Indian Journal of Natural Sciences www.tnsroindia.org.in ©IJONS

Vol.8 / Issue 45 / December 2017 *International Bimonthly* *ISSN: 0976 – 0997*

RESEARCH ARTICLE

Rice Area Estimation in Tiruvarur District of Tamil Nadu using VH Polarized Sentinel 1A SAR Data

Mugilan Govindasamy Raman[1]*, Ragunath Kaliaperumal[2] and Sellaperumal Pazhanivelan[3]

Department of Remote Sensing and GIS, Tamil Nadu Agricultural University, Coimbatore -641003, Tamilnadu, India.

Received: 12 Sep 2017 Revised: 20 Sep 2017 Accepted: 01 Oct 2017

***Address for correspondence**
Mugilan Govindasamy Raman
Department of Remote Sensing and GIS,
Tamil Nadu Agricultural University,
Coimbatore -641003, Tamilnadu, India.
E.mail: mugilantnau@gmail.com

ABSTRACT

A research study on 'Rice Area estimation in Tiruvarur district of Tamil Nadu using VH Polarized Sentinel 1A SAR data' was conducted during *rabi* 2016 (Samba season) to estimate rice area in Tiruvarur district. Multi temporal Sentinel 1A satellite data with VH polarization at 20 m spatial resolution was acquired between September, 2016 and January, 2017 at 12 days interval and processed using MAPscape-RICE software. Continuous monitoring was done for crop parameters and validation exercise was done for accuracy assessment. Spectral dB curve of rice was generated using temporal Sentinel 1A SAR data. The dB values showed a minimum at agronomic flooding and a peak at maximum tillering stage and decreased thereafter. A total rice area of 91007 ha was estimated in Tiruvarur district during samba season 2016-17 using VH polarization.

Keywords: Rice, Sentinel 1A SAR, VH Polarization, Spectral dB curves

INTRODUCTION

The importance of agriculture for the Indian society can be hardly be over emphasized, as its role in the economy, employment, food security, national self reliance and general well being, does not need reiteration. The need for timely and reliable information on crop area and production for tactical and strategic decision making by all the stake holders in agriculture, such as producers, processors, resource managers, marketing finance and the government is well known. Crop growth and yield are determined by a number of factors such as genetic potential of crop cultivar, soil, weather, cultivation practices (date of sowing, amount of irrigation and fertilizer) and biotic stresses. Accurate crop identification can achieve a good estimation for crop sown acreage, planting structure and spatial distribution, as well as provide key input parameters for crop yield estimation. Hence study on crop identification is important for making national food policy and economy plan. With the launch and continuous

availability of multi-spectral (visible, near-infrared) sensors on polar orbiting earth observation satellites (LANDSAT, SPOT, IRS, etc) remote sensing (RS) data has become an important tool for area and yield estimation. Remote sensing data provide timely, accurate, synoptic and objective estimation of crop identification, crop monitoring, acreage and yield estimation. In view of the advantages of high temporal resolution, wide coverage and low cost, remote sensing has been used in a wide range of earth observation activities and thus provides a useful tool for crop recognition and planting acreage monitoring at a large scale. Since the 1980's, optical remote sensing has been widely used to identify various crops, however, optical images are not often available in the key growth period of crops, owing to the cloudy and rainy weather. Thus, it has a negative effect on the accuracy and timeliness of crop area monitoring. As a new technology with an advantage of all weather, all-time, high resolution and wide coverage, Synthetic Aperture Radar (SAR) has been widely applied in agricultural condition monitoring which provides a strong complement and support for crop identification in data and technology aspect. As the updating and improvement of function parameters and performance index of radar sensors, it has been an important field of agriculture remote sensing in getting the information of crop sown acreage, growing condition and yield by SAR. In order to increase the accuracies of crop identification and area estimation, we need to have a better understanding of the crop and the underlying soil characteristics that influence the radar backscatter throughout the growing season and identify the suitable methodologies to extract crop information from SAR imagery and evaluate the multi temporal SAR data for crop identification.

MATERIALS AND METHODS

Synthetic Aperture Radar (SAR) has the advantage of operating at wavelengths not impeded by cloud cover or a lack of illumination and can acquire data over a site during day or night time under all weather conditions. Sentinel-1A, with its C-SAR instrument, can offer reliable, repeated wide area monitoring. Sentinel-1A is a European radar imaging satellite launched in 2014. It is the first Sentinel 1 satellite launched as part of the European Union's Copernicus programme. It provides dual polarization capability, very short revisit times and rapid product delivery. For each observation, precise measurements of spacecraft position and attitude are available. The satellite carries a C-band Synthetic Aperture Radar which will provide images in all light and weather conditions with VH (Vertical–Horizontal) and the data obtained at twelve days interval. Sentinel1-A has four standard operational modes, designed for interoperability with other systems. Level-1 ground range (GRD) product obtained by interferometric wide (IW) swath mode (1) of High Resolution (HR) is used for this research. The characteristics of IW1-GRD-HR product are given in Table1. In order to have a full coverage during the crop growing period of rice, the satellite data were downloaded for 19th September 2016 to 17th January 2017 at 12 days interval from https://scihub.copernicus.eu/dhus/.

GIS and other softwares viz., MAPscape-RICE, ArcGIS, QGIS, RiceYES and ORYZA growth model will be used in the study to perform different operations to achieve results.A fully automated processing chain developed by Holecz *et al*. (2013) will be used to convert the multi-temporal space-borne SAR SLC data into terrain-geocoded σ° values. The processing chain is a module within the MAPscape-RICE software.

The multi-temporal stack of terrain-geocoded σ° images was input to a rule-based rice detection algorithm in MAPscape-RICE. The temporal evolution of σ° was analyzed from an agronomic perspective, which also required *a priori* knowledge of rice maturity, calendar and duration and crop practices from field information and knowledge of the study location. The temporal signature was frequency and polarization dependent and also relied on the crop establishment method and, to some extent, on crop maturity. This implied that general rules could be applied to detect rice, but that the parameters for these rules needed to be adapted according to the agro-ecological zone, crop practices and rice calendar. The Rule-based rice detection algorithm for multi-temporal C-band σ° is presented in Fig.1 with the parameters used in the MAPscape-RICE software.

The choice of parameters a, b, c, d, e and f was guided by a simple statistical analysis of the temporal signature of σ° values in the monitored fields. The criteria used to guide the selection of parameters. The mean, minimum, maximum and range of σ° were computed for the temporal signature of each monitored field. Then, we computed the minima and maxima of those mean σ° values across fields, the maxima of the minimum σ° values across fields, the minima of the maximum σ° value across fields and the minimum and maximum of the range of σ° values across fields (Holecz *et al*., 2013). These six statistics, which we call temporal features, concisely characterize the key information in the rice signatures of the observed fields, and each one relates directly to one parameter. Hence, the value of the six temporal features from the monitoring locations at each site can be used to guide the choice of the six parameter values as shown in Table 2.

The Error matrix and Kappa statistics are used for evaluating the accuracy of the estimated rice area. The class allocation of each pixel in classified image is compared with the corresponding class allocation on reference data (Crop Cutting Experiment data) to determine the classification accuracy. The pixels of agreement and disagreement are compiled in the form of an error matrix, where the rows and columns represent the number of all classes and the elements of matrix represent the number of pixels in the testing dataset (Lillesand 1994). The accuracy measures, such as overall accuracy, producer's accuracy and user's accuracy are estimated from the error matrix (Congalton, 1991). The overall accuracy, which is the percentages of correctly classified cases lying along the diagonal, was determined as follows:

$$\text{Overall Accuracy} = \frac{\Sigma(\text{Correctly classified classes along diagonal})}{\Sigma(\text{Row Total or Column Total})}$$

The producer's accuracy (errors of omission) of each class was computed by dividing the number of samples that were classified correctly by its total number of reference samples as follows:

$$\text{Producer's Accuracy} = \frac{\text{Number of correctly classified class in a column}}{\text{Total number of items verified in that column}}$$

The user's accuracy (errors of commission) of each class was computed by dividing the number of correctly classified samples of that class by its total number of samples that were verified as belonging to the class as follows:

$$\text{User's Accuracy} = \frac{\text{Number of correctly classified item in a row}}{\text{Total number of items verified in that row}}$$

Another measure of classification accuracy is the kappa coefficient, which is a measure of the proportional (or percentage) improvement by the classifier over a purely random assignment to classes (Richards, 1993). The kappa coefficient can be estimated from the formula given below.

$$\hat{K} = \frac{NA - B}{N^2 - B}$$

For an error matrix with **r** rows, and hence the same number of columns,

Where,

A = the sum of **r** diagonal elements, which is the numerator in the computation of overall accuracy

B = sum of the r products (row total x column total)

N = the number of pixels in the error matrix (the sum of all r individual cell values)

Field observations will be performed throughout the rice and non-rice fields within the study area. Monitoring sites will be fixed in major rice growing blocks of the study area and these fields will be selected with the farmers' consent, prior to the start of the rice season and the image acquisition schedule. Observations will be made on or as close to the image acquisition date as possible. Observations will include latitude and longitude from hand held GPS

receivers, descriptions and photos of the status of the field, plant height, water depth, weather conditions and crop stage. A validation exercise will be conducted for each footprint to assess the accuracy of the rice classification. Random stratified sampling method will be adopted to collect land cover information at approximately 106 locations throughout the district with these points split 12/94 between non-rice points and rice points. Map validation assessments will be conducted in season, in the reproductive or ripening stage before harvesting. Locations will be chosen such that the land cover was homogeneous in a 50 m radius around each GPS point for 20 m resolution imagery.

RESULTS AND DISCUSSION

This study on 'Rice Area estimation in Tiruvarur district of Tamil Nadu using VH Polarized Sentinel 1A SAR data' has attempted to estimate the rice area using SAR images from Sentinel 1A satellite, which is a freely available data. Single (VH) polarized data are available from these sensors, which pave way to explore the interaction of the polarizations to determine crop characteristics. The strength of different polarization in rice area estimation was studied and the results on the characteristics of the study area, rice area mapping for VH polarization, rice area map are discussed in this Chapter.A dB stack was generated using eleven sets of Sentinel-1A data (Table 3) acquired after basic processing viz., orbital and radiometric correction, geo-coding, mosaicking and speckle filtering. Temporal signatures were extracted in VH polarization for each monitoring field and used to generate the dB curves for rice fields for VH polarization. The temporal signature for a selected representative pixel in VH polarization was generated to visualize the resulting rule based classification (Fig.2).

A detailed analysis of temporal signatures of rice for VH polarization were done separately for deriving parameters used to classify rice pixels in MAPscape-RICE software. The eleven parameters derived from the temporal signatures of VH polarization for analysis were, mean value of Built-up area, minimum value at tillering, minimum and maximum crop cycle duration, maximum value at start of season, start of season to last acquisition, minimum primary and secondary variation, maximum value and days of temporary water. The temporal signatures for the selected rice pixels in VH polarization are presented in Fig.3 and the parameters used for classification are given in the Table 4.

VH polarization signatures showed a minimum dB value at agronomic flooding and a peak at maximum tillering stage. At flooding the minimum dB value ranged from -19.56 to -18.79 with an average of -19.23. At peak tillering stage in VH polarization average was found to be -16.35 with a range of -15.77 to -16.92 across Tiruvarur district (Table 5), Rice crop shows significant temporal behavior and a large dynamic range (−14.4 to −8.41dB) during its growth period (Inoue *et al*., 2002, Suga and Konishi, 2008, Oh *et al*., 2009 and Kim *et al*., 2009). The minimum primary variation was found to be 2.5 dB corresponding to growth at vegetative and maximum tillering stage in VH polarization.

The lowest values at emerging were due to less back scattering from less vegetation cover with rougher surface which was the moment to capture the start of the season for each pixel. This might be the due to soil moisture variation or sowing which made the soil surface smoother (Karjalainen *et al*., 2004). Nelson *et al*., 2014 recorded a similar minimum at early stage of rice crop with X-band (TerraSAR-X and Cosmosymed) SAR data across Asia in Philippines and Thailand.Rice map generated from VH polarization of Sentinel 1A SAR data recorded a total area of 91007 ha (Fig.04). Block wise statistics showed that, rice area in the blocks ranged from 2880 ha to 13418 ha, where Muthupettai block recorded the largest area followed by 12730 ha in Needamangalam, 11895 ha in Kottur and 10178 ha in Valangaiman block. The lowest area was found in the Tiruvarur block followed by Koradacheri with 5798 ha and Nannilam block with 8103 ha. The other blocks viz., Mannargudi, Thiruthuraipoondi and Kudavasal had 9461 ha, 8298 ha and 8246 ha respectively (Table.6)

The generated rice area map was validated using ground truth points collected throughout Tiruvarur district during different time of visit coinciding with crop stages and satellite pass. Both rice and non-rice points were collected with latitude and longitude values during the visits. There were 106 points collected which includes 94 rice points and 12 non-rice points. The number of non-rice points collected was less, since in Tiruvarur district the major crop grown is rice and very less area with other crops. The ground truth points collected for validation are depicted in the Fig.5.Validation was carried out using confusion matrix and classification accuracy was calculated. The two classes of Rice and Late rice available in the rice area map were considered as a single class for map accuracy. The accuracy assessments in the field were generally conducted in season, in the reproductive or ripening stage before harvesting, but in some cases the field assessment was conducted post season and rice stubble and farmer survey were used to confirm that the observed post harvest situation reflected the presence of a rice crop during the monitoring season. The results of confusion matrix show that the number of true positives (actual rice that classified as rice) was 74 points, the number of false positives (actual non rice that classified as rice) was 1 point. The number of false negatives (actual rice that classified as non rice) was 20 points and the number of true negatives (actual non rice that classified as non rice) was 22 points.

The user accuracy of Rice and Non rice points were 78.7% and 95.7% respectively. The Producers accuracy of Rice and Non rice points were 98.7% and 52.4% respectively. The overall accuracy of both rice and non rice points are 82.1%. The average accuracy and reliability was about 87.2% and 75.5% respectively. The overall Kappa index was 0.64 (Table 7). In VH polarization the direct seeded rice area was well pronounced showing more agreement with the ground truth data in the southern parts of the district. More of Late rice pixels were classified in VH polarization. Though there were good agreement in the lower parts of the district, the Western and Northern parts of the district that dominate transplanted rice was not captured fully, which lead to low accuracy.

REFERENCES

1. Congalton, R.C. 1991. A review of assessing the accuracy of classifications of remotely sensed data. Remote Sensing Environment, 37, pp. 35-46.
2. De Zan, F. and A. M. Guarnieri. 2006. TOPSAR: Terrain Observation by Progressive Scans. *IEEE Transactions on Geoscience and Remote Sensing,* 44(9), pp. 2352–2360.
3. Holecz, F., M.F.L. Barbieri, A. Collivignarelli, T.D.M. Gatti, Nelson, G. Setiyono, Boschetti, P.A.B. Manfron, J.E. Quilang. 2013. An operational remote sensing based service for rice production estimation at national scale. In: Proceedings of the Living Planet Symposium, Edinburgh, UK, 9-11.
4. Inoue., Y. T. Kurosu, H. Maeno, S. Uratsuka, T. Kozu, K. Dabrowska-Zielinska, J. Qi. 2002. Season - long daily measurements of multifrequency (Ka, Ku, X, C, and L) and fullpolarization backscatter signatures over paddy rice field and their relationship with biological variables. Remote Sens. Environ., 81: 194–204.
5. Karjalainen, M., H. Kaartinen, J. Hyyppa, H. Laurila and R. Kuittinen. 2004. The Use of ENVISAT Alternating Polarization SAR Images in Agricultural Monitoring in Comparison with RADARSAT-1 SAR Images. *XXth ISPRS Congress,* July 12-23, 2004 Istanbul, Turkey. XXXV (B7), pp. 132-137.
6. Kim, Y.H., S.Y. Hong and Y. H. Lee, 2009. Estimation of paddy rice growth parameters using L-, C-, X-bands polarimetric scatterometer. Korean J. Remote Sens., 25, 31–44.
7. Lillesand, T.M. and Kiefer, R.W., 1994. Remote sensing and photo interpretation. John Wiley and Sons: New York, p.750.
8. Nelson, A., Setiyono, T., Rala, A.B., Quicho, E.D., Raviz, J.V., Abonete, P.J., Maunahan, A.A., Garcia, C.A., Bhatti, H.Z.M., Villano, L.S. and Thongbai, P. 2014. Towards an operational SAR-based rice monitoring system in Asia: Examples from 13 demonstration sites across Asia in the RIICE project. *Remote Sensing*, *6*(11), pp.10773-10812.
9. Oh, Y, S.Y., Hong, Y. Kim, J.Y. Hong and Y.H. Kim. 2009. Polarimetric backscattering coefficients of flooded rice fields at L- and C-bands: Measurements, modeling, and data analysis. IEEE Trans. Geosci. Remote Sens., 47, 2714–2721. on 1 June 2014).
10. Richards, J.A. 1993. Remote Sensing Digital Image Analysis. Springer, Heidelberg, New York.

11. Suga, Y. and Konishi, T. 2008, October. Rice crop monitoring using X, C and L band SAR data. In *SPIE Remote Sensing* (pp. 710410-710410). International Society for Optics and Photonics.

Table 1. Characteristics of Sentinel1-A (IW1-GRD-HR) Data (DeZan and Guarnieri., 2006)

Parameters	Characteristics
Pixel value	Magnitude detected
Coordinate system	Ground range
Polarization options	Single(HH or VV) or Dual (HH+HV or VV+VH)
Resolution (range x azimuth in meters)	20.4x21.7
Pixel spacing (range x azimuth in meters)	10x10
Incidence angle (degree)	32.9
Radiometric resolution	1.7 dB
Ground range coverage (km)	251.8
Absolute location accuracy (m) (NRT)	7
Equivalent Number of Looks (ENL)	4.4
Number of looks (range x azimuth)	5 x 1
Range look bandwidth (Hz)	14.1
Azimuth look bandwidth (Hz)	327
Look overlap (range, azimuth)	0.250, 0.000
Bits per pixel	16

Table 2. Site-specific parameters for the rule-based classification and the criteria used to select them based on temporal features.

Parameter	Relationship between Parameter and Temporal Feature
a = lowest mean	a < (i) minima of the mean σ° across all rice signatures
b = highest mean	b > (ii) maxima of the mean σ° across all rice signatures
c = maximum variation	c > (vi) maxima of the range in σ° across all rice signatures
d = max value at SoS	d > (iii) highest minima in σ° across all rice signatures
e = min value at peak	e < (iv) lowest maxima in σ° across all rice signatures
f = minimum variation	f < (v) minima of the range in σ° across all rice signatures

Table 3. Sentinel 1A data acquisition dates during Samba 2016 for Tiruvarur district

S.No	Date of Acquisition
1	19 Sep 2016
2	01 Oct 2016
3	13 Oct 2016
4	25 Oct 2016
5	06 Nov 2016
6	18 Nov 2016

S.No	Date of Acquisition
7	30 Nov 2016
8	12 Dec 2016
9	24 Dec 2016
10	05 Jan 2017
11	17 Jan 2017

Table 4. Classification parameters used for rice pixel delineation in VH polarization data

S.No	Parameter	VH
1.	Mean Value of Water (dB)	-21.00
2.	Max Value of Temporary Water (dB)	-22.00
3.	Days of Temporary Water (days)	65
4.	Mean Value of Built up Areas (dB)	-14.00
5.	Max Value at Start of Season (dB)	-16.00
6.	Min Primary Variation (dB)	2.50
7.	Min Secondary Variation (dB)	0.00
8.	Min Value at Tillering (dB)	-20.00
9.	Minimum Cycle Duration (days)	80
10.	Maximum Cycle Duration (days)	120
11	SOS to Last Acquisition (days)	10

Table 5. Temporal dB values of Rice fields across Tiruvarur district (VH Polarization)

Satellite Pass no.	Field 1	Field 2	Field 3	Field 4	Field 5	Field 6	Field 7	Field 8	Average
19-Sep-2016	-18.124	-19.277	-17.845	-17.763	-18.728	-17.886	-17.928	-17.702	**-18.1566**
01-Oct-2016	-19.732	-19.763	-18.983	-18.792	-19.01	-19.11	-19.564	-18.906	**-19.2325**
13-Oct-2016	-18.525	-18.839	-18.504	-19.009	-18.372	-18.904	-19.062	-18.824	**-18.7549**

25-Oct-2016	-17.582	-18.078	-18.072	-18.519	-17.815	-18.297	-17.972	-18.211	**-18.0683**
06-Nov-2016	-16.679	-17.887	-17.05	-17.626	-17.593	-17.857	-16.942	-17.343	**-17.3721**
18-Nov-2016	-16.179	-16.982	-16.485	-16.341	-16.583	-17.238	-16.313	-16.891	**-16.6265**
30-Nov-2016	-16.442	-16.327	-16.763	-15.769	-15.987	-16.746	-15.834	-16.921	**-16.3486**
12-Dec-2016	-15.902	-16.293	-16.417	-15.333	-16.066	-16.632	-15.547	-17.044	**-16.1543**
24-Dec-2016	-15.438	-15.697	-15.998	-15.234	-16.022	-16.409	-15.251	-16.171	**-15.7775**
05-Jan-2017`	-15.11	-15.557	-16.059	-13.931	-14.843	-15.329	-14.278	-15.074	**-15.0226**
17-Jan-2017	-15.455	-15.361	-15.979	-15.013	-15.652	-15.787	-15.224	-15.255	**-15.4658**

Table 6. Block wise rice area derived from VH Polarization for Tiruvarur district (Area in Ha)

Block Name	Rice	Late Rice	Total Rice area
Nannilam	8083	20	8103
Kudavasal	8246	0	8246
Valangaiman	10165	14	10178
Koradacheri	5790	8	5798
Tiruvarur	2788	93	2880
Needamangalam	12726	4	12730
Mannargudi	9461	0	9461
Kottur	11851	44	11895
Thiruthuraipoondi	8131	167	8298
Muthupettai	13174	244	13418
Total			**91007**

Table 7.Confusion matrix for accuracy assessment of rice classification

Actual class from survey	Predicted class from the map			
	Class	**Rice**	**Non-Rice**	**Accuracy**
	Rice	74	20	78.7%
	Non-Rice	1	22	95.7%
	Reliability	98.7%	52.4%	82.1%

Average accuracy	**87.2%**
Average reliability	**75.5%**
Overall accuracy	**82.1%**
Kappa index	**0.64**

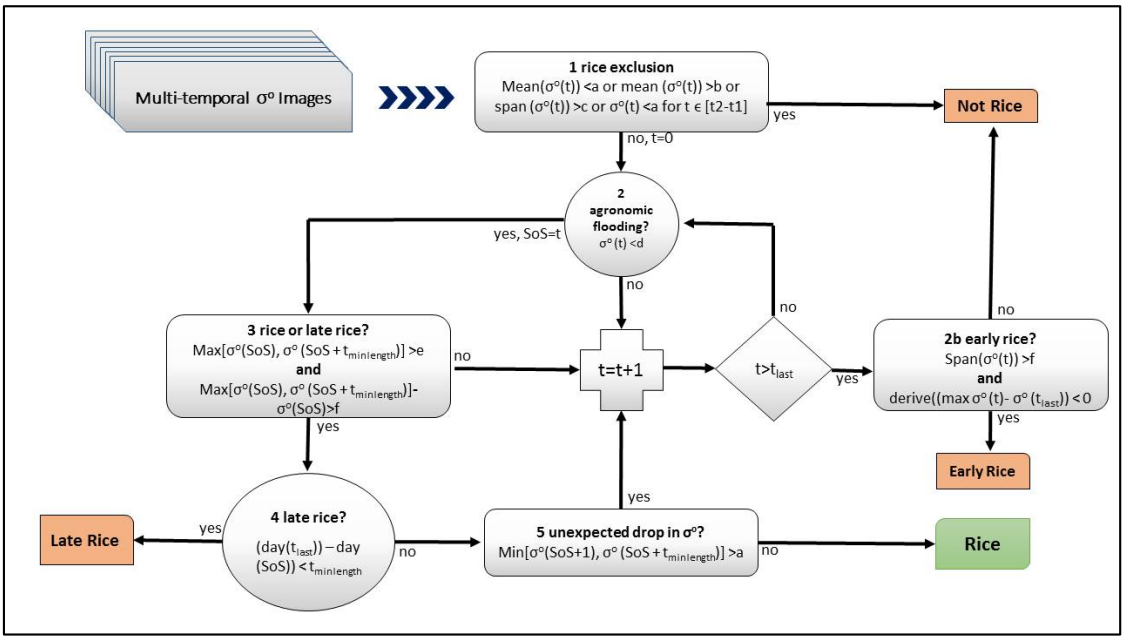

Fig.1.Rule-based rice detection algorithm for multi-temporal C-band σ° in MAPscape-RICE

a =lowest mean
b =highest mean
c = maximum variation
d = maximum value at SoS
e = minimum value at maximum peak
f = minimum variation
t = time
t_2-t_1 = maximum time under water
tmin length= minimum number of days of season length
tmax length= maximum number of days of season length
t_{last} = date of the last acquisition
SoS = Start of Season

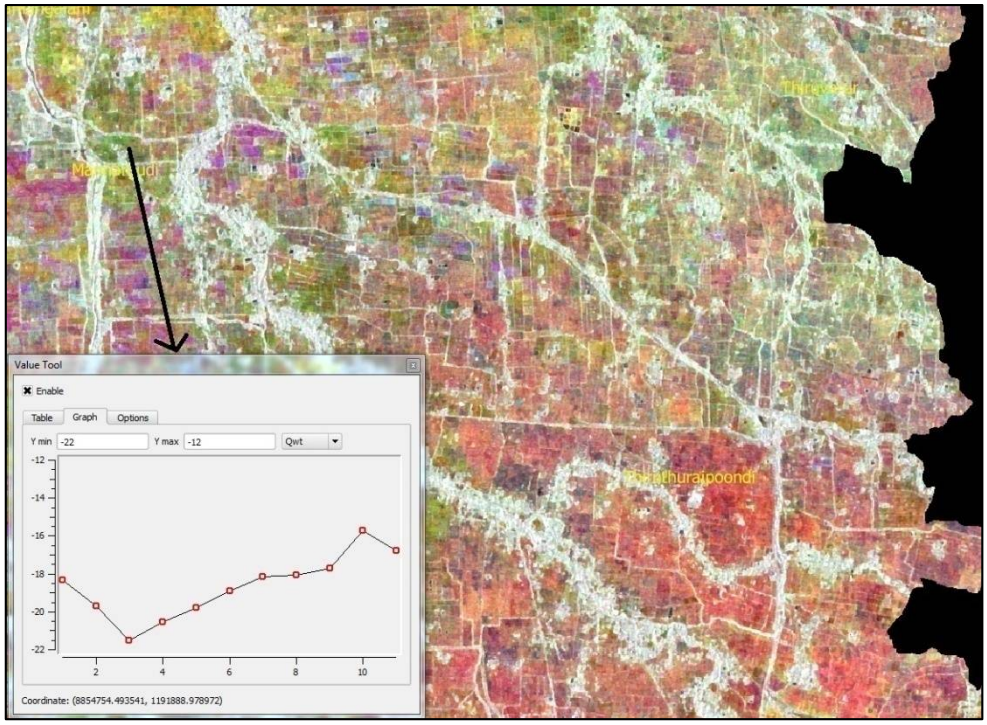

Fig.2.dB stack generate with Sentinel 1A data and Rice temporal curve VH

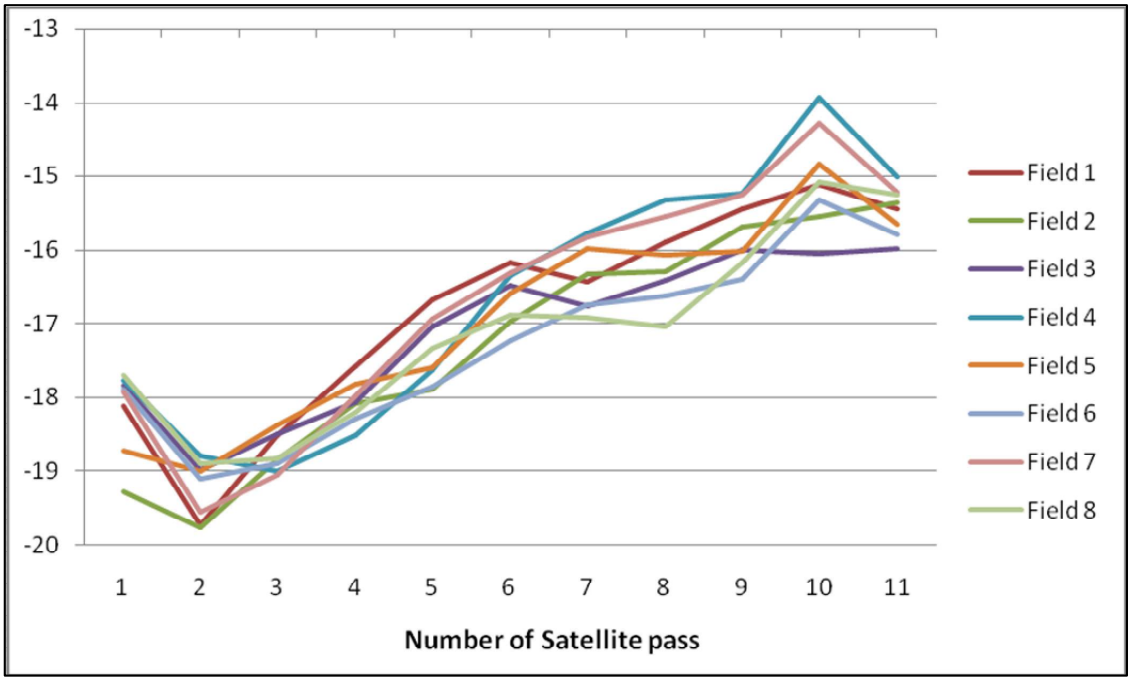

Fig.3.Temporal dB curves for rice at selected sites VH

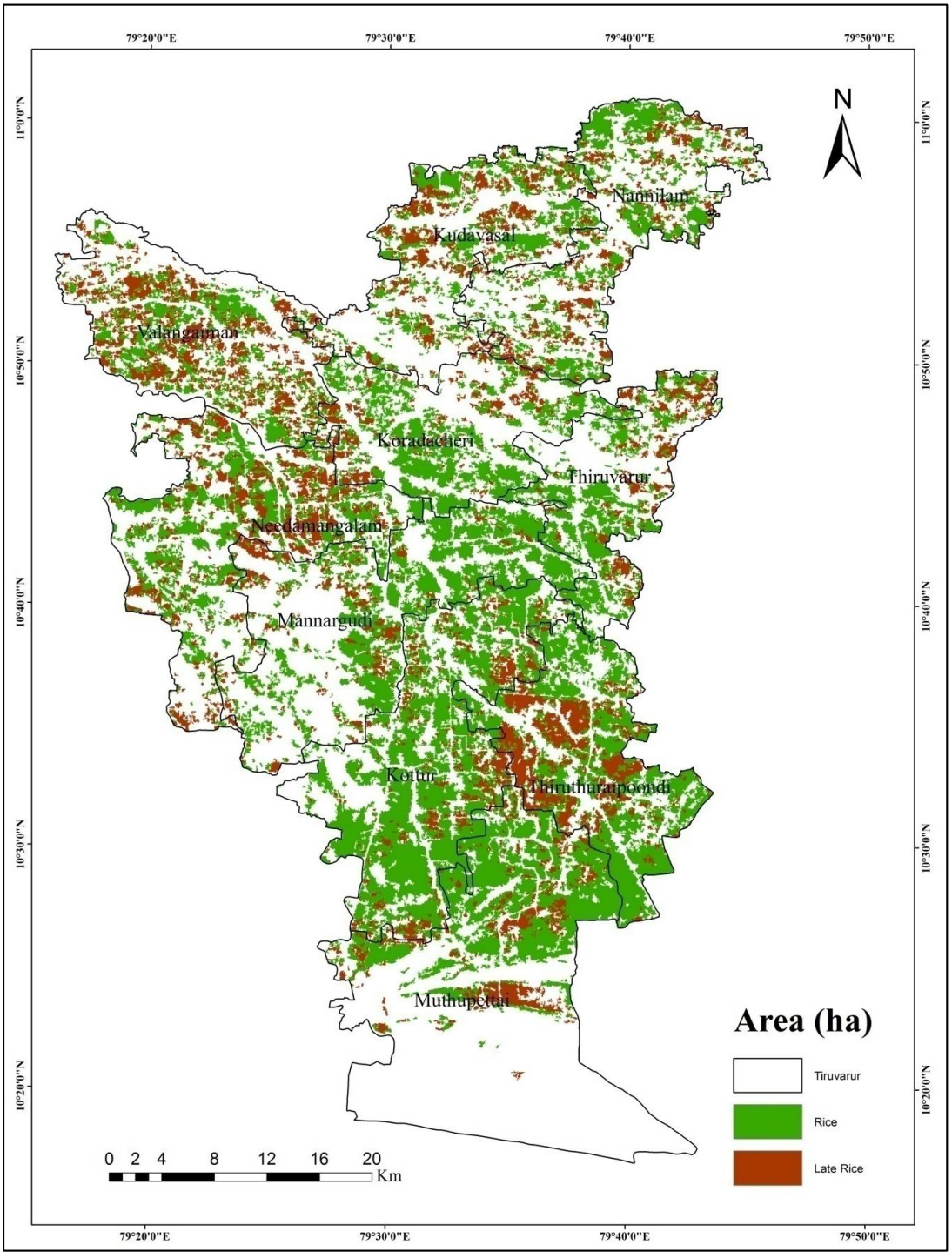

Fig.4 Rice area map of Tiruvarur district generated using VH Polarization

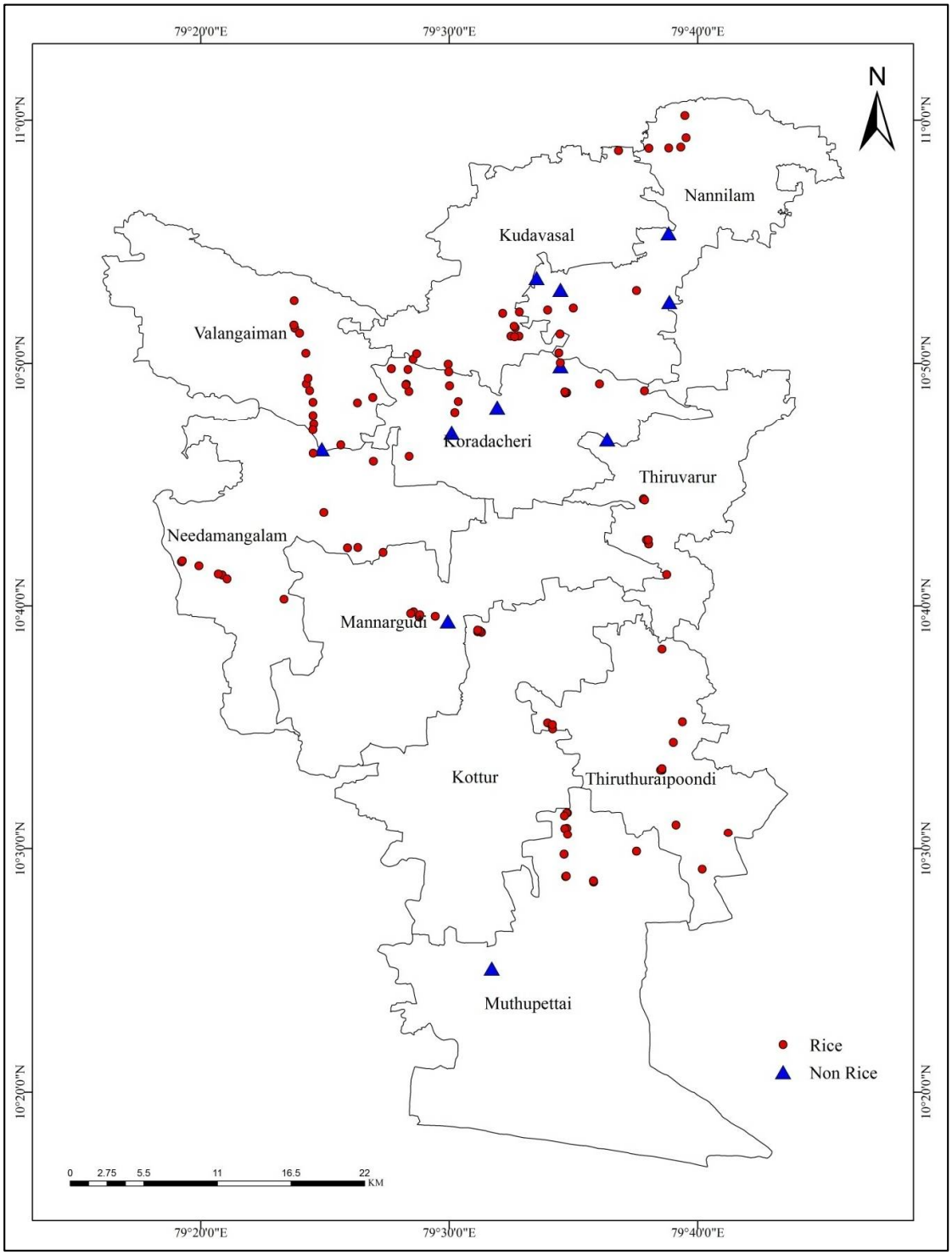

Fig.5. Rice area map validation points (rice and non-rice) across Tiruvarur district

Indian Journal of Natural Sciences www.tnsroindia.org.in ©IJONS

Vol.8 / Issue 45 / December 2017 *International Bimonthly* *ISSN: 0976 – 0997*

RESEARCH ARTICLE

Ultrastructure of Renal Tubules in the Indian Grass Skink, Eutropis carinata

S.Samson and M.Bhagya*

Department of Studies in Zoology, Manasagangotri, University of Mysore, Mysuru, 570006, Karnataka, India.

Received: 07 Sep 2017 Revised: 28 Sep 2017 Accepted: 30 Oct 2017

***Address for correspondence**
Dr.M.Bhagya
Professor in Zoology
Department of Studies in Zoology,
University of Mysore, Manasagangotri,
Mysuru, 570006, Karnataka,India.
Email: bhagya.uomzoology@gmail.com

ABSTRACT

The light microscopic and ultrastructural examinations of renal tubule in the lizard *Eutropis carinata* reveals that, proximal convoluted tubule that bears low microvillus brush border and dark staining cytoplasm.The presence of diffused secretory vacuoles within the cells of PCT and lack of inter sellular spaces is unique to E. carinata. The intermediate segment bears tuft of cilia in the apical portion of the cells and the lumen shows the presence of electron lucent mucoid substances. Distal convoluted tubule has lightly stained cytoplasm filled with electron lucent amorphous substances. The similarities and variations in the microstructure of the renal tubules in *E. carinata* with other reptiles are discussed.

Keywords : Proximal convoluted tubule, Distal convoluted tubule, Intermediate segment, *Eutropis carinata*.

INTRODUCTION

The major functional attributes of the kidney are, formation of urine, maintaining systemic hemodynamics and regulation of fluid volume of the body. It is also involved in acid base balance, synthesis and release of hormones. These functions are achieved due to unique structural organization of the uriniferous tubule, consisting of the nephron and the collecting tubule, which has been regarded as the functional unit of the kidney (Dantzler, 2003). However, studies have shown that the nephron of the reptilian kidney shares a degree of anatomical similarities with the mammalian kidney in possessing Bowman's capsule (renal corpuscle), proximal convoluted tubule, distal tubule, collecting duct and ureter (Peek and McMillan, 1979). However variations do exists in the extant of nephron among reptiles. Reptilian nephron lack loop of henle and instead have a short intermediate segment (Davis *et al.,* 1976; Peek

and McMillan, 1979). The density of nephrons in reptilian kidney is far less compared to mammalian kidney (Peek and McMillan, 1979). The kidney of the squamate reptiles (snakes and lizards) however, has a reputation beyond the general functions of the kidney. In these reptiles a portion of a nephron known as Renal sexual segment (RSS) hypertrophies and becomes highly secretory during sexually active season, whose secretions have a pivotal role in sperm sustenance, motility and also mating behaviour (Cuellar, 1966; Prasad and Reddy, 1972; Devine, 1975; Ross and Crews, 1977; Shine *et al.,* 2000).

Interestingly, comparative studies have also revealed marked variations in the ultrastructure of the nephron within a variety of reptilian species (Gabri, 1983; Khalil *et al.,* 1974). The first histological description of the squamate nephron was made by Gampert (1866) on the European natricine grass snake, *Natrix natrix*. Since then, the reptilian kidney has been investigated in variety of snakes and lizards by ultrastructural, histological, histochemical and physiological techniques (Kuhnel and Krisch, 1974; Sever *et al.,* 2002; Siegel *et al.,* 2009; Krohmer, 2004; Rheubert *et al.,* 2011).

Peek and McMillan (1979) reported the ultrastructural features of the tubular nephron in Garter Snake *Thamnophis sirtalis.* Their studies revealed that, although a nephric loop (loop of Henle) is lacking, the renal tubules appear to be structurally well adapted for efficient ion and water re-absorption. The most prominent features are well developed microvilli in the proximal tubule and elaborate lateral folds, particularly in the distal tubule and collecting ducts. Allam *et al.,* (2013) provided a comparative account on the histochemical, histological and ultrastructural features of the nephron of four snakes, *Eryx jaculus; Psammophis sibilans; Naja haje* and *Echis pyramidum*, belonging to different families. The glomerulus of the snakes, *P. Sibilans* and *N. haje* was comparatively larger possessing wider urinary space. The epithelial cells of the proximal convoluted tubule (PCT) of all the 4 snakes showed well developed brush border. Ciliated cells were present in the intermediate segment. Small microvilli are noticed in the distal convoluted tubule (DCT). The collecting tubule showed more mucous cells in *N. haje* than the other snakes. Thus, their study revealed several structural similarities and differences among the four snakes.

Davis *et al.,* (1976) studied the anatomy and ultrastructure of the kidney in the lizard *Sceloporus cyanogenys.* They reported that, beginning with the glomerulus and Bowman's capsule the nephron segments are sequentially: proximal tubule; intermediate ciliated segment consisting of a proximal and distal part; distal tubule, which can be divided into two segments, followed by connecting tubule and initial collecting duct. They also reported that the initial collecting ducts from several nephrons open into the collecting duct, which is not reported in other lizards.Schmidt-Nelson and Davis (1968) performed a comparative study of the nephron in crocodiles (*Crocodylus johnstoni* and *Crocodylus porosus*), blue tongued lizards (*Tiliqua scincoides),* banded sea snakes (*Laticauda colubrine*) and green turtles (*Chelonia mydes*). Their reports revealed that renal tubules have intercellular spaces. The fluid movements across renal tubules of reptiles are correlated with the width of the tubular intercellular spaces. In the proximal tubules, where transport is always isosmotic, the spaces are open whenever the tubular epithelium is transporting, but closed when no transport is taking place.

Roberts and Schmidt-Nelson (1966) performed a comparative study of the nephron in three lizards, *Hemidactylus* species (geckos), horned toads (*Phrynosoma cornutum*) and Galapagos lizards (*Tropidurus* species). In all these species, the luminal surfaces of the proximal tubular cells have a brush border. Cytoplasm contains small population of vesicles and large membrane bound vacuoles. The basal cytoplasm of the distal tubular cells is divided into processes bounded by the plasma membrane.Although Scincidae is the largest family of lizards that encompasses ~1,200 species (European Molecular Biology Laboratory Reptile Database, 2006), an ultrastructural study on the different portions of the kidney tubule, (other than RSS) is scarce and fragmentary. Such studies expand our knowledge in understanding the structural modifications in the reptilian nephron that has enabled the reptiles to cope up even with the hostile environmental conditions whether in land, marine or fresh water habitats (Gambarian, 1978).

Therefore, the present study was designed to examine the ultrastructural details of proximal convoluted tubule (PCT), intermediate segment (IS) and distal convoluted tubule (DCT) of the nephron in the lizard *Eutropis carinata* (Scincidae). So far no studies have been reported in this aspect of the kidney in Indian reptiles.

MATERIALS AND METHODS

Sexually mature male *Eutropis carinata,* commonly known as grass skink, were collected from woody areas in and around Mysore University Campus that spread over 739 acres of pristine woody habitat (Longitude 76.6°, Latitude 12.3°) in Mysuru district, Karnataka, India. The lizards were euthanized by exposure to ether, a procedure approved by the Institutional Animal Ethics Committee of University of Mysore and CPCSEA for handling and sacrifice of animals. Kidneys were removed free from connective tissue, fat and blood and utilized for light as well as electron microscopic examinations.

For examination with light microscopy, kidney tissues were fixed in 10% neutral buffered formalin, processed through graded series of alcohol, embedded in paraffin wax, and five micron thick cross sections were cut using LIECA-RM 2125 microtome. Sections were stained with hematoxylin-eosin for general histology (Kiernan, 1990). The stained sections were examined and photographed under compound Zeiss polarised AX-400EB projector microscope**.**

For examination with electron microscopy, small pieces of kidney tissue were fixed in 3% glutaraldehyde in 0.1M phosphate buffer pH 7.2 for 24 hrs, post fixed in osmium tetroxide, dehydrated in ethanol and embedded in epoxy resin. Semithin (1µm) and ultrathin (500-700 A°) plastic sections were cut using a LEICA EM UC6 ultramicrotome. Semithin sections were stained with Toluidine blue and utilized for examination with light microscopy and the ultrathin sections were placed on copper grids, doubly stained with uranyl acetate followed by lead citrate and examined with a Techani G2 electron microscope at 60KV accelerating voltage.

RESULTS

The proximal convoluted tubule (PCT)

Light microscopic examinations showed that the PCT is made up of monolayer of low columnar epithelium. In the toluidene stained sections the epithelial cells are filled with dark staining cytoplasmic contents. The nuclei of these cells appear eccentric/ basal that usually possesses nucleolus at the centre. The apical portion of the epithelial cells bears tuft of microvilli that are lightly stained provides a characteristic brush border appearance (Fig's 1 and 2). Transmission electron microscopic examination revealed that, at the proximal region of the PCT, the apical portion of the epithelial cells bears long, thick tuft of microvilli that are closely stacked (Fig. 3). The cytoplasmic contents of these cells appear electron dense which is very distinct from that of DCT. The nucleus is basally positioned, spherical and heterochromatic with centralized nucleolus.The cytoplasm consists of more number of electron dense mitochondria that are intermixed with small lucent vacuoles (Fig. 4 and 5). The intercellular canaliculi that are very extensive in the cytoplasm are highly labyrinthine (Fig. 5). The lumen is filled with slightly electron dense amorphous substance (Fig. 3). At the distal portion of the PCT, the epithelial cells are low columnar and possess light and dark cells that are arranged alternatively (Fig. 6). Closer examination reveals that the nucleus of the dark cell are highly indented and heterochromatic, where as the nucleus of the light cell is roughly spherical and euchromatic (Fig. 7 and 8). The cytoplasm of the light cells encloses randomly distributed diffused secretory vesicles. Whereas the cytoplasm of the dark cell lack diffused secretory vesicles but bears few lucent vacuoles (Fig. 7 and 8). The diffused secretory vesicles of the lighter cells are crowded at the apical portion of the cytoplasm and also in the lumen. The microvilli of these cells are short and distended (Fig. 6 and 8). The lateral and basal plasma membranes are highly labyrinthine (Fig. 7). Erythrocytes are generally noticed between the tubules (Fig. 8).

The intermediate segment (IS)

This segment of the nephron is much obscured and extremely rear in light microscopic examinations. The diameter of the tubule is comparatively smaller than PCT and DCT. The epithelium of IS is made up of single layer of cuboidal cells whose cytoplasmic contents appear lighter. The lumen is reduced to a narrow slit (Fig. 1). Transmission electron microscopic examination of IS showed that, the apical portion of cuboidal epithelial cells bears a rim of cilia. The cytoplasm is abundant in mitochondria and fewer dense bodies. Lateral plasma membrane is labyrinthine. Nucleus is spherical, euchromatic and centrally positioned (Fig. 9). Upon closer view, the cristae of the mitochondria are highly dilated and enclose electron lucent amorphous substance (Fig. 10). The tuft of cilia at the apical portion of the cell that projects into the lumen are long, filamentous and possess prominent axoneme. The lumen is narrow and filled with electron lucent mucoid substances that are intermixed with cilia (Fig's 11 and 12).

The distal convoluted tubule (DCT)

Light microscopic examinations showed that the PCT is made up of monolayer of low columnar epithelium. In the toluidene stained sections the epithelial cells are filled with dark staining cytoplasmic contents. The nuclei of these cells centralized that usually possesses nucleolus at the centre (Fig. 1). Transmission electron microscopic examination showed that, the cytoplasm of the columnar cells of the DCT encloses highly electron lucent amorphous substance intermixed with small clusters of electron lucent mucoid substance (Fig's 13 and 14). The cytoplasm shows abundant mitochondria, distended Golgi vesicles. The RER that are appears lighter, distended and obscured. Basal membranes are non-labyrinthine (Fig's 13 and 14). The nucleus is roughly spherical and euchromatic (Fig. 15).

DISCUSSION

One of the characteristic features of PCT in *E. carinata* is the presence of dark cytoplasm and the presence of low microvillus brush border. This feature of PCT is same in desert snakes as reported by Allam *et al.,* (2013); Garter Snake *Thamnophis sirtalis* (Peek and McMillan, 1979) and in lizards and crocodiles studied thus far (Davis *et al.,* 1976; Schmidt-Nelson and Davis, 1968; Roberts and Schmidt-Nelson, 1966; Rheubert *et al.,* 2011). The dark staining cytoplasm of the PCT as shown in the present study is mainly due to the electron dense cytoplasm that bears abundant electro dense mitochondria. The presence of more number of mitochondria reflects the active flux of salts in the epithelial cells of the PCT as noticed in other reptiles (Schmidt-Nelson and Davis, 1968; Roberts and Schmidt-Nelson, 1966). Another cytological feature that is more pronounced as reported in reptiles is the presence of intercellular spaces. The comparative reports on snakes, lizards, crocodiles and turtles given by Schmidt-Nelson and Davis, (1968) the intercellular spaces has a vital role in transport of fluids. The spaces widen during the transit of fluids that increases the rate of flow and narrows (constrict) when there is no transport which is highly transitory. Also, comparative account on the PCT of three lizard species given by Roberts and Schmidt-Nelson (1966), shows that the lateral and basal plasma membrane are folded. However, in *E. carinata* the cells of the PCT do not show inter cellular spaces but do show highly labyrinthine lateral and basal plasma membrane.

Roberts and Schmidt-Nelson (1966) reported that the cytoplasm of PCT contains small population of vesicles and large membrane bound vacuoles. It is interesting to note that, the cells of the PCT at distal portion in *E. carinata* is filled with diffused secretory vesicles and are being released into the lumen in large clusters. Although it is known that PCT secretes certain substances in mammals, the secretory activity of PCT in lizards is reported for the first time.

The intermediate segment is a short portion of the nephron that connects PCT and DCT in *E. carinata*. The characteristic feature of this portion of nephron is the presence of elongated tuft of cilia at the apical portion of the simple cuboidal cells. The cilia projects deep into the lumen with their terminal ends usually pointing towards the distal region of the nephron as reported for the lizard *Hemidactylus turcicus* (Rheubert *et al.,* 2011) and other snakes

(Allam *et al.,* 2013). However in *Hemidactylus turcicus* (Rheubert *et al.,* 2011) the cytoplasm contains dark staining substances which are in contrast with the *E. carinata* in which the cytoplasm is lighter filled with electron lucent amorphous substance. It is speculated that the role of cilia in the IC might be related to low blood pressure that reflects low filtration pressure in the kidney.The cytoplasmic contents of the cells of the DCT in *E. carinata* appear lighter in light microscopic examinations. The most obvious reason as revealed through ultrastructural observations could be due to the presence of highly electron lucent cytoplasmic contents. In the lizard *Hemidactylus turcicus,* the cells of the DCT bears apical cilia (Rheubert *et al.,* 2011), which is contrast with *E. carinata* that bears short microvilli. The presence of rough distended endoplasmic reticulum, mitochondria and Golgi vesicles in the cytoplasm as observed for *E. carinata* reflects a product synthesis. This in turn shows the secretory activity of this segment of the nephron. This is in line with the presence of diffuse secretory material in the cytoplasm of the PCT as reported for *Hemidactylus turcicus,* (Rheubert *et al.,* 2011).

The structural variations and similarities of the nephron in *E. carinata* with other reptiles are significant. This structural change in the nephrons reflects the unique physiological adaptations that have enabled the lizard to colonize and thrive in various environmental conditions.

REFERENCES

1. Allam, A.A. and Abo-Eleneen, R.E., 2013. Comparative histological, histochemical and ultrastructural studies of the nephron of selected snakes from the Egyptian area. *Biologia*, *68*(3), pp.546-558.
2. Cuellar, O., 1966. Oviducal anatomy and sperm storage structures in lizards. *Journal of Morphology*, *119*(1), pp.7-19.
3. Dantzler, W.H., 2003. Regulation of renal proximal and distal tubule transport: sodium, chloride and organic anions. *Comparative Biochemistry and Physiology Part A: Molecular & Integrative Physiology*, *136*(3), pp.453-478.
4. Davis, L.E., Schmidt-Nielsen, B., Stolte, H. and Bookman, L.M., 1976. Anatomy and ultrastructure of the excretory system of the lizard, *Sceloporus cyanogenys*. *Journal of morphology*, *149*(3), pp.279-326.
5. Devine, M.C., 1975. Copulatory plugs in snakes: enforced chastity. *Science*, *187*(4179), pp.844-845.
6. Gabri, M.S., 1983. Seasonal changes in the ultrastructure of the kidney collecting tubule in the lizard *Podarcis (= Lacerta) taurica*. *Journal of Morphology*, *175*(2), pp.143-151.
7. Gambarian, S.P., 1978. Micro-dissection study of the kidneys of reptiles living under different ecologic conditions. *Zhurnal evoliutsionnoi biokhimii i fiziologii*, *14*(6), pp.533-538.
8. Gampert, O., 1866. Ueber die Niere von *Tropidonotus natrix* und der Cyprinoiden. *Zeit Wissen Zool*, *16*, pp.369-373.
9. Khalil, A., Nasr, A.N. and Gabri, M.S., 1974. Studies on the histology and histochemistry of the sexual segment of *Mabuya quinquetaeniata* (Lacertilia: Scincidae). *Bull. Fac. Sci. Assiut Univ*, *3*, pp.31-46.
10. Kiernan, J.A., 1990. Histological and Histochemical Methods: Theory and Practice, edn 2. Ed Kiernan J.A. New York: Pergamon Press.
11. Krohmer, R.W., 2004. Variation in seasonal ultrastructure of sexual granules in the renal sexual segment of the northern water snake, *Nerodia sipedon sipedon*. *Journal of Morphology*, *261*(1), pp.70-80.
12. Kühnel, W. and Krisch, B., 1974. On the sexual segment of the kidney in the snake (*Natrix natrix*). *Cell and tissue research*, *148*(3), pp.417-429.
13. Peek, W.D. and McMillan, D.B., 1979. Ultrastructure of the tubular nephron of the garter snake *Thamnophis sirtalis*. *Developmental Dynamics*, *154*(1), pp.103-127.
14. Prasad, M.R.N. and Reddy, P.R.K., 1972. Physiology of the sexual segment of the kidney in reptiles. *General and Comparative Endocrinology*, *3*, pp.649-662.
15. Rheubert, J.L., Murray, C.M., Siegel, D.S., Babin, J. and Sever, D.M., 2011. The sexual segment of *Hemidactylus turcicus* and the evolution of sexual segment location in Squamata. *Journal of Morphology*, *272*(7), pp.802-813.

16. Roberts, J.S. and Schmidt-Nielsen, B., 1966. Renal ultrastructure and excretion of salt and water by three terrestrial lizards. *American Journal of Physiology--Legacy Content*, *211*(2), pp.476-486.
17. Ross, P. and Crews, D., 1977. Influence of the seminal plug on mating behaviour in the garter snake. *Nature*, *267*(5609), pp.344-345.
18. Schmidt-Nielsen, B. and Davis, L.E., 1968. Fluid transport and tubular intercellular spaces in reptilian kidneys. *Science*, *159*(3819), pp.1105-1108.
19. Sever, D.M., Stevens, R.A., Ryan, T.J. and Hamlett, W.C., 2002. Ultrastructure of the reproductive system of the black swamp snake (*Seminatrix pygaea*). III. Sexual segment of the male kidney. *Journal of Morphology*, *252*(3), pp.238-254.
20. Shine, R., Olsson, M.M. and Mason, R.T., 2000. Chastity belts in gartersnakes: the functional significance of mating plugs. *Biological Journal of the Linnean Society*, *70*(3), pp.377-390.
21. Siegel, D.S., Aldridge, R.D., Clark, C.S., Poldemann, E.H. and Gribbins, K.M., 2009. Stress and reproduction in *Boiga irregularis* with notes on the ultrastructure of the sexual segment of the kidney in squamates. *Canadian journal of zoology*, *87*(12), pp.1138-1146.

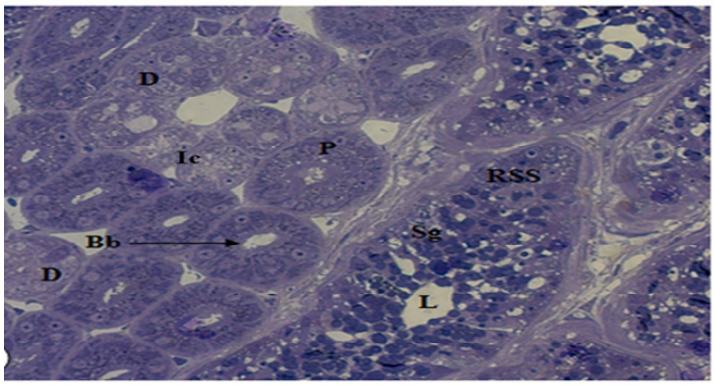

Fig: 1. Section through the renal tubule shoeing Proximal convoluted tubule (P), Distal convolutrd tubule (D), Intermediate segment (Ic) and Renal sexual segment (RSS). Bb, brush border; Sg, secretory granules.

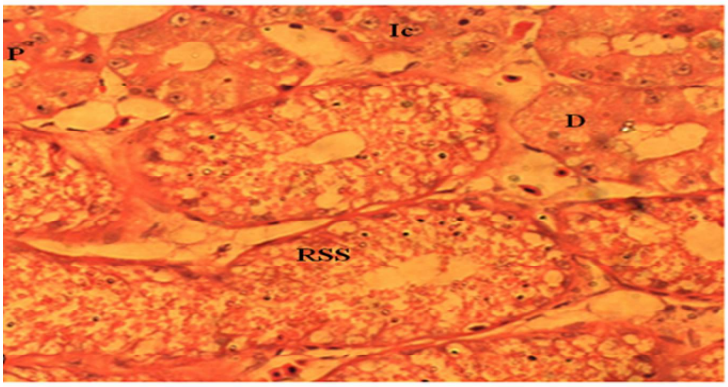

Fig: 2. Section through the renal tubule shoeing proximal convoluted tubule (P), Distal convolutrd tubule (D), Intermediate segment (Ic) and Renal sexual segment (RSS). Bb, brush border; Sg, secretory granules.

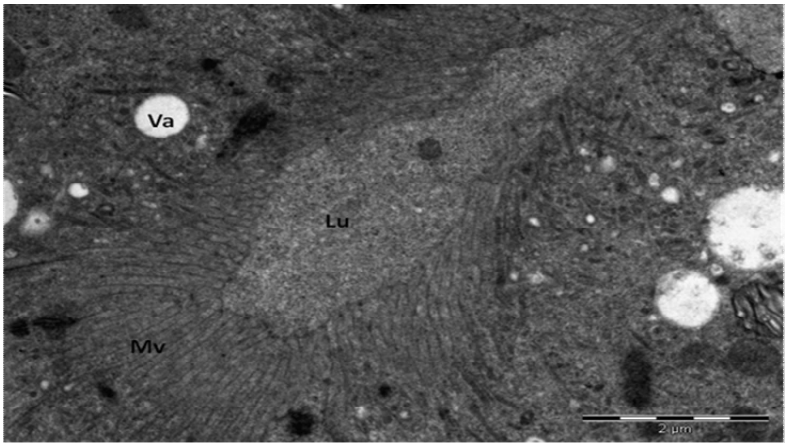

Fig: 3. Apical portion of PCT showing lumen (Lu) and microvilli (Mv).

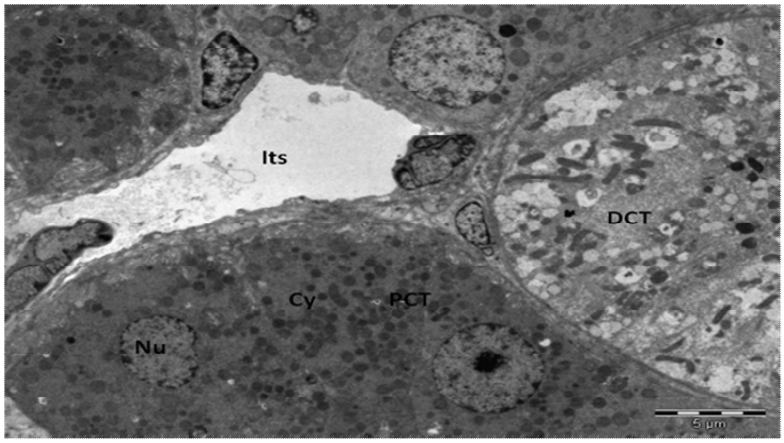

Fig: 4. Portion of PCT and DCT showing light and dark cytoplasmic content (cy) and vast inter tubular space(Its)

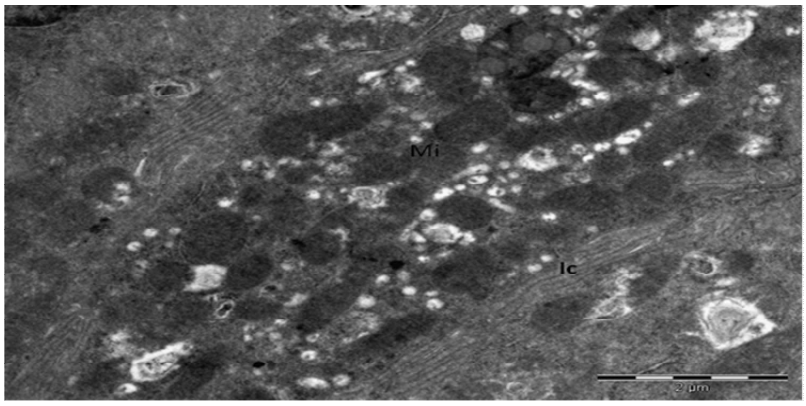

Fig: 5. Portion of PCT showing dark cytoplasmic content (cy) mitochondria (Mi) and Intercellular canaliculi (Ic)

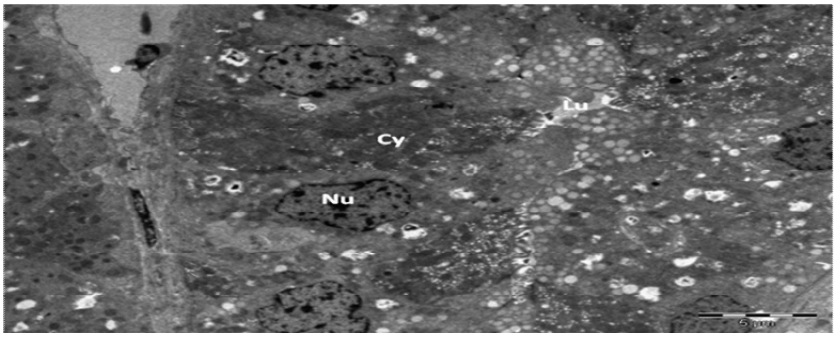

Fig: 6. Portion of PCT showing dark cytoplasmic content (cy) mitochondria (Mi).

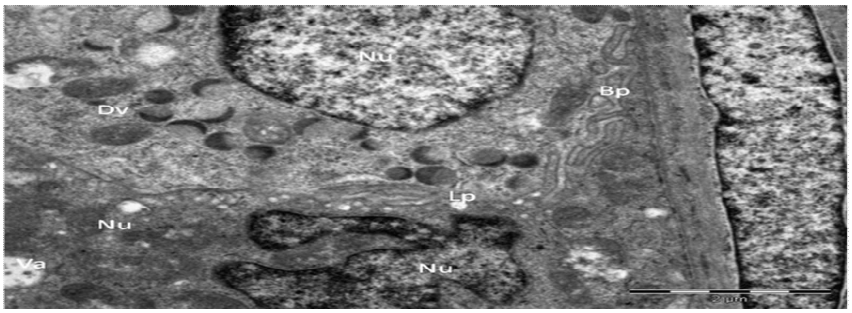

Fig: 7. Portion of PCT showing alternating dark and light cells with indented and circular nucleus. The cytoplasm of light cells show diffused secretory vacuoles.

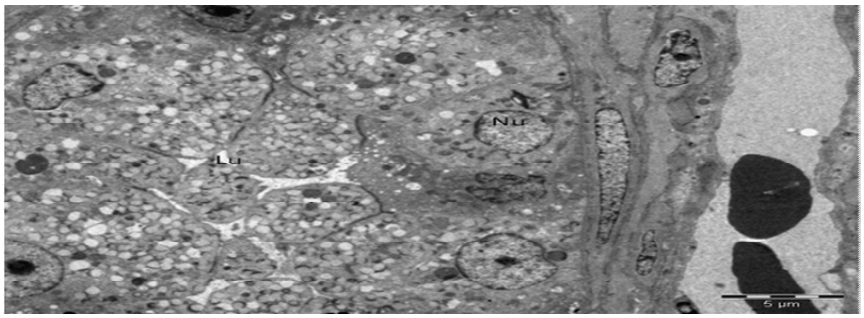

Fig: 8. PCT showing alternating dark and light cells with indented and circular nucleus. The cytoplasm of light cells show diffused secretory vacuoles. Lumen filled with diffused vacuoles.

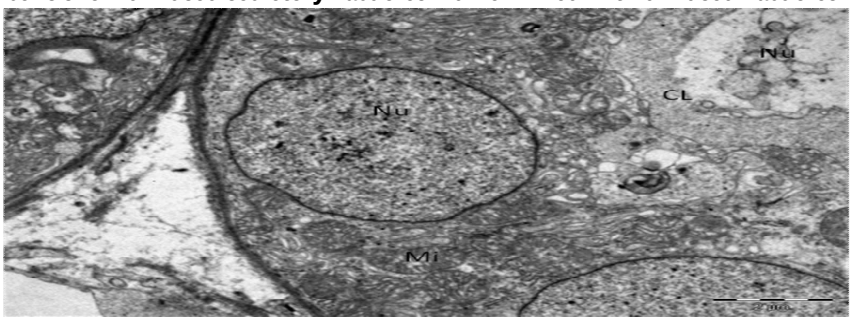

Fig: 9. Intermediate segment showing cuboidal cell and apical ciliary rim. Lumen filled with diffused material.

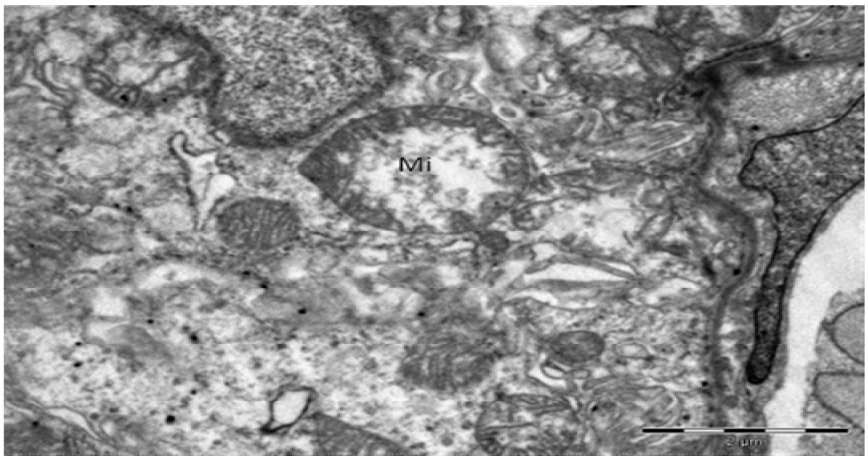

Fig: 10. Intermediate segment showing mitochondria enclosing amorphous substance

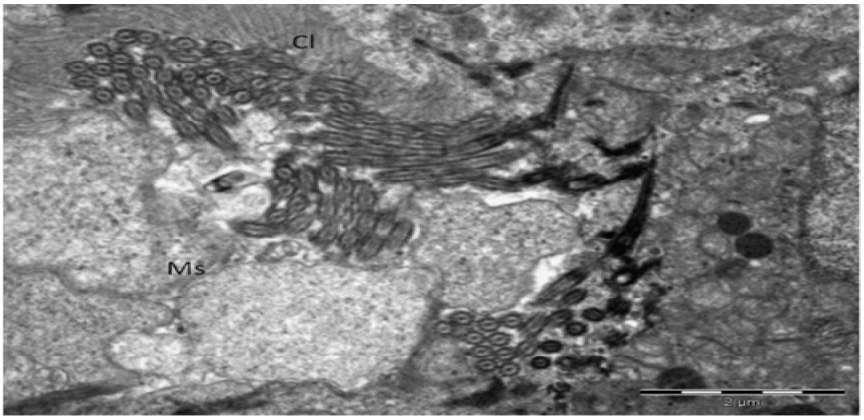

Fig: 11. Intermediate segment showing apical portion of the cell bearing cilia and lumen filled with mucoid substances.

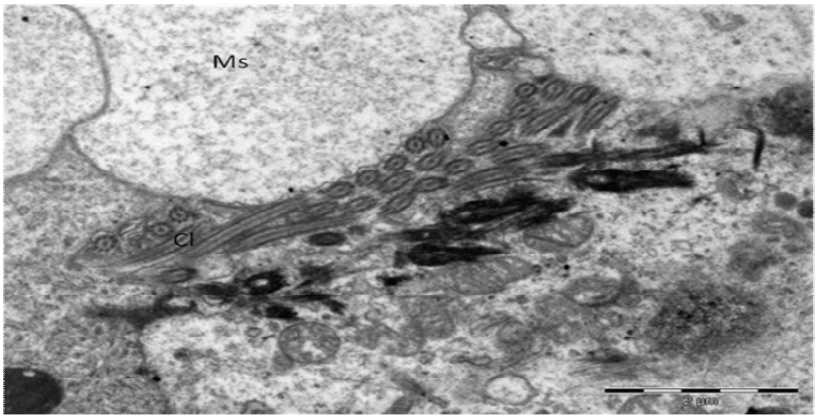

Fig: 12. Intermediate segment showing apical portion of the cell bearing cilia and lumen filled with mucoid substances.

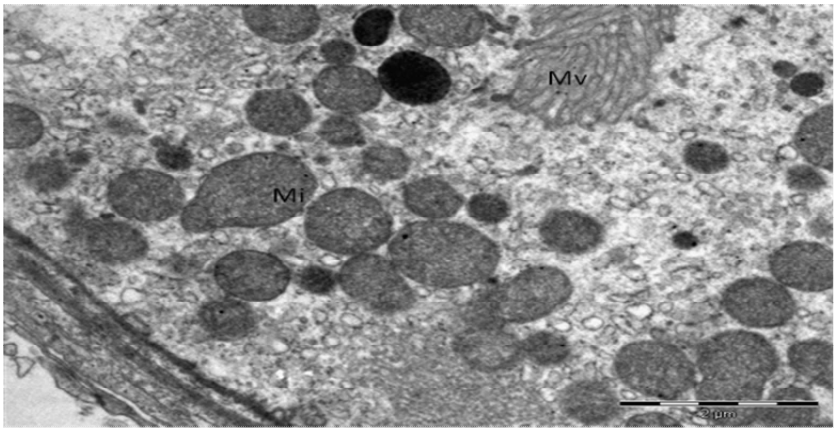

Fig: 13. The distal convoluted tubule showing electron lucent cytoplasm and apical microvilli.

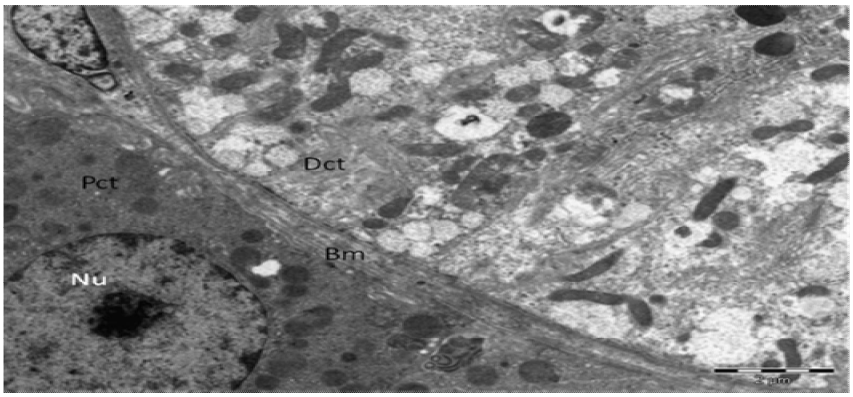

Fig: 14. The distal convoluted tubule showing electron lucent cytoplasm and proximal tubule showing electron dense cytoplasm.

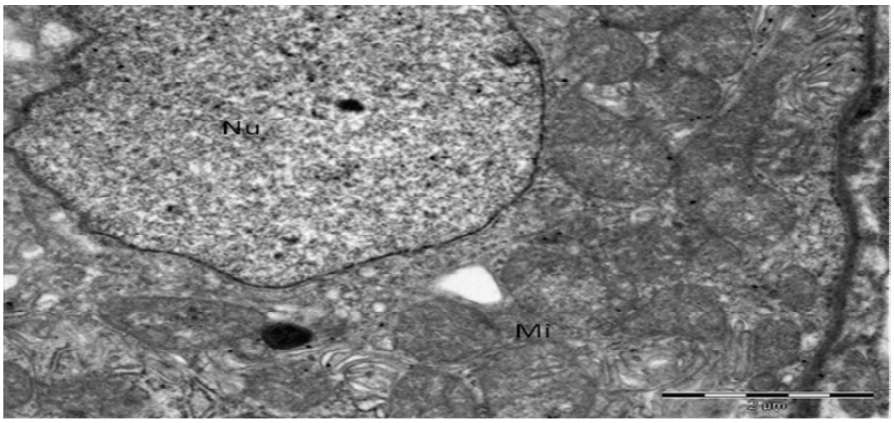

Fig: 15. The distal convoluted tubule showing the euchromatic nucleus.

Indian Journal of Natural Sciences www.tnsroindia.org.in ©IJONS

Vol.8 / Issue 45 / December 2017 *International Bimonthly* *ISSN: 0976 – 0997*

RESEARCH ARTICLE

Effect of Different Pretreatment for Bioethanol Production from Corncobs Substrate

Yasir M. Yousif[1]* and Hind S.Abdulhay[2]

[1]Department of Biology, College of Science, University of Anbar, Anbar, Iraq.
[2]Department of Biology, College of Science, University of Baghdad, Baghdad, Iraq.

Received: 13 Sep 2017 Revised: 17 Oct 2017 Accepted: 25 Oct 2017

*Address for correspondence
YasirMohsinYousif
Department of Biology,
College of Science, University of Anbar,
Anbar, Iraq.
Email: y.alani83@yahoo.com

ABSTRACT

Biomass is a renewable resource, whose utilization has received great attention due to environmental considerations and the increasing demand for energy worldwide. Toobtain high concentration of ethanol from cellulosic materials, corncobs was pretreated with diluted acid (H_2SO_4 0.5%) and two type of ionic liquids (ILs) and cellulase enzyme, and observed effect it on the substrate for conversion cellulose and hemicellulose to monosaccharides and ethanol production. Fermentation process was conducted using *Saccharomyces cerevisiae* under anaerobic condition. All the pretreatment methods have been shown to effectively solubilize and hydrolyze cellulose and hemicellulose into monomeric sugars. The best reducing sugar after 3 days when pretreatment with hexamethylphosphoramide and enzyme were 42.7g/L and 41.7g/L, respectively. But pretreatment with diluted sulfuric acid was 39.6 g/L after 4 days. The concentration of ethanol was measured every two days using ethanol sensor. The lowest mean concentration of ethanol produced from corncobs sample without pretreatment, diluted acid, ethyl acetoacetate, hexamethylphosphoramide and enzyme were 0.863, 1.516, 3.103, 5.793 and 3.293 g/L, respectively after 3 days fermentation.While the higher concentration of ethanol for the same samples (without pretreated and pretreated as above) were in the following order 19.889, 70.276, 30.25, 68.306 and 57.186 g/L, respectively after 9 days of fermentation..

Keywords: Bioethanol; corncobs; diluted acid; enzyme; fermentation.

INTRODUCTION

Bioenergy is a form of renewable energy derived from an available biological material. Forms of bioenergy include power, heat, and solid, liquid, and gas fuels. Uses of these various forms of bioenergy include industrial, residential, and commercial applications. Biofuel refers to liquid and gas fuels used for transportation and industrial processes [1].Corn culture is one of the agricultural activities that most generate residues, because the corncob represents little considering the whole plant. Therefore, after the harvest the leaf (straw), stem, and cob are left in the field; these residues are well known as corn stover [2].It can be recycled as a fuel, after milling, in a boiler furnace, as most lignocellulosic material. Corncobs is a potential sugar source that can be used for many purposes, therefore this material can be used as sugar source for second generation ethanol [3-4]. Routes most studied till now have been the use of chemical pretreatment with acids or bases, followed by enzymatic hydrolysis, of which the acid pretreatment is considered as one of the very important techniques and targets for high yields of sugars from lignocellulosics[5]. The pretreatment is complete to break the matrix in order to reduce the degree of crystallinity of the cellulose and increase the fraction of amorphous cellulose, the most suitable form for enzymatic attack [6-7].

MATERIALS AND METHODS

Collection of samples

Fresh corncobs were gathered (without any part of plant) and washed with distilled water to remove the suspended impurity then placed in plastic bag. Corncobs were sliced into small pieces and then sun-dried for 3 days before ball-milled [8], and grinding in high speed multi-function comminutor (25000 r/min) to procurement grains 50-300 mesh fractions , then ground and sieved to obtain 80–120 mesh fractions [9]. The samples were dried to constant weight at 105°C in oven overnight. Then it was transported to the laboratory where the experiments were done.

Corncobs composition

The fibre composition of the raw material was estimated in regard to the quantities of cellulose, hemicellulose and lignin [10] in Advisory Office at the College of Agriculture - University of Baghdad. The contents of cellulose, hemicellulose and lignin were detected gravimetrically according to the modified neutral (Neutral Detergent Fibre = NDF) and acid detergent method (Acid Detergent Fibre = ADF) [11]. The hemicellulose content was calculated as the difference between NDF(cellulose, hemicellulose and lignin) and ADF. Lignin was detected indirectly by determination ADF (lignin and cellulose) and clear as the difference between ADF and cellulose [10].
The experiments were done in two ways:

a. Without pretreatment Corncobs

One hundred grams of dried corncobs were weighted and prepared for fermentation process.

b. Pretreatment Corncobs

Acid hydrolysis: One hundred grams of dried corncobs pretreated with diluted H_2SO_4 (0.5%) at 121°C for 60 min. After that, the residues were washed by distilled water until neutral pH generated[12]. The pH was 3.5 and washed with deionized water and NaOH were added to regulate the pH to 5 [13].

Ionic liquid hydrolysis : The solubility of lignocellulosic materials in Ionic liquid**s**(ILs) was performed at 130°C by mixing 100g of dried corncobs with two kind of ILs (Hexamethylphosphoramide $C_6H_{18}N_3OP$ and Ethyl acetoacetate

$C_2H_{10}O_3$) 1:10 w/v with magnetic stirring. After incubating the solution in the ILs for 20 min at 130°C, the pretreated corncob powder was precipitated with deionized water. The precipitate was washed with deionized water [14]. Dried washed solids in oven overnight at 45°C and then weighed to determine dry weight yield and stored at 4°C until further use [15].

Enzymatic hydrolysis : Enzymatic hydrolysis was carried out at 50ºC, 0.01 M citrate buffer (pH 4.7) in 150 rpm shaking incubator for 72 h of saccharification. The activity of cellulase was 30 FPU/g of solid [14]. The suspensions were placed in a thermostatic bath at 80◦C for 30 min, to denature the enzyme. Next, the residues were washed with deionized water, and the solid was separated by centrifugation (10,000 rpm, 15 min) and suspended in deionized water. Acolloidal suspension of cellulose was obtained and stored at 4◦C in a closed container [16]. Determined release of soluble reducing sugars by 3,5 dinitrosalicylic acid DNS assay using D-glucose as a standard [17].

Preparation of yeast culture

The yeast *S. cerevisiae*were purchased from Baghdad local market. Before using in fermentation, the yeast was activated. About 1 g of dry yeast was added to 20 ml of 5% sterilized glucose solution, activated at 38ºC for 1h, cooled from 38ºC to 30ºC, and then used in the experiment. The yeast concentration was approximately 10^8 cells/mL [13].

Fermentation of raw materials

The activated yeast were added to corncobs sample for each experiment (with pretreatment and without pretreatment) in sterilized circumstances in order to prevent any contamination [13]. Added one liter of distilled water to each mixture, then autoclaved in 121ºC for 20 min. and left for fermentation 9 days. It was kept in glass tank with pH 4.8 and air outlet to let the carbon dioxide formed to escape [18]. During that the ethanol concentration was determined every two days by using ethanol sensor device.

Distillation and Dehydration

This process is designed to increase the ethanol concentration up to maximum available purity. The columns use the differences in the boiling points of water and ethanol to will boil and separate the ethanol. The distillation process is a raise the concentration of alcohol from low purity to high purity [19]. One liter of fermented raw materials was placed in flask and heated to preset evaporation temperature by a digital heating mantle at 80 ºC for 3hours. The cooling water supply was opened while the evaporating temperature was kept constant during the process. The vapor was condensed and collected in a flask. The concentration of ethanol was measured at 20 ºC and 250 ml of condensate was obtained from each liter of fermented raw materials. To raise the ethanol concentration to 99.5%, the extractive distillation was used in the present work. The drying agents used were calcium oxide (CaO) [18]. So, 5 g of CaO were added to the ethanol and mixed well for 10 minute. The mixture was heated and evaporated again at 80°C. The output of this process was 99.5% ethanol.

Statistical analysis

In order to determine the impact of ethanol in corncobs, using analysis of variance, F-test, t-test in complete randomized design (CRD). To explain the differences between means, calculate least significant differences (LSD) values at $p \leq 0.05$, and expressed that as (Mean ± SEM) [20].

RESULTS AND DISCUSSION

The compositions of corncobs are shown in table (1). The parts of corncobs were mainly composed of cellulose (glucan), hemicellulose (xylan and arabinan) and lignin, also a few content of proteins, lipids, crude fibers and ash were determined before pretreatment.Thepercentage of hemicellulose and cellulose have been considered as important factors in determining the hydrolysis degrees of relatively refined cellulosic substrates.

Influence of different pretreatment methods

The effect of different pretreatment methods on glucose and ethanol returns for corncobs samples as shown in (figure-1) was studied to determine the most effective material for the production of bioethanol.All the pretreatment methods (diluted acid, ILs, enzymes) has been shown to effectively solubilize and hydrolyze cellulose and hemicellulose into monomeric sugars, removing it from the cellulose fibers. The best reducing sugar after third day when pretreatment with hexamethylphosphoramide and enzyme were 42.7g/L and 41.7g/L, respectively.While pretreatment with diluted sulfuric acid after fourth day was 39.6 g/L.

The results agreed with Kahar*et al.*, (2010) who indicated the highest conversion of corncobs to sugars was obtained at 0.5% (v/v) H_2SO_4, giving 8 g of sugars from 10 g of corncobs; i.e., the sugar yield was 80% (w/w). For instance, the sugar yield under H_2SO_4 pretreatment was 1.6 times higher than that without acid pretreated.

Production of ethanol from banana peels

High ethanol production depends on a high cellulose and hemicellulose concentration. Increases in cellulose and hemicellulose content are best affected by removal of non-cellulose components by pretreatment. The presence of lignin restricts the access of effective materials to substrate and preventing saccharification.When comparing different pretreatments in the same days, it found that there were differences between the pretreatments. At the 3rdday of fermentation there were no significant differences found in the ethanol production between pretreatment with diluted acid and without pretreatment, while there are differences between them and other pretreatment. Furthermore non-significant differences were noticed between enzyme pretreatment and ethyl acetoacetate, while significant differences with other treatments. The higher production of ethanol after 3days was 5.793 g/L when pretreated with hexamethylphosphoramide, while the lowest production was 0.863 g/L for samples which not treated. The higher production of ethanol after 5 days was 16.277 g/L when pretreated with hexamethylphosphoramide, while the lowest production was 3.947 g/L for samples which not treated. After 7 days of fermentation, the higher production of ethanol after seven days was 36.243 g/L when pretreated with hexamethylphosphoramide, while the lowest production was 8.027 g/L for samples which not treated. The fermentation continued for the ninth day because it was found that the concentration of ethanol increased significantly and markedly and in some pretreatments increased to double. The pretreatment of corncobs with diluted acid and hexamethylphosphoramide were showed the highest concentration of ethanol, 70.277 g/L and 68.307 g/L, respectively.While the lowest concentration of ethanol after 9 days fermentation was 19.890 g/L for the untreated substrate (figure-2). As it appears in table (2).

Abdulhay and Aljoborey, (2015) mentioned an increase in ethanol amount during the days of fermentation rise can be returned to the contact time between substrate and yeast.This result agreed with badger (2002) and revealed that fermentation of cellulosic material needs several days to achieve a good result. Also, the obtained result coincide with Alkhafagi*etal.*, (1999) reported that the best time of fermentation was 5-7 days.

Finally, the above results of ethanol that obtained from corncobs agreed with Zhang *et al.*, (2010) referred a higher ethanol concentration (69.2 g/L) was obtained, corresponding to an 81.2% overall ethanol yield, using H_2SO_4–NaOH

treated corncob and batch SSF. Because strong acid–strong alkali removed more non-cellulosic material and caused a greater disruption of biomass structure.The results agreed with Li *et al.*, (2010) indicated that the two-phase simultaneous saccharification and fermentation (TPSSF) using 12 hours soaking in aqueous ammonia (SAA-treated) corn stover resulted in the highest ethanol concentration 22.3 g/L after 120 h fermentation, which was equivalent to 84% of the theoretical ethanol yield based on the total carbohydrates (glucanandxylan) in the untreated corn stover.

The results correspondent with Zhu *et al.*, (2014) showed a relatively high final ethanol concentration 70.1g/L was achieved when fed-batch simultaneous saccharification and co-fermentation (SSCF) was conducted with temperature 38^{o}C at pH ranged from 4.8–5.6. Yeast feeding, combined with substrate feeding and enzyme feeding, was demonstrated to be an efficient approach for SSCF with time and high dry matter of corncobs loading.

The liquid of fermentation stage was heated and condensed then the ethanol purity was measured. Ethanol purity was 66% when corncobs without pretreatment, while 89% when corncobs with pretreatment.After dehydration stageethanol purity was 99.5 % this result agreed with Dohetry and Malone (2001) studied the effect of different drying agents on alcohol concentration and found that ethylene glycol and CaO give highest concentration.

CONCLUSION

From the obtained results of this study, corncobs have high contents of cellulose and hemicellulose. The different pretreatments gave different efficiency to turn the basic material into monosaccharides. The maximum amount of ethanol from corncobs was 70.276 g/L after 9 days fermentation.

REFERENCES

1. Jose, S., and Bhaskar, T. (2015). Biomass and biofuels advanced biorefineries for sustainable production and distribution. Taylor and Francis Group, LLC.
2. Gil, M., Schott, D.,Arauzo, I.,Teruel, E. (2013). Handling behavior of two milled biomass: SRF poplar and corn stover. Fuel Proc. Technol. 112:76-85 .
3. Kadam, K.L., McMillan, J.D. (2003). Availability of corn stover as a sustainable feedstock for bioethanol production. Biores. Technol. 88:17-25.
4. Mosier, N., Wyman, C., Dale, B.,Elander, R., Lee, Y.Y.,Holtzapple, M.T,Ladish, C.M. (2005). Features of promising technologies for pretreatment of lignocellulosic biomass. Biores. Technol. 96:673-686.
5. Sarkar, N.,Ghosh, S.K.,Bannerjee, S.,Aikat, K. (2012). Bioethanol production from agricultural wastes: An overview. Renewable Energy, 37:19-27.
6. Sanchez, Ó.J, Cardona, C.A. (2008). Trends in biotechnological production of fuel ethanol from different feedstocks. Bioresource Technology, 99:5270-5295.
7. Souza, E.L.,Lieblb, G.F.,Marangonia, C.,Sellina, N.,Montagnolia, M.S., Souza, O. (2014). Bioethanol from fresh and dried banana plant pseudostem. Chemical Engineering Transactions, 38:271-276 .
8. Kahar, P., Taku, K., Tanaka, S. (2010). Enzymatic digestion of corncobs pretreated with low strength of sulfuric acid for bioethanol production . Journal of Bioscience and Bioengineering. 110(4):453-458 .
9. Sun, S.,Fei, L.M., Yuan, T.Q.,Xu, F., Sun, R. (2013). Effect of ionic liquid/organic solvent pretreatment on the enzymatic hydrolysis of corncob for bioethanol production. Part 1: Structural characterization of the lignins . Industrial Crops and Products Journal. 43:570-577 .
10. Pointner, M.,Kuttner, P.,Obrlik, T.,Jager, A.,Kahr, H. (2014). Composition of corncobs as a substrate for fermentation of biofuels . Agronomy Research. 12(2):391-396 .
11. Van Soest, P.J., Robertson, J.B., Lewis, B.A. (1991). Methods for dietary fiber, neutral detergent fiber, and nonstarch polysaccharides in relation to animal nutrition. Journal of Dairy Science. 74(10):3583-3597.

12. Li, P.,Cai, D.,Luo, Z., Qin, P., Chen, C., Wang, Y., Zhang, C., Wang Z., Tan, T. (2016). Effect of acid pretreatment on different parts of corn stalk for second generation ethanol production . Bioresource Technology. 206:86-92 .
13. Lu, J., Li, X.Z., Zhao, J.,Qu, Y. (2012). Enzymatic saccharification and ethanol fermentation of reed pretreated with liquid hot water. Journal of Biomedicine and Biotechnology.V9.
14. Li, Q., Jiang, X., He, Y., Li, L., Xian, M., Yang, J. (2010). Evaluation of the biocompatibile ionic liquid 1-methyl-3-methylimidazolium dimethylphosphite pretreatment of corncob for improved saccharification . Appl. Microbiol. Biotechnol. 87:117-126.
15. Allison, B.J., Cádiz, J.C.,Karuna, N.,Jeoh T., Simmons, C.W. (2016). The effect of ionic liquid pretreatment on the bioconversion of tomato processing waste to fermentable sugars and biogas. Appl. Biochem. Biotechnol. 179:1227-1247.
16. Tibolla, H.,Pelissari, F.M., Rodrigues, M.I.,Menegalli, F.C. (2016). Cellulose nanofibers produced from banana peel by enzymatic treatment: Study of process conditions. Ind. Crops Prod. In press .
17. Miller, G.L. (1959). Use of dinitrosalicylic acid reagent for determination of reducing sugar. Analysis Chemistry, 31:426-428.
18. Aljoborey, A.D.,Abdulhay, H.S. (2014). Production of bioethanol from reed (*Phragmitesaustralis*). International Journal of Sciences: Basic and Applied Research.15(2):145-150.
19. Ebraheem, A.K. (2013). Production and analysis of bioethanol from dates syrup. M.Sc thesis. College of Engineering. Babylon University.
20. Horwitz, W., Latimer, G.W. (2005). Official methods of analysis of AOAC 18. Gaithersburg, Md: AOAC International.
21. Badger, P.C. (2002). Ethanol from cellulose: A general review, In: Trends in new crops and new uses, edited by Janick, J. and Whipkey, A., ASHS Press, Alexandria, VA.
22. Alkhafaji, J.K., Alaqasim, S.A.,Hamood, M.R.,Aldijili, A.H.,Almahdawy, M.S. (1999). Industrial chemistry.2nd edition, D al-atheer for publishing, Mosul University.
23. Abdulhay, H.S.,Aljoborey, A.D. (2015). Bioethanol production using date syrup wastes. The second biological science conference. College of education for girls. Kufa university in16-17/12/2015.
24. Zhang, M., Wang, F., Su, R., Qi, W., He, Z. (2010). Ethanol production from high dry matter corncob using fed-batch simultaneous saccharification and fermentation after combined pretreatment. Bioresource Technology. 101:4959-4964.
25. Li, X., Kim, T.H.,Nghiem, N.P. (2010). Bioethanol production from corn stover using aqueous ammonia pretreatment and two-phase simultaneous saccharification and fermentation (TPSSF). Bioresource Technology 101:5910-5916.
26. Zhu, J.Q., Qin, L., Li, B.Z., Yuan, Y.J. (2014). Simultaneous saccharification and co-fermentation of aqueous ammonia pretreated corn stover with an engineered Saccharomyces cerevisiae SyBE005. Bioresource Technology. 169:9-18.
27. Doherty, M., Malone, M.F. (2001). Conceptual design of distillation systems. McGraw Hill: New York.

Table 1: Compositional analysis of corncobs on dry matter

Component	% w/w
Cellulose	39.84
Hemicellulose	28.75
Lignin	11.45
Proteins	9.0
Lipids	5.35
Crude fibers	4.15
Ash	1.40

Table 2: Static comparison for ethanol production among the days and among the different pretreatment for corncobs samples

Treatments / Ethanol con.	without	H_2SO_4	Ethyl acetoacetate	Hexamethyl phosphoramide	Enzyme	LSD P ≤ 0.05
3 rd day	0.863 Cd	1.516 Cd	3.103 Bd	5.793 Ad	3.293 Bd	
	±	±	±	±	±	1.222
	0.105	0.327	0.423	0.566	0.367	
5 th day	3.947 Dc	7.647 Cc	7.983 Cc	16.277 Ac	11.843 Bc	
	±	±	±	±	±	3.245
	0.321	0.335	1.502	1.669	0.221	
7 th day	8.027 Bb	35.013 Ab	12.813 Bb	36.243 Ab	31.823 Ab	
	±	±	±	±	±	5.507
	0.188	3.116	1.707	1.345	0.897	
9 th day	19.890 Da	70.277 Aa	30.250 Ca	68.307 Aa	57.187 Ba	
	±	±	±	±	±	9.349
	1.315	3.056	1.229	5.434	1.379	
LSD P ≤ 0.05	2.236	7.158	4.270	9.570	2.772	

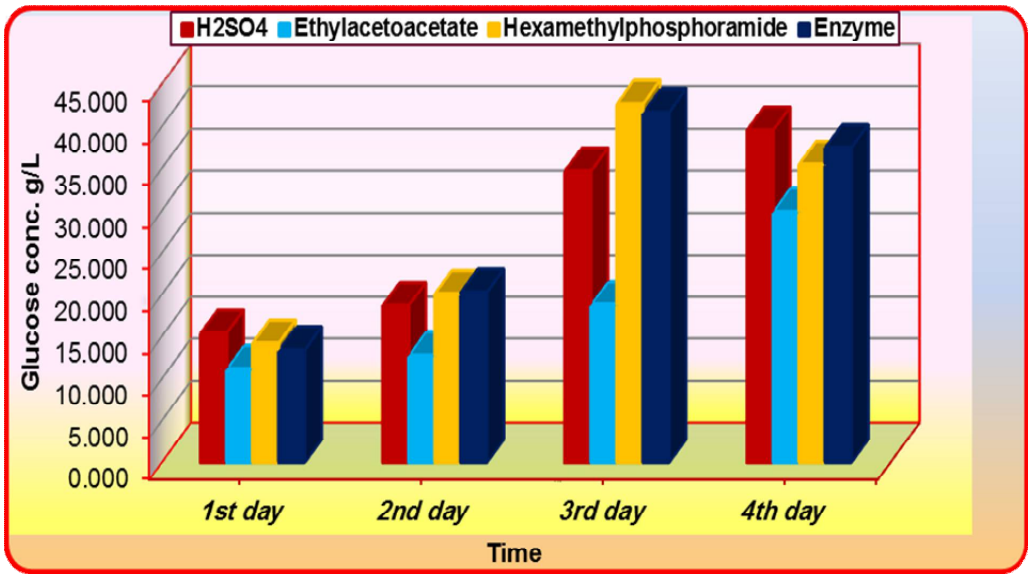

Figure 1. Concentration of reducing sugar from corncobs samples after pretreatment with diluted H_2SO_4, ILs and enzyme

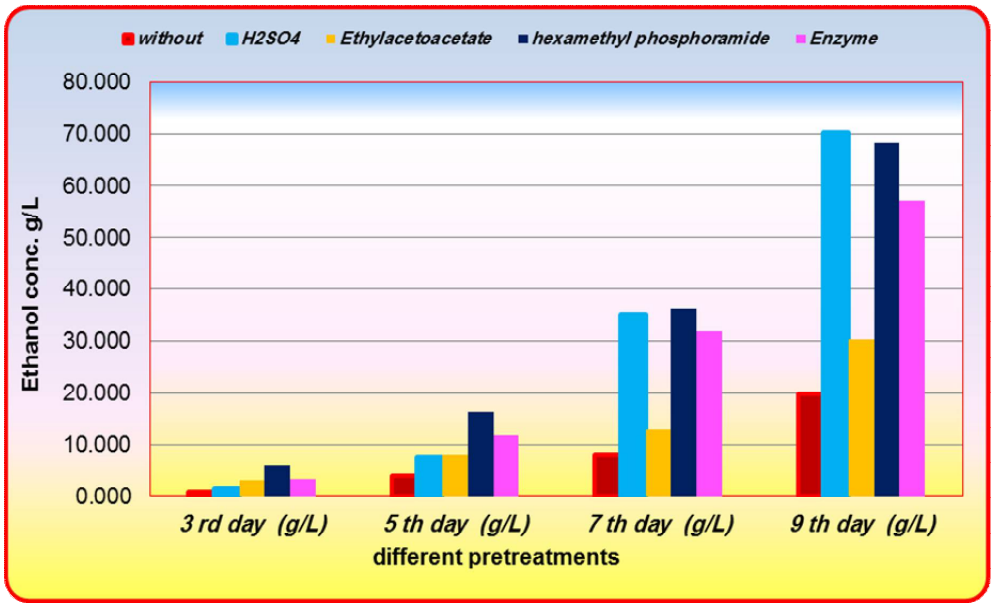

Figure 2.The mean concentration of ethanol from corncobs samples (pretreatment and without pretreatment) after 3, 5, 7 and 9 days of fermentation

Indian Journal of Natural Sciences www.tnsroindia.org.in ©IJONS

Vol.8 / Issue 45 / December 2017 *International Bimonthly* *ISSN: 0976 – 0997*

RESEARCH ARTICLE

Seroprevalence of Antibodies to Mycoplasma ovipneumoniae in Sheep in South Karnataka

M.Shivakumar[1]*, P.T.Ramesh[2] and T.Suryanarayana[3]

[1]Associate Professor, Dept. of Veterinary Medicine, Veterinary College, Hassan, Karnataka,India.
[2]Professor, Dept. of Veterinary Medicine, Veterinary College, Bangalore, Karnataka,India.
[3]Assistant Professor, Dept. of Veterinary Medicine, Veterinary College, Bangalore, Karnataka,India.

Received: 18 Sep 2017 Revised: 18 Oct 2017 Accepted: 31 Oct 2017

***Address for correspondence**
Dr. M.Shivakumar
Associate Professor,
Dept.of Veterinary Medicine,
Veterinary College, Hassan – 573 202.
Karnataka,India.
Email: shiva5kid@gmail.com

ABSTRACT

A total of 360 sheep from 24 different flocks were screened for antibodies to *mycoplasma ovipneumoniae* using indirect ELISA. Overall 212 sera samples gave positive result which accounted for 58.88 %. The highest sero-positive animals were noticed in the lambs which are less than six months old (92.22%) followed by the sheep aged more than three years 65.58%. A significant difference was noticed in the ELISA positive cases among different age groups.

Keywords: Mycoplasma ovipneumoniae, ELISA, particulate antigen, seroprevalence.

INTRODUCTION

Mycoplasmal pneumonia in sheep has been associated with *M. ovipneumoniae, M. capricolum* subsp. *capricolum, M. mycoides* subsp. *mcoides* LC and *M. arginini*. *M. ovipneumoniae* is the most commonly isolated mycoplasma from the upper respiratory tract of normal sheep and can be significant in respiratory disease in both sheep and goats. During times of stress, subclinical infection may predispose sheep to atypical pneumonia with paroxysmal coughing (Azizi *et al*., 2011). *Mycoplasma* infections cause indirect economic losses as a result of emaciation, delayed market weight and infertility, due to the subacute or chronic pneumonia in small ruminants (Mohkber Dezfouli *et al*., 2011).

MATERIALS AND METHODS

Flocks which showed signs of respiratory tract infection were selected for the study. Blood samples were collected from four different age groups viz, < 6 months, 6 months -1 year, 1-3 years and >3years. A total of 360 sheep from 24 different flocks were selected for screening of *mycoplasma ovipneumoniae* using indirect ELISA.15 sheep from each flock and a total of 90 animals in each age group were sampled for the purpose of screening.

Serum from animals suffering from mycoplasma infection was used as a positive control as detected by plate agglutination test and slide agglutination test with particulate antigen was carried out as described by Uma (2011). Control reference negative serum was kindly provided by IAH & VB (Karnataka) and the indirect ELISA was standardized as described by Lin *et al,* 2008. The samples were screened at 50µl of 1:100 dilution of sheep serum, the plates were coated with 7.0 µg/ ml of antigen and a conjugate dilution of 1:8000 was used in the present study. In this study mean ± 3 SD of reference negative samples was found to be 0.113 (table1) while the field positive control showed an OD nearing 1.013. The OD of positive reactants ranged from 0.114 to 1.099 while in the negative reactants it ranged from 0.03 to 0.113. Samples with an OD of greater than 0.113 were considered positive by the indirect ELISA.

RESULTS AND DISCUSSION

Of the 360 samples screened, 212 sera showed positive result in the present study to ELISA which accounted for 58.88 %. The highest sero-positive animals were noticed in the lambs which were less than six months old (92.22%) followed by sheep aged more than three years 65.58%. The other middle age group sheep i.e., 6 month-1year and 1-3 year showed sero-positivity of 28.88% and 47.77% respectively (Table 2).The chi-square test was used to obtain the difference in sero-prevalence among various age groups. A significant difference was observed in the ELISA positive cases in different age groups ($p<0.001$) in the Chi square test. The percentage of positive animals was high in extreme age group animals.

Overall, a total of 212 sera showed positive result to ELISA which accounted for 58.88 %. The results are in near agreement with the findings of Justice-Allen *et al*. (2011) who detected antibodies to *M. ovipneumoniae* in 47% of the tested bighorn sheep, which was in contrast to Massimo *et al.* (2012) who reported only sixty-four of the 246 (26.01%) samples from 13 flocks were seropositive to *M. ovipneumoniae*.The highest sero-positive animals using indirect ELISA in the present study were noticed in the lambs which were less than six months old (92.22%), followed by the sheep aged more than three years (65.58%). The other middle age group sheep i.e., 6 month-1year and 1-3 year had sero-positivity of 28.88% and 47.77% respectively.

In the young lambs 92.22 % of sero-prevalence may be due to increased susceptibility and also due to the fact that this microorganism is associated with *M. arginini* from young lambs with a chronic disease that has been termed the "coughing syndrome" (Azizi *et al*., 2011). Furhter, Bottinelli *et al*. (2016) reported that *M. ovipneumoniae* is thought to be the cause of atypical or ovine non-progressive pneumonia. Probably this pathogen infects lambs which are most susceptible to the infection by this pathogen during the first months of life. Massimo *et al.* (2012) reported that the proportion of sero-positive sheep appeared to increase with age from 2 to 10 years. In the present study also, there was an increase in the seropositive animals with increase in age whilst the very young animals aged < 6 months were affected most.

The variation in the seroprevalence observed in different age groups may be due to chronicity of the disease which persists for several weeks, with variable morbidity and mortality rates between flocks (Massimo *et al.* 2012). Chisquare test ($P < 0.001$) indicated a significant difference in ELISA positive cases between age groups in the present

study which is in agreement with the findings of Shahid *et al*. (2016) who reported a statistically significant difference in the isolation of *Mycoplasma ovipneumoniae* among various age groups.

The low positive cases in the middle age groups may be due to the fact that the animals are more immune at this age and capable of resisting the infection. The immune system of very young animals and extremely aged animals may not be in a position to resist the infection and that may be the probable reason for high sero-positivity. There is no evidence or supportive data to substantiate, but this may be a probable reason for the high percentage of infection.

CONCLUSION

Sero-prevalence study using ELISA was useful for detecting antibodies to *M. ovipneumoniae* using whole cell antigen. Young age groups and advanced age group animals had a higher sero-prevalence. Further studies are necessary to validate the pathogenicity of *M. ovipneumoniae* alone or combined with other bacteria, and its economic impact on the flocks requires further studies.

REFERENCES

1. LIN, Y.C., MILES, R.J., NICHOLAS, R.A.J., KELLY, D.P. AND WOOD, A.P. 2008. Isolation and immunological detection of Mycoplasma ovipneumoniae in sheep with atypical pneumonia and lack of a role for Mycoplasma arginini. *Research in Veterinary Science.*, 84: 367–373.
2. AZIZI, S. TAJBAKHSH, E. REZAII, A. NEKOUEI, S.H and NAMJOO, A.R., 2011. The role of *Mycoplasma ovipneumoniae* and *Mycoplasma arginini* in pneumonic lungs of slaughtered sheep. *Revue Méd. Vét.,* 162 (6) 310-315.
3. JUSTICE-ALLEN, A.E., LUEDTKE, C. J and OVERSTREET, M., 2011. Prevalence of *Mycoplasma ovipneumoniae* in desert bighorn sheep in Arizona. *Desert Bighorn Council Transactions:* Volume 51, PP: 1-10.
4. MOHKBER DEZFOULI. M. R., SADEGHIAN. S., JAVANBAKHT. J., HOBE NAGHI R AND LAKZIAN. A., 2011. A study of occurrence and histopathology of *Mycoplasma* infection in sheep in Tehran suburb, Iran. *Journal of Infectious Diseases and Immunity*., 3(6): 106-111.
5. UMA, 2011. Studies on pathology and pathogenesis of mycoplasmosis in small ruminants. PhD thesis submitted to Department of Pathology, Bangalore, Karnataka Veterinary, Animal and Fisheries Sciences University, Bidar.
6. MASSIMO, G., ROBIN, A. J. N., MIROSLAV, H., BARBARA, B., TAKESHI, O.,RICCARDO, O., SHINGO, T., EISHU, T., HIROAKI, M., NORIMOTO, O.,KAZUO, K., ATSUSHI, K., RYÔ, H., AND ROGER, D. A., 2012. Seroepidemiological survey of sheep flocks from Northern Japan for *Mycoplasma ovipneumoniae* and *Mycoplasma Agalactiae. Trop. Anim. Health. Prod*., 44:395–398.
7. BOTTINELLI, M., SCHNEE, C., LEPRI, E., STEFANETTI, V., FILIPPINI, G., GOBBI, M., SEBASTIANELLI, M., ANTENUCCI, P., RAMPACCI, E., COLETTI, M and PASSAMONTI, F., 2016. Investigation on mycoplasma populations in pneumonic dairy lamb lungs using a dna microarray assay. Manuscript accepted for publication in *Small Ruminant Research. http://dx.doi.org/doi:10.1016/j.smallrumres*.2016.12.038.
8. SHAHID, A., SAJJAD, U.R., IFTIKHAR, H., GHULAM, M., MOHAMMAD, A. A., ZAFER, A., MOHAMMAD, M.T., MUHAMMAD, I.U and MUHAMMAD, A. K., 2016. Bimolecular identification of *M.ovinpeumoniae* from nasal swab samples of sheep from various districts of Balochistan, Pakistan. *Int. j. of Advan. Biol. and Biomed. Res.*, 4(1):32–39.

Indian Journal of Natural Sciences www.tnsroindia.org.in ©IJONS

Vol.8 / Issue 45 / December 2017 *International Bimonthly* *ISSN: 0976 – 0997*

RESEARCH ARTICLE

Effects of Different Irrigation Water and Nitrogen Treatments on Culm Mechanical Properties and Yield of Rice

Minhui Li[1,2], Peng Zhou[3], Xu Yang[1,2], Xiaohou Shao[1,2], Tingting Chang[1,2]*, Xinyu Mao[1,2], Yujie Zhang[1,2], and Wenbo Wu[1,2]

[1]Key Laboratory of Efficient Irrigation-Drainage and Agricultural Soil-Water Environment in Southern China, Ministry of Education, Nanjing 210098, China.
[2]College of Water Conservancy and Hydropower Engineering, Hohai University, Nanjing 210098,China.
[3]Zhejiang Zhongye Survey and Design Co., Ltd, Hangzhou 310002 China.

Received: 13 Oct 2017 Revised: 25 Oct 2017 Accepted: 03 Nov 2017

***Address for correspondence**
Tingting Chang
College of Water Conservancy and Hydropower Engineering,
Hohai University,
Nanjing 210098, China.
Email : changtingting225@163.com

ABSTRACT

In order to study the effects of different water stress levels and different nitrogen application rates on the lodging resistance and yield of rice, the pot experiment was conducted with Nanjing 5055 as the research object, and analyzed the effects of irrigation water and nitrogen interaction on culm mechanical properties (*LI*, *Wt*, *DE*, *BR* and *BM*) and yield of rice, and clarify its relevance. The results showed that different water and nitrogen treatments had a significant effect on culm mechanical properties and yield of rice, and the lodging resistance of rice was inversely proportional to the length of the first and second internodes, and it was proportional to the area of culm tube bundle. In the case of no stress, low nitrogen treatment is beneficial to the increase of crop yield, while the rice itself has the high quality lodging ability, and under the same stress situation, the rice is cultivated under the condition of low nitrogen more suitable, the relative lodging performance is stronger, the yield higher. These results suggest a reasonable amount of irrigation water and N, and will be much more beneficial to increasing grain yield and N use efficiency in rice production.

Keywords: Rice; Irrigation Water Amount; Nitrogen application; Culm mechanical properties; Yield

INTRODUCTION

Rice is one of the major grain crops in the world, water and nitrogen are the necessary factors for the growth and yield of rice, water and nitrogen deficit are the important reasons for the further increase the production of rice which in growth critical period (Haefele S M, 2008,Ye Y S, 2013). However, such as in the wind, heavy rain, easily lead to stalk lodging, and increasingly become a major obstacle to improve rice production in the realization of rice high yield, super high yield target (Yuan Zhihua, 2003.Setter T L, 1997). Lodging not only affects the yield, but also makes the quality worse. According to the study, a higher yielding cultivation condition leads to lower crop production by lodging. After the rice lodging, the photosynthetic products were synthesized, transported and stored, and the grain maturity and grain weight decreased. Maturity and grain weight are closely related to the quality of rice, so lodging is also a major obstacle to high-quality rice production (Huang Yanling, 2008).

The amount of water required for the rice is actually far less than the actual irrigation, unreasonable use of water resources caused a serious waste of resources (Kato Y,.2006,Boyer J S, 2004). It is well known that the main component of rice production cost is nitrogen fertilizer, the amount of nitrogen fertilizer in rice is about 24% of the total consumption of nitrogen fertilizer. At present, the addition of nitrogen fertilizer can increase the yield of rice, but the efficiency of nitrogen use is obviously low. It is estimated that the rice growing demand can still be met even if reduced 28% of global nitrogen use(Mueller N D, 2004), waste of resources becomes a serious problem in agricultural production. Since the 1970s, China's use of synthetic nitrogen has increased by 271% (Ju X T, 2009), and the use of nitrogen has increased crop yields, but this has also caused serious damage and degradation in the 1990s (Liu J, 2005). Rational use of water resources and nitrogen fertilizer and how to improve the efficiency of water resources and nitrogen use is particularly important.

In recent years, there are a lot of researches on the lodging of rice in China or abroad, such as Setter T have indicated that the rice lodging rate for each 2% increase in production will be reduced by 1%, severe lodging and even cause 50% reduction in rice production(Setter T, 1997). Lodging mainly divided into root lodging and stalk lodging, in southern China, the lodging mainly stalk lodging (Zhang W J,2014,Zhang Fengzhuan 2010). The lodging resistance of rice was related to the morphological characteristics of rice(such as plant height, center of gravity height, culm dry weight, et al.), mechanical properties(such as culm breaking resistance, bending stress, cross section modulus, et al.) and the chemical composition of stem(such as cellulose, lignin, soluble sugar, nitrogen, et al.).

There are many studies on the effects of water and nitrogen on the lodging resistance and yield of rice. However, there are few studies on the effect of water and nitrogen interaction on mechanical properties and yield and its composition, and it need further discussion. In this paper, water and nitrogen interaction is associated with rice lodging resistance, and attempts to analyze and evaluate the difference of lodging resistance of different nitrogen treatments under different irrigation treatments are studied. By comparing the causes of rice stalk lodging, the appropriate rice irrigation and fertilization model, to provide a basis for the development of reasonable water and fertilizer system in rice. The effects of nitrogen stress on the yield of rice were studied, and the effects of water stress and nitrogen nutrition on the yield of rice were discussed, the aim of this experiment was to provide the theoretical basis and practical basis for efficient rice production.

MATERIALS AND METHODS

Experimental site

The experiments are initiated in Jiangsu Province Hydraulic Research Institute coastal test base (latitude 31°57' N, longitude 118°50′ E), from May 15 to October 15, 2016. The experiments area is a subtropical humid monsoon climate, and the average annual rainfall is about 1029.5mm, the average yearly temperature is approximately 15.8°C

and the frost-free period is 225d. The soil of the experimental site was a clay loam soil with following properties: The soil water content and soil water holding capacity were 30.9% and 42.1% , the total nitrogen content was 62.9 mg·kg^{-1}, the available nitrogen content was 47.4 mg·kg^{-1}, the total phosphorus content was 33.0 mg·kg^{-1}, the available phosphorus content was 10.37 mg·kg^{-1}.

Experimental design

The tested rice varieties were Nanjing 5055. Using pot experiment, basin diameter 29 cm, pelvic floor diameter 26 cm, height 35 cm. Experiment with 10.5 kg per pot of soil, before the test the soil dried and sieved, and then into the basin, and even fertilization. Soil samples by the sun, crushed, sieved into the barrel, the barrel after the dry capacity of the soil 1.29 g/cm^3. Raise rice seedlings on May 10, when the three leaves of one mind, choose the same size of the seedlings transplanting on June 24; Each pot transplanted 3 points, 2 per hole, the seedlings were triangular arrangement; October 15 harvest, the whole growth period of 158d. Fertilized basal fertilizer (among them $CO(NH_2)_2$ is 0.15 g/kg, $Ca(H_2PO_4)_2$ is 0.65 g/kg, and KCl is 0.15 g/kg) on June 21. Insecticides were sprayed on July 7 and August 10 for locust and leaf borers in paddy fields.

In this experiment, pot experiment was used to test three water stress levels and three nitrogen application levels, a total of 9 varieties were treated. The rice plants were planted on May 24, and were transplanted when the rice leaves were in the middle of the leaves. The size of each seedling was almost the same, each pot was transplanted 3 points, 2 per hole, 9 times for each treatment. To ensure that each treatment of the same base fertilizer. During the stress period, ensure that the pot is weighed with an electronic balance of 1 g per day at about 8:00 every morning, when the basin water level is below the lower limit of water control, the basin will be replenished to the upper limit. During the non-stress period, the treatment was kept shallow water, and the depth of the water layer was about 10~20 mm. The whole growth period of artificial grass, in addition to water and nitrogen measures, the other agricultural measures are the same. Rice plants began to stress at the end of tillering and early jointing, and the stress lasted 9 days. the experiment set 2 factors and 3 levels, (1).Degree of water stress: not drought treatments (full irrigation), recorded as CK; Light drought treatments (soil water holding capacity of 70% to 80%), recorded as C1; Heavy drought treatment (soil water holding capacity of 60% to 70%), recorded as C2; (2). After the drought and water at the same time topdressing nitrogen fertilizer: no nitrogen treatment (no fertilization after rehydration), recorded as N0; Light nitrogen treatments (the amount of nitrogen is about 80 mg/kg after rehydration), recorded as N1; Heavy nitrogen treatments (the amount of nitrogen is about 160 mg/kg after rehydration), recorded as N2. A total of 9 treatments, and each treatment has 9 times repeat. Specific test design as shown in Table1:

Main tested indices and methods

The test began sampling from August 7 to October 4. After the end of the test, the measurement data were collated and analyzed. Rice enter to the heading stage on August 23, and harvest October 15. The results were measured on August 23 (heading stage), September 1 (grain filling stage), September 10 (milk stage) and September 28 (yellow ripening stage), determination of various indicators, the entire growth period were measured 4 times.

Physical indicators

BR (breaking resistance): Place the stalk level, the stems on both sides of the fixed, fixed at both ends of 2.5 cm, the middle of 10 cm test part of the vacant. With the electron stalk strength testing machine, the sensor is constantly moving down, the stem pressure and the deflection are increasing, and when the stem reaches the maximum pressure, the pressure is the bending force. Each measured a total of three times the measured data, the final results of each treatment to take three averages.

Bending moment of rice: Using the following formula(Ma Jun, 2004):

$$BM=H\times G\times 0.001\times 9.8 \quad (1)$$

Where, BM is the bending moment, H is the internode base to spike length(cm), G is the internode base to spike top fresh weight(g).

BR and D, Base lodging is the main form of rice stalk lodging (Li Xiaokun, 2012), so the study of the base above the 15 cm stalk to test.

LI (lodging index): Using the following formula(Li Min, 2012):

$$LI=BM/BR\times 100 \quad (2)$$

Where, LI is the lodging index (cm $g\cdot g^{-1}$), BM is the bending moment (cm g), BR is the breaking resistance (g).

Yield

Measurement of effective panicle rate, number of grains, number of thousand grains, yield and other data.Each treatment takes 4 pots to measure production, and the final result takes the average of each treatment.

Statistical analysis: Data was analyzed using the SPSS 13.0. The differences among treatments were analyzed by Duncan's new multiple range test.

RESULTS AND DISCUSSION

Effects of different water and nitrogen treatments on bending strength of culm

The flexural modulus of the rice and the bending strength are directly related to the diameter and cross-sectional area of the culm, the increase of the cross-sectional area is beneficial to increase the modulus of the bending section, and decreased the bending strength. It can be seen from Table 2, the cross-sectional area of heavy drought treatment is the smallest under the conditions of no nitrogen application, and the cross-sectional area of sufficient irrigation and light drought treatment is not much different. Under the influence of cross-sectional area, the Wt of light drought and non-nitrogen application treatment is higher than the treatment of sufficient irrigation, while the Wt of heavy drought and non-nitrogen fertilizer was reduced to 12.7% compared with the sufficient irrigation. While the bending strength under light drought treatment decreased by 9.2%, heavy drought treatment is increased by 16.5%, the gap is more obvious. This shows that heavy drought treatment with the same material of the culm, was more difficult to cause rice lodging. In the case of low nitrogen, the cross section modulus and stress are not much different under the three levels of water stress. Under the high nitrogen treatment, Compared to the sufficient irrigation, the Wt ratio increased by 19.3% and the stress increased by 21.7% under the light drought treatment. The bending modulus and flexural strength under heavy drought treatment were better than the sufficient irrigation treatment, but the promotion is not obvious. In order to improve the mechanical strength of the culm, it is more suitable for light drought treatment without nitrogen application, while under the condition of low nitrogen, the difference of the three treatments is not obvious, and in the case of high nitrogen, the light drought treatment is more suitable. Considering that the same nitrogen application, the light drought treatment is more conducive to improve the mechanical strength of the culm; under the condition of sufficient irrigation, no nitrogen treatment is more

favorable; Under the condition of light drought, high nitrogen treatment is more favorable; Under the condition of heavy drought, low nitrogen is more favorable.

Effects of different water and nitrogen treatments on culm destruction energy

The cumulative damage energy of the culm is the ability of the culm to resist the sustained and continuous deformation, which is an important index of the lodging resistance of the culm. It can be seen from Table 2, under the conditions of no nitrogen application, the relationship of damage energy is: C1> C2> CK, and the damage energy of rice under the influence of water stress is higher, which indicates that the rice culm is more energy, culms are more resistant to stress. Under the condition of sufficient irrigation, the relationship of damage energy is N0> N1> N2, the energy of the culm under no nitrogen treatment is higher, and the culm force is stronger. At the same time, with the increase of nitrogen application rate, the lower energy of the culm, indicating that the nitrogen fertilizer will lead to the continuous weakening of the culm capacity, the occurrence of rice bending, the more prone to fatigue damage. The treatment without reference to nitrogen under the condition of sufficient irrigation as CK, the damage energy under the treatment of heavy drought and low nitrogen treatment was higher than the other treatments. At this time the rice has a stronger culm energy, a strong resistance to sustained stress and the ability to continue to deform.

Effects of different water and nitrogen treatments on *LI*, *BR* and *BM* of culm

The lodging index LI is an important parameter to judge the rice lodging performance. The larger of the LI, the greater the possibility of rice lodging. It can be seen from Table 2, under the condition of nitrogen application, the LI under the treatment of heavy drought and low nitrogen treatment showed the highest lodging resistance, while the LI was highest under heavy drought and high nitrogen treatment. Under the condition of no nitrogen application, the LI under the light drought treatment was higher than the high nitrogen treatment, and the difference between the heavy drought treatment and the non-drought treatment was not significant, compared with the LI of each treatment, the BR of each treatment was not significant, the BM in the light drought treatment is relatively large, which is the product of plant height and fresh weight is larger, resulting in the LI becomes larger. Under the condition of low nitrogen application, The LI is lowest under heavy drought and low nitrogen treatment, the rice at this time is more resist lodging. By comparison, BM and BR under heavy drought treatment were larger, BM was 2.4% and 2.3% higher than sufficient irrigation and light drought treatment, and 10.1% and 3.1% of BR, the BM relationship under different treatments was similar, the BR value directly affects the lodging resistance of rice under low nitrogen condition.

The results showed that the rice LI had exceeded the critical value in the process of nitrogen treatment, but there was no lodging phenomenon in the experiment process, which indicated that the rice varieties could be different, even though the rice lodging index exceeded the critical value, but the rice itself has strong lodging resistance, so rice will not be lodged. Under low nitrogen treatment, LI was close to the critical value of 200, while the high nitrogen treatment was far more than 200, this indicated that under nitrogen treatment, low nitrogen treatment of rice lodging resistance is stronger. Under different water stress, LI under no nitrogen treatment was significantly less than under nitrogen treatment, while LI under low nitrogen treatment was lower than the high nitrogen treatment. By numerical comparison, BM under no nitrogen treatment was significantly less than nitrogen treatment, and the BR under no nitrogen treatment was significantly larger, so resulting the LI is relatively small with non-nitrogen treatment. And then compared with low nitrogen and high nitrogen treatment, the difference of BM under different treatments was not significant, while the BR with high nitrogen treatment was significantly lower than low nitrogen treatment, which resulted in the increase of LI under high nitrogen treatment. Through the above comparison, it is found that the difference of LI is mainly caused by the change of the bending force BR. It can be seen from Table 2 that the resistance of rice affected by water stress is significantly larger than sufficient irrigation treatment, which indicated that drought stress will help increase the resistance of rice.

The test of the bending force measured by the base of more than 15cm part, which measured interval between the two sections. In the different irrigation mode, the bending resistance decreased with the increase of nitrogen application rate, which indicated that the more nitrogen was applied, the more likely to be lodged in rice; The resistance under no nitrogen treatment was: C2> CK> C1; The resistance under nitrogen treatment (low nitrogen and high nitrogen) was: C2> C1> CK, this indicated that the rice under the influence of water stress had lower lodging potential.

For the BM under different treatments, the heavy drought treatment was the largest under the condition of no nitrogen application. With adequate irrigation treatment as a control, the BM was reduced 2.9% under the light drought treatment, while promoted to 4.9% under the heavy drought treatment; under the condition of low nitrogen application, BM under heavy drought treatment is still the largest, and the difference between light and non-drought is not significant. Under the condition of high nitrogen application, the BM was reduced by 1.9% the light drought treatment, while promoted to 2.1% under the heavy drought treatment, this indicated that moderate bending stress can reduce the bending moment, but the drought stress exceeding the limit will cause the bending moment to increase.

Correlation analysis of rice culm traits and mechanical properties and lodging index

In this paper, the relationship between rice culm traits and mechanical properties and lodging index was analyzed under different water and nitrogen interaction. The results are shown in the following table (*, ** denote significance at the 0.05 and 0.01 probability levels, respectively).

Correlative relationship between morphological traits and lodging index of rice culm

According to Table 3, the relationship between flag leaf area and lodging index was showing a very significant positive correlation, the correlation coefficient is the largest (r=0.9.19**); There was a significant positive correlation between stem stalk and lodging index, the correlation coefficient is the second (r=0.855**); There was a significant positive correlation between the plant height and the second internode wall thickness and the lodging index(r=0.864**); There was a significant positive correlation between the stalk and the lodging index(r=0.671*).

Correlation between mechanics index and lodging index of rice

It can be seen from Table 3, there was a significant negative correlation between rice flexion and lodging index, and the correlation coefficient was the highest (r=-0.981**); There was a significant positive correlation between the bending moment and the lodging index (r=0.966**); There was no significant positive correlation between flexural modulus and lodging index (r=0.567).

In conclusion, there was a significant positive correlation between the flag leaf area, the stalk of the second internode, the thickness of the second internode, the plant height and the bending moment were significantly positively correlated with the lodging index, and the correlation coefficient of the bending moment was the largest (r=0.966**), followed was plant height (r=0.819 **), and followed was second culm diameter from top(r=0.887**). There was a significant negative correlation between rupture force and cumulative damage energy and lodging index(r=-0.981** and r=-0.787**).Comprehensive comparison can be learned that the impact of rice lodging index is the greatest resistance to rice, effectively improve the resistance of rice, can effectively reduce the possibility of lodging.

Effects of different water and nitrogen treatments on yield of rice

It can be seen from Table 4, under the condition of light and heavy drought, the yield of N1 and N2 treatments is significantly higher than N0 treatment, and the yield of CK and C1 is N1> N2. Under the condition of N0, the yield of C1N0 and C2N0 was 2.13% and 5.21% higher than CKN0 respectively. Under the condition of N1 and N2, the yield of CK treatment was less than that of C1 and C2, and the increase of yield was proportional to the drought degree of rice. The yield of CK was CKN1> CKN2>CKN0; The yield of C1N1 and C2N1 treatments was increased by 45.51% and 45.13% respectively compared with C1N0 treatment under the condition of C1. The yield difference between nitrogen treatment and non-nitrogen treatment was obvious, the yield of nitrogen treatment was much higher than that non-nitrogen treatment, C2N1 and C2N2 were increased 74.63% and 79.21% than C2N0 respectively, the results showed that water stress was affected rice plant growth, and caused the yield decreased during the jointing period of the rice. After the end of the stress, the application of nitrogen fertilizer directly affects the rice yield, and the application of nitrogen fertilizer will obviously increase the rice yield. Under the condition of CK and C1, the excess nitrogen fertilizer could inhibit the yield of rice, and the yield under N0 and N2 treatment was lower than N1 treatment. The effect of water and nitrogen interaction under the condition of C2 was more significant, the yield is proportional to the amount of nitrogen applied, this may be because the Nanjing 5055 relatively strong drought tolerance, and the application of nitrogen fertilizer after drought will have a certain compensation effect on rice plants, thus promoting the yield increase.

Effects of water and nitrogen treatments on yield factors

The grains of N1 and N2 were significantly higher than N0 under the condition of C1 and C2, and the number of grains in CK and C1 was N1> N2, which the regular pattern was the same as the yield. The total grain number increased with the increase of nitrogen content under the condition of C1, but the filled grain rate was significantly larger under the condition of N1, this indicated that the fertilization could increase the total grain number under the condition of C1.

The 1000-grain weight of CK and C2 treatments were less than C1 under the condition of N0; The 1000-grain weight of N1 and N2 treatments were lower than non-nitrogen treatment those which under the same water condition, and N0> N2> N1. The 1000-grain weight of N1 and N2 treatments were less than CK under the condition of C2, this is significantly different with yield, grain number, filled grain rate and other indicators, this phenomenon indicated that the nitrogen application rate under heavy drought could increase the compensation with the increase of nitrogen content, but the application of high nitrogen will also increase the yield, the increase in the number of grains may increase the late hybridization of rice competition, resulting in reduced 1000-grain weight. Therefore, a reasonable range of nitrogen application of rice yield has a substantial role in promoting.

The impact of lodging on the yield of rice

In general, the filled grain rate of rice varieties will be significantly reduced by lodging, but in this test, only N0 treatment have partially tilted under the condition of C2, and have not serious lodging situation, combined with the yield point of view, C2NO treatment of rice in line with the general regular, and can not clearly show that lodging on rice yield has an impact, it indicated that the varieties of rice itself may have a good lodging resistance.

Correlation analysis of yield factor and yield

It can be seen from Table 5, Table 6 and Table 7, the correlation between yield and yield components have great difference under different water and nitrogen conditions. Under the condition of CK, the number of grains was positively correlated with total grain number and yield, but negatively correlated with 1000 grain weight; The 1000

grain weight was negatively correlated with all the indexes, which was negatively correlated with grain number, total grain number and yield. Under the condition of C1, the number of grains was negatively correlated with the 1000 grain weight, and was positively correlated with the other indexes, which was positively correlated with the yield; The 1000 grain weight was negatively correlated with all the indexes. Under the condition of C2, the number of grains was positively correlated with the total grain number; The 1000 grain weight was the same as CK and C1, was negatively correlated with all the indexes; The 1000-grain weight was negatively correlated with the other indexes under different water conditions, the indicator is not conducive to other indicators. Under the condition of C1 and C2, the indicators only one or two significant correlation, but under the condition of CK, a number of indicators were significantly related. It can be seen that under the same water condition, the yield of rice under different nitrogen application was positively correlated with the number of grains, indicating that the number of grains was an important factor affecting rice yield, and the more the number of grains was, the higher of the yield.

It can be seen from Table 8, Table 9 and Table 10, the correlation analysis showed that the filled grain rate was positively correlated with other indexes except the total grain number under the condition of N0; The 1000-grain weight was positively correlated with the yield, and was negatively correlated with the other indexes. Under the condition of N1, the number of grains was significantly positively correlated with total grain number, filled grain rate and yield, and negatively correlated with 1000-grain weight; The filled grain rate was negatively correlated with 1000-grain weight, which was positively correlated with the other indexes; The yield was positively correlated with all the indexes, and significant positively correlated with the number of grains, total number of grains and filled grain rate. Under the condition of N2, the number of grains was significant positively correlated with the yield; The 1000-grain weight was negatively correlated with all the other indexes. The above data show that under the condition of N0 and N2, the effect of different water treatments on the yield factors of rice is relatively simple, and the significant correlation index is only one or two, and under the condition of N1, different water treatment will affect the multiple rice yield factors.

CONCLUSION

Different water and nitrogen treatments had significant effects on culm mechanical properties and yield of rice, the shorter the first and second internodes, the stronger the resistance to lodging, the longer the third, the stronger the lodging resistance of rice. As the amount of nitrogen applied increases, the length of the first, second and third internodes become shorter. The increase in the thickness of the first section is related to the wall thickness and the plant lodging resistance, to increases the first internode thickness, the lodging resistance become stronger. The lodging resistance of rice was inversely proportional to the length of the first and second internodes, and it was proportional to the area of culm and tube, this is consistent with the actual production. The yield under heavy drought and high nitrogen treatment reached the highest and the yield under heavy drought and low nitrogen treatment was not the same, but the yield of these two treatments was significantly higher than other treatments. Cultivate the first, the second section is relatively short, and the third section between the longer rice varieties can effective to prevent the rice from lodging. The nitrogen fertilizer directly affects the rice yield and the reasonable nitrogen fertilizer can effectively increase the rice yield. In this experiment, the low nitrogen treatment was beneficial to the increase of yield under the condition of no coercion, and at the same time, the rice had high quality lodging ability, but under the same stress condition, the rice was cultivated more suitable under low nitrogen condition, more powerful, higher yield.

ACKNOWLEDGEMENTS

This work was financially supported by Postgraduate Research & Practice Innovation Program of Jiangsu Province (SJCX17_0129), and Fundamental Research Funds for the Central Universities (2017B755X14).

REFERENCES

1. Haefele S M, Jabbar S M A, Siopongco JDLC, et al. 2008. Nitrogen use efficiency in selected rice (Oryza sativa L.) genotypes under different water regimes and nitrogen levels. Field Crops Research, 107(2): 137-146.
2. Ye Y S, Liang X Q, Chen Y X, et al. 2013. Alternate wetting and drying irrigation and controlled-release nitrogen fertilizer in late-season rice. Effects on dry matter accumulation, yield, water and nitrogen use. Field Crops Research, 144(20): 212-224.
3. Yuan Zhihua, Zhao Anqing, Su Zongwei, et al. 2003. Dynamic analysis of rice stem lodger resistance, Journal of Biomathematics, 18 (2): 234-237.
4. Setter,T.L., Laureles,E., Mazaredo,A.M. Loding reduces yield of rice by self-shading and reduction in canopy photosynthesis. Field Crops Rice, 1997, 49: 95-106.
5. Huang Yanling, Shi Yingyao, Shen Guangle, et al.2008. Study on the Relationship Between Rice Lodging Resistance and Culmtraits & the Yield Factors.Chinese Agricultural Science Bulletin, 24(4), 203-206.
6. Kato Y, Kamoshita A, Yamagishi J. Growth of Three Rice Cultivars (Oryza sativa L.)under Upland Conditions with Different Levels of Water Supply:2.Grain Yield .Plant production science, 2006, 9(4): 435-445.
7. Boyer J S, Westgate M E. Grain yields with limited water.Journal of Experimental Botany, 2004, 55(407): 2385-2394.
8. Mueller N D, Gerber J S, Johnston M, et al. Closing yield gaps through nutrient and water management.Nature, 2012, 490(7419): 254-257.
9. Ju X T, Xing G X, Chen X P, et al. Reducing environmental risk by improving N management in intensive Chinese agricultural systems. Proceedings of the National Academy of Sciences, 2009, 106(9): 3041-3046.
10. Liu J, Diamond J. China's environment in a globalizing world. Nature, 2005, 435(7046): 1179-1186.
11. Setter T, Laureles E, Mazaredo A. Lodging reduces yield of rice by self-shading and reductions in canopy photosynthesis.Field Crops Research, 1997, 49(2/3): 95-106.
12. Zhang W J, Li G H, Yang Y M, et al. Effects of nitrogen application rate and ratio on lodging resistance of super rice with different genotypes. Journal of Integrative Agriculture, 2014, 13(1): 63-72.
13. Zhang Fengzhuan, Jin Zhengxun, Ma Guohui, et al.Correlation analysis between lodging resistance and morphological characters of physical and chemical components in rice culm. Crops, 2010, 46(7): 15-19. (in Chinese with English Abstract)
14. Shen Guangle, Shi Yingyao, Huang Yanling, et al. Study on rice lodging resistance character and correlation between the culm traits and lodging resistance traits. Scientia Agricultura Sinica, 2007, 23(12): 58-62. (in Chinese with English Abstract)
15. Li Guohui, Zhong Xuhua, Tian Ka, et al. Effect of nitrogen application on stem lodging resistance of rice and its morphological and mechanical mechanisms. Scientia Agricultura Sinica, 2013, 46(7): 1323-1334. (in Chinese with English Abstract)
16. Guo Xiangping, Zhen Bo, Wang Zhenchang, et al. Increasing lodging resistance performance of rice by alternating drought and flooding stress. Transactions of the Chinese Society of Agricultural Engineering (Transactions of the CSAE), 2013, 29(12): 130-135. (in Chinese with English Abstract)
17. Kashiwagi T, Sasaki H, Ishimaru K, et al. Factors responsible for decreasing sturdiness of the lower part in lodging of rice(Oryza sativa L.). Plant Production Science, 2005, 8(2):166-172.
18. Takayuki K, Naoki H, Kazuhiro U, et al. Lodging resistance locus prl5 improves physical strength of the lower plant part under different conditions of fertilization in rice (Oryza sativa L.). Field Crop Research, 2010, 115: 107-115.
19. Ma Jun, Ma Wenbo, Tian Yanhua, et al. The culm lodging resistance of heavy panicle type of rice. Acta Agronomical Sinica, 2004, 30(2): 143-148. (In Chinese with English abstract)
20. Li Xiaokun, Li Yunchun, Lu Jianwei, et al. Effect of different factors on lodging of rice after flood and waterlogging induced by consecutive rainfall. Journal of Natural Disasters, 2012, 21(6): 99-103. (In Chinese with English abstract)

21. Li Min, Zhang Hongcheng, Yang Xiong, et al. Comparison of Culm Characteristics with Different Nitrogen Use Efficiencies for Rice Cultivars. Acta Agronomica Sinica, 2012, 38(7): 1277-1285.

Table 1. Experimental design

Treatment	Water stress degree	Nitrogen application rate	Soil moisture content	Stress duration(d)	Additional nitrogen fertilizer (mg·kg^{-1})
CKN0	Sufficient irrigation	0	Keep the shallow layer 10-20mm	0	0
CKN1	Sufficient irrigation	Low N application	Keep the shallow layer 10-20mm	0	80
CKN2	Sufficient irrigation	High N application	Keep the shallow layer 10-20mm	0	160
C1N0	Light drought	0	70%-80%	9	0
C1N1	Light drought	Low N application	70%-80%	9	80
C1N2	Light drought	High N application	70%-80%	9	160
C2N0	Serious drought	0	60%-70%	9	0
C2N1	Serious drought	Low N application	60%-70%	9	80
C2N2	Serious drought	High N application	60%-70%	9	160

Table 2. Different water and nitrogen treatments on culm mechanical properties

Treatments	S/mm^2	DE/(10^{-3}J)	Wt/($m^3\times10^{-8}$)	σ /MPa	BM/(N×cm)	BR/N	LI
CKN0	55.95	27.56	4.33	3.15	13.73	9.62	142.80
CKN1	61.24	23.64	5.52	3.14	17.57	7.72	227.56
CKN2	64.75	19.80	5.64	2.95	19.09	6.59	289.60
C1N0	52.30	31.98	4.38	2.86	15.33	9.27	165.39
C1N1	65.04	27.26	5.66	3.22	17.60	8.32	211.57
C1N2	73.90	25.90	6.73	3.59	18.74	6.94	270.22
C2N0	50.64	29.54	3.78	2.63	14.40	9.65	149.18
C2N1	57.28	27.53	5.18	3.05	18.01	8.59	209.70
C2N2	66.19	24.78	5.73	3.02	19.50	7.00	271.75

Table 3. Correlation between rice lodging index and various resistance-related traits

Lodging related characteristics	Items	Lodging index
Culm morphological traits	Plant height	0.819**
	Panicle length	0.494
	Ear height	0.319
	Panicle fresh weight	0.269
	Total fresh weight	0.581
	Gravity center height, GCH	0.303
	Ratio of GCH to plant height	-0.565
	First Culm diameter from top	0.671*
	Second Culm diameter from top	0.852**
	Third Culm diameter from top	-0.107
	First Culm wall thickness from top	0.392
	Second Culm wall thickness from top	0.839**
	Third Culm wall thickness from top	0.138
	First internode from top	0.102
	Second internode from top	0.155
	Third internode from top	-0.588
	First Plumpness of internode from top	0.199
	Second Plumpness of internode from top	-0.277
	Third Plumpness of internode from top	-0.067
	Area of flag	0.919**
Culm mechanical traits	Wt	0.567
	DE	-0.787*
	BR	-0.987**
	Bending stiffness	-0.409
	BM	0.966**

Table 4. Effects of different water and nitrogen treatments on yield of rice

Treatments		Number of grains (grain/basin)	Total grain number (grain/basin)	Filled grain rate /%	1000-grain weigh t/g	Yield /g
Irrigation amount	Nitrogen application					
CK	N0	1858.37	2167.03	85.76	24.69	45.53
	N1	3398.70	3718.75	91.39	24.08	78.17
	N2	2728.57	3112.80	87.66	24.35	66.85
C1	N0	1852.88	2072.46	82.31	25.1	46.50
	N1	2755.47	3078.84	89.51	24.29	67.64
	N2	2753.96	3400.16	80.99	24.36	67.47
C2	N0	1995.69	2251.84	88.62	24.75	47.90
	N1	3717.78	4031.01	92.23	23.73	85.65
	N2	3576.75	3940.28	90.77	24.25	85.64

Table 5. Correlation analysis on yield factors of different nitrogen application in CK condition

CK	Number of grains	Total grain number	Filled grain rate	1000-grain weight	Yield
Number of grains	1				
Total grain number	0.999*	1			
Filled grain rate	0.966	0.952	1		
1000-grain weight	-1.000**	-0.998*	-0.968	1	
Yield	0.995*	0.999*	0.936	-0.994*	1

Note: *, ** denote significance at the 0.05 and 0.01 probability levels, respectively.

Table 6. Correlation analysis on yield factors of different nitrogen application in C1 condition

C1	Number of grains	Total grain number	Filled grain rate	1000-grain weight	Yield
Number of grains	1				
Total grain number	0.972	1			
Filled grain rate	0.371	0.145	1		
1000-grain weight	-0.997*	-0.952	-0.441	1	
Yield	1.000**	0.971	0.377	-0.997*	1

Note: *, ** denote significance at the 0.05 and 0.01 probability levels, respectively.

Table 7. Correlation analysis on yield factors of different nitrogen application in C2 condition

C2	Number of grains	Total grain number	Filled grain rate	1000-grain weight	Yield
Number of grains	1				
Total grain number	1.000*	1			
Filled grain rate	0.943	0.933	1		
1000-grain weight	-0.896	-0.883	-0.993	1	
Yield	0.992*	0.995	0.894	-0.883	1

Note: * denote significance at the 0.05 probability levels.

Table 8. Correlation analysis on yield factors of different irrigation treatment in N0 condition

N0	Number of grains	Total grain number	Filled grain rate	1000-grain weight	Yield
Number of grains	1				
Total grain number	0.867	1			
Filled grain rate	0.856	1.000*	1		
1000-grain weight	-0.409	-0.809	-0.822	1	
Yield	0.899*	0.562	0.543	0.032	1

Note: * denote significance at the 0.05 probability levels.

Table 9. Correlation analysis on yield factors of different irrigation treatment in N1 condition

N1	Number of grains	Total grain number	Filled grain rate	1000-grain weight	Yield
Number of grains	1				
Total grain number	1.000**	1			
Filled grain rate	1.000*	1.000*	1		
1000-grain weight	-0.944	-0.943	-0.936	1	
Yield	1.000**	1.000*	0.999*	0.948	1

Note: *, ** denote significance at the 0.05 and 0.01 probability levels, respectively.

Table 10. Correlation analysis on yield Factors of different irrigation treatment in N2 condition

N2	Number of grains	Total grain number	Filled grain rate	1000-grain weight	Yield
Number of grains	1				
Total grain number	0.948	1			
Filled grain rate	0.727	0.472	1		
1000-grain weight	-0.994	-0.908	-0.797	1	
Yield	1.000**	0.949	0.725	-0.994	1

Note: ** denote significance at the 0.01 probability levels.

Indian Journal of Natural Sciences www.tnsroindia.org.in ©IJONS

Vol.8 / Issue 45 / December 2017 *International Bimonthly* *ISSN: 0976 – 0997*

RESEARCH ARTICLE

Empirical Relationship to Optimize the Blending Ratio for the Biomasses in the Fluidised Bed Gasification

M.Ramarao[1]*, S.Jayakrishna[2], P.Senthilkumar[3], M.Mathan Mohan[4] S.B.Malsoor[5], Adesh Bhil[6], and V.B.Manjunta[7]

[1]Associate Professor, Department of Mechanical Engineering, Holy Mary Institute of Technology & Science College of Engineering, Bogaram (v), keesara(m),Ranga reddy(Dist),Hyderabad, Telangana,-501301.

[2]Professor,Department of Mechanical Engineering, Holy Mary institute of technology & Science College of Engineering, Bogaram (v), keesara(m),Ranga reddy(Dist),Hyderabad, Telangana,-501301.

[3]Associate professor, Department of Mechanical Engineering, St. Joseph of College of Engineering Tamilnadu, India.

[4]Research Scholar,Annamalai University,Chidambaram,TamilNadu,India.

[5]Assistant ProfessorDepartment of Mechanical Engineering, Holy Mary Institute of Technology & Science College of Engineering, Bogaram (v), keesara(m),Ranga reddy(Dist),Hyderabad, Telangana,-501301.

[6]Assistant Professor,Department of Mechanical Engineering, Holy Mary institute of technology & Science College of Engineering, Bogaram (v), keesara(m),Ranga reddy(Dist),Hyderabad,Telangana,-501301.

[7]Asst.professor, Department of Mechanical Engineering, Holy Mary Institute of Technology & College of Engineering, Hyderabad, Telangana,-501301, India.

Received: 24 Sep 2017 Revised: 22 Oct 2017 Accepted: 06 Nov 2017

*Address for correspondence

M. Ramarao

Associate Professor,
Department of Mechanical Engineering,
Holy Mary Institute of Technology & Science College of Engineering,
Bogaram(v),keesara(m),Ranga reddy(Dist),
Hyderabad,Telangana,-501301,India.
Email: ramaraoenergy1983@gmail.com

ABSTRACT

The objective of this work was to assess the combined effects of the rice husk, wheat and coconut shell in a fluidized gasification process, where the focus was to quantify the relationships between the response variables and vital operating factors. With a view to the shortcomings of the classical “one factor-at-a-time” method in identification of the effect of experimental factors and their interactions, a statistical design of the experiment based on response surface methodology (RSM) was used. The response

variables used in this work were gasification efficiency, tar yield and carbon conversion with different bed materials such as silica and limestone. Using RSM, the effects of individual operating factors and their interactions were categorically determined, which were not otherwise possible by the classical design of experiment methodology. Using the resultant response variable correlations, gas efficiencies were optimized as a function of the different blending ratios and bed materials using respectively. In order to validate the optimized parameters, a comprehensive three-dimensional numerical model is developed to simulate gasification in a fluidized bed reactor using Eulerian–Lagrangian approach. The model predicts product gas efficiency and carbon conversion efficiency in good agreement with experimental data. The formation and development of flow regimes and distributions of gas compositions inside the reactor are also discussed.

Keywords: Rice Husk; Wheat Husk, Coconut Shell, Fluidized bed gasifier; Response surface methodology and Computational fluid dynamics.

INTRODUCTION

An agricultural residue that could be utilized for the recovery of energy is rice husk because of its reasonably high energy content (12–18 MJ/kg). Today in many countries, most of the surplus rice husks are disposed by direct burning in open heaps, which results in loss of energy as well as emission of various pollutants to the atmosphere [1–4]. Gasification as a process of converting carbonaceous materials into gaseous products using a gasifying medium such as air, oxygen, and steam has been considered as an alternative to combustion of low density biomass materials [5]. Further, the gasification process is typically 80–85% thermodynamically efficient in converting the organic content of the feed into a fuel gas mixture containing carbon dioxide, carbon monoxide, hydrogen, methane, excess steam and also nitrogen (if air is used as a gasifying agent), in addition to some minor organic compounds, tars, other minor components such as ammonia, and sulfur compounds. Besides, the gasification process generates a clean fuel gas which can be utilized in a combined cycle power generation system with enhanced efficiency. An integrated gasification combined cycle system offers a generating efficiency in the order of 40%, which is higher than that for a conventional direct combustion pulverized coal fired plant (~34%) [6].

Co-gasification technology of coal and biomass offers advantages, such as reduction of air pollutants (e.g., NOx and SOx) and volatile organic compounds [7], improved gasification reactivity (alkali and alkaline earth metal in biomass ash behave as catalysts in coal gasification [8], and increase in gas yield. Thus, it is becoming increasingly important, because it allows for the use of coal in a more environmentally friendly way and contributes to the implementation of biomass gasification on a commercial scale [9]. However, with a view to enhance the reduction of air pollutants and volatile matter, co-gasification of agro-based biomass is appreciated. Hence it tends to discover a substitute for the coal for the co gasification. Agro based biomass is the only source of carbon-based renewable fuels and the sustainable exploitation of this resource is essential to secure the energy security. Wheat husk and coconut shell are high in sulfur content and vanadium and nickel contents (EPA-regulated elements), whereas rice husk are high in moisture and ash content and low in sulfur content. Blending the above three is regarded as a promising option to improve the slag flow difficulties of high ash content husk because of the relatively low ash content of coconut shell, which reduces the risk of slag plugging the reactor tapping system. Mixing biomass also helps to reduce the sulfur loading in flue gas, which in turn results in lowering downstream processing requirements [10] Blending also helps to alleviate the high Ni and V difficulties of oil sand coke gasification, such as destroying the refractory binder, slagging and fouling on economizer heat-transfer surfaces, problems with burners and the syngas cooler, and formation of low-melting-point sodium vanadate, which deposits in the syngas cooler [11]. Furthermore, there is a chance that blending coke with coal can enhanced the conversion through catalytic activity of alkali metals in coal ashes, although the results reported in the literature are not consistent in this respect. Last but not the least; blending

is one of the promising options that can further help to reduce the environmental impacts and footprints of the oil and gas industry.

Modeling and simulation can also be helpful for optimizing the biomass gasifier design and its operation (start up, shutdown, etc.) with minimal temporal and financial costs [12]. The reported mathematical models for biomass gasifier are primarily classified into three groups: thermodynamic equilibrium models, kinetics models and multiphase computational fluid dynamics (CFD) models. Due to the complexity of the gasification process, i.e., involving many phases and various chemical and physical interactions among them existing work is focused on kinetics models and equilibrium models [12]. Only a few multiphase CFD trials have been reported to simulate fluidized bed biomass gasifier.

From the literature review, it is understood that there are a large number of fluidized bed biomass gasifiers developed worldwide for co-gasification; unfortunately most of these projects are struggling to reach commercialization. Very few investigations have been done related to the prediction of the gas efficiency, gas yield and tar yield , incorporating the process parameters like temperature, equivalent ratio and steam to biomass ratio alone. The main objective of this research is to develop an empirical relationship to predict the gas efficiencies with respect to blending ratio of different biomasses and also to optimize the processing parameters for the above said gasification using desirability approach, Furthermore, a three-dimensional Eulerian–Lagrangian model is developed to validate the optimized performance of the fluidized bed biomass gasification by simulating the complex granular flow and chemical reaction simultaneously. The experimental data and the predicted vales have been analyzed, compared and discussed in the present work.

MATERIALS AND METHODS

Feedstock and inert bed materials

The feed stock selected to study the fluidized bed gasification were coconut shell, rice husk and wheat husk with different biomass ratio. These biomaterials were collected from rural industries of Cuddalore district, India. The proximate and ultimate analyses of coconut shell, rice husk and wheat husk used as feed stock are presented in Table 1. The inert bed materials used were silica and lime stone and its particle size distribution were selected as 0.400 mm using sieve analysis. The properties of these materials and the procedures followed in finding out physical and chemical properties are mentioned in detail. Absolute specific gravity of the selected materials was measured using specific gravity bottle method. To minimize the complexities, resulting from the non-uniform particle size distribution in the bed, the average particle diameter was used to represent the particle size. Sieve analysis is commonly used to predict the particle size distribution of the feed stock having size of 70-500 µm. The test materials were dried and then sieved in a set of standard sieves and particle size distribution was observed [12]. Using oven method (110°C till reaching standard borne dry weight), moisture content of feed stock was measured (ASTM, E – 871). Proximate composition such as volatile matter (ASTM, E – 872) and ash (ASTM, E – 830) and fixed carbon (by weight difference) was found out by ASTM procedures. The elemental composition of the feed stock was found out using Elemental Analyzer (Carlo Erba EA 1108) coupled with auto sampler AS-200 and data processor DP 200-PRC. The minimum fluidization velocity was measured using pressure drop method. U tube manometers are used to measure the pressure drop below and above the distributor plate and at different heights of fluidized bed reactor. The air velocity corresponding to the peak pressure drop gives the experimental value of minimum fluidization velocity [13].

Experimental Set up

A pilot scale fluidized bed rice husk gasifier (capacity: 20 kg/h) had been developed and installed in the laboratory to carry out the experimental investigation. The schematic diagram of the setup is shown in Fig. 1. Table 2 shows the design and operating features of Fluidized Bed Gasifier. The cylindrical gasifier with 108 mm inside diameter up to a height of 1400 mm made of carbon steel material having inside refractory lining of thickness 0.1 m. The gasifier is fitted with a multiple hole distributor plate of 105 mm diameter was used for air distribution The ash discharge systems were provided for periodical disposal through the lock hopper arrangements. Silica sands and lime stone as bed materials were initially put into the gasifier through the screw feeder and air was introduced at the bottom of gasifier to maintain the bed in fluidized state. The air flow, after the discharge of blower, was controlled by a regulating valve and the flow was then estimated by an orifice meter placed in the supply pipe on the basis of pressure drops recorded across it. The orifice had been calibrated prior to the experiment with two reference instruments; namely a digital micromanometer (make: Furnace Control, England) and a thermal anemometer (make: Dantec, Denmark). The pressure drops across the orifice were recorded in the manometer and the corresponding flow rates were measured by the anemometer; the calibration curve was thus generated by plotting the flow rates along abscissa and the corresponding pressure drops along the ordinate.

During experiment, the pressure drops were noted to get the corresponding air flow rates from the curve at different equivalence ratios. External electric heating was used for preheating the bed materials as well as the refractory lining during start up. The electric heating was switched onto and the gasifier was allowed to run until the bed temperature was 450°C. The raw rice husk was then fed through the under-bed feeding system having a screw feeder. The feed rate was controlled by the screw feeder fitted to a variable speed drive and it push the solid fuel immediately into the gasifier preventing pyrolysis outside the chamber. Supply of air was then regulated to maintain the desired equivalence ratio.

The cyclone at the outlet of gasifier was used to separate the solid particles from the fuel gas mixture. The bag filter placed after the cyclone further cleaned up the gas by capturing dust and other smaller particles. The water cooler and an ice trap system were used in series to cool the fuel gas to separate the tar through condensation. A second orifice meter (50 mm diameter) was positioned in the fuel gas pipe (108 mm diameter) to estimate the gas yields. The calibration of the orifice was done prior to the experimental work by following the similar procedure as it was done in case of orifice meter in airline to generate a separate calibration curve. While the gasifier was running, the pressure drops across the orifice were noted in manometer to get the corresponding gas flow rates from the curve. The flow rates thus obtained corresponding to gas temperatures was then corrected by the temperature factor to get the actual flows at NTP. Equivalence ratio is very important in gasification process as it determines the fraction of the fuel that is burnt and thereby it controls the bed temperature. It also affects the fluidization of the bed. The lower limit of equivalence ratio is decided by the minimum quantity of air required to burn a portion of the fuel to release enough heat to support the endothermic reactions, to meet the sensible heat losses in gas, char and ash, and to maintain the required bed temperature of the reactor. As rice husk has high ash content, it requires larger fraction of the fuel to be burnt – this ultimately demands a higher equivalence ratio [14]. In Hartiniati et al. [15], it is reported that the equivalence ratio was maintained between 0.30 and 0.48 during experimentation in a pilot scale fluidized bed gasifier fueled by mixture. Later on, Mansaray et al. [16] also investigated the rice husk and wheat husk gasifier performance in a fluidized bed system by varying the equivalence ratio at 0.25, 0.30 and 0.35. In view of these observations, the gasifier was operated with equivalence ratios of 0.20-0.50 in the present investigation to get the experimental results.

Experimental Design Matrix

From the studies [17-26] producer gas and the carbon conversion efficiency have been identified. The biomasses such as coconut shell, rice husk and wheat husk are used in the present investigation. Owing to a wide range of factors,

the use of five factors and central composite rotatable design matrix was chosen to minimize number of experiments. The number of tests required for the CCRD includes the standard 2k factorial with its origin at the center, 2k points fixed axially at a distance, say α, from the center to generate the quadratic terms, and replicate the tests at the center; where k is the number of variables. The axial points are chosen such that they allow rotatability, which ensures that the variance of the model prediction is constant at all points equidistant from the design center. By adding axial points which extend, the design will provide protection against the curvature from twisting. Hence, the design was extended up to ± α (axial point). The value of α is chosen to maintain rotatability. To maintain rotatability, the value of α depends on the number of experimental runs in the factorial portion of the central composite design, which is given by Equation (3.1)

$$\alpha = [\text{number of factorial points}]1/4 \quad (3.1)$$

If the factorial is a full factorial, α is evaluated from the Equation (3.2)

$$\alpha = [23]1/4 = \pm 1.682 \quad (3.2)$$

It can be noted that when $\alpha > 1$, each factor is run at five levels ($-\alpha$, -1, 0, +1, $+\alpha$) instead of the three levels of -1, 0, and +1. The reason for running the central composite designs with $\alpha > 1$ is to have a rotatable design. However, the factorial portion can also be a fractional factorial design of resolution. The center values for the variables were carried out at least six times for the estimation of error, and single runs for each of the other combinations. Replicates of the test at the center are very important as they provide an independent and more uniform estimate of the prediction variance over the entire design. Table 3.4 presents the ranges of factors considered. For the convenience of recording and processing the experimental data, the upper and lower levels of the factors are coded as +1.682 and -1.682 respectively. The coded values of any intermediate value can be calculated by using the Equation (3.3)

$$Xi = 1.682\,[2X - (Xmax - Xmin)] / (Xmax - Xmin) \quad (3.3)$$

where,

Xi is the required coded value of a variable X, and X is any value of the variable from Xmin to Xmax

Xmin is the lower level of the variable.

Xmax is the upper level of the variable.

Xmax is the upper level of the variable.

Design matrix consisting of 20 sets of coded conditions (comprising full replication 8 factorial points, 6 corner points and six center points) was chosen in this investigation. Table 3 represents the ranges of factors considered, and Table 4 shows the 20 sets of coded and actual values with experimental results.

Experimental Testing

During experimentation, special care was taken to maintain the desired bed temperatures as the selected feedstock were coconut shell, rice husk and wheat husk. One of the important features of biomass gasification is that the bed temperature can be kept as low as 700–900°C, thereby preventing sintering and agglomeration of this ash which would otherwise cause serious operational problems during the conversion process [27]. The upper temperature is fixed by slagging phenomena which primarily depends upon the ash composition and the reaction atmosphere (like oxidation or reduction). Above this temperature, silica and potassium oxide in ash fuses on the surface of rice husk char particles forming a glass-like barrier that prevents the further reaction of the remaining carbon [28]. Some studies [29, 30] also indicate that oxidation of biomasses at a temperature higher than 900°C results in a physical structural transformation of silica from its original amorphous state to a crystalline state thereby encapsulating residual carbons. Once the structural changes of silica occurs, the combined carbon becomes unavailable for further oxidation reactions even at higher temperatures. In view of this, the gasifier was operated in the range of 700–950°C when the experiments were carried out with equivalence ratio 0.2 and 0.5.

The gasification temperature was raised up to 700°C only in case of equivalence ratio of 0.25. The gasifier temperatures were recorded using Ni–Cr–Ni thermocouples with a digital display system. The gas sampling system was composed of probes fitted with septum. The sampling point was located at the outlet pipe of gasifier. The gas sampling probe made of glass was 50 mm in diameter and 500 mm in length. A syringe of volume capacity of 10 ml was used to collect the gas sample. The sample was analyzed in the Gas Chromatograph (Make – Chemito, model – GC1000) to get the raw experimental data and those were compared with the predicted values of the developed model. The energy content of the gas is assessed through the variable CCE (carbon conversion efficiency). This variable represents the ratio between the energy content of the permanent gas and the energy content of the initial biomass feedstock without taking into account the heat input in the reactor:

$$CCE = [(M_{CO\%} + M_{CH4\%} + M_{CO2\%}) * 12] / M_{feed\ rate}$$

$$GE = HHV_{gas} / HHV_{biomass}$$

where HHV for the biomass is calculated from;

$$HHV_{biomass} = (CO\%* 3018 + H_2\%* 3052 + CH_4\%* 9500)*0.01*4.1868\ (kJ/Nm^3)$$

At the end of the experiment the residual tar were weighed and stored in a sealed recipient for further characterization. The tar yield is expressed as the ratio of the residual tar to the initial mass of biomass

$$Y_{Tar}\% = [(M_{Tar}) / (M_{biomass})] \times 100$$

Computational domain, initial and boundary conditions

Computational Analysis is further enhancing to correlate the experimental and statistical evaluation. The validation among the experimental, statistical computational analysis gives a better understanding the gasification behavior of biomass blends. The Eulerian–Eulerian model was implemented using the commercially available Computational Fluid Dynamics software FLUENT12.0 (ANSYS, Inc., USA). The reactor domain has been discretized with a uniform Cartesian grid. The grid cell size is 4 mmx2mmx8.75 mm (Δx, Δy & Δz). Inlet and boundary conditions are modeled to match the experiments as close as possible. Heated air flows through the distributor with 25 holes. The biomass feeding rate from the experiment is transformed into the particle injection rate. At the outlet, gas phase adopts out-flow boundary condition and outlet pressure is fixed to atmosphere. The reactors is filled at the beginning of the calculation with 30 g silica sand and lime stone with the volume fraction 0.48 each separately [31]. To prevent excessive compression of particles, the solid close pack volume fraction is set as 0.5. The initial conditions are corresponding to the conditions of the real reactor after heated up with pure nitrogen. The particle normal-to-wall momentum retention coefficient is 0.2 and the tangent–to-wall retention coefficient is 0.99. The time step of $2.0x10^{-4}$s is used. Equivalence ratio (ER), and average relative error (ARE) are referred from the previous literature [32, 33]. For modeling of solid particles the following assumptions have been made as the gas phase species are ideal gas, particles are assumed as isotropic material and the properties change along the radius (for sphere particles) and the solid and gas (inside the particle) are in local thermal equilibrium.

RESULTS

Developing Empirical Relationship

In the present investigation, to correlate the process parameters and the quality of the producer gas, a second order quadratic model was developed. In this study, the RSM provides a quantitative form of relationship between the desired response (Quality of the Producer gas) and the independent input variables (Biomass ratio), Coconut shell (C), Rice husk (R), and Wheat husk (W), and can be expressed as a function, as in Equation (3)

Quality of the Producer gas (Q) = f (C, R, W)..... (3)

The empirical relationship must include the main and interaction effects of all factors and hence the selected polynomial is expressed as follows:

$$Y = bo + \sum bi\ xi + \sum bii\ xi^2 + \sum bij\ xi\ xj \quad \ldots\ldots (4)$$

For three factors, the selected polynomial could be expressed as

Quality of the Producer gas (Q) = { $b_0 + b_1 (C) + b_2 (R) + b_3 (W) + b_{11} (C^2) + b_{22} (R^2) + b_{33} (W^2) + b_{12} (CR) + b_{13}(CW) + b_{23} (RW)$ } ..... (5)

where b_0 is the average of responses () and b_1, b_2, b_3... b_{11}, b_{12}, b_{13}... b_{22}, b_{23}, b_{33}, are the coefficients that depend on their respective main and interaction factors, which are calculated using the expression given below,

$$B_i = (\sum (Xi,Yi)\ )/n \quad \ldots\ldots\ldots\ldots\ldots\ldots\ldots\ldots\ldots\ldots\ldots\ldots\ldots\ldots\ldots\ldots (6)$$

Where 'i' varies from 1 to n, in which Xi the corresponding coded value of a factor and Yi is is the corresponding response output value (Biomass Blend) obtained from the experiment and 'n' is the total number of combination considered. All the coefficients were obtained applying central composite rotatable design matrix including the Design Expert statistical software package. After determining the significant coefficients (at 95% confidence level), the final relationship was developed including only these coefficients. The final empirical relationship obtained by the above procedure to estimate producer gas generation, tar yield and carbon conversion efficiency of biomass blend under fluidized bed gasification is given below;

Gas Efficiency (Silica)

Producer Gas (GE S) = +73.015 -2.546 *(C) -0.528 *(S) -0.397 (W) -4.305 x 10^{-3} *(CS) + 9.277x 10^{-3} (CS) +9.446x 10^{-3} *(SW) + 0.072* (C^2) +3.208x 10^{-3} (S^2) +0.053*(W^2)

Gas Efficiency (Limestone)

Producer Gas (GE L) = +82.768 -2.768*(C) -0.570 *(S) -0.539(W) -5.185x 10^{-3} *(CS) + 0.0126* (CW) +0.013* (SW) + 0.079* (C^2) +3.150x 10^{-3} (S^2) +0.054*(W^2)

Carbon Conversion Efficiency (Silica)

Producer Gas (CCE S) = +90.592 -2.759*(C) -0.557*(S) -0.539(W) -5.185x 10^{-3} *(CS) + 0.0126* (CW) +0.013* (SW) +0.0139* (SW) + 0.078* (C^2) +2.887x 10^{-3} (S^2) +0.052*(W^2)

Carbon Conversion Efficiency (Limestone)

Producer Gas (CCE L) = + 86.722 -2.759*(C) -0.557*(S) -0.539(W) -5.185x 10^{-3} *(CS) + 0.0126*(CW) +0.013*(SW) + 0.078*(C^2) +2.887x 10^3 (S^2) +0.052*(W^2)

Tar yield (Silica)

Producer Gas (TY S) = +14.657 -0.499 *(C) -0.138 *(S) -0.163 (W) -5.342 x 10^{-4} *(CS) -1.236x10^{-3} (CW) + 8.975x 10^{-4} * (SW) + 0.014* (C^2) +1.384x 10^{-3} (S^2) + 0.015* (W^2)

Tar yield (Limestone)

Producer Gas (TY L) = +10.657 - 0.499 *(C) -0.138 *(S) -0.163 (W) -5.342 x 10^{-4} *(CS) -1.236x10^{-3} (CW) +8.975x 10^{-4} * (SW) + 0.014* (C^2) + 1.384x 10^{-3} (S^2) + 0.015* (W^2)

The Analysis of Variance (ANOVA) technique was used to find the significant main and interaction factors. The results of second order response surface model fitting as Analysis of Variance (ANOVA) are given in the Table 5. The determination coefficient (r^2) indicated the goodness of fit for the model. The Model F-value of (CCE_L = 5.76, CCE_S = 5.76, GE_L = 5.88, GE_S = 6.24 , TY_S = 4.66, TY_L = 4.66, implies the model is significant. There is only a 0.01% chance that a "Model F-Value" this large could occur due to noise.

Optimizing the Diffusion Bonding Parameters

In this investigation, the RSM was used to optimize the process parameters for biomass gasification. RSM is a collection of mathematical and statistical techniques that are useful for designing a set of experiments, developing a mathematical model, analyzing for the optimum combination of input parameters, and expressing the values graphically [19]. To obtain the influencing nature and optimized condition of the process on shear strength and bonding strength, the surface and contour plots, which are the indications of possible independence of factors, have been developed for the proposed empirical relation by considering two parameters in the middle level and two parameters in the X- and Y-axes as shown in Fig. 2, 3 and 4 respectively. These response contours can help in the prediction of the response for any zone of the experimental domain [28].The apex of the response plot shows the maximum achievable gas efficiency, carbon conversion efficiency and lowest tar yield.

The gasification behavior of the biomass blends over different combinations of the independent variables is shown through a two-dimensional view of the contour plots. The contour plots are represented as a function of two factors at a time, holding the other factors at a fixed level. All the contour plots revealed that at low and high levels of the variables, the response is minimal; however, it is noted that there existed a region with a color difference, where neither an increasing nor a decreasing trend in the gasification behavior was observed. This phenomenon confirms that there was an optimum for the gasification mixing variables, in order to maximize the gasification capacity. Figure 2 shows the interaction effects of the rice husk and the coconut shell on the gasification behavior of the biomass blends. It is observed that, the stationary point is far outside the region of exploration for fitting the second order model. The contour surface is assumed to be a rising ridge. In this type of ridge system, the least or most number of contours was assumed to be an optimal degree of solution. Elliptical contours exist in the interaction plots for all the gasification tests. It can be seen that an inverse relationship between rice husk and the coconut shell on the gasification behavior of the biomass blends was found in all the plots. Figure 2 shows the effect of rice husk and the coconut shell on the gasification behavior of the biomass blends. It was observed that on increasing rice husk and the coconut shell on the gasification behavior of the biomass blends, the gas efficiency increases. It was authenticated by the fact that the interaction between rice husk and the coconut shell on the gasification behavior of the biomass blends shows an appreciable level of significance. Also it suggested that, the rice husk was more sensitive than coconut shell on the gasification behavior of the biomass blends. Thus, the contour plots, clearly show the effect of gasification behavior of the biomass blends; and independently show that the gas efficiencies increased on increasing rice husk and the coconut shell. Figure 3 shows the interaction effects of the coconut shell and the wheat husk on the gasification behavior of the biomass blends. It shows the wheat husk also played an important role on the gasification behavior of the biomass blends; this was evident from the equation and contour plots. The interaction between the coconut shell and the wheat husk was distorted, which was reflected by the corresponding p-values, but, it was clear that, the wheat husk was more sensitive than the coconut shell. Further, it was seen that, on increasing the wheat husk and coconut shell the gasification behavior increase. Circular contours were found and the optimal value falls at the center of the concentric circles. Fig. 4 shows the effects of the rice husk and the wheat husk on the gasification behavior of the biomass blends. It was observed that the interaction of the rice husk and the wheat

husk was appreciably significant on the gasification behavior of the biomass blends. This was evident from the corresponding p-values, and deduced from the curvature of the contour. It was noted that, on the gasification behavior of the biomass blends especially carbon conversion efficiency decreased with increasing rice husk and with the increment in the wheat husk. The trend observed in the other responses was different as increases with increase in the composition and blends. As an interactive factor, the rice husk is more sensitive than the wheat husk during the gasification.

In order to optimize the process parameters to maximize the gasification efficiency, a combined analysis is done based on their desirability criteria. Desirabilities range from zero to one for any given response. The program combines the individual desirabilities into a single number and then searches for the greatest overall desirability. A value of one represents the ideal case. A zero indicates that one or more responses fall outside desirable limits. A total number of cycles (10 cycles) per optimization were given. This is a complex combination of response surfaces, increasing the number of cycles will give more opportunities to find the optimal solution. The Duplicate solution filter establishes the epsilon (minimum difference) for eliminating duplicate solutions. The program using Design Expert software randomly picks a set of conditions from which to start its search for desirable results. Multiple cycles improve the odds of finding multiple local optimums, some of which will be higher in desirability than others. After grinding through 10 cycles of optimization, the results appear as the most optimal parameters are coconut shell with 26.80%, rice husk with 4.58% and wheat husk with 15.34% with the desirability of 0.70. Fig. 5 shows histogram of desirability is generated for the optimal solution of process parameters found via numerical optimization.

Computational Validation

In order to validate the computational and statistical model and to verify the accuracy of the simulation, the predicted results are compared with experimental data measured further shown in Table 6. It is observed that in the fluidized bed, air was used as the fluidizing agent and introduced into the reactor below the distributor. The system contains four types of particles: silica sand, limestone, carbon and ash. Flow patterns transformation colored with particle volume fraction is shown in Fig. 6. The large bubbles or intense slugs (void structures) form when gas flows up the distributor. The growth can be observed whereas the coalescence and eruption are difficult to identify because of the high gas velocity. Particles gradually move up driven by gas-particle interactions. After t = 0.4 s, the particle profile shows the relatively steady state. The particle volume fraction decreases along the reactor height.

Effect of Coconut shell

Two series of tests have been performed with silica and limestone as bed material. The main difference in both series is the blending ratio (BR) used. As a biomass blend, coconut shell plays a vital role in biomass gasification process. In this present work, though it was an autothermal gasifier, the fuel gas was evaluated at various intermediate coconut shell ratio in the biomass blend until it reached the maximum ratio for a given rice husk and wheat husk. Table shows the experimental data of gas species taken at coconut shell ratio between 0 to 30% of the total blend. It was seen that the calculated values fits good from the experimental data, although the similar trends (increase or decrease) were observed regarding the changes of species concentrations. It is found that with the increase of coconut shell ratio, the carbon conversion efficiency, gas efficiency and tar yield increases. It is noted that for both the bed materials the carbon conversion efficiency, gas efficiency and tar yield increases with the increase in coconut shell ratio. This may be explained with Le Chatelier's principle which states that higher concentration of coconut shell ratio favors the reactants in exothermic reactions and the products in endothermic reaction. Therefore, the endothermic reaction was strengthened with increasing coconut shell ratio, which resulted in more H_2 and less CH_4 concentrations.

It is well-known how the addition of limestones to the bed changes the product distribution in processes of combustion, incineration, gasification, and pyrolysis of biomass. These calcinated solids mainly react with some

contaminants like HCl, SO_2, PAHs, etc., and eliminate them in some extent from the fuel gas. The in-bed use of limestone in biomass gasification seems also to have found commercial application. Many researches [34, 35, 36] used in-bed limestone and dolomite, respectively, for biomass gasification with steam, and in the earlier research [34] dolomite for biomass gasification with air but under pressure. Since there was some lack of knowledge in biomass gasification with air at atmospheric pressure, hence the present research was made for this purpose. All the runs were made with silica and limestone to study the effect of biomass blending ratio on the gas efficiency, carbon conversion efficiency and tar yield. The biomass blends used with the limestone bed materials shows better performance than the silica bed materials. This is due to the low heating value (LHV) of the gas decreases somewhat with lime stone. This is attributed to the in-bed tar elimination reactions which increase the H_2, CO, and CH_4 contents in the producer gas. For the just said reasons, gas yield increases with limestone bed materials. Thus it reduces the tar yield because the rates of the in-bed char elimination reactions (partial oxidation, steam, and dry (CO_2) gasification, etc.) increase on limestone bed materials. As is observed, the carbon conversions of the producer gas with limestone bed materials vary significantly as tabulated in the Table 4. The high reactivity of limestone can be explained by its high initial porosity. Limestone has also earlier been found to behave differently than the other silica under gasification. When comparing the porosity with the reactivity of the sorbents, the higher the porosity, the higher the final conversion. This is in agreement with the work of previous research [37]. Due to the decomposition of CaCO3 to CaO, the porosity of the limestone was increased, thus increasing the conversion rate.

Effect of Rice Husk

Rice husk is a predominant biomass used for the gasification. Table 4 shows both theoretical values and experimental data of gas species taken at rice husk ratio between 0 to 60% of the total blend. The influences of addition of rice clearly demonstrated that, because of the thermal instability of carbon, a higher percentage of rice husk results in a lesser degree of carbon conversion in both silica and limestone bed material. However, the carbon conversion with lime stone as a bed material is comparatively higher than the silica bed materials. Compared to thermodynamic equilibrium the syngas contains less CO. The syngas also contains 1.3% CH_4 which is not predicted at all at equilibrium (~10-4 %). A possible explanation could be that the heterogeneous reactions involved in char gasification are too slow to be completed within the residence time of the reactor at the current gasification conditions. This will thereby result in less CO_2 and CO. The syngas can also have become shifted in the quench, which could also explain differences between the measured syngas composition after the quench compared to the syngas composition at equilibrium. Generally, increasing the rice husk will increase the gas efficiency since the heating value of the produced gas will increase with pressure [38] as a result of CH_4 production through the steam reforming reaction. On the other hand, with silica bed material increasing rice husk will decrease the heating value of produced gas and hence lower the gas efficiency.

In terms of tar yield, with the increase of rice husk, the tar yield increases. On comparing the bed materials, the limestone bed material possesses lesser tar yield. According to the course of the catalytic reaction, the tar needs to be absorbed first by the active sites of the bed material, which is not only affected by the physical properties of the bed material but also by the transfer behavior of the volatiles. In this experiment, calcium oxide was fine and was prone to enter the freeboard, which had no bubbles, with good contact between the bed material and the tar; thus, the tar cracking would be improved. The tar conversion increases apparently as rice husk rises. The addition of rice husk favors the conversion of tar. It is well-known that the polarities of the active site of silica could not affect the π-electron cloud's stability of condensed aromatic compounds in tar, so the addition of silica decelerates the cracking of condensed aromatic compounds and results in the quick decrease of tar yield.

Effect of Wheat husk

Major constituents of wheat husk such as hydrogen, nitrogen, oxygen and minerals such as calcium. It is observed for each gasification trial and are represented in Table 4. The data with the increase of wheat husk, the carbon

conversion efficiency, gas yield increases. High reactivity of biomass causes an increase in volatile matter, which subsequently gets converted to free radicals and therefore improves the decomposition, oxidation and gasification reactions. It is reported that due to both high reactivity and high contents of hydrogen and oxygen in biomass, carbon conversion during co-gasification is greater than other biomass gasification alone and this tends to increase with increasing biomass content in the fuel. It is reported that higher conversion of fuel during co-gasification causes an increase in the gas yield [39]. In the co-gasification, higher gas yield is reported with an increase in wheat husk composition in the fuel as a consequence of higher concentration of hydrocarbons. In earlier research [39], gas yield increases with an increase in biomass ratio due to transfer of hydrogen radicals from biomass that causes more decomposition of fuel. In addition, gas yield reaches to a maximum value when the fuel blend consists of 30% of wheat. This is due to the reaction of oxygen content and carbon content in biomass, CO increases. They also state that by increasing the cracking of tar by means of volatiles present in biomass such asH_2O andH_2 radicals, CH_4 increases. The wheat husk as a biomass plays a key role in the production of tar during co-gasification in comparison with other feedstock components. It is observed that in co-gasification of wheat husk with rice husk with, tar contents are decreased, although it is reported that the structure of tar that is formed is harder than that formed by individual biomass. It is also claimed that the synergetic effects of wheat husk with coconut shell causes a decrease in tar contents during cogasification. It is also observed that the use of high air/fuel ratio with higher contents of biomass during co-gasification, due to which less tar yield is produced. It is further confirmed that tar production in co-gasification of biomass is lower than in the gasification of individual fuels as a result of synergetic effects between both fuels. The investigation of wheat contents in cogasification shows a decrease in tar production, when wheat proportion increases in fuel blends as wheat has less complex structure than biomass [40].

CONCLUSION

1. The present study was focused on the co-gasification of biomass blends in a pilot scale fluidized bed reactor installed in the laboratory. The gasifier was operated at bed temperatures ranging from 750 °C to 950 °C with varying equivalence ratios of 0.35 to investigate the fuel gas compositions.
2. The empirical relation was developed in order to quantify the gas efficiency of fuel gas. This model gave results with high accuracy showing similar trends in predicting the variation of gas species concentrations in line with experimental data.
3. It was noticed that the carbon conversion efficiency, gas efficiency and tar yield increases with the increase in rice husk, wheat husk and coconut shell. However, with the increase of rice husk, the carbon conversion efficiency reduces.
4. On comparing the efficiency of the producer gas, the lime stone bed material shows better performance than the silica bed material.

REFERENCES

1. Bridgwater, A.V.: The technical and economic feasibility of biomass gasification for power generation. Fuel. 74(3), 631–53 (1995).
2. Boateng, A.A., W.P. Walawender, L.T Fan and C.S.Chee : Fluidized bed steam gasification of rice hull. Bio resource Technology. 40(2), 235–9 (1992).
3. Beagle, E.: Rice husk conversion to energy, In Agricultural services bulletin. 31. Rome, Italy. FAO (1978).
4. Luan, T.C. and T.C. Chou: Recovery of silica from the gasification of rice husks/coal in the presence of a pilot flame in a modified fluidized bed. Ind Eng Chem Res. 29 (9). 1922-1927 (1990).
5. Ghaly, A.E., A.M. Al-Taweel and Mackay: GDM project report renewable energy division. Canada, Ottawa, Ontario: Energy Mines and Resources; 1986.
6. Schimmoller, B.K.: Coal gasification striking while the iron is hot. Power Eng. 30–40 (2005).

7. Jones J. M., M.Kubaki, K.Kubica K., A.B. Ross and A.Williams: Devolatilization characteristics of coal and biomass blends. J. Anal. Appl. Pyrolysis, 74, 502−511 (2005).
8. Rizkiana, J., G. Guan, W.B.Widayatno, X. Hao X. Li, W. Huang and A. Abudula: Promoting effect of various biomass ashes on the steam gasification of low-rank coal. Appl. Energy, 133, 282–288 (2014).
9. Hernandez, J.J., G. Aranda-Almansa and C.Serrano: Co-gasification of biomass wastes and coal–coke blends in an entrained flow gasifier: An experimental study. Energy Fuels, 24, 2479–2488 (2010).
10. Peter, M.K.: Energy production from biomass (part 2): Conversion Technologies. Bioresource Technology, 83 (1) 47–54 (2002).
11. Sims, REH: Bioenergy to mitigate for climate change and meet the needs of society, the economy and the environment. Mitigation and Adoption Strategies for Global Change, 8: 349–370 (2003.).
12. Ahmed, T.Y., Ahmad, M.M., Yusup, S., Inayat, A., Khan, Z., 2012. Mathematical and computational approaches for design of biomass gasification for hydrogen production: A review. Renewable and Sustainable Energy Reviews 16, 2304–2315.
13. Lin, C.L., M.L. Wey and S.D. You: The effect of particle size distribution on minimum fluidization velocity at high temperature. Powder Technol.126, 297–301(2002).
14. Natarajan, E., A. Nordin and A.N.Rao: Overview of combustion and gasification of ricehusk in fluidized bed reactors. Biomass Bioenergy. 14(5/6), 533–46 (1998).
15. Hartiniati, A., A.Soemardjo and M.Youvial: Performance of a pilot scale fluidized bedgasifier fuelled by rice husks. In: Proceedings of international conference onpyrolysis and gasification, 257–63 (1989).
16. Bin ZainalAlauddin, Z.A., L. Pooya, M. Mohammadi and A.R. Mohamed: Gasification of lignocellulosic biomass in fluidized beds for renewable energy development. Areview.Renewable and Sustainable Energy Reviews 14, 2852–2862 (2010).
17. Mansaray, K.G., A.E. Ghaly, A.M. Al-Taweel, F. Hamdullahpur and Ugursal : Air gasification of rice husk in a dual distributor type fluidised bed gasifier. Biomass Bioenergy. 17, 315–332 (1999).
18. Simin Shabani, MojtabaAghajani Delavar and Mohammadreza Azmi : Investigation of biomass gasification hydrogen and electricity co-production with carbon dioxide capture and storage, international jornal of hydrogen energy 38, 3630-3639 (2013),
19. Koc, R., N.K. Kazantzis and Y. Hua Ma: A process dynamic modeling and control framework for performance assessment of Pd/ alloy-based membrane reactors used in hydrogenproduction. Int J Hydrogen Energy 36, 4934-51.(2011)
20. Mathieu, P. and R. Dubuisson: Performance analysis of a biomass gasifier. Energy Convers. Manage. 43, 1291–1299 (2002).
21. Lin, C.L., M.L. Wey and S.D. You: The effect of particle size distribution onminimum fluidization velocity at high temperature. Powder Technol. 126 (2002), 297–301.
22. Drift, A.V., J. Doorn and J.W. Vermeulen: Ten residual biomass fuels for circulating fluidized-bed gasification. Biomass Bioenergy 20, 45–56 (2009).
23. Luoa, S., B. Xiao, Z. Hua, S. Liua, Y. Guana and L. Caia : Influence of particle size on pyrolysis and gasification performance of municipal solid waste in a fixedbed reactor. Bioresour Technol.101(16), 6517–6520 (2010).
24. Susana Martı´nez-Lera and Jose´ TorricoJavier Pallare´s Antonia Gil: Design and first experimental results of a bubbling fluidized bedfor air gasification of plastic waste, J Mater Cycles Waste Manag. 15, 370–380(2013)
25. Risberg M., Ohrman O.G.W., Gebart B.R., Nilsson P.T., Gudmundsson A. and Sanati M. Influence from fuel type on the performance of an air-blown cyclone gasifier, Fuel 116, 751–759 (2014).
26. Mansaray, K.G., A.E. Ghaly, A.M Al-Taweel, F. Hamdullahpur and V. Ugursal: Air gasification of rice husk in a dual distributor type fluidized bed gasifier. Biomass Bioenergy.17, 315–32 (1999).
27. Kaupp Albrecht : Gasification of rice hulls. Theory and practices. Deutsches Zentrum Fuer Entwicklungs Technologien (GATE): Eschborn; (1984).
28. Schiefelbein, G.F.: Biomass thermal gasification research, recent results – UnitedStates DOE's research program. Biomass 19, 145–59 (1989).

29. Bin Zainal Alauddin Z.A., L. Pooya, M. Mohammadi and A.R. Mohamed: Gasification of lignocellulosic biomass in fluidized beds for renewable energy development, Renewable and Sustainable Energy Reviews 14, 2852–2862 (2010).
30. Kurkela, E.; P. Stahlberg: Air Gasification of Peat, Wood and Brown Coal in Pressurised Fluidized Bed Reactor. I. Carbon Conversion, Gas Yield, and Tar Formation. Fuel Process. Technol. 31, 1-21 (1992)
31. Wang, X.F., Jin, B.S., Zhong, W.Q., 2009. Three-dimensional simulation of fluidized bed coal gasification. Chemical Engineering and Processing 48, 695–705.
32. Buragohain, B., Mahanta, P., Moholkar, V.S., 2012. Performance correlations for biomass gasifiers using semi-equilibrium non-stoichiometric thermodynamic models. International Journal of Energy Research 36, 590–618.
33. Nikoo, M.B., Mahinpey, N., 2008. Simulation of biomass gasification in fluidized bed reactor using ASPEN PLUS. Biomass and Bioenergy 32, 1245–1254
34. Corella, J., M. P Aznar, J. Delgado, E. Aldea and P. Martı´nez, : Fuel and Useful Gas by Steam Gasification of Biomass in Fluidized Bed Followed by Tar Cracking Fluidized Bed of Dolomite/ Limestone/ Magnesite. In Biomass for Energy Industry and Environment (6th EC Conference); Grassi, G., et al., Eds.; Elsevier Applied Science: London, pp 714-721 (1992).
35. Walawender, W. P., D. Hoveland and L. T. Fan : Steam Gasification of Alpha Cellulose in a Fluid Bed Reactor. In Fundamentals of Thermochemical Biomass Conversion; Overend, R. P., et al., Eds.; Elsevier Applied Science: London; pp 897-910 (1985).
36. Illerup, J. B., K.Dam-Johansen and Lunden, K; High-Temperature Reaction between Sulfur Dioxide and Limestone-VI. The Influence of High Pressure. Chem. Eng. Sci., 48, 2151-2157 (1993).
37. Mathieu, P. and R.Dubuisson : Performance analysis of a biomass gasifier. Energy Convers. Manage..Eqivalent ratio & Feed rate. 43, 1291–1299 (2002).
38. Fermoso, J, B. Arias, M.V. Gil, M.G. Plaza, C. Pevida and JJ Pis :. Cogasification of different rank coals with biomass and petroleum coke in a high-pressure reactor for H2-rich gas production. Bioresource Technol 101(9):3230-5 (2010).
39. Seo, M.W., J.H. Goo, S.D. Kim, S.H. Lee and Y.C. Choi:. Gasification characteristics of coal/biomass blend in a dual circulating fluidized bed reactor. Energy Fuel; 24:108-18 (2010).
40. Collot, A.G, Y. Zhuo, D.R. Dugwell and R. Kandiyoti Co-pyrolysis and co-gasification of coal and biomass in bench-scale fixed-bed and fluidised bed reactors. Fuel; 78(6):667-79 (1999).

Table 1.Ultimate and proximate analysis

Ultimate Analysis				Proximate Analysis			
Components	Percent			Component	Percent		
	Coconut Shell	Rice Husk	Wheat Husk		Coconut Shell	Rice Husk	Wheat Husk
Carbon	53.73	50.48	40.1	Volatile matter	72.93	70.60	84.1
Hydrogen	6.15	6.51	6.4	Fixed carbon	19.48	2.97	5.68
Sulphur	0.02	0.20	0.36	Moisture	6.98	9.45	9.92
Nitrogen	0.86	1.49	1.35	Ash	0.61	17.09	1.63
Oxygen	38.45	41.40	51.79	Calorific Value	20.88	19.81	17.94

Table 2. Design and operating features of Fluidized Bed Gasifier

Parameters	Range
Type of gasifier	Fluidized Bed Gasifier
Geometrical parameters	Diameter (Inner) : 108 mm Total height : 1400 mm
Heating Type	External electric heating
Cooling medium	Water
Feedstock capacity	5-20 kg / h (depending on the type of fuel)
Feeding equipment	Screw feeder
Gasifying agents	Air&Steam
Operating temperature	650-950 ºC
Heating rate	1-60°C/min
Main process variables	Bed Temperature, Pressure, Feed rate, Equivalence ratio and Particle size.
Fuel gas treatments	Cyclone, Water scrubber, Dry filter

Table 3.Important factors and their levels

Factors	Units	Notation	Factors levels				
	%		-1.682	-1	0	+1	+1.682
Coconut Shell		C	0	6	15	24	30
Rice Husk		R	0	12	30	48	60
Wheat Husk		F	0	5	12.5	20	25

Table 4 Experimental Results

EX. No	Coco nut Shell (%)	Rice husk (%)	Wheat husk (%)	Carbon Conversion Efficiency-Silica (%)	Carbon Conversion Efficiency-Limestone (%)	Gas Efficiency Silica (%)	Gas Efficiency Limestone (%)	Tar Yield Silica (%)	Tar Yield Limestone (%)
1	6	12	5	64.55	69.78	53.34	61.66	11.476	7.956
2	24	12	5	50.15	55.38	40.48	47.76	8.596	5.076
3	6	48	5	55.87	61.1	46.75	52.98	9.74	6.22
4	24	48	5	36.21	41.44	28.04	33.82	7.808	4.288
5	6	12	20	79.97	85.2	70.83	77.08	14.56	11.04
6	24	12	20	66.97	72.2	57.32	64.58	11.96	8.44
7	6	48	20	76.71	81.94	66.14	73.82	13.908	10.388
8	24	48	20	62.37	67.6	53	59.98	11.04	7.52
9	0	30	12.5	66.87	72.1	56.16	63.98	11.94	8.42
10	30	30	12.5	75.07	80.3	63.76	72.68	13.58	10.06
11	15	0	12.5	67.67	72.9	58.55	64.78	12.1	8.58
12	15	60	12.5	43.97	49.2	34.35	41.58	9.36	5.84
13	15	30	0	43.17	48.4	34.02	40.28	9.2	5.68
14	15	30	25	79.77	85	69.92	77.38	14.52	11

15	15	30	12.5	50.77	56	41.58	47.88	8.72	5.2
16	15	30	12.5	61.77	67	50.56	58.88	10.92	7.4
17	15	30	12.5	50.77	56	42.76	47.88	8.72	5.2
18	15	30	12.5	52.77	58	42.6	49.88	9.12	5.6
19	15	30	12.5	48.77	54	38.9	45.88	8.32	4.8
20	15	30	12.5	48.07	53.3	39.9	45.18	8.18	4.66

Table 5.ANOVA Test Results

Source	Carbon Conversion Efficiency (Silica)		Carbon Conversion Efficiency (Limestone)		Gas Efficiency (Silica)		Gas Efficiency (Limestone)		Tar Yield (Silica)		Tar Yield (Limestone)	
	F value	p-value Prob>F	F value	p-value Prob>F	F value	p-value Prob>F	F value	p-value Prob>F	F value	p-value Prob>F	F value	p-value Prob>F
Model	5.68	0.0047	5.76	0.0057	5.88	0.0053	6.24	0.0042	4.66	0.0123	4.27	0.0101
A-Coconut shell	3.08	0.1021	3.23	0.1025	2.91	0.1191	3.39	0.0952	2.29	0.1612	2.11	0.1587
B-Rice husk	6.95	0.0231	7.05	0.0241	7.00	0.0245	7.77	0.0192	3.07	0.1105	3.00	0.1008
C-Wheat husk	25.4	0.0002	28.25	0.0003	29.08	0.0003	31.79	0.0002	21.03	0.0010	19.24	0.0009
AB	0.10	0.7244	0.11	0.7515	0.11	0.7494	0.084	0.7775	0.032	0.8617	0.030	0.8601
AC	0.09	0.7315	0.11	0.7471	0.11	0.7451	0.068	0.7997	0.030	0.8665	0.024	0.7844
BC	0.48	0.4698	0.53	0.4833	0.54	0.4797	0.28	0.6071	0.063	0.8075	0.060	0.8044
A^2	11.01	0.0058	11.04	0.0077	11.54	0.0068	10.87	0.0080	10.68	0.0084	10.01	0.0077
B^2	0.2	0.6078	0.24	0.6376	0.29	0.6040	0.34	0.5743	1.55	0.2421	1.32	0.2358
C^2	2.05	0.1500	2.38	0.1537	2.57	0.1401	2.86	0.1218	5.62	0.0392	4.98	0.0228

Table 6. Validation of Test Results

Description	Coconut Shell (%)	Rice Husk (%)	Wheat Husk (%)	Carbon Conversion Efficiency		Gas Efficiency		Tar Yield		Desira-bility (%)
				(Lime stone) (%)	(Silica) (%)	(Lime stone) (%)	(Silica) (%)	(Limestone) (%)	(Silica) (%)	
RSM	26.8	14.58	15.34	74.07	68.84	66.42	58.62	11.78	8.26	0.68
Test				73.25	67.12	66.11	57.21	11.62	8.01	--
CFD				75.01	68.85	66.72	58	11.66	7.41	--
Max. Error (%)				1.1	2.4	0.4	2.4	1.3	1.9	--

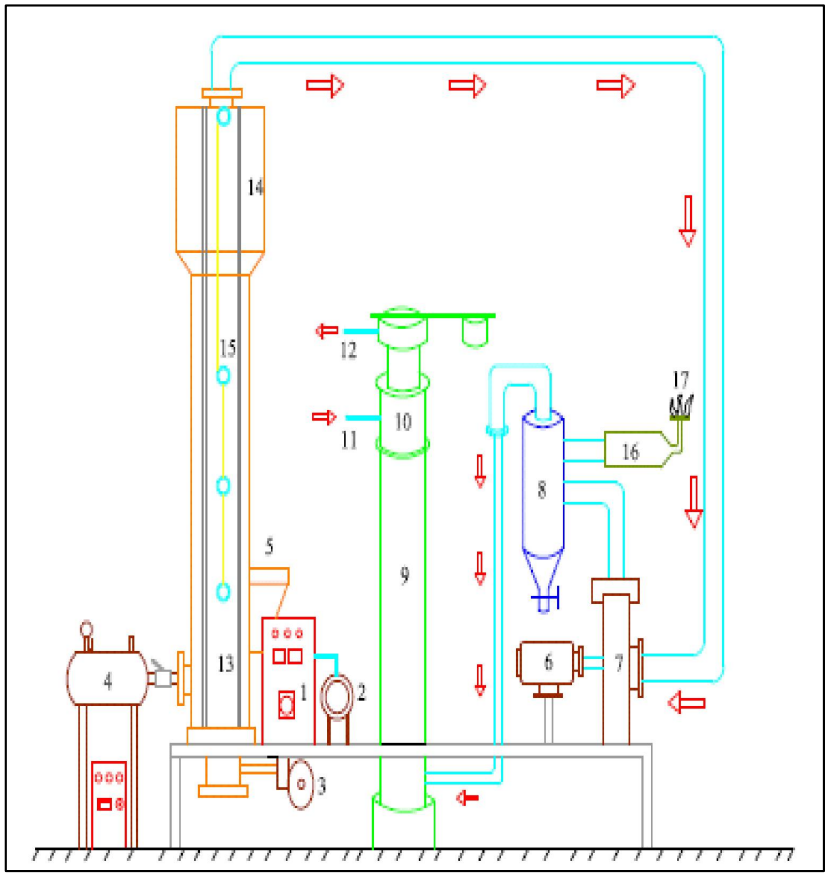

1- control panel; 2- variable displacement drive motor; 3- air blower;
4- steam generator; 5- biomass hopper; 6- blower motor;
7- suction blower; 8- cyclone; 9- water scrubber;
10- dry filter; 11- water inlet; 12- to gas analyser;
13- fluidized bed; 14- free board; 15- thermocouple;
16- burner; 17- flare;

Fig.1.Experimental Setup

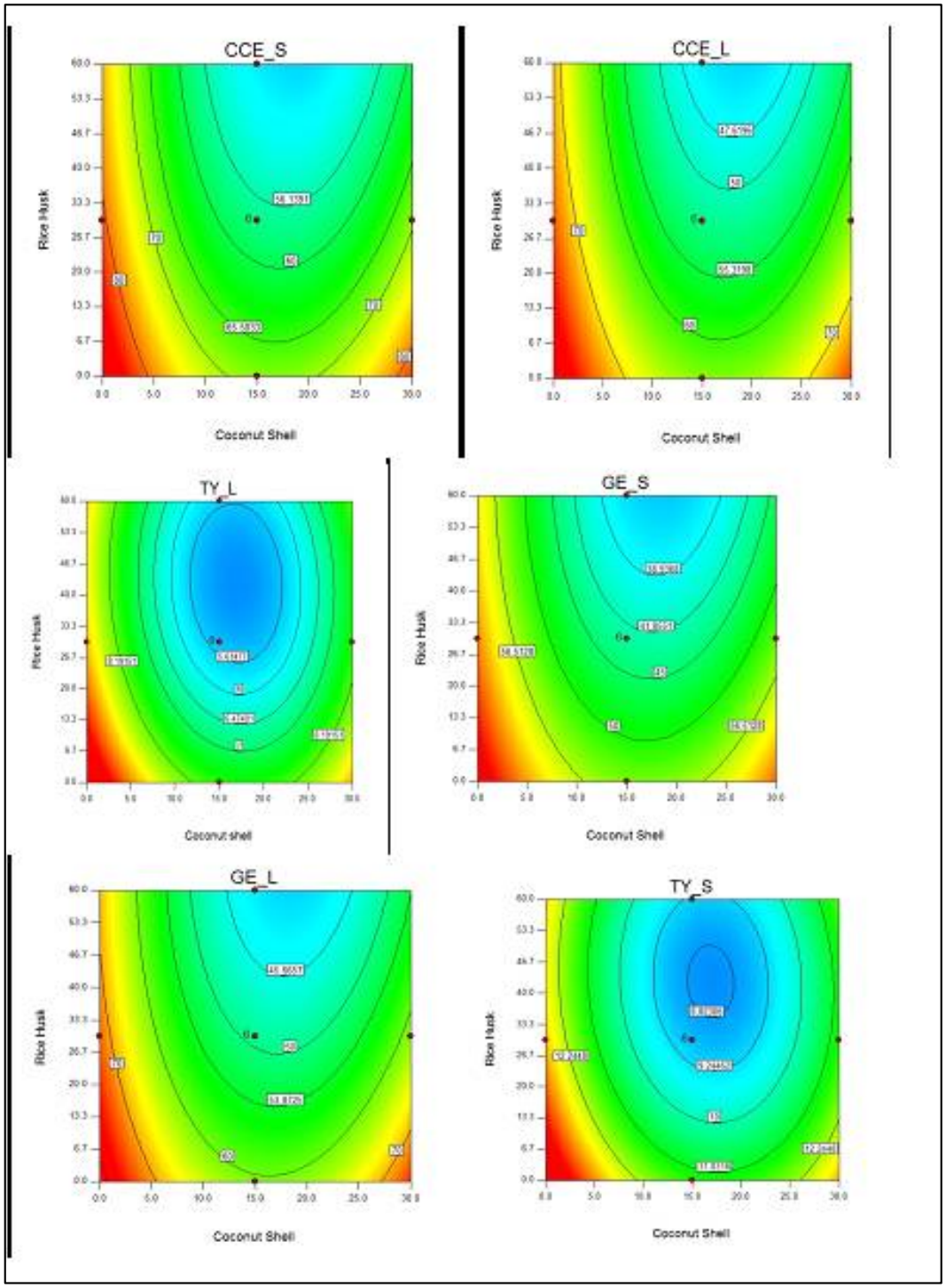

Fig. 2. Response Contour Plots Showing the Effect of Interaction Factors (Coconut Shell & Rice husk)

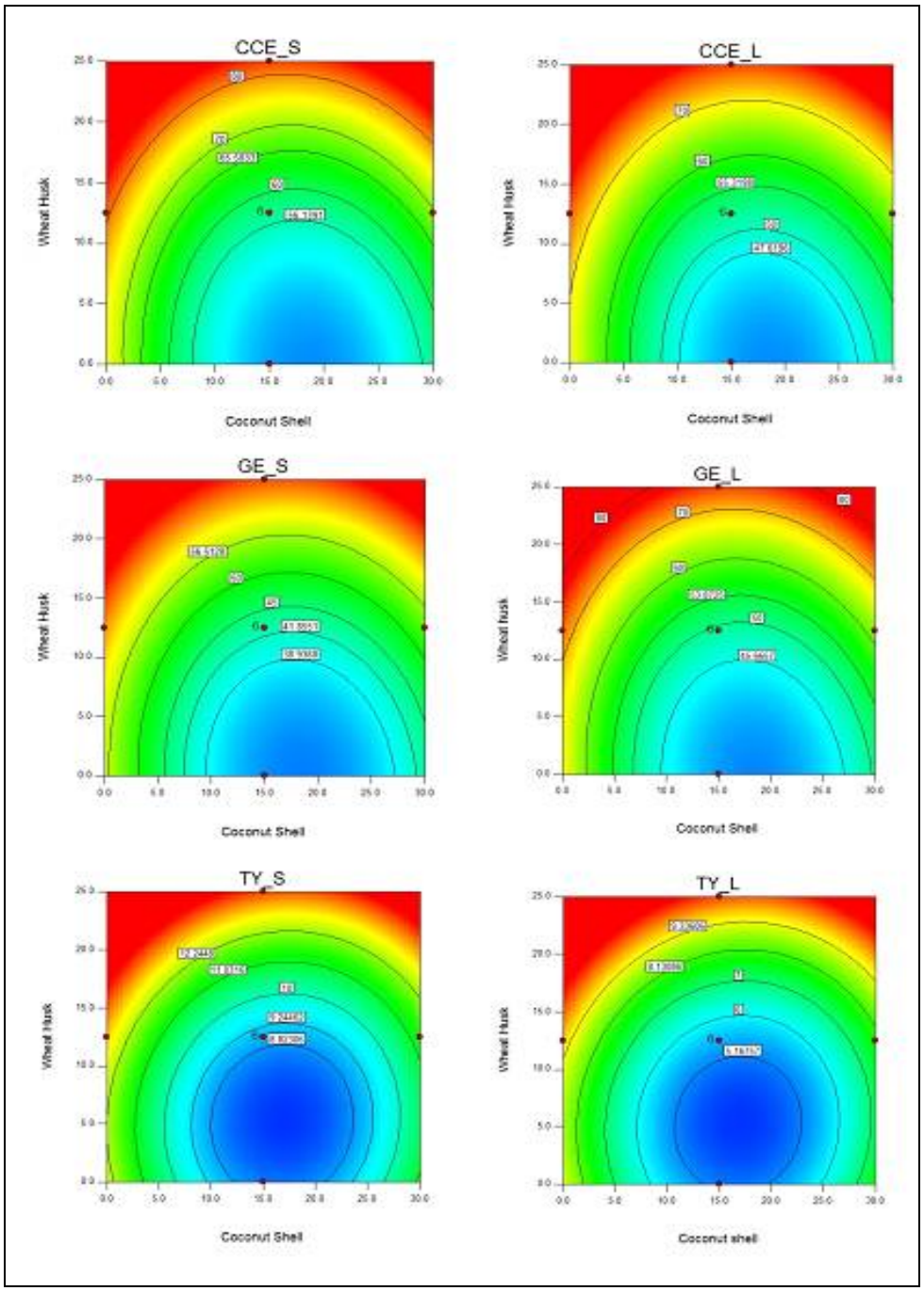

Fig. 3.Response Contour Plots Showing the Effect of Interaction Factors (Coconut Shell & Wheat husk)

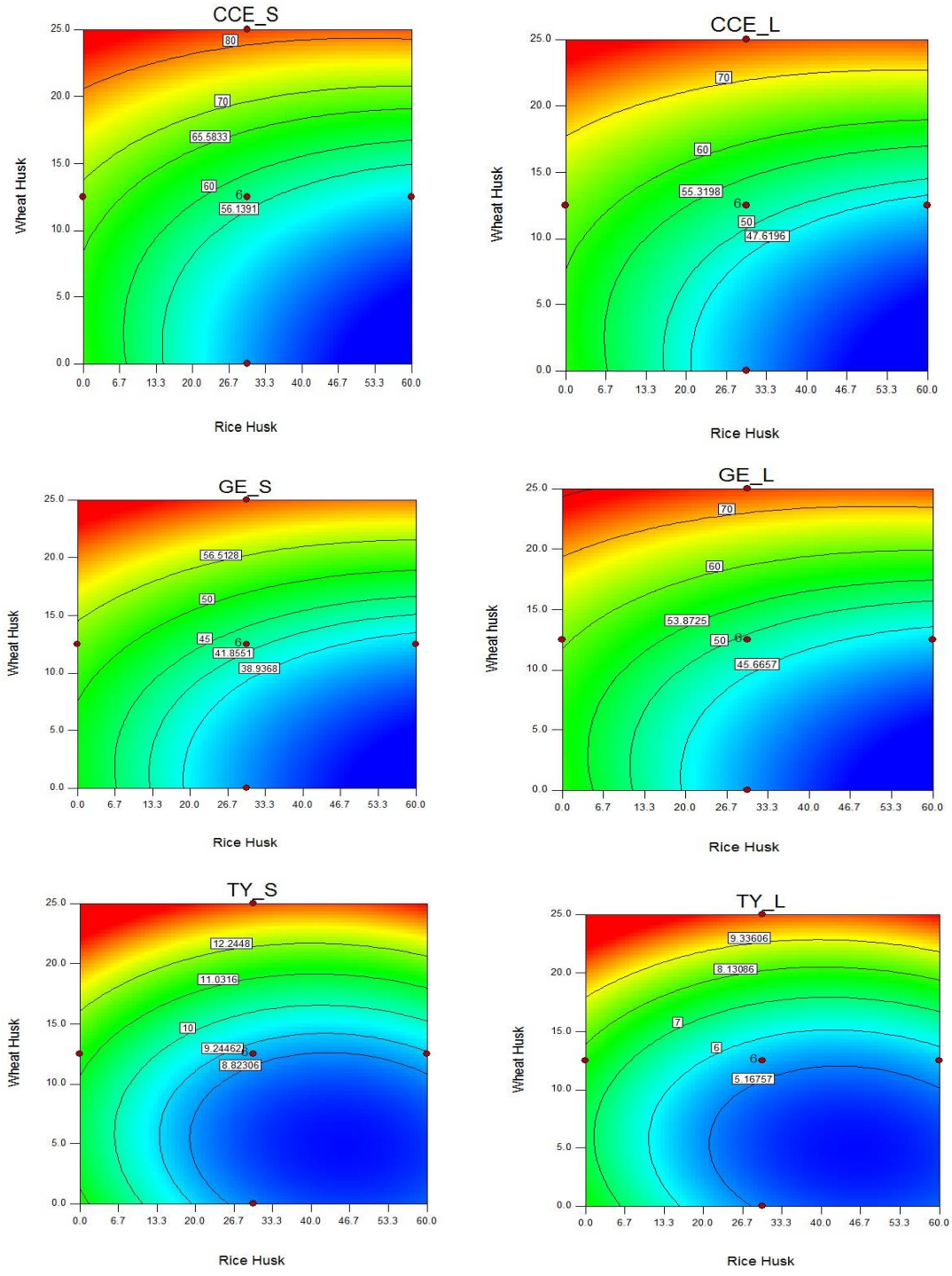

Fig. 4.Response Contour Plots Showing the Effect of Interaction Factors (Rice husk & Wheat husk)

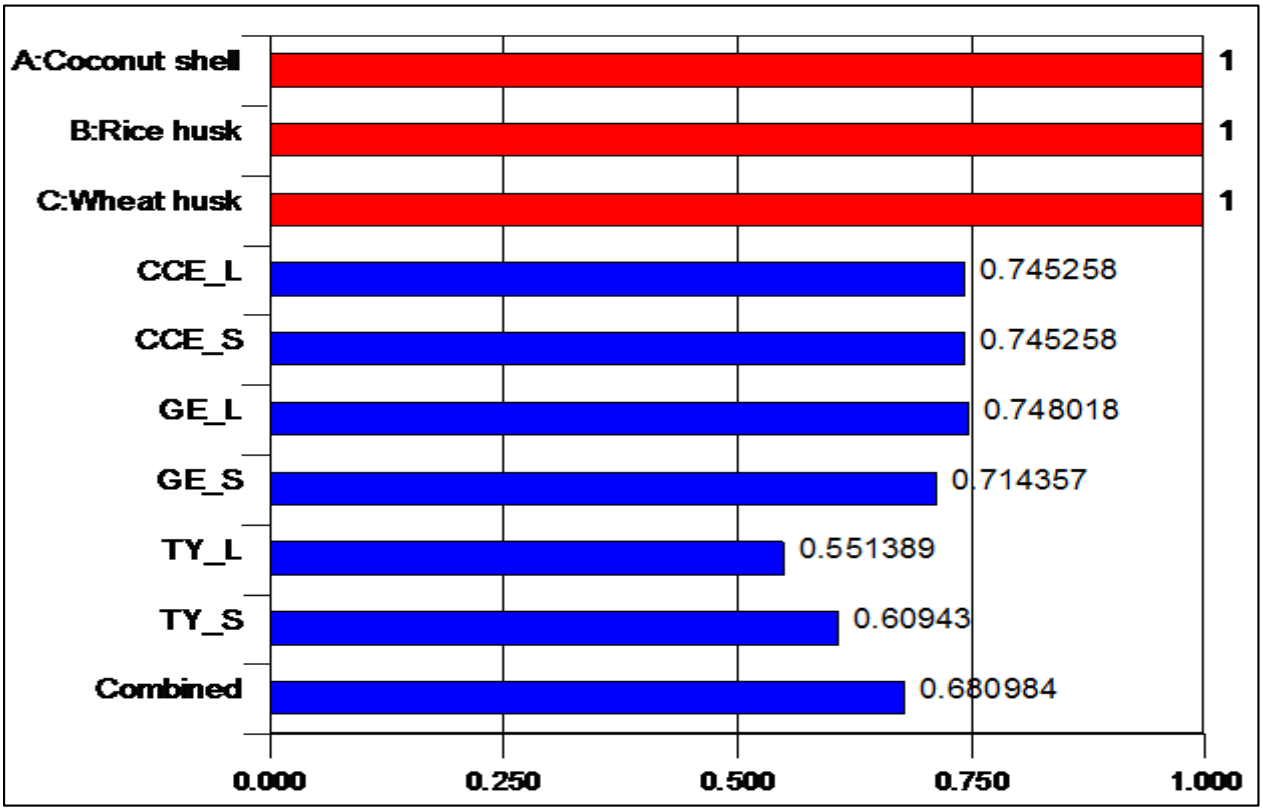

Fig. 5. Desirability for Optimal Solution

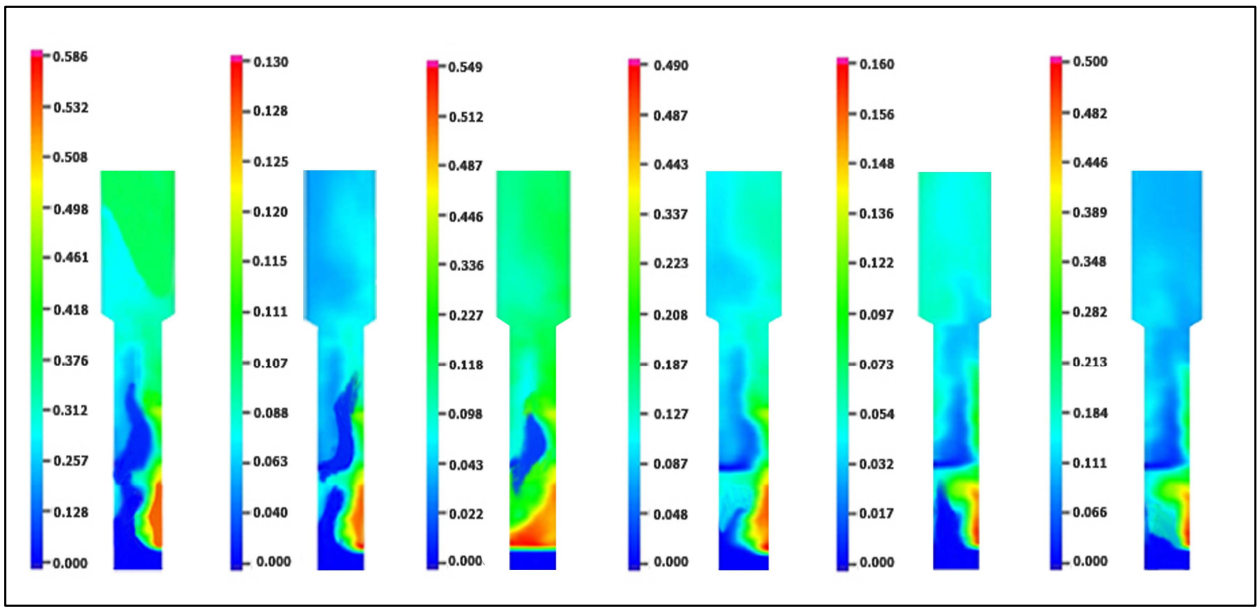

Fig. 6. Flow patterns transformation colored with particle volume fraction

Indian Journal of Natural Sciences www.tnsroindia.org.in ©IJONS

Vol.8 / Issue 45 / December 2017 *International Bimonthly* *ISSN: 0976 – 0997*

RESEARCH ARTICLE

Optical Emission Spectroscopy for Studying Plasma Parameters for Gold Plasma Generated by Exploding Wire in Fe_3O_4 Water Colloidal and Au Decorated Fe_3O_4 Water Colloidal Plasma Generated by Laser Induced Breakdown.

Hammad R. Humud* and Noor K. Fadhil

Department of Physics, College of Science, University of Baghdad, Baghdad, Iraq.

Received: 10 Oct 2017 Revised:22 Oct 2017 Accepted: 06 Nov 2017

*Address for correspondence
Hammad R. Humud
Department of Physics,
University of Baghdad,
Iraq.
E-mail:dr.hammad6000@yahoo.com

ABSTRACT

The aim of this work is studying the plasma parameters for two types of plasma, gold plasma was generated by exploding wire in Fe_3O_4 water colloidal(GP) and Au decorated Fe_3O_4 water colloidal plasma was generated by pulse laser using optical emission spectroscopy. The emission spectra of the gold plasma were generated by exploding wire and Au decorated Fe_3O_4 water colloidal plasma generated by Laser induced breakdown (LIB) have been recorded and analyzed. The plasma electron temperature (T_e) was calculated by Boltzmann plot and the ratio method. The electron density (n_e) was calculated by Stark broadening for exploding wire plasma. It was found that the electron density (n_e) increases from (4.1×10^{17}- 5.5×10^{17}) cm^{-3} and the electron temperature is decreased from 0.868 eV to 0.793 eV with increasing the exploding current from 75 to 160 A and for Au decorated Fe_3O_4 water colloidal plasma generated by LIB it was found that electron density (n_e) increases from (6×0^{17}- 10×10^{17}) cm^{-3} and the electron temperature is decreased from 0.831 eV to 0.824 eV with increasing laser power from 400 to 800 mJ. The electron density n_e and electron temperature T_e are with the same order for the two plasm types, this confirms that the gold plasma generated by exploding wire is identical with plasma produced by LIB.

Keywords: Exploding wire, laser, plasma diagnostic, Boltzmann plot, Plasma parameter.

INTRODUCTION

Optical emission spectroscopy is one of plasma diagnostics technique this technique was used to obtain information about the properties of plasma such as the chemical compositions, temperature and density of electrons [1,2]. Laser Induced Breakdown Spectroscopy (LIBS) is an atomic emission spectroscopy technique can be used to analyze any material regardless of physical state: solid or liquid or gas [3]. LIBS is a diagnostics technique based on the analysis of plasma emission spectral created by a laser beam which focused on a sample surface or sample colloidal [4]. Emission spectrum often consists of a number of characteristic atomic or ionic spectral lines. The electron temperature of plasma was calculated using two methods the first one Boltzmann method which depends on the following relationships

$$\ln\left(\frac{\lambda_{ji} I_{ji}}{hcA_{ji} g_j}\right) = \frac{-1}{KT}(E_j) + \ln\left(\frac{N}{U(T)}\right) \text{ ---------- (1)}$$

The second one was the ratio Method

$$\frac{I_1}{I_2} = \frac{g_1}{g_2}\frac{A_1}{A_2}\frac{\lambda_2}{\lambda_1} e^{[-\left(\frac{E_1 - E_2}{KT}\right)]} \text{ ..... (2)}$$

where λ_{ji} is the wavelength, I_{ji} is the intensity, g_j is the statistical weight and A_{ji} is the transition probability, the transition between states of upper level (j) and lower level (i), respectively. E is the energy of excited state in eV and k is Boltzmann constant.

The subscript 1 and 2 refer to the spectral lines of the same selected element.

The electron density (ne) of plasma was calculated using Stark broadening.

$$n_e(cm^{-3}) = \left(\frac{\Delta\lambda_{1/2}}{2\omega}\right) 10^{16} \text{ ----------(3)}$$

where $\Delta\lambda_{1/2}$ is the FWHM of Stark broadened spectral peak , ω is the electron impact parameter [5].The plasma coupling parameter (Γ) was calculated by

$$\Gamma = \left(\frac{Z^2 e^2}{4\pi\, \varepsilon_0\, a\, K_B\, T}\right) \text{ ---------- (4)}$$

where Z is the charge of the ions (Z=1 for hydrogen ions), ε_0 is the vacuum permittivity, (e) is the elementary charge and (a) mean inter particle distance given by $a = \left(\frac{3}{4\pi n_i}\right)^{1/3}$.

If Γ > 1 the plasma is strongly coupled, if Γ << 1 the plasma is ideal, If Γ< 1 the plasma weakly coupled non-ideal since $\Gamma\ \alpha\ \left(\frac{n^{1/3}}{T}\right)$ [6].

Debye length (λ_D) which calculated by [7]:

$$\lambda_D = \sqrt{\frac{\varepsilon_0 k T_e}{n_e e^2}} \quad \text{----------(5)}$$

plasma frequency which calculated by [8].

$$\omega_{pe} = \sqrt{\frac{e^2 n_e}{\varepsilon_0 m_e}} \quad \text{---------- (6)}$$

m_e is the electron mass.

EXPERIMENTAL PART

The basic circuit for exploding the gold wires is shown in Fig.1. The spectrum emitted from gold plasma generated by exploding wire in Fe_3O_4 water colloidal was recorded by spectrograph. The gold plate and gold wire 21Karats (Karats measure the parts per 24) contains 12.5% of Cu. The emitted spectrum produced by the exploding wire carried by optical fiber to the spectrograph to be analyzed where the spectrograph connected to a computer. The diameter of gold wire is 0.3 mm and 2 cm long. The Fe_3O_4 nanoparticles concentration was 16mg/l with an average particle size 40 nm. 30 cm^3 of the colloidal was placed in a 100 cm^3 container.

Initially the fabricated Au decorated Fe_3O_4 water colloidal by explosion wire technique with a concentration of 16mg/l. The colloids were irradiated by second harmonic Q-switched Nd/YAG laser system was providing pulses of 532 nm wavelength with maximum energy of 1000 mJ per pulse and the pulse width is 10 ns. The laser beams were irradiated the Au decorated Fe_3O_4 colloids after focusing by 15 cm focal length lens. The Au decorated Fe_3O_4 water colloidal was exposed to different laser energy 400, 600 and 800mJ. The optical spectrum emitted from Au decorated Fe_3O_4 water colloidal was carried by optical fiber to be analyzed using a spectrometer connected with a computer to record the data as shown in Fig. 2.

RESULTS AND DISCUSSION

Fig. 3 shows the optical emission spectrum emitted from gold plasma generated by exploding wire in Fe_3O_4 water colloidal with different current 75, 100 and 160 A. It can be noticed that the peaks intensities increase as a result of increasing the current. The electron temperature (T_e) were calculated by Boltzman plot using six of CuI lines 424.90, 427.51, 515.32, 529.25, 570.02, and 578.21nm.

Fig. 4 shows the electron temperature T_e which equal to the 1/slope of fitting line. The fitting equations and the R^2 were shown in this figure for all fitting lines. R^2 is a statistical coefficient indicating the goodness of the linear fit which takes a value between 0 and 1. The better one of R^2 has a value closer to one.

Fig. 5 shows the 656.279 nm hydrogen line peak profile, where full width at half maximum was found using Gaussian fitting to calculate electron density for different samples using Stark effect depending on the standard values of broadening for this line [9].

Fig.5 shows the variation of electron density (n_e) which calculated using Stark broadening effect and electron temperature (T_e) was calculated by Boltzman plot from this figure its notice that the electron density (n_e) increasing from (4.1×10^{17} to 5.5×10^{17})cm^{-3} with increasing current from 75 to 160A, while electron temperature (T_e) was decreasing.

Fig.7 shows the variation of plasma ideality with current, the plasma ideality increases while current was increasing. Its notice that the plasma ideality takes the values 0.199, 0.223 and 0.243 these values are less than 1 so that the plasma is ideal [6].

Table1 shows the calculated electron density (n_e), electron temperature (T_e), plasma frequency (f_p), Debye length (λ_D) and plasma ideality for gold plasma generated by exploding wire in Fe_3O_4 water colloidal at different current, all calculated parameters were satisfied the plasma conditions.

Fig.8 shows the optical emission spectra for Au decorated Fe_3O_4 water colloidal plasma generated by LIB for different laser energies in the spectral range (280- 460)nm.

Fig.9 shows the Gaussian fitting for 656.279 nm hydrogen line (Hα). The full width at half maximum used to calculate electron density for different samples using Stark effect depending on the standard values of broadening for this line [11.12].

Fig.10 shows the electron temperature (T_e) which was calculated by the Ratio Method and the electron density which was calculated by Stark effect. from this Fig it can be notice that the electron temperature decrease from 0.421 to 0.384 eV and the electron density was increase from (6×10^{17} to 10×10^{17}) cm^{-3} with increasing the laser pulse energy from (400-800) mJ.

Fig.11 shows the variation of plasma ideality with three different laser energy 400,600 and 800mJ, the plasma ideality is equal to 0.465, 0.397 and 0.605 for these laser energies. It notices that the plasma ideality values are less than 1 this mean that the plasma is ideal [7].

Table 2 shows the calculated electron density (ne) ,electron temperature (Te), Debye length (λD),plasma frequency (fp) , and plasma ideality (Γ) for Au decorated Fe_3O_4 water colloidal plasma generated by LIB for different laser energies . All calculated parameters were satisfied the plasma conditions.

CONCLUSIONS

Studying plasma parameters for the gold plasma generated by exploding wire in Fe_3O_4 water colloidal and Au decorated Fe_3O_4 water colloidal plasma generated by LIB shows that gold plasma electron temperature decrease while the electron density increases with increasing current, also Au decorated Fe_3O_4 water colloidal plasma behave by the seam meaner with increasing the laser power. The electron density n_e and electron temperature T_e are with the same order for the two plasm types this confirms that the gold plasma was generated by exploding wire is identical with plasma produced by LIB. This makes it possible to say that the gold plasma generated by exploding wire is local thermal equilibrium (LTE) plasma type.

REFERENCES

1. P. Wankhede, P. K. Sharma, and A. K. Jha, "Synthesis of Copper Nanoparticles through Wire Explosion Route" , J. Eng. Res. Appl., Vol. 3, No. 6, pp. 1664–1669, (2013).
2. D. M. Devia, L. V Rodriguez-Restrepo, and E. Restrepo-Parra, "Methods Employed in Optical Emission Spectroscopy Analysis," Eng. Sci., Vol. 11, No. 21, pp. 239–267, (2015).
3. Xi Jiang, "Dual-Pulse Laser Induced Breakdown Spectroscopy in the Vacuum Ultraviolet with Ambient Gas: Spectroscopic Analysis and Optimization of Limit of Detection of Carbon and Sulfur in Steel", Dublin City University, Ph.D. thesis, (2012)

4. M. Simileanu, W. Maracineanu, J. Striber. ,C. Deciu, D. Ene, L. Angheluta R. Radvan, and R. Savastru , "Advanced research technology for art and archaeology – ART4ART mobile laboratory", J. Optoelectron. Adv. Mat. Vol. 10,No. 2, pp.470–473 (2008).
5. H. H. Ley, A. Yahaya and R. K. Raja Ibrahim ,Analytical Methods in Plasma Diagnostic by Optical Emission Spectroscopy: A Tutorial Review ,journal of since and technology , vol. 6, No. 1,(2014)
6. A.Mohmoud, E. Sherbini, A. Aziz, and S. Alaamer, "Measurement of Plasma Parameters in Laser-Induced Breakdown Spectroscopy Using Si-Lines" , World J. Nano Sci. Eng., Vol. 2, pp. 206–212, (2012).
7. A. Descoeudres, Ch. Hollenstein, R. Demellayer and G. walder. " optical emission spectroscopy of electrical discharge maching plasma ", J. Phys. D: Appl. Phys. vol. 37 ,pp. 875–882 ,2004.
8. A. Konies "Basic Plasma Physics, Ch2.", Summer University for Plasma Physics, Max-Planck-institute,(2004).
9. A. Dinklage, T. Klinger, G. Marx and L. Schweikhard "Plasma Physics Confinement, Transport and Collective Effects", Lect. Notes Physics, Springer, Berlin Heidelberg, vol.21, pp.153, (2005).
10. J. E. Sansonetti and W. C. Martin "Handbook of basic atomic spectroscopic Data", J. Phys. Chem. Ref. Data, vol. 34, No. 4, pp. 1559–2259,(2005).
11. A. Lesage, "Experimental Stark Widths and Shifts for Spectral Lines of Neutral and Ionized Atoms", J. Phys. Chem., vol. 31, No. 3, pp. 819–927,(2002).

Table 1: Plasma Parameters for Gold Plasma Generated by Exploding Wire in Fe_3O_4 Water Colloidal for Different Current

Current (A)	T_e (eV)	H_α FWHM (nm)	n_e*10^{17} (cm^{-3})	f_p (Hz) $*10^{12}$	$\lambda_D *10^{-6}$(cm)	plasma ideality
75	0.868	4.100	4.1	5.750	1.081	0.199
100	0.820	4.900	4.9	6.286	0.961	0.223
160	0.783	5.500	5.5	6.660	0.886	0.243

Table 2: Au Decorated Fe_3O_4 water colloidal Plasma Generated by LIB Plasma Parameters for Different Laser Energies

Laser energy (mJ)	T_e (eV)	H? FWHM (nm)	n_e*10^{17} (cm^{-3})	f_p (Hz) $*10^{12}$	?$_D$ $*10^{-6}$(cm)	Plasma ideality
400	0.421	6.000	6.0	6.956	0.062	0.465
600	0.543	8.000	8.0	8.032	0.061	0.397
800	0.384	10.000	10.0	8.980	0.046	0.605

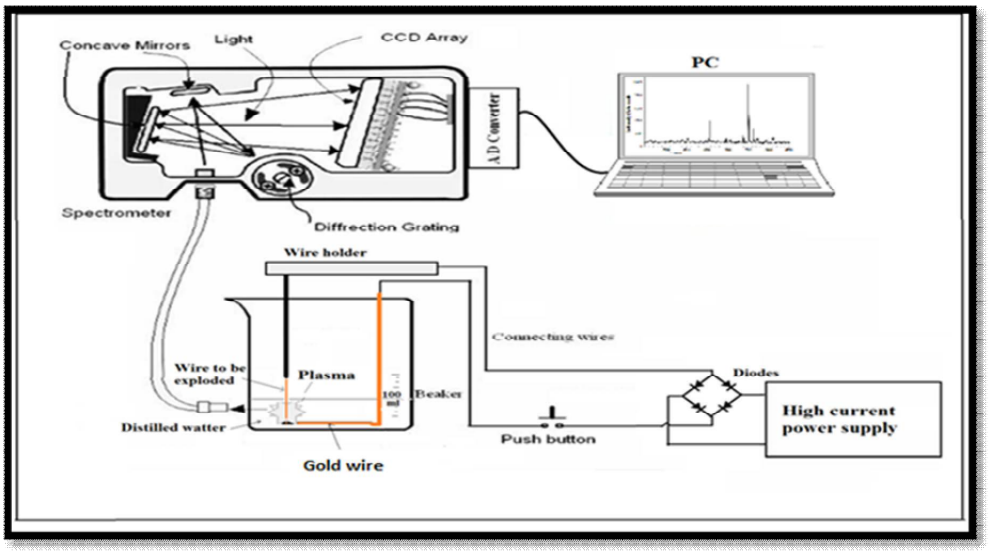

Fig. 1: Schematic Diagram for the Basic Circuit used for the Generation and characterization of the Gold Plasma Generated by Exploding Wire in Fe_3O_4 Water Colloidal

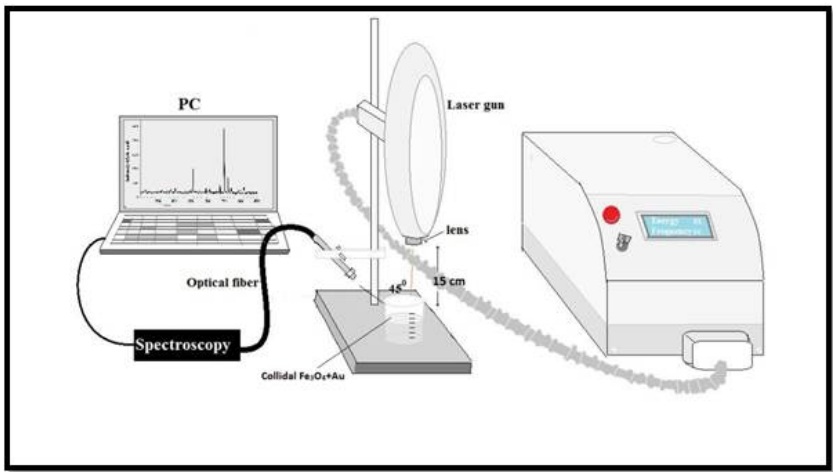

Fig. 2: Schematic Diagram for Au Decorated Fe_3O_4 Colloids Irradiated by Laser

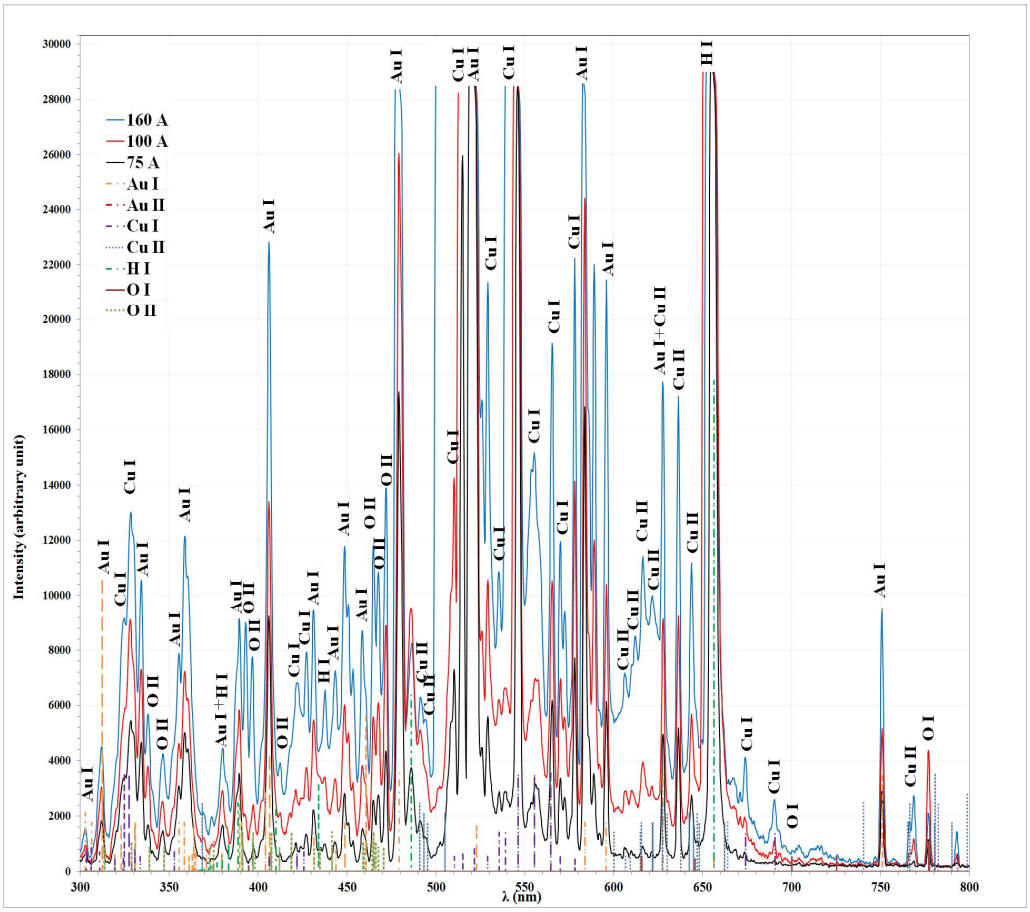

Fig. 3: Optical Emission Spectra from Gold Plasma Generated by Exploding Wire in Fe_3O_4 Water Colloidal.

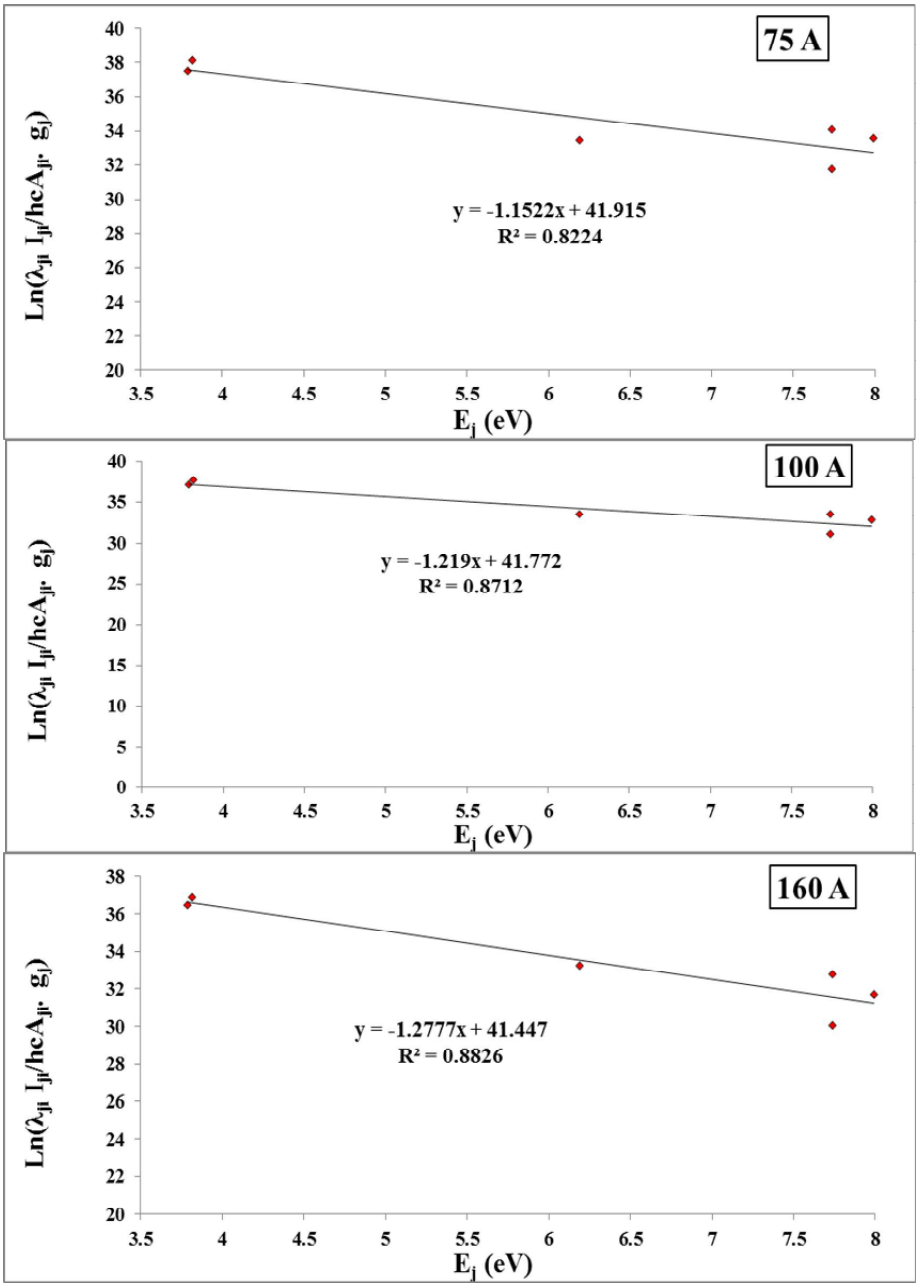

Fig. 4: Boltzmann Plot from the Cui Lines Emitted from Gold Plasma Generated by Exploding Wire in Fe_3O_4 Water Colloidal with Different Current.

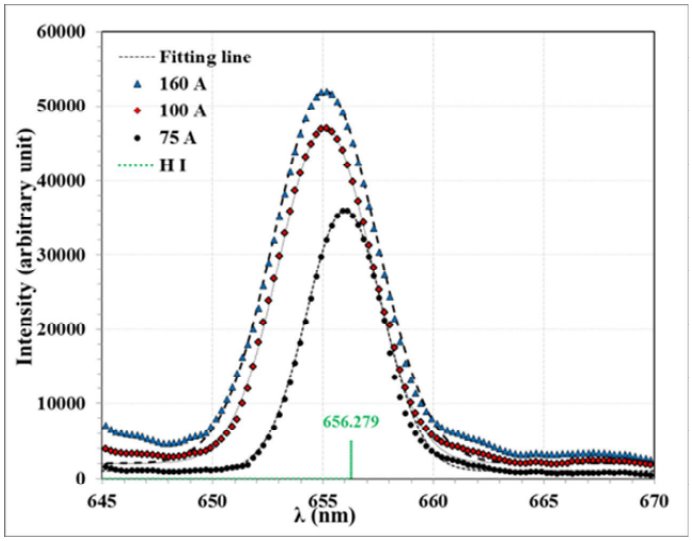

Fig. 5: Hα 656.279 nm Peaks Broadening and There Gaussian Fitting for Different Current.

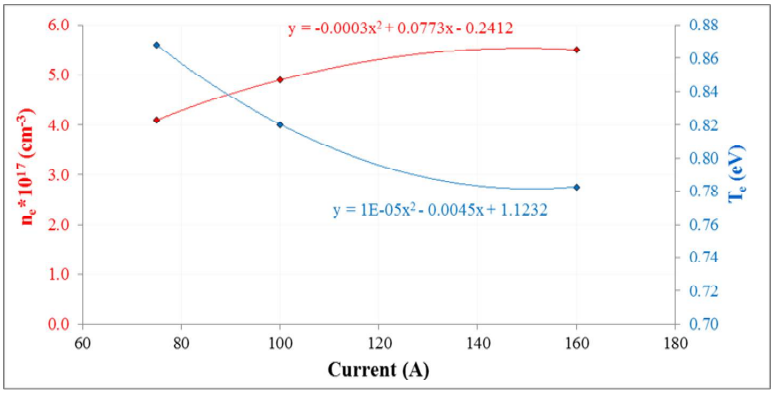

Fig. 6: T_e and N_e for Gold Plasma Generated by Exploding Wire in Fe_3O_4 Water Colloidal

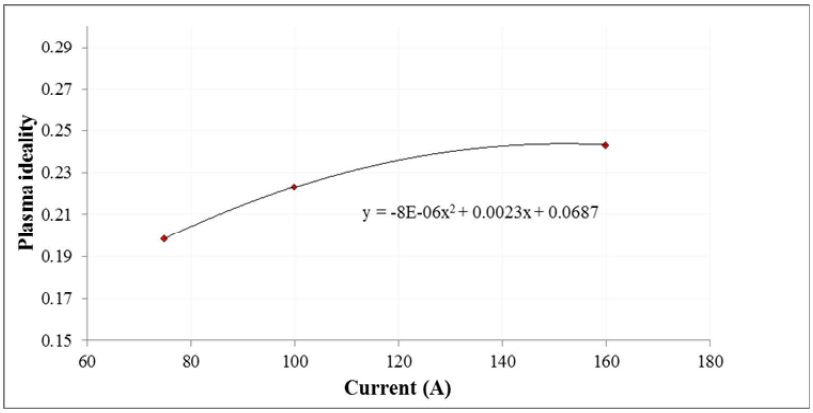

Fig .7: Gold Plasma Generated by Exploding Wire in Fe_3O_4 Water Colloidal Ideality for Different Current

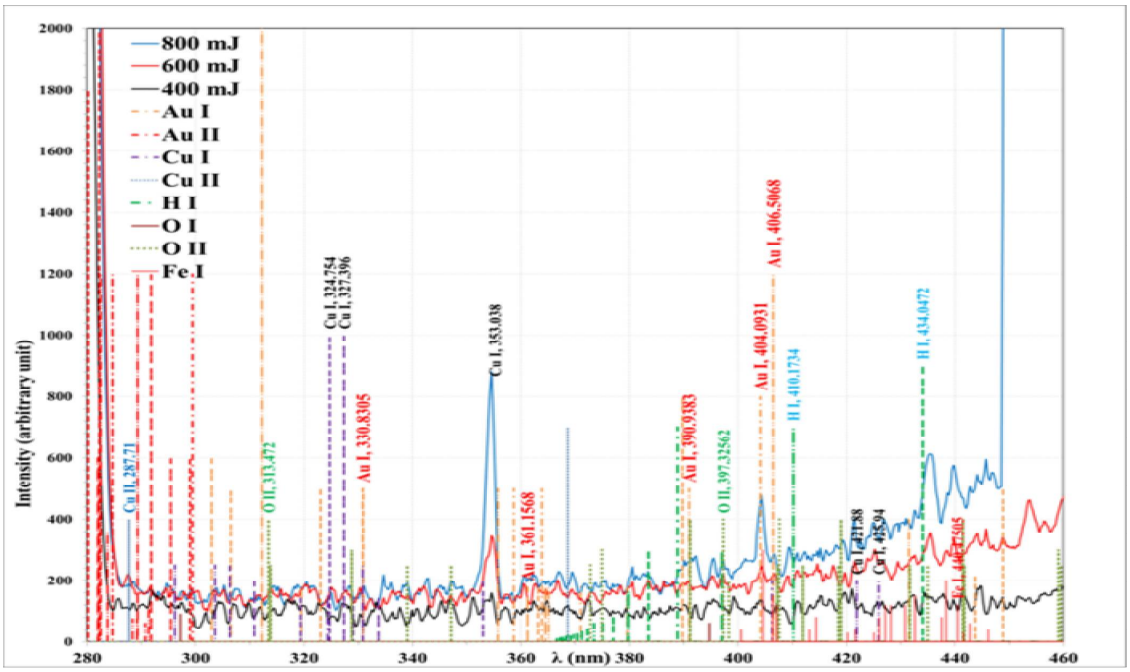

Fig. 8: Emission Spectra for Au Decorated Fe_3O_4 Water Colloidal Plasma Generated by LIB for Different Laser Energies

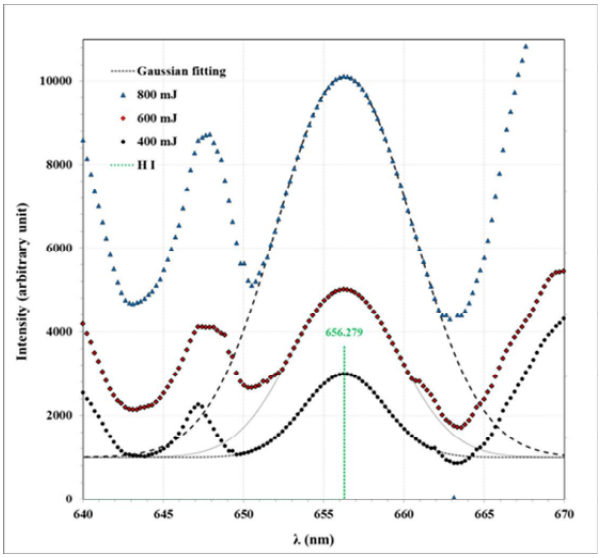

Fig. 9: Hα(656.279 nm) Peaks Broadening and There Gaussian Fitting for Different Laser Energies

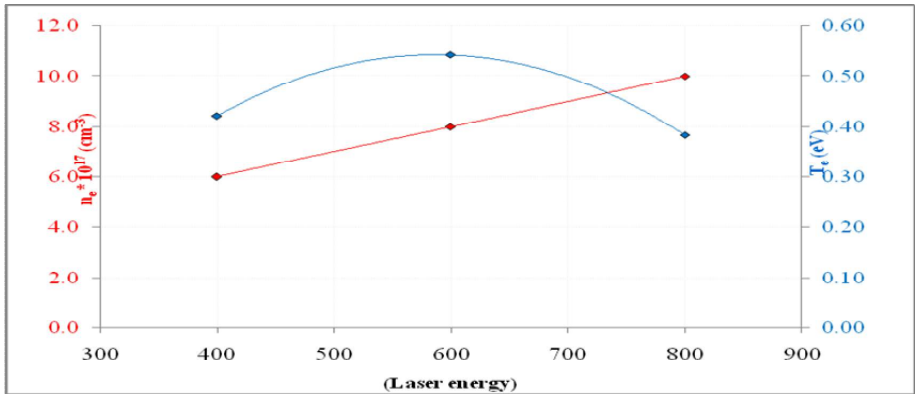

Fig. 10: The Electron Temperature (T_e) and Density (n_e) for Au Decorated Fe_3O_4 Water Colloidal Plasma Generated by LIB for Different Laser Energies

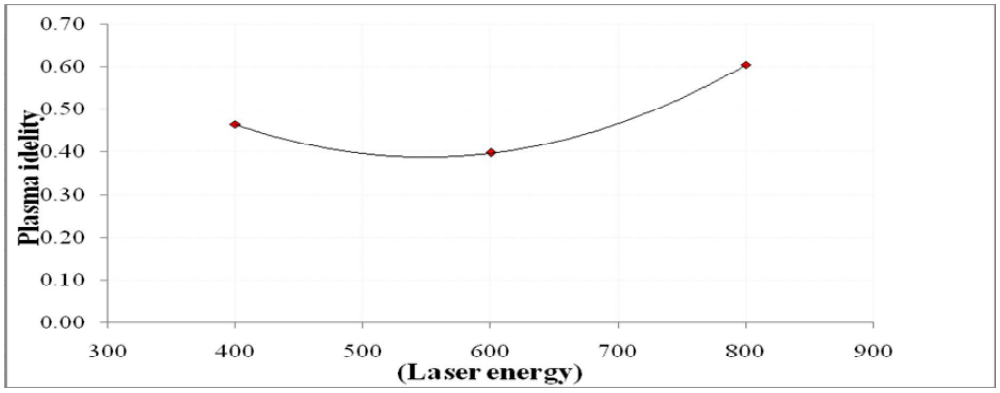

Fig .11:Au Decorated Fe_3O_4 Water Colloidal Plasma Generated by LIB Ideality for Different Laser Energies

Indian Journal of Natural Sciences www.tnsroindia.org.in ©IJONS

Vol.8 / Issue 45 / December 2017 *International Bimonthly* *ISSN: 0976 – 0997*

RESEARCH ARTICLE

Thermal Conductivity of PVA/Rice Starch and PVA/Pistachia (Biodegradable) Blends

Zainab Raheem Muslim[1] and Tamara NabeelJabbar[2]

[1]Department of Physics, College of Science, Baghdad University, Iraq.

Received: 05 Oct 2017 Revised: 18 Oct 2017 Accepted: 08 Nov 2017

*Address for correspondence
Zainab Raheem
Department of Physics,
College of Science, Baghdad University,
Iraq.
Email: ruqia.f.k@gmail.com

ABSTRACT

In this paper, polymer-based on biomaterials is prepared fromPolyvinyl alcohol (PVA)powder PVA polymer blend was prepared & PVA with rice starch ,as well as PVA with plant resin (Pistachia) in different weights usingcasting way .The thermal conductivity of the prepared blends was studied using a Lees'disk. It was observed that by increasing the weight percentage of starch, the thermal conductivity was increased and by increasing the weight percentageof plant resin thermal conductivity was decreased.

Key words: Polyvinyl alcohol(PVA), Thermal conductivity,blends.

INTRODUCTION

The durability properties which make plastics ideal for many applications such as in packaging, building materials and commodities, as well as in hygiene products, can lead to waste-disposal problems in the case of traditional petroleum-derived plastics, as these materials are not readily biodegradable and because of their resistance to microbial degradation, they accumulate in the environment. These facts have helped to stimulate interest in biodegradable polymers and in particular biodegradable biopolymers [1].

Starch is totally biodegradable and is an environmentally friendly material. In addition starch has a low cost. Nevertheless, since starch is highly sensible to water and has relatively poor mechanical properties compared to other petrochemical polymers, its use is limited. A solution may be to blend it with other synthetic polymers. Many biodegradable starch-based thermoplastic blends have been developed and studied extensively. A lot of research work deals with the development of blends of starch with synthetic biodegradable polymers. These blends present several advantages [2, 3].

The material properties can be adjusted to the needs of the application by modifying the composition. The blending process is low cost compared to the cost of the development of new synthetic materials. These kinds of blends are intended to be more biodegradable than traditional synthetic plastics[4].Historically, trunk exudates of Pistachialentiscus(mastic gum) have been used for the treatment of stomach ulcers. Archaeologists in 1982 found a late Bronze Age shipwreck with 100 jars filled with mastic that had been used by the Egyptians for medicinal purposes [5].

The genus Pistachiafrom the Anacardiaceaefamily consists of eleven species of trees found in some Mediterranean countries and in Southern and Central America [6]. Substantial work has been done on characterization of chemical composition of Pistachialentiscusand some other species which are widely spread around the Mediterranean countries as well as the Zagros Mountains and particularly in western and northern Iran and eastern and northern Iraq [7].

THERMAL CONDUCTIVITY

Thermal conduction is the phenomenon by which heat is transported from high to low temperature regions of a substance. The property that characterizes the ability of a material to transfer heat is the thermal conductivity [8].The measurement of thermal conductivity according to "Fourier's law" [9].

$$q = - k \frac{dT}{dx} \quad \ldots\ldots\ldots\ldots\ldots\ldots\ldots (1)$$

Where q denotes the heat flux, or heat flow, per unit time per unit area (area being taken as that perpendicular to the flow direction), k is the thermal conductivity, and dT/dx is the temperature gradient through the conducting medium.

Heat conduction in metallic solids takes place through, both lattice vibrations (phonons) and free electrons. In non-metals since there are no free electrons, the contribution to thermal conduction is only due to the lattice vibrations. Free electrons (due to their high mobility) conduct heat energy more effectively than phonons and hence metals are better conductors of heat than non-metals [10].

$$K ((T_B-T_A)/d_S) = e [T_A + (2/r) (d_A + (1/4) d_S) T_A + (1/2) r d_S T_B] \ldots\ldots\ldots\ldots (2)$$

where (T_A,T_B,T_C) are the temperature degree at each disk A,B,C respectively, (d_s)is thickness of specimens, r is radius of each disks also the specimens (all are of same radius) and e represents the amount of the imposed heat calculated by the following equation:

$$IV = \pi r^2 e (T_A+T_B) + 2\pi r e \left[d_A T_A + d_S \frac{1}{2}(T_A+T_B) + d_B T_B + d_C T_C\right] \ldots\ldots\ldots\ldots (3)$$

Where: I is current through the heater, V is applied voltage and (d_A), (d_B), and (d_C) are the thickness of copper disks A, B and C respectively.

MATERIALS AND METHODS

The polymer used in the study was Elvanol grade HV poly (vinyl alcohol) (PVA)(from DuPont chemicals). The molecular weight is 125,000 (weight average) and the purity 99.9%.

Rice starch (Thai Flower brand) used was obtained from Bangkok Starch Industrial Co. Ltd.Pistachiawere bought from the local market.The granules were ground to powder for 5min in a mill fitted.

Films Preparation

Polyvinyl alcohol (PVA) powder were prepared by dissolving (6g) of PVA powder in 100 mL of distilled water at 80 °C and waiting for PVA to dissolves about 1 hour using magnetic stirrer. Then 50 ml of distilled water was added to 3g of rice starch to prepared solution of PVA/ rice starch blends. And 50 ml ofdistilled water was added to 3g ofPistachiato prepared solution of PVA/Pistachia blends. Finally Mixing (2,3and4)ml of PVAsolution with (4,3and2)ml of rice starch solution and (2,3and4)ml of PVAsolution with (4,3and2)ml of Pistachiasolution then casting the samples in cups and waiting for 3 days to dry.

Results and Discussion

Thermal conductivity of blends materials depends on the thermal conductivity of the filler and matrix and the weight percentage of the filler, Moreover, the filler/matrix interface plays an important role in thermal conductivity of the blends, since the conductance of the heat in non-metallic materials occurs by the flow of polymeric chains vibration energy or phonons, along the temperature gradient in the material, therefore, for a two phase system, interfacial contact between phases is very important, because phonons are very sensitive to surface defects at the interface .
Two types of blends were used; PVA/PR & PVA/RS blends. The results of this test showed that the highest values of thermal conductivity were achieved by increased the ratios of rice starch fillers as shows in figure (4).

This is attributed to the smaller particles size (492.53 nm) , thermal conductivity of these blendsmaterials depend on several factors, first of all on the filler concentration, the ratio between the properties of the components, the size and the shapes of the filler particles .

Small particle size has large surface area, which means large thermal interface resistance. The decrease of the filler size significantly increases the surface-to-volume ratio which in turn increases the phonon scattering at the interfaces.

When the content of filler increases & the particle size increased (1083.10 nm) of the plant resin thethermal conductivity decreased as shows in Figure (5).

Atomic Force Microscopy Test 4.

Surface topology of the Plant resin and Rice starch were studied by Atomic Force microscope (AFM) analysis. The AFM pictures morphology for the surface in the three dimensions is shown in Figures 6 (a,b) and 7 (a, b). The pictures are shown a uniform surface; indicate that the particle has uniform dimensions.Result of the test show that the high distribution of particles size was in 1083.10nm and low distribution was in 492.53.

CONCLUSIONS

Thermal conductivity of PVA/RS was higher than PVA/PR because of the particle size of RS bigger than PR and the increases the phonon scattering at the interfaces.

REFERENCES

1. N. Lucas, C. Bienaime, C. Belloy, M. Queneudec, F. Silvestre, J.E .Nava-Saucedo, “Polymer biodegradation: mechanisms and estimation techniques”, Chemosphere, 73, 429-442, 2008.

2. D. Briassoulis, "An overview on the mechanical behavior of biodegradable agricultural films", J. Poly. Environ. 12, 65-81, 2004.
3. G.Scott,D.Gilead, "Degradable Polymers: Principles and Applications; Chapman and Hall: London", UK; pp. 247-258, 1995.
4. L.Chen, S.Imam, S.Gordon, R.V. Greene, "Starch- polyvinyl alcohol crosslinked film— performance and biodegradation", J. Environ. Polym. Degr., 5, 111-117,1997.
5. S.Thomas, D. Stefanos, E.Chmielewska, W.Chmielewska, Distribution, "Development and Structure of Resin Ducts in Pistachialentiscus" var. chia Duhamel. Flora, *195*, 83-94, 2000.
6. V.P. Papageorgiou,Sagredos, A.N. Moser, R. GLC-MS "Computer Analysis of The Essential Oil of Mastic Gum", Chem. Chron., New Ser. 1981, 10, 119-124. Pharmaceuticals, 110, 2009.
7. M.S. Sharifi,"Fractionation and analysis of trunk exudates from pistacia genus in relation to antimicrobial activity". Ph. D thesis, College of Health and Science, University of Western Sydney, Australia, 2006.
8. W. D. Callister and D. G. Rethwisch," Fundamentals of Materials Science and Engineering: An Integrated Approach", John Wiley and Sons,2012.
9. P. R. Childs, "Practical Temperature Measurement", Butterworth-Heinemann,2001.
10. M. S. Vijaya and G. Rangarajan ", Materials Science", Tata McGraw-Hill publishing company limited, 2003.

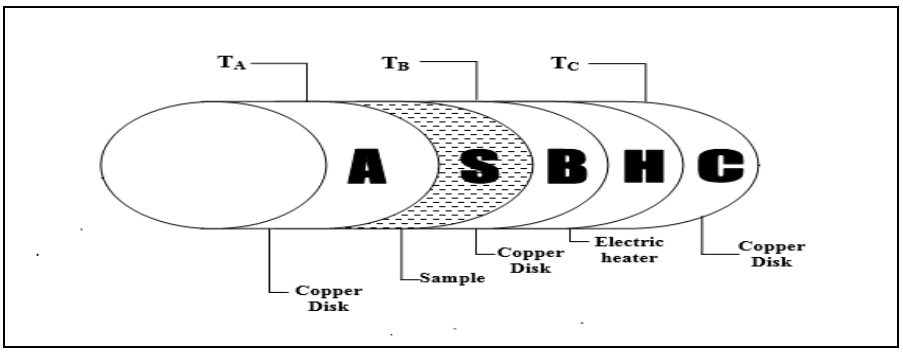

Figure 1: Lee's disk for calculating thermal conductivity.

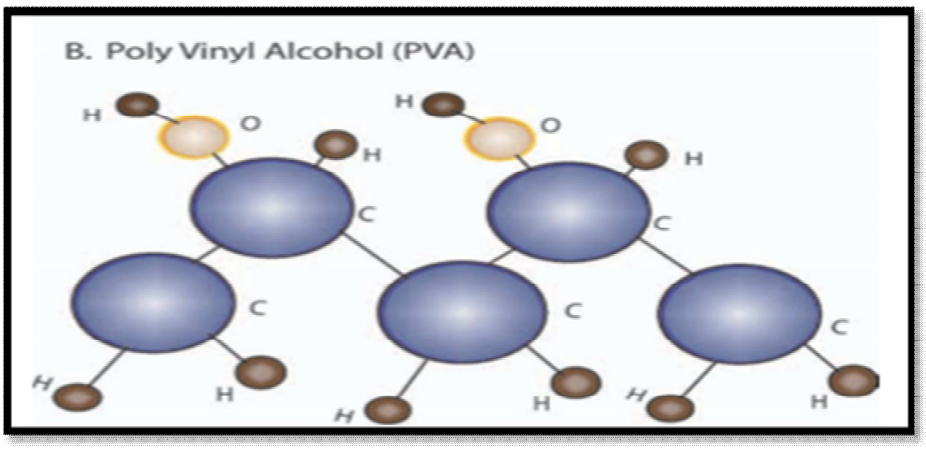

Figure 2: Poly(vinlyalcohol) PVA Structure.

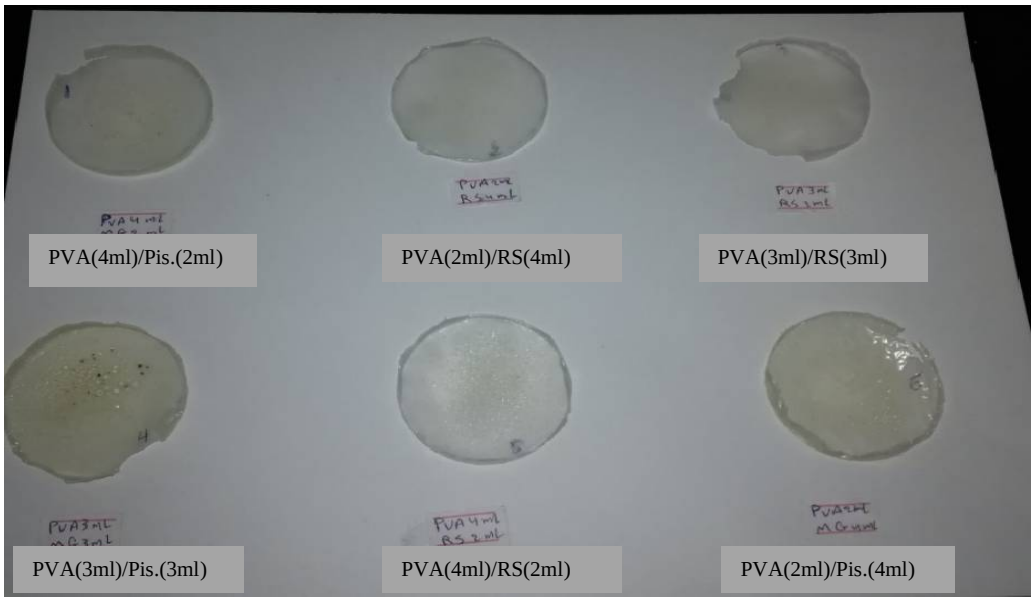

Figure 3:PVA blends

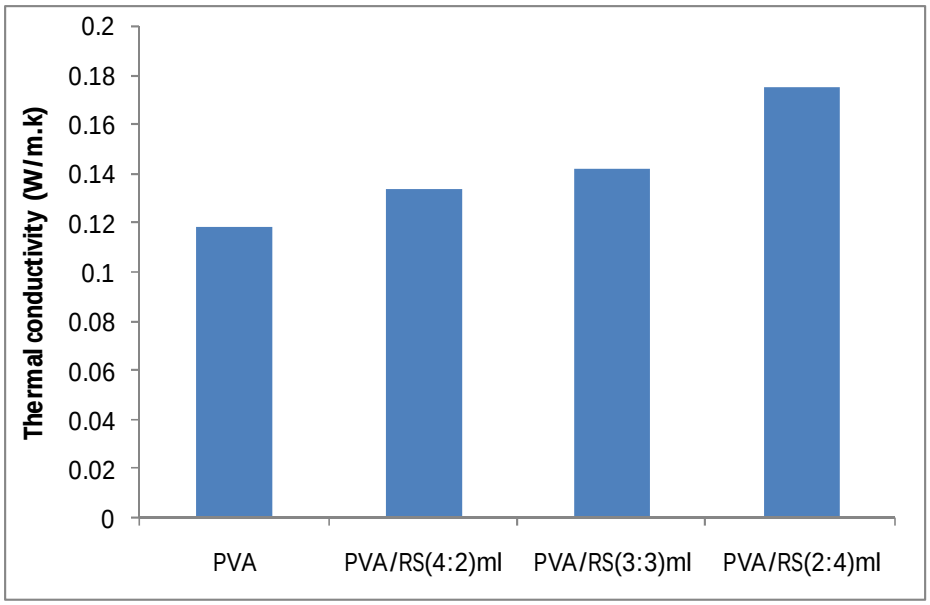

Figure 4: Thermal conductivity of PVA/ rice starch blends

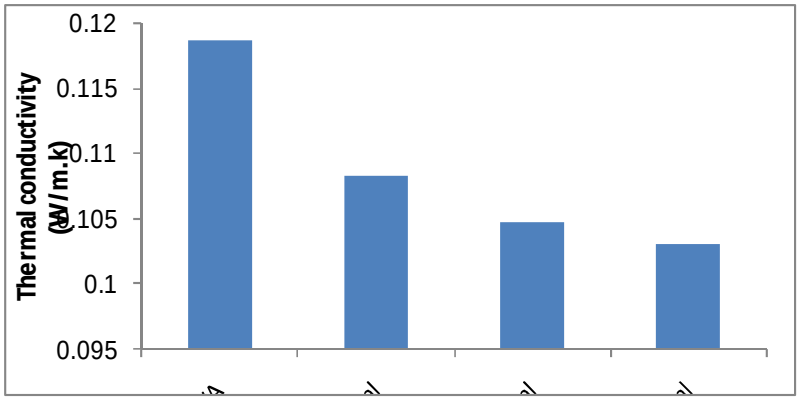

Figure 5: Thermal conductivity of PVA /plant resin blends

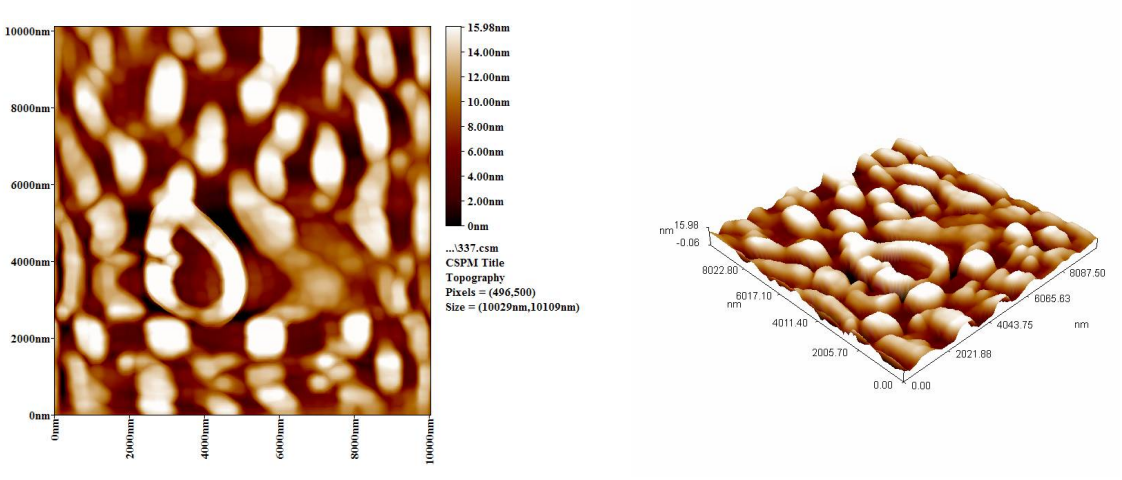

a **b**

Figure 6: (a) and (b) AFM image of Plant resin in 2D and 3D view

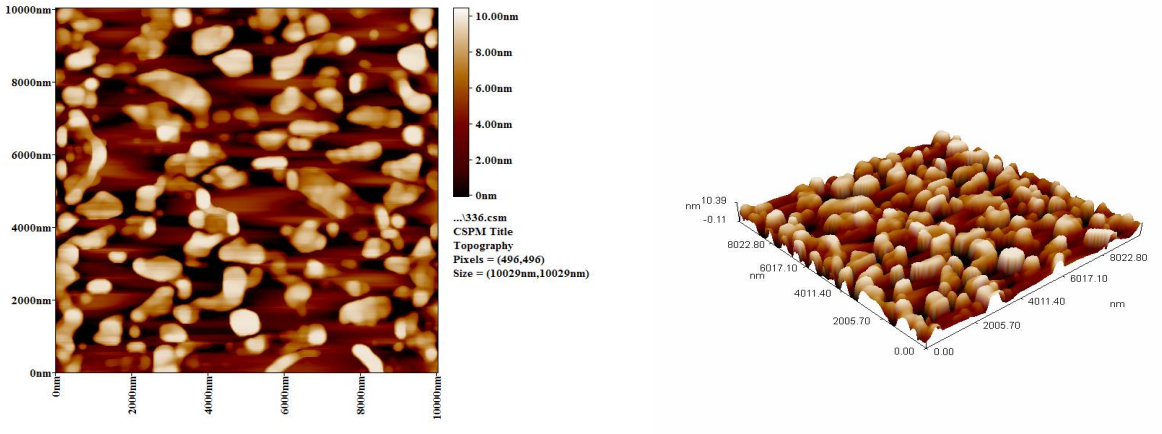

a **b**

Figure 7:(a) and (b) AFM image of Rice starch in 2D and 3D view

Indian Journal of Natural Sciences www.tnsroindia.org.in ©IJONS

Vol.8 / Issue 45 / December 2017 *International Bimonthly* *ISSN: 0976 – 0997*

RESEARCH ARTICLE

Elastic Electron Scattering Form Factors and Density Distributions for ^{21}Ne, ^{23}Na, ^{29}Si and ^{31}P nuclei using Hartree-Fock Calculations

Ahmed N.Abdullah* and Wasan Z. Majeed

Department of Physics, College of Science, University of Baghdad, Baghdad, Iraq.

Received: 20 Sep 2017 Revised: 22 Oct 2017 Accepted: 11 Noc 2017

***Address for correspondence**
Ahmed N. Abdullah
Department of Physics,
College of Science, University of Baghdad,
Iraq.
Email: Ahmednajim@scbaghdad.edu.iq

ABSTRACT

Nuclear structure of ^{21}Ne, ^{23}Na, ^{29}Si and ^{31}P nuclei have been investigated using Hartree Fock (HF) calculations with selected effective nuclear interactions, namely the Skyrme parameterizations SVI, SKB, SGI, SKM*, MSK7, SLY4 and Skxs25 are used. Results of the binding energy and charge, proton, neutron and matter root mean square (rms) radii of these nuclei are studied. The results of rms radii with Skxs25 parameterizations showed good agreement with experimental values, thus this parameterization is used to calculated the charge, proton, neutron and matter density distributions. Good agreement is found with the measured charge density. Besides the elastic charge electron scattering form factors of these nuclei are investigated. The calculated charge form factors almost coincide with the experimental data for all nuclei in the low range of momentum transfer and the deviation occurs at high momentum transfer.

Keywords: Hartree – Fock , electron scattering, rms matter radii, Density Distributions.

INTRODUCTION

The electron scattering from the nucleus at high energy gives important information about the nuclear structure. Information obtained from the high energy electron scattering by the nuclei depends on the magnitude of the de Broglie wave length that is associated with the electron which is compared with the range of the nuclear forces. When the energy of the incident electron is in the range of 100 MeV and more, the de Broglie wave length will be in the range of the spatial extension of the target nucleus. Thus with this energy, the electron represents a best probe to study the nuclear structure [1].

The Hartree-Fock method with an effective interaction with Skyrme forces is widely used for studying the properties of nuclei. this method is successfully used for a wide range of nuclear characteristics such as binding energy, rms charge radii, neutron and proton density, electromagnetic multipole moments, etc. The Hartree-Fock description of

nuclear properties yields good results not only for stable even-even spherical and deformed nuclei, but also for neutron-rich and neutron -deficient nuclei [2]. Alzubadi [3] has been investigated the ground state properties of the sulfur isotopes covering a wide range from the line of stability up to the dripline region ($^{30-44}$S) using . For this purpose, the Hartree–Fock mean field theory in coordinate space with a Skyrme parameterization SkM* has been utilized. Radhi et al., [4] studied inelastic electron scattering form factors, energy levels and transition probabilities for positive and negative low-lying states using shell model and Hartree-Fock calculations. Abdullah [5] has been studied the ground-state properties of some Te-isotopes such as the proton and charge and matter densities, the corresponding root mean square radius, neutron skin thickness and charge form factor using Skyrme–Hartree–Fock method with Skyrme interactions namely; SKB, SGI, SKM, SKX, MSK7 and SLy4. The calculated results were compared with the experimental results. The ground state nuclear density distributions, form factors and rms radii of unstable ^{17,18,19,20}F isotopes were calculated in shell model and Hartree- Fock method by Majeed et al., [6] using SDPF- model space which consist the active shells 2*s* 1*d* and 2*p*1*f* above the inert core and effective nucleon –nucleon interaction Skyrme forces for Hartree- Fock calculations. Abdullah [7] has been studied the ground-state properties of some Sn-isotopes such as the proton and charge and matter densities, the corresponding root mean square radius, neutron skin thickness and charge form factor using Skyrme–Hartree–Fock method with Skyrme interactions namely; SII, SIII, SV, SKXce, SLy4 and SKT. The calculated results were compared with the experimental data and the relativistic mean field theory (RMFT) results.

In this research, the nuclear structure of ^{21}Ne, ^{23}Na, ^{29}Si and ^{31}P nuclei are investigated. The Hartree Fock (HF) calculations is performed using selected effective nuclear interactions, namely the Skyrme parameterizations SVI [8], SKB [9], SGI [10], SKM* [11], MSK7 [12], SLy4 [13] and Skxs25 [14].

THEORETICAL FORMULATIONS

The expectation value of the HF Hamiltonian of the system is given by [15]:

$$\left\langle \phi_{HF} \left| \hat{H} \right| \phi_{HF} \right\rangle = \sum_{i=1}^{A} \left\langle \phi_i \left| \hat{T} \right| \phi_i \right\rangle + \frac{1}{2} \sum_{ij}^{A} \left\langle \phi_i \phi_j \left| \vec{\upsilon}(i,j) \right| \phi_i \phi_j \right\rangle \quad (1)$$

where $\vec{\upsilon}(i,j)$ contains all parts of nucleon– nucleon forces. This forces consists of some two-body terms together with a three-body term [16]:

$$\hat{V}_{Skyrme} = \sum_{I \prec J} V_{ij}^{(2)} + \sum_{i \prec j \prec k} V_{ijk}^{(3)} \quad (2)$$

With

$$V_{ij}^{(2)} = t_0(1 + x_0 p_\sigma)\delta(\vec{r}) + \frac{1}{2} t_1[\delta(\vec{r})\vec{k}^2 + \vec{k}^{\sim 2}\delta(\vec{r})] + t_2 \vec{k}^{\sim}\delta(\vec{r})\vec{k} + iW_0(\vec{\sigma}_i - \vec{\sigma}_j).\vec{k} \times \delta(\vec{r})\vec{k} \quad (3)$$

$$V_{ijk}^{(3)} = t_3 \delta(\vec{r}_i - \vec{r}_j)\delta(\vec{r}_j - \vec{r}_k) \quad (4)$$

The relative momentum operators $\vec{k} = (\nabla_i - \nabla_j)/2i$, acting to the right and $\vec{k}^{\sim 2} = -(\nabla_i - \nabla_j)/2i$, acting to the left.

The neutron, proton or charge densities in the Skyrme–Hartree–Fock (SHF) theory are given by [17]

$$\rho_g(\vec{r}) = \sum_{\beta \in g} w_\beta \psi_\beta^+(\vec{r})\,\psi_\beta(\vec{r}), \qquad (5)$$

where g is used for proton, neutron and charge densities, ψ_β is the single-particle wave function of the state β and w_β represents the occupation probability of the state β.

The charge form factor, $F(q)$, is obtained from the charge density by the Fourier–Bessel transform [18]:

$$F(q) = 4\pi \int_0^\infty r^2 j_0(qr)\rho_c(r)dr \qquad (6)$$

where q is the momentum transfer.

The rms radii of neutron, proton and charge densities can be calculated using equation (5) with the following formula [19]:

$$r_g = < r_g^2 >^{1/2} = \left[\frac{\int r^2 \rho_g(r) dr}{\int \rho_g(r) dr} \right]^{1/2} \qquad g = n, p, c \qquad (7)$$

A quantity of both theoretical and experimental interest, the neutron skin thickness t, can then be defined as the difference between the neutron rms radius and the proton rms radius as [17]:

$$t = t_n - t_p \qquad (8)$$

RESULTS AND DISCUSSION

The nuclear structure of ^{21}Ne, ^{23}Na, ^{29}Si and ^{31}P nuclei are studied using self-consistent mean field with selected Skyrem forces (SVI, SKB, SGI, SKM*, MSK7, SLY4 and Skxs25). The Skyrme force parameters of the sets are given in Table-1.

The calculated binding energies per nucleon for the nuclei with the experimental data are shown in Table-2. The binding energy for ^{21}Ne and ^{23}Na calculated using SKM* are agree with the experimental data, while for ^{29}Si and ^{31}P nuclei the SGI parameterizations are more close to experimental data than the calculated results with the other parameterizations.

The calculated charge and matter rms radii of the nuclei under study are tabulated and compared with available experimental data in Tables 3 - 4, respectively. From Table-3, it clear that the calculated charge rms using Skxs25 parameterizations calculation gives excellent agreement with experimental data. Thus, this parameterization is used to calculate the density distributions and electron scattering form factors for these nuclei. It is obvious from Table-4 that the matter rms radii calculated with MSK7 parameterizations are more close to experimental data than those of other parameterizations. The proton and neutron rms radii calculated with different Skyrme parameterizations for

selected nuclei are given in Tables 5- 6, respectively. From these Tables, it is seen that the proton rms radii are increased from (2.845-2.889) fm for ^{21}Ne to (3.105-3.186) fm (for ^{31}P) with the increasing of proton number, while the neutron rms radii are increased from (2.862-2.920) for ^{21}Ne to (3.059-3.179) fm for ^{31}P with the increasing of proton number. The calculated neutron skin thickness (*t*) with Skxs25 parameterizations are given in Table 6. It has been shown from Table 6, as the proton number of nuclei increase the neutron skin thickness (*t*) values increase from 0.029 fm for ^{21}Ne to 0.046 fm for ^{31}P.

Figures 1(a)-1(d) display the calculated charge density distributions (solid curve) for ^{21}Ne, ^{23}Na, ^{29}Si and ^{31}P, respectively obtained with SHF using Skxs25 parameterization compared with the experimental data (dotted symbols) [20,23]. It is clear from this figure that the calculated and experimental charge densities are agree well in the fall of region and differ more in the nuclear interior as a consequence of the shell oscillations of the mean field densities.

Figure (2) shows the proton (a) and charge (b) densities of ^{21}Ne, ^{23}Na, ^{29}Si and ^{31}P nuclei. It is evident from this figure that the difference in these densities are related to the shell structure of nuclei. The surface part increasing in the interior density. The proton and charge densities differ very slightly from each other.

Also, the matter density distribution of ^{21}Ne, ^{23}Na, ^{29}Si and ^{31}P nuclei are calculated using Skxs25 parameterization and displayed in figure 3(a)-3(d), respectively with the experimental data (dotted symbols) [20,23]. The results are agree well in the fall of region and differ more in the nuclear interior.

In figure 4, the calculated elastic charge form factors (solid curve) are plotted for ^{21}Ne [Fig. 4(a)], ^{23}Na [Fig. 4(b)], ^{29}Si [Fig. 4(c)] and ^{31}P [Fig. 4(d)] nuclei using Skxs25 parameterization along with the experimental data (dotted symbols) [20, 23, 24, 25]. It is apparent from this figure that the theoretical curves and the experimental curves for all nuclei almost coincide in the range of momentum transfer $q \leq 2.5$ fm^{-1}. The deviation occurs at high momentum transfer. Since the form factor in this range of momentum transfer is mainly sensitive to the details of the inner part of the charge density distribution, its occurrence indicates that the theoretical charge density distribution has a departure from the experimental one around the center of the nucleus. The result of Skxs25 Skyrme parameterization predicted successfully the position of first diffraction minimum for ^{21}Ne and ^{29}Si but predicts the existence of a second diffraction minimum at medium q in disagreement with experimental data.

SUMMARY AND CONCLUSION

In this study, nuclear structure of ^{21}Ne, ^{23}Na, ^{29}Si and ^{31}P nuclei using HF calculations with Skyrme parameterizations SVI, SKB, SGI, SKM*, MSK7, SLy4 and Skxs25 have been investigated. The binding energy for ^{21}Ne and ^{23}Na calculated using SKM* are agree with the experimental data, while for ^{29}Si and ^{31}P nuclei the SGI parameterizations are more close than the calculated results with the other parameterizations.

Results of rms radii showed excellent agreement with experimental data when the Skxs25 Skyrme parameterizations are used, while the other parameterizations results showed an overestimation in the calculated rms radii. It is clear from the result of the density distribution that the calculated density are quite consistent with the experimental data excepted in the central region. Also, the proton and charge densities differ very slightly from each other. It is apparent from the results of charge form factors that the theoretical and experimental curves almost coincide in the range of momentum transfer $q \leq 2.5$ fm^{-1} and the deviation occurs at high momentum transfer.

REFERENCES

1. R. Roy and B. P. Nigam; "Nuclear Physics: Theory and Experiment", John and Sons, New York (1967).
2. E. Tel, S. Okuducu, G. Tanır, N. N. Aktı, M. H. Bolukdemir, Commun. Theor. Phys. (Beijing, China) 49 (2008) 696–702.
3. A. A. Alzubadi, Indian J Phys , 89(6) (2015) 619–627.
4. R. A. Radhi, A. A. Alzubadi and E. M. Rashed, Nucl. Phys. A 947 (2016) 12.
5. A. N. Abdullah, Iraqi Journal of Science 58, 1A, (2017) 71-78.
6. W. Z. Majeed and A. R. Ridha, Indian Journal of Natural Sciences 8, 44, (2017) 12733-12744.
7. A. N. Abdullah, Diyala Journal for Pure Sciences 13 (3) (2017) 182-194.
8. M. Beiner, H. Flocard, and N. van Giai, Nucl. Phys. A238, 29 (1975).
9. H. S. Kohler, Nucl. Phys. A257, 301 (1976).
10. N. V. Giai and H. Sagawa, Phys. Lett. 106 B (1981).
11. J. Bartel, P. Quentin, M. Brack, C. Guet, and M. B. Hakansson, Nucl. Phys. A 386, 79 (1982).
12. S. Goriely, F. Tondeur and J. M. Pearson Atomic Data and Nuclear Data Tables 77, 311–381 (2001).
13. E. Chabanat, P. Bonche, P. Haensel, J. Meyer, and T. Schaeffer, Nucl. Phys. A 635, 231 (1998).
14. B. A. Brown, G. Shen, G. C. Hillhouse, J. Meng and A. Trzcinska, Phys. Rev. C 76 (2007) 034305.
15. L. Guo-qiang, Commun. Theor. Phys. 13 (1990) 457.
16. D. Vautherin, D. M. Brink, Phys. Rev. C5 (1972) 626.
17. H. Aytekin *et al*., Turk J Phys 32 (2008) , 181 – 191.
18. G. Q. Li, *Journal Physics* G 17 (1991) 1-34.
19. M. Wang *et al*., *Chinese Physics* C 36, (2012) 1603-2014.
20. H. de Vries, C.W. de Jager, C. De Vries, Atomic Data and Nucl. Data Tables 36,(1987) 495-536.
21. I. Angeli and K.P. Marinova, *Data and Nuclear Data Tables* 99 (2013) 69-95.
22. A. Ozawa, T. Suzuki and I. Tanihata, Nuclear Physics A 693 (2001) 32–62.
23. G. Fricke *et al*., At. Data Nucl. Data Tables 60, 177 (1995).
24. P. P. Singhal, A. Watt and R. R. Whitehead, J. Phys. G 8, 1059 (1982).
25. B. B. P. Sinha and G. A. Peterson Phys. Rev., C6 1657 (1972).

Table (1): The Skyrme Force Parameters.

Parameter	SVI [8]	SKB [9]	SGI [10]	SKM*[11]	MSK7 [12]	SLy4 [13]	SKxs25 [14]
t_0 (MeV.fm^3)	-1205.6	-1602.78	1603.0	-2645.0	-1828.23	-2488.91	-2887.813
t_1 (MeV.fm^5)	765.0	570.88	515.9	410.0	259.4	486.82	315.504
t_2 ((MeV.fm^5)	35.0	-67.70	84.5	-135.0	-292.84	-546.39	-329.305
t_3 MeV.fm$^{3\alpha}$)	5000	8000	8000	15595	13421.7	13777.0	18229.807
t_4(MeV.fm^5)	150	125	115	130	118.807	123	163.933
x_0	0.05	-0.165	-0.02	0.09	0.577	0.834	-0.186
x_1	0.0	0.0	-0.5	0.0	-0.5	-0.344	-0.248
x_2	0.0	0.0	-1.731	0.0	-0.5	-1.0	-0.601
x_3	1.0	-0.286	0.138	0.0	0.783	1.354	-0.409
α	1.0	0.333	0.333	0.167	0.333	0.167	0.167

Table (2): The Calculated Values of Binding Energy Per Nucleon in MeV.

Nuclei	SVI	SKB	SGI	SKM*	MSK7	SLy4	SKxs25	Exp. [19]
^{21}Ne	7.422	7.546	7.602	7.777	7.675	7.688	7.608	7.971
^{23}Na	7.520	7.643	7.676	7.914	7.827	7.800	7.735	8.111
^{29}Si	8.222	8.289	8.293	8.575	8.489	8.450	8.204	7.167
^{31}P	8.221	8.344	8.343	8.642	8.564	8.526	9.741	8.225

Table (3): The Calculated Values of Charge Rms Radii.

Nuclei	SVI	SKB	SGI	SKM*	MSK7	SLy4	SKxs25	Exp. [20, 21]
^{21}Ne	2.961	2.958	2.953	2.925	2.919	2.946	2.962	2.969±0.003
^{23}Na	3.021	3.020	3.013	2.980	2.974	3.005	2.995	2.993±0.002
^{29}Si	3.161	3.168	3.155	3.123	3.121	3.143	3.127	3.130±0.005
^{31}P	3.268	3.258	3.244	3.200	3.191	3.226	3.188	3.188±0.002

Table (4): The Calculated Values of Matter Rms Radii.

Nuclei	SVI	SKB	SGI	SKM*	MSK7	SLy4	SKxs25	Exp. [22]
^{21}Ne	2.905	2.895	2.898	2.865	2.854	2.889	2.904	2.83±0.07
^{23}Na	2.952	2.945	2.946	2.911	2.900	2.937	2.935	2.83±0.03
^{29}Si	3.085	3.080	3.080	3.041	3.034	3.069	3.061	----
^{31}P	3.182	3.165	3.165	3.117	3.102	3.147	3.081	----

Table (5): The Calculated Values of Proton Rms Radii.

Nuclei	SVI	SKB	SGI	SKM*	MSK7	SLy4	SKxs25
^{21}Ne	2.888	2.886	2.880	2.851	2.845	2.873	2.889
^{23}Na	2.944	2.943	2.935	2.902	2.896	2.928	2.917
^{29}Si	3.077	3.084	3.071	3.038	3.036	3.059	3.039
^{31}P	3.186	3.176	3.161	3.116	3.106	3.143	3.105

Table (6): The Calculated Values of Neutron Rms Radii.

Nuclei	SVI	SKB	SGI	SKM*	MSK7	SLy4	SKxs25	*t* (SKxs25)
^{21}Ne	2.920	2.904	2.914	2.878	2.862	2.903	2.918	0.029
^{23}Na	2.960	2.948	2.955	2.919	2.903	2.946	2.951	0.033
^{29}Si	3.092	3.076	3.088	3.045	3.033	3.078	3.082	0.043
^{31}P	3.179	3.155	3.168	3.118	3.097	3.150	3.059	0.046

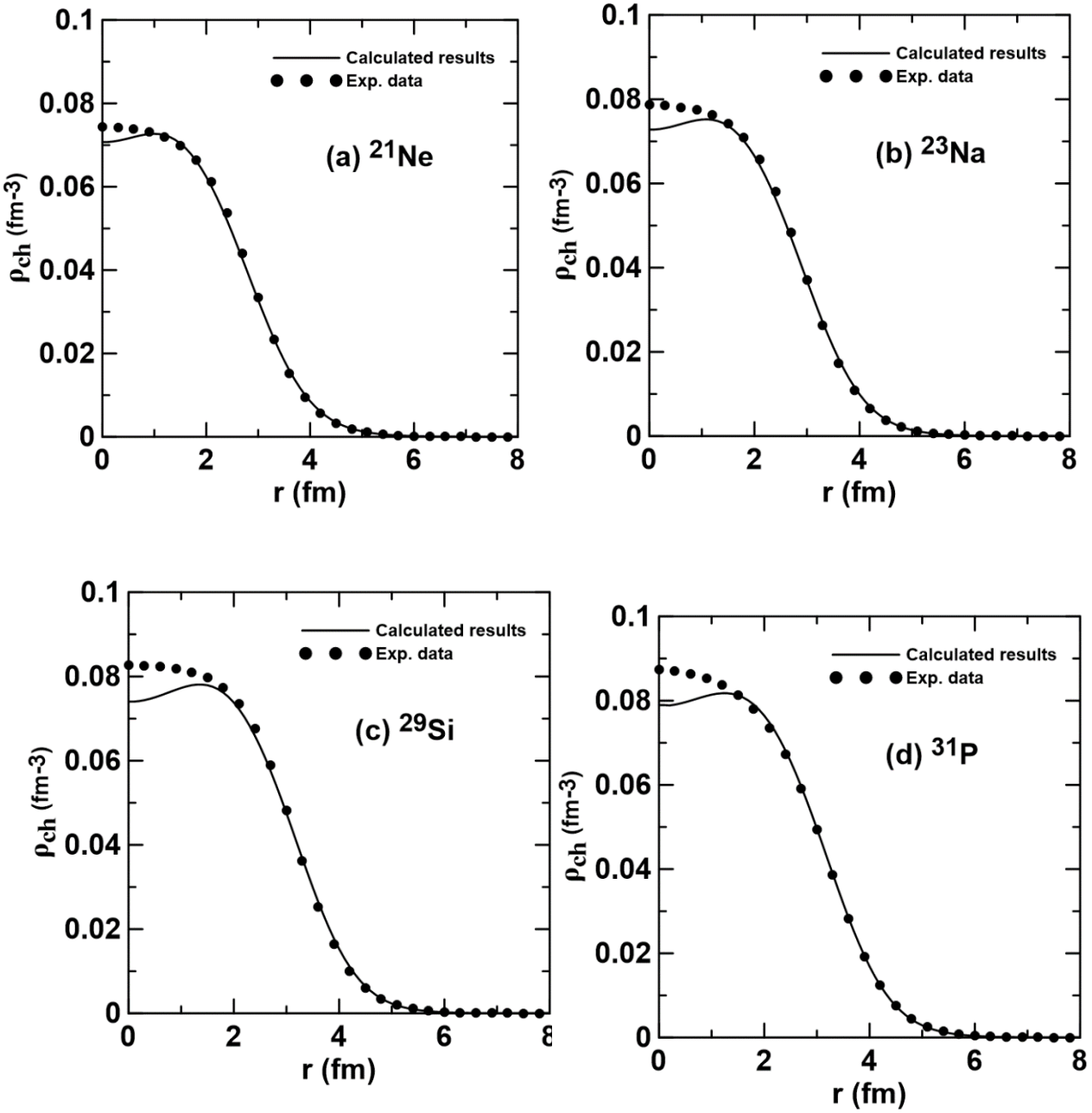

Fig.1: Charge Density Distributions of (a) ^{21}Ne, (b) ^{23}Na, (c) ^{29}Si and (d) ^{31}P.

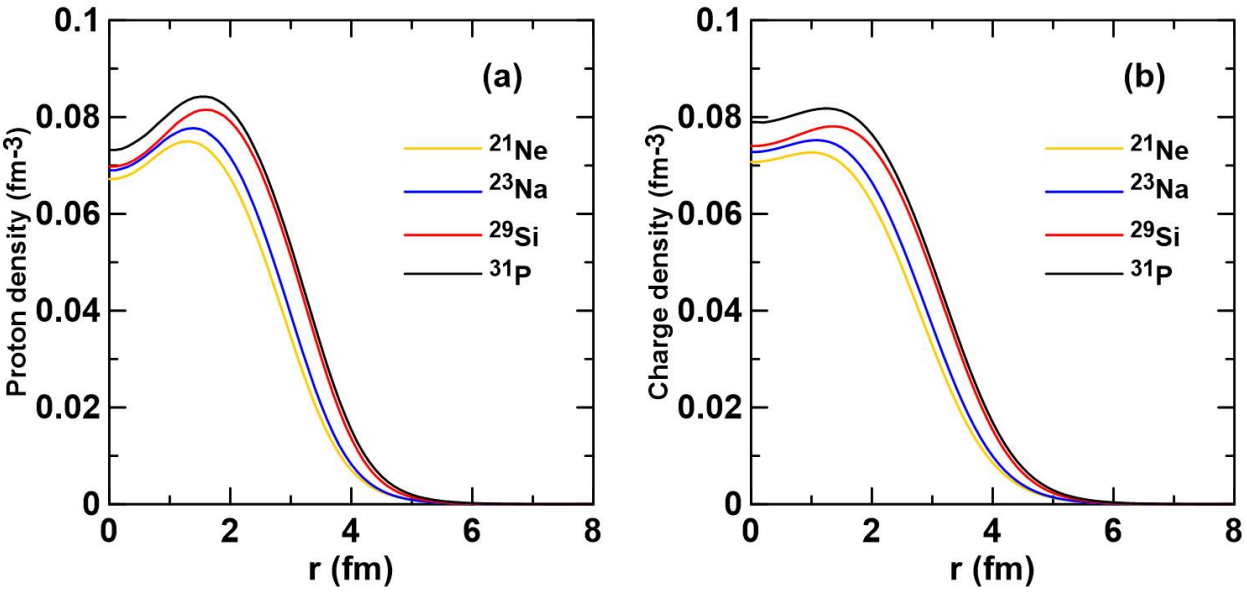

Fig.2: Charge (a) and Proton (b) Densities Distributions of ^{21}Ne, ^{23}Na, ^{29}Si and ^{31}P nuclei.

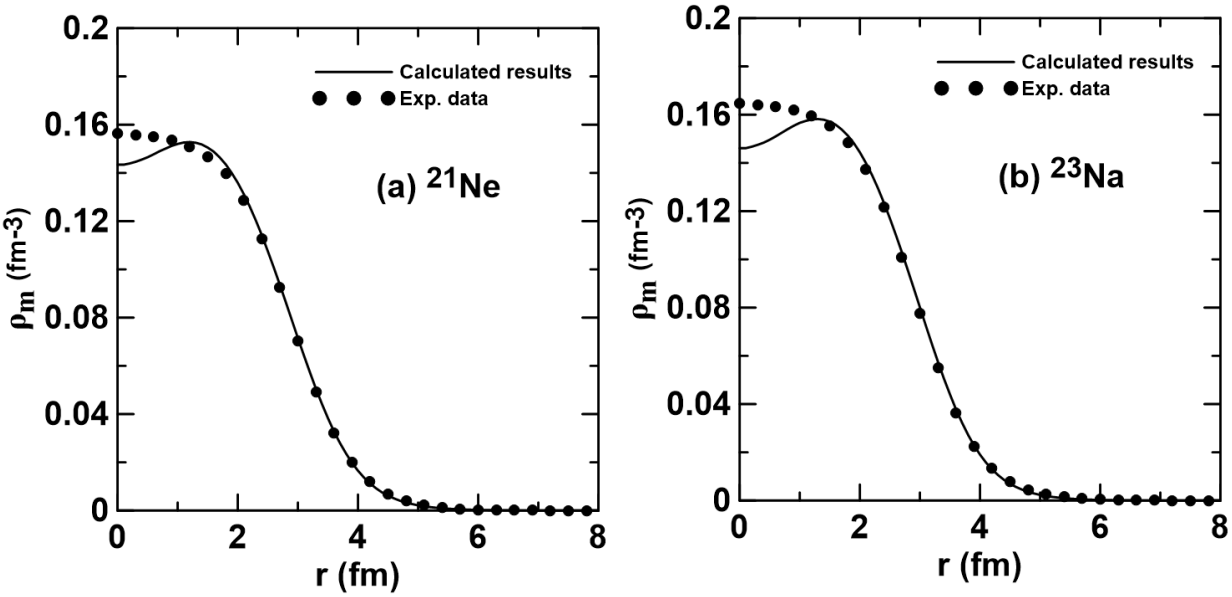

Fig. 3

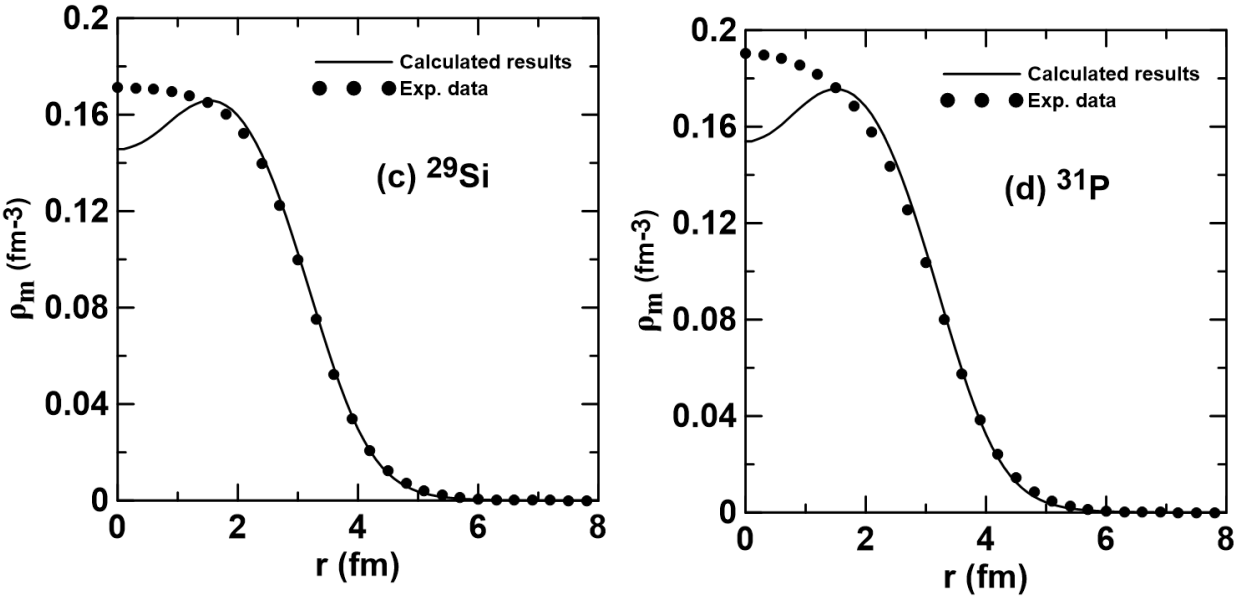

Fig. 3: Matter Density Distributions of (a) ^{21}Ne, (b) ^{23}Na, (c) ^{29}Si and (d) ^{31}P.

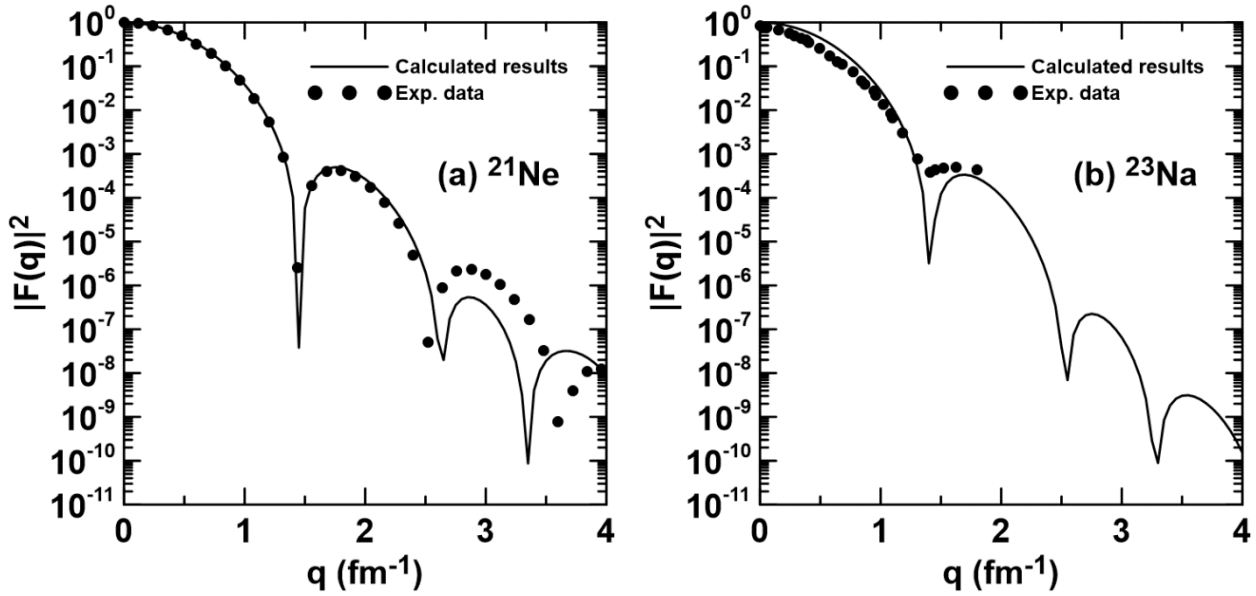

Fig.4

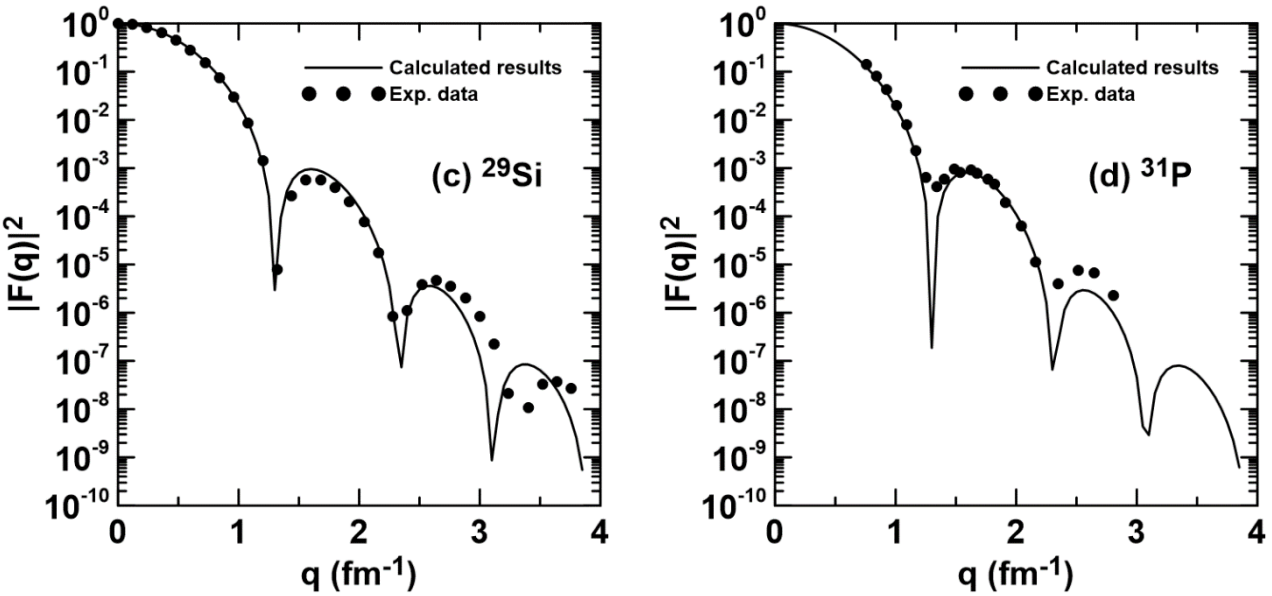

Fig.4: Elastic Charge form Factors of of (a) ^{21}Ne, (b) ^{23}Na, (c) ^{29}Si and (d) ^{31}P.

Indian Journal of Natural Sciences www.tnsroindia.org.in ©IJONS

Vol.8 / Issue 45 / December 2017 *International Bimonthly* *ISSN: 0976 – 0997*

RESEARCH ARTICLE

Phytotheraputic Clinical Study of Tribulus terrestris Extract on Diverse Types of Renal Stone

Zena Munther Qaragholi[1*], Montadhar Hameed Alhussaini[2] , Huda F. Hassan[3], Oday Kareem Luaibi[4], Zainab Saleh[5] and Wesam Yaseen[6]

[1]A. Lecturer, Department of Pharmacognosy and Medicinal Plants-College of Pharmacy-University of Baghdad, Iraq.
[2]M.B.CH.B., F.I.C.M.S., C.A.B.S/ Lecturer, Urology Department-College of medicine-University of Baghdad,Iraq.
[3]A. Prof.,Department of Pharmacology and Toxicology College of Vet.Medicine- University of Baghdad.
[4] Lecturer,Department of Internal Medicine. College of Vet.Medicine-University of Baghdad, Iraq.
[5]Chemist,Department of Pharmacognosy and Medicinal Plants-College of Pharmacy-University of Baghdad, Iraq.
[6]Pharmacist, Ministry of Health,Iraq.

Received: 17 Oct 2017 Revised: 28 Oct 2017 Accepted: 15 Nov 2017

[*]**Address for correspondence**
Zena Munther Qaragholi
A. Lecturer,
Department of Pharmacognosy
Medicinal Plants-College of Pharmacy-University of Baghdad,
Baghdad, Iraq.
Email: zenaqaragholi@yahoo.com

ABSTRACT

The current study evaluated the phytochemical constituents and the antilithiatic properties of *Tribulus terrestris.Tribulus terrestris* powder (250 g) was extracted using 500ml, 70% ethanol in a soxhlet apparatus. A number of phtytochemical tests where conducted to study the phytochemical properties of the herbal extract including tests for alkaloids, flavonoids, saponins, glycosides and phenols. Moreover, a clinical evaluation was conducted to evaluate the effect of the extract on different types and sizes of kidney stones. Fifty patients (32 males-18 females) aged between 18 -65 years. Were diagnosed with different types and in different locations of renal stones. Stone sizes ranged between 7mm to 18 mm. *Tribulus terrestris* extract 500 mg 60 Caps from Swanson Superior Herbs was prescribed twice daily for a month to be taken with large amounts of water along with daily exercise.The ethanolic extract of *Tribulus terrestris* contained clearly saponin glycosides and gave a great effect in treating different types and sizes of kidney stone in male and female patients.

Therefore, this study suggests the possibility of using *Tribulus terrestris* as a therapeutic agent to treat urolithiasis.

Keywords: ethanolic extract**,** *Tribulus terrestris* and urolithiasis.

INTRODUCTION

Tribulus terrestris is a perennial plant from the caltrop Family called *Zygophyllaceae* widely spread around the world.[1] *Tribulus terrestris* naturally occurs in Iraq and named " Qutub". This plant has been used traditionally in Iraq by the local herbalists in the treatment of many diseases including kidney stone without knowing its chemical components and pharmacological mechanism. Therefore, this plant was chosen for this study to reach a scientific approach for Iraqi traditional medicine. Moreover, recurrence and persistent side effects of resent treatment for urolithiasis such as extracorporeal shock wave lithotripsy has restricted their uses therefore an alternate treatment using phytotherapy is recommended for use. *Tribulus terrestris* appears to be able to reduce kidney stone formation in vitro (specifically calcium oxalate stones) in rodents. which may be due to multiple components[2-4].

This plant has many pharmacological activities including; Analgesia, as some studies has indicated that *Tribulus* may possess pain-reducing properties. [5] Also, *Tribulus terrestris* effects cardiac Tissue as the saponins in this plant are able to reduce infarct size in hearts exposed to ischemia / reperfusion and oxidation in *Vitro*.[6] Moreover, there are some evidence that it contributes to the reduction in total cholesterol[7] In addition, it has an immunomodulatory activity as the Saponins isolated from the fruits of *Tribulus terrestris* demonstrated dose-dependent increase in phagocytosis, indicating stimulation of nonspecific immune response.[8] Also, an antidiabetic activity was noted for the saponins from *Tribulus terrestris* possesses hypoglycemic properties.[9]*Tribulus terrestris* significantly reduced the level of serum glucose, serum triglyceride, and serum cholesterol. The decoction of *Tribulus terrestris* showed inhibition of gluconeogenesis in mice[10][11]. A significant decrease in the postprandial blood glucose level of rats was found after administration of saponin from *Tribulus terrestris.* The plant produced dilation of coronary artery and improved the coronary circulation [11]. Also, *Tribulus terrestris* posses an antidepressant and anxiolytic activity, a β-carboline alkaloid present in *Tribulus terrestris*, is one of the main active constituents that contributes to the above-mentioned activities. [12] Furthermore, there are some evidence that hepatoprotective activity *Tribulus terrestris*.[13] Furthermore, there are some facts for the anti inflammatory activity of *Tribulus* [14-17]

There are three forms of kidney stones First, calcium-containing stones, there are the most commonly occurring to an extent of 75-90% these typically contain calcium oxalate either alone or in combination with calcium phosphate, Calcium oxalate stones are found in two different forms, calcium oxalate monohydrate (COM) and calcium oxalate dihydrate (COD).[24] Secondly, struvite which is bout 10–15% of urinary calculi are composed of magnesium ammonium phosphate Struvite stones (also known as "infection stones", urease or triple-phosphate stones), form most often in the presence of infection by urea-splitting bacteria. Using the enzyme urease, these organisms metabolize urea into ammonia and carbon dioxide. This alkalinizes the urine, resulting in favorable conditions for the formation of struvite stones.[25] Thirdly, Uric acid stones which are the third main type of kidney stones as about 5–10% of all stones are formed from uric acid. There are other types as people with certain rare inborn errors of metabolism have a propensity to accumulate crystal-forming substances in their urine. For example, those with cystinuria, cystinosis, and Fanconi syndrome may form stones composed of cystine. Cystine stone formation can be treated with urine alkalinization and dietary protein restriction. People afflicted with xanthinuria often produce stones composed of xanthine. People afflicted with adenine phosphoribosyltransferase deficiency may produce 2,8-dihydroxyadenine stones, alkaptonurics produce homogentisic acid stones, and iminoglycinuria produce stones of glycine, proline and hydroxyproline. Urolithiasis has also been noted to occur in the setting of therapeutic drug use, with crystals of drug forming within the renal tract in some people currently being treated with agents such as indinavir, sulfadiazine and triamterene.[26-27].

MATERIALS AND METHODS

Plant Material

Dryed plant was purchased from the local market (Herbal store), then identified by the Department of Pharmacognosy and medicinal plants- College of Pharmacy- University of Baghdad. Later, the plant was grinded by an electric mill then the powder was used for extraction.

Extraction Procedure

Tribulus terrestris powder (250 g) was extracted with 500ml, 70% ethanol in a soxhlet apparatus for four hours then evaporated to dryness by a rotary evaporator.[18] As in (Figure 1)

Phytochemical Tests

Alkaloid Tests

- **Wagner's Test:** (Iodine in Potassium Iodide) Plant extract was treated with few drops of Wagner's reagent. [19]
- **Mayer's Test:** (Potassium Mercuric Iodine Solution) Plant extract was treated with few drops of Mayer's reagent. [19]
- **Dragendorff's Test:** (Potassium Bismuth Iodide) Plant extract was was treated with few drops of Dragendorff's reagent. [19]
- **Hager's Test:** (Saturated aqueous solution of picric acid) Plant extract was treated with few drops of the reagent [20]

Flavonoid Test

Sodium Hydroxide Test

About 5 mg of the compound was dissolved in water, warmed and filtered. 10% aqueous sodium hydroxide was added to 2 ml of this solution. [21]

Glycoside Test

Baljet Test

We took the plant extract and added sodium picrate reagent.

Phenols Test

Ferric Chloride Test

The ferric chloride test is used to determine the presence or absence of phenols in a given sample (for instance natural phenols in a plant extract). Phenols form a violet complex with Fe (III), which is intensely colored. The color may vary from blue, green or even red depending upon the nature of the phenol. As in (figure 8)[22].

Saponin Test

Haemolytic test: was used to identify saponin glycosides.

Procedure : Two test tubes were used and each placed with 5 ml of a 10 % solution of blood in normal saline. One of them , 5 ml of normal saline solution was added and to the other one 5 ml of the extract of plant prepared added by shaking with normal saline solution , and then filtered. Both tubes were shake gently [23]

Kidney Stone

Clinical evaluation of the effect of *Tribulus terrestris* on different types and sizes of kidney stones

50 patients (32 male) and the rest were females aged between 18 -65 years. Were diagnosed with different types and in different locations of renal stones. Stone sizes ranged between 7mm to 18 mm. *Tribulus terrestris* Extract 500 mg 60 Caps from Swanson Superior Herbs.

RESULTS

Phytochemical Tests

Alkaloid Tests

Wagner's Test: Formation of reddish brown precipitate indicates the presence of alkaloids. Shown in (Figure 2)

Mayer's Test: Formation of creamy white precipitate indicates presence of alkaloids. As shown in (figure 3)

Dragendorff's Test: Formation of reddish brown precipitate indicates presence of alkaloids. As in (figure 4)

Hager's Test:

The filtrate when treated with Hager's reagent as in (figure 5) the appearance of yellow color precipitate indicates the presence of alkaloids[20].

Flavonoid Test

Sodium hydroxide Test

This test produces a yellow coloration. A change in color from yellow to colorless on addition of dilute hydrochloric acid is an indication for the presence of flavonoids. As in (figure 6)

Glycoside Test

Baljet Test

Glycoside was proven to be present in the extract as a yellow to orange color appeared as in (figure 7)

Phenols Test

Ferric Chloride Test

The ferric chloride test is used to determine the presence or absence of phenols in a given sample (for instance natural phenols in a plant extract). Phenols form a violet complex with Fe (III), which is intensely colored. The color may vary from blue, green or even red depending upon the nature of the phenol. As in (figure 8)[22].

Saponin Test

Haemolytic test: Results are shown in (figure 9)[23].

Kidney stone

Clinical evaluation of the effect of *Tribulus terrestris* on different types and sizes of kidney stones

Results after one month of treatment were as the following divided into three groups:

- First group: Complete recovery from kidney stone was noticed from ultrasound examination in 23 patients (15 male, 8 female). Stone size ranged from (7-13)mm
- Second group: Partial response to the extract was found from ultrasound examination in 17 patients (10 male, 7 female). Stone size ranged from (12-18)mm
- Third Group: Patients showed no response to the herbal extract as shown from the ultrasound examination in 10 patients (7 male, 3 female). Stone size ranged from (15-19)mm.

DISCUSSION

There is growing evidence that CaOx nephrolithiasis is associated with renal injury. Hyperoxaluria is a major risk factor for calcium oxalate nephrolithiasis, and calcium oxalate urinary stones are the most common type of urinary stone. High level of oxalate produced a variety of changes in the renal epithelial cells, such as an increase in free radical production and a decrease in antioxidant status, followed by cell injury and cell death. These changes are significant predisposing factors for the facilitation of crystal adherence and retention. Due to significant side effects and failure to prevent recurrence by the present day treatment procedures for urolithiasis, in this study we used alternative treatment modalities using herbal products. A dramatic advancement in using *Tribulus terrestris* for urolithiasis treatments has been proposed. In the present study, the anticalcifying properties of *Tribulus terrestris* commonly called “gokhru” were explored clinically[3].

Tribulus terrestris extract contain saponins substance showed great results in 23 patients as they showed complete recovery and 17 patients showed 50% recovery. This comes in agreement with other previous researches for saponins obtained from medicinal plants[28].

Therefore, This finding suggests the type of kidney stones were COM crystals as the property of saponins is important in the prevention of kidney stone formation. Thus, it inhibits CaOx crystal aggregation and also the binding of the crystals to the renal epithelial surface.[29-31] Moreover, the rest of the patients showed no response to the extract which suggests the type of their kidney stone was different.

CONCLUSION

It can be concluded that the extract of *Tribulus terrestris* has shown to possess an ability to inhibit CaOx crystallization. Our study suggests the possibility of using *Tribulus terrestris* as a therapeutic agent to treat urolithiasis and further characterization of its active phytochemical compounds could lead to a new candidate drug for patients with urolithiasis.

REFERENCES

1. Flowering Plants of the Santa Monica Mountains, Nancy Dale, 2nd Ed., 2000, 21.p. 200
2. Aggarwal A, et al. A novel antilithiatic protein from Tribulus terrestris having cytoprotective potency. Protein Pept Lett. 2012. ;19(8):812-9.
3. Aggarwal A, et al. Diminution of oxalate induced renal tubular epithelial cell injury and inhibition of calcium oxalate crystallization in vitro by aqueous extract of Tribulus terrestris. Int Braz J Urol. 2010 ;36(4):480-8.
4. Shirfule AL, Sangamwar AT, Khobragade CN. Exploring glycolate oxidase (GOX) as an antiurolithic drug target: molecular modeling and in vitro inhibitor study. Int J Biol Macromol. 2011: 1;49(1):62-70.
5. Heidari MR, et al. The analgesic effect of Tribulus terrestris extract and comparison of gastric ulcerogenicity of the extract with indomethacine in animal experiments. Ann N Y Acad Sci. 2007; 1095:418-27.
6. Wang SS, et al. Mechanisms of gross saponins of Tribulus terrestris via activating PKCepsilon against myocardial apoptosis induced by oxidative stress. Yao Xue Xue Bao. 2009: 44(2):134-9
7. Murthy AR, Dubey SD, Tripathi K Anti-hypertensive effect of Gokshura (Tribulus terrestris Linn.) - A clinical study. Anc Sci Life. 2000: 19(3-4): 139–145.
8. Tilwari A, Shukla NP, Devi U. Effect of five medicinal plants used in Indian system of medicines on immune function in Wistar rats. Afr J Biotechnol. 2011; 10: 16637-45.
9. Li M, Qu W, Wang Y, Wan H, Tian C. Hypoglycemic effect of saponin from Tribulus terrestris. Zhong Yao Cai. 2002; 25: 420-2. [PubMed]
10. Li M, Qu W, Chu S, Wang H, Tian C, Tu M. Effect of the decoction of Tribulus terrestris on mice gluconeogenesis. Zhong Yao Cai. 2001; 24: 586-8. [PubMed]
11. Amin A, Lotfy M, Shafiullah M, Adeghate E. The protective effect of Tribulus terrestris in diabetes. Ann N Y Acad Sci. 2006; 1084: 391-401. [PubMed]
12. Deole YS, Chavan SS, Ashok BK, Ravishankar B, Thakar AB, Chandola HM. Evaluation of antidepressant and anxiolytic activity of Rasayana Ghana tablet (a Compound Ayurvedic formulation) in albino mice. Ayu. 2011; 32: 375-9. [PMC free article] [PubMed]
13. Kavitha P, Ramesh R, Bupesh G, Stalin A, Subramanian P. Hepatoprotective activity of Tribulus terrestris extract against acetaminophen-induced toxicity in a freshwater fish. In Vitro Cell Dev Biol Anim.2011; 47: 698-706. [PubMed]
14. Oh JS, Baik SH, Ahn EK, Jeong W, Hong SS. Anti-inflammatory activity of Tribulus terrestris in RAW264.7 Cells. J Immunol. 2012; 88: 54.2
15. Kiran B, Lalitha V, Raveesha KA. In Vitro Evaluation of Aqueous and Solvent extract of Tribulus terrestris L. leaf against Human bacteria. Int J Pharm Tech Res. 2011; 3: 1897-903.
16. El-Sheikh TM, Bosly HA, Shalaby NM. Insecticidal and repellent activities of methanolic extract ofTribulus terrestris L. (Zygophyllaceae) against the malarial vector Anopheles arabiensis (Diptera: Culicidae) Egypt Acad J Biolog Sci. 2012; 5: 13-22.
17. Oh HK, Park SJ, Moon HD, Jun SH, Choi NY, You YO. Tribulus terrestris inhibits caries-inducing properties of Streptococcus mutans. J Med Plants Res. 2011; 5: 6061-6.
18. Ahmed A. Hussain, Abbas A. Mohammed, Heba. H. Ibrahim, and Amir H. Abbas,. Study the Biological Activities of Tribulus Terrestris Extracts. World Academy of Science, Engineering and Technology. 2009: pp: 433-435.

19. Nair R., Phytochemical Analysis Of Successive Re-extracts of the Leaves of MoringaOleiferaLam. Department of Applied Zoology, Mangalore University, Mangalagangothri, Karnataka India, Int J Pharm Pharm Sci, 2013: Vol 5, Suppl 3, 629-634
20. C.K. Kokate, Practical Pharmacognosy, 4 th Edn, 1994, p.108-109.
21. Bello IA, Ndukwe GI, Audu OT, Habila JD (2011). "A bioactive flavonoid from Pavetta crassipes K. Schum". Organic and Medicinal Chemistry Letters 1 (1): 14. doi: 10.1186 / 2191-2858-1-14. PMC 3305906. PMID 22373191.
22. "Ferric Chloride - Pyridine Test Page". Chemistry.ccsu.edu. Retrieved 2013-09-11.
23. Parker sD., Latif Z., Gray A. L Natural Products Isolation. 2 ed. Humana Press, Totowa, New Jersey, 2005, 515p.
24. Reilly, RF, Jr, Ch. 13: "Nephrolithiasis". In Reilly Jr & Perazella 2005, pp. 192-207.
25. Weiss, M; Liapis, H; Tomaszewski, JE; Arend, LJ (2007). "Chapter 22: Pyelonephritis and Other Infections, Reflux Nephropathy, Hydronephrosis, and Nephrolithiasis". In Jennette, JC; Olson, JL; Schwartz, MM; Silva, FG. Heptinstall's Pathology of the Kidney 2 (6th ed.). Philadelphia: Lippincott Williams & Wilkins. pp. 991-1082.
26. Merck Sharp & Dohme Corporation ."Patient Information about Crixivan for HIV (Human Immunodeficiency Virus) Infection". Crixivan® (indinavir sulfate) Capsules. Whitehouse Station, New Jersey: Merck Sharp & Dohme Corporation. 2010 Retrieved.2011-07-27.
27. Schlossberg, D; Samuel, R. "Sulfadiazine". Antibiotic Manual: A Guide to Commonly Used Antimicrobials (1st ed.). Shelton, Connecticut: People's Medical Publishing House. 2011: pp. 411-12.
28. Fouada A, Yamina S, Addi Nait M, Mohammed B, Abdlekrim R. In Vitro and in Vivo Antilithiasic Effect of Saponin Rich Fraction Isolated From Herniaria hirsute. J Bras Nefrol Volume XXVIII - n - Dezembro de 2006. pp 199-203.
29. Kumar V, Farell G, Deganello S, Lieske JC: Annexin II is present on renal epithelial cells and binds calcium oxalate monohydrate crystals. J Am Soc Nephrol. 2003; 14: 289-97.
30. Shukla A, Mandavia D, Barvaliya M, Baxi S, and Tripathi C. Evaluation of anti-urolithiatic effect of aqueous extract of *Bryophyllum pinnatum* (Lam.) leaves using ethylene glycol-induced renal calculi. Avicenna J Phytomed. 2014 May-Jun; 4(3): 151–159.
31. Hennequin C, Lalanne V, Daudon M, Lacour B, Drueke T: A new approach to studying inhibitors of calcium oxalate crystal growth. Urol Res. 1993; 21: 101-8.

***Fig.1. Tribulus terrestris* cap was prescribed twice daily for a month to be taken with large amounts of water and day by day exercise**.

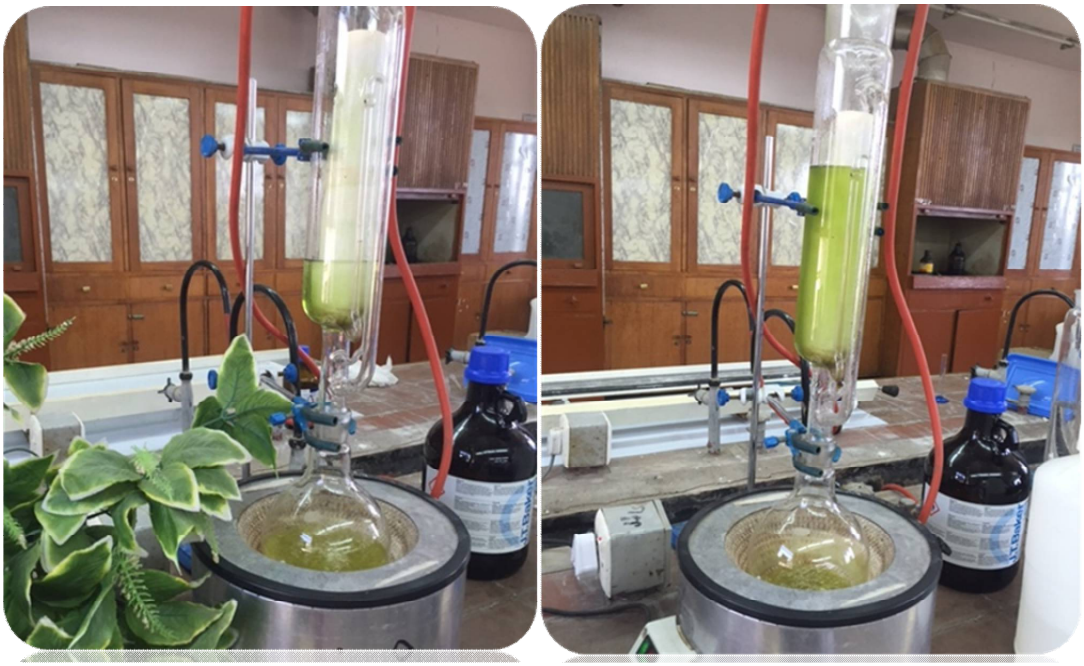

Figure 1: Extraction method using soxhlet apparatus.

Figure 2: Wagner's Test.

Figure 3: Mayer's Test.

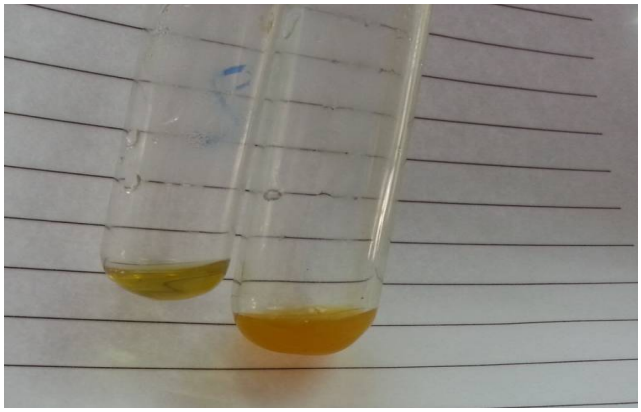

Figure 4: Dragendroff's Test

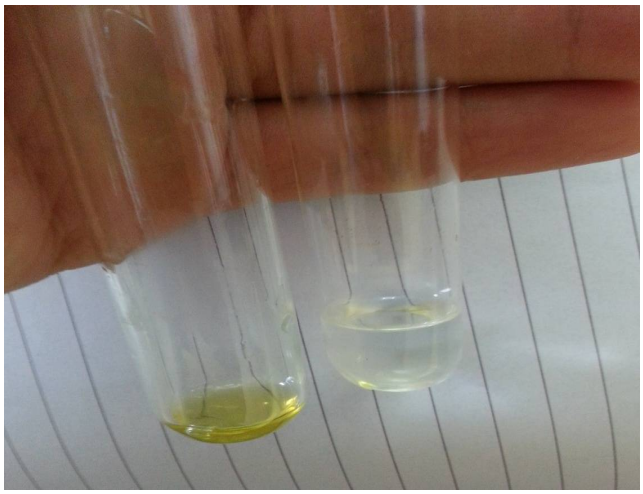

Figure 5: Hager's Test

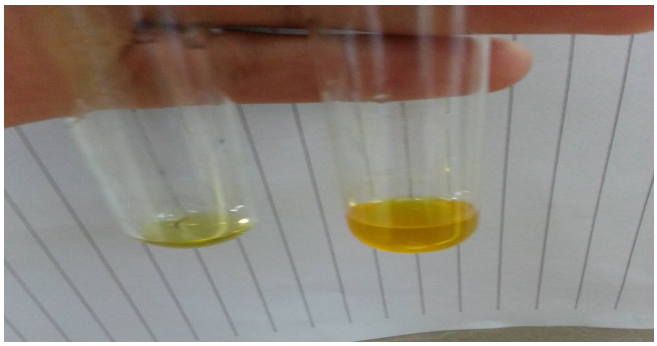

Figure 6: Sodium Hydroxide Test

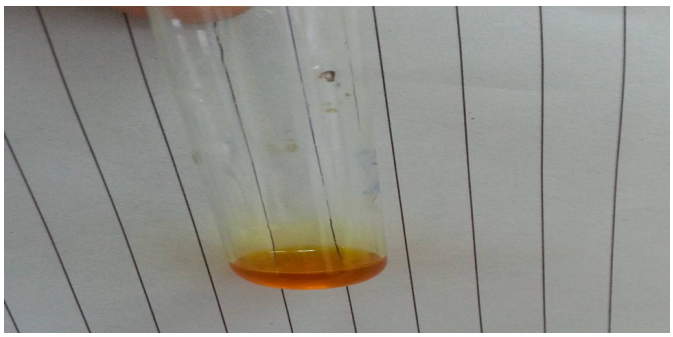

Figure 7: Baljet Test.

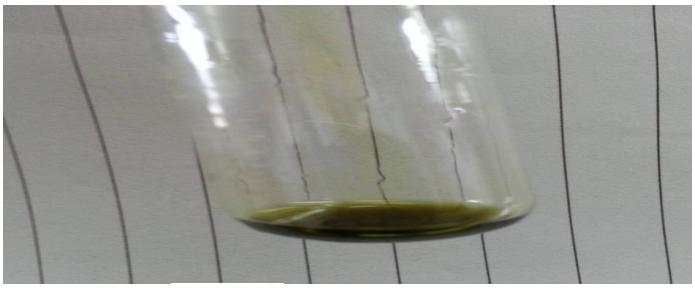

Figure 8: Ferric Chloride Test

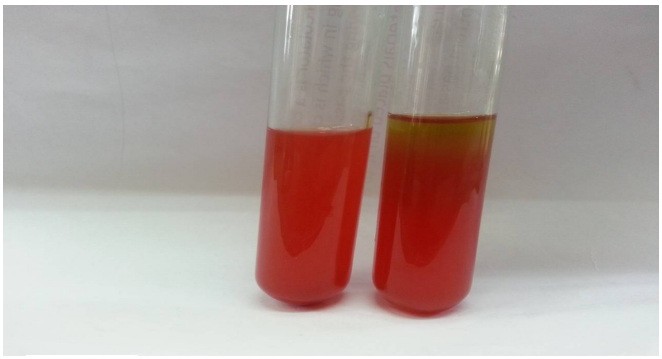

Figure 9: Haemolytic Test for Saponin Glycosides.

Indian Journal of Natural Sciences www.tnsroindia.org.in ©IJONS

Vol.8 / Issue 45 / December 2017 *International Bimonthly* *ISSN: 0976 – 0997*

RESEARCH ARTICLE

Hematological Effects of *Spinagia oleracea* Leaf Extract on Mice Treated with Chloramphenicol

Huda F.Hasan[1*], Zena M.Qaragholi[2], Oday Kareem Luaibi[3], Abdullah A. Jabbar[4], Mays Kh.Abbas[4] and Mouj M.Khalil[4]

[1]Assist. Prof. PhD/ Dept. of Pharmacology, College of Veterinary Medicine, University of Baghdad,Iraq.
[2]Lecturer, M.S.c/ Dept. of Pharmacognosy and Medicinal Plants, College of Pharmacy, University of Baghdad,Iraq.
[3]Assist. Prof. PhD/Dept.of Veterinary Internal and Preventive Medicine, Collage of Veterinary Medicine, University of Baghdad,Iraq.
[4]B.V.S.M.College of Veterinary Medicine,University of Baghdad,Iraq.

Received: 10 Oct 2017 Revised: 25 Oct 2017 Accepted: 15 Nov 2017

[*]**Address for correspondence**
Huda F. Hasan
Assist. Prof. PhD,
Dept. of Pharmacology
College of Veterinary Medicine,University of Baghdad,
Baghdad, Iraq.
Email: dr.hudaalqaraghuli@yahoo.com

ABSTRACT

Research was done to assess the potential use of the alcoholic extract of *Spinacia oleracea* leaves in the treatment of anemia in chloramphenicol - treated albino mice. Fifteen mice were divided into three equal groups and were given treatment orally for 14 days, the first group (T1) was treated with Chlormphenicol (25mg/kg) per day, the second group (T2) was treated with Chloramphenicol (25mg/kg) and *Spinacia oleracea* (100mg/kg) while the third group (T3) was treated with distilled water only . Hematological parameters used. Results of T2 showed a significant increase in packed cell volume (PCV%), hemoglobin (Hb), RBCs count, total WBCs count, neutrophil%, lymphocyte%, monocyte%, esinophil% and basophil% as compared with T1 while no significant difference when compared with T3. The histolopathological section of liver in T1 showed the main lesions were characterized by sever coagulative necrosis , pyknotic or disappear of nuclei of hepatocyte as well as dilated sinusoid with inflammatory cell infiltration in the lumen and vacular degeneration and congestion of blood vessels. The histopathological section in T2 showed kupffer cell proliferation, and disappearing of necrosis with mononuclear cells infiltration particularly Lymphocyte aggregation around blood vessels and central vein. From this study established the use of *Spinacia oleracea* has prevented the adverse effects of

chloramphenicol on blood cells when given together and the extract can be mentioned as a plant of considerable importance for improving hematological parameters.

KEYWORDS: *Spinacia oleracea*, chloramphenicol and Hematological parameters.

INTRODUCTION

Spinacia oleracea,is an annual plant with a short growth cycle, is considered as one of the most common leafy vegetable crop, which belongs to family Chenopodiacea (Hanif *et al*., 2006). Spinach is a highly desirable leafy vegetable with a good cooking adoptability, a high nutritive value and many important vitamins and minerals . It is used as cocked during the winter seasons, or as canned as well as frozen product , the *Spinacia oleracea* had an important role in enhancement the hematological indices due to presence of vitamin, iron and mineral contents of the leaves of *Spinacia oleracea*. (Martini,2007). Body Blood is a bodily fluid in animals that delivered necessary substance such as nutrients and oxygen to the cells and transports metabolic waste products away from those same cells. The components of blood include plasma (the liquid portion, which is contained water, proteins, salts, lipids and glucose), red blood cells and white blood cells, and cell fragments called platelets.Blood was played an important role in regulating the body's systems and maintaining homeostasis (Mortense*etal,2005*).Other functions included supplying oxygen and nutrient to tissues, removing waste, transported hormones and other signals throughout the body, and regulated body pH and core body temperature (Vieira*etal*.,*2008*) there aresome disease of blood such as anemia, hemophilia,leukemia and lymphoma.Several therapeutic drugs during the periods of treatment the diseasewere caused anemia such as chloramphenicol including major side effects but less common another effect included (e.g. pale skin, sore throat and fever, weakness and unusual bleeding or bruising) and minor side effect also less common such as diarrhea, nausea or vomiting (Ogbe *etal*., 2010), The increase in hematological indices by Spinacia oleracea extract may be due to presence of vitamin and mineral contents of the leaves of Spinacia oleracea (Gaikwod *et al*., 2010),the aim of this study is to evaluate the hematological effect of alcoholic extract of *Spinaciaoleracea*leaves in mice treated chloramphenicol.

MATERIAL AND METHODS

Spinacia Oleracea Leaves Extraction

The fresh plant material of *Spinacia oleracea* leaves was dried under the shade, then grinded. Later, one hundred grams of the powder was boiled in a magnetic stirrer with 1.5 liter of 70% ethanol for 72 hour at 40-45 C^{o} . Then the extract was sieved by using sterile guaze to get rid of coarse particulars, the solution then was filtered through Whitman filter. The filtrate was evaporated under vacuum in a rotary evaporator at 45 C^{o} after that, the extract was poured into a clean and sterile petridishes (12x2 cm) and kept in incubator at temperature of 45 C^{o} . (Maridass and John,2008).

Preparation of Stocks Solutions of the Extract of the Plant and Chloramphenicol

100 mg of the dried extract was dissolved in distilled water until the volume was completed to 10 ml. To make a concentration of 10mg/ml, the stock solution was prepared for a dose of (100mg/kg) mg/kg, 0.1 ml of the stock solution was given to each 10 gm mouse(Luka *et al* ., 2014). The stock solution of recommended dose of chloramphenicol (25mg/kg)body weight was prepared by dissolving 250mg in distilled water until the volume was completed to 100ml. to make a concentration of 2.5mg/ml, 0.1 ml of the stock solution was given to each 10 gm mouse (Saba *et al*., 2000) .

Experimental Animals

Fifteen albino Swiss mice weighting 28-30g were obtained from the animal house of the Ministry of Industry and Minerals/AL Razi research center. Mice were housed in plastic cages .30x10x10 cm putting. Standard rodent diet (commercial feed pellets) and tap water was freely available. Housing condition was maintained at 28± 2c and light / dark cycle (14/10 hours). The litter of cages was changed every 7 days.

Experimental Groups

Fifteen mice were divided into three equal groups treated orally by stomach tube for 14 days:

- The first group (T1) was treated by recommended daily dose of (25mg/kg) body weight of Chlormphenicol.
- The second group (T2) was treated by Chloramphenicol (25mg/kg) and extract of *Spinacia oleracea* (100mg/kg) body weight.
- The third group (T3) was treated by distilled water only.

Collection of Blood Sample

At the end of the experiment period, mice were anaesthetized by diethyl ether and the samples of blood have been obtained by cardiac perforate from anesthetized rats using disposable syringes of insulin.

Blood Tests

Hemglobin Test

The principle of this test is the dilution of the blood in the solution consists of potassium cyanide and potassium ferric cyanide ; in this case both of hemoglobin will rapidly convert into cyanohamogiobin by using Drabkin's Reagent 0.02 milliliter of bloo was pulled and mixed with 5 milliliter of reagent, left 5 min. then read was taken by using spectro-photometer according to the method mentioned by (Varly *et al*.,1980). Packed Cell Volume (P.C.V. Packed cell volume was measured by using micro-hematocrit-capillary tubes. After being filled with blood 2 to 3 up to their length. Other side of tubes was blocked by clay and been set in micro-hematocritreaer according to the method mentiond by (Archer,1985). While the white the blood cells and red blood cells Counting measured by using Thomas's solution to dilate blood to count WBCs and RBCs by haemocytometer method counting the type of pipette that used to pull up dilution fluid with WBCs and RBCs were counted in squares (squares of corners) Number of Counted WBCs/4x20x10=WBCs x50, WBCs/cm^3 blood. RBCs count= n/80x400x200x10. Furthermore, differential Counting of WBCs determined according to (Close,1974) one drop of blood was dripped on the slid then this drop was spread with one stroke and after getting dried, slide was dyed with leishman's stain and left 10 min. then washed with tap water, slide was examined under microscope (power of adjustment was 100) slid was examined in zigzag line up and down until 100 cells were counted (every type was identified to calculate the percentage of cell.

Histopathlogical Study

Specimen of 1-2 cm from liver was taken and kept in 10% neutral buffered formalin for fixation , processed routinely in histokinette, cut at 5mm thickness by microtome and stained with haematoxylin and eosin stain then examined under light microscope.(Luna,1968).

Statistical Analysis

SAS (2012) is the Statistical Analysis System- was used to result of changed factors in parameters of study. Least significant difference LSD test at (P□0.05) was used to significant compare between means in this study.

RESULTS

Hematological Parameters

The hematological parameters (packed cell volume (PCV%), hemoglobin (Hb), RBCs count, total WBCs count, neutrophil%, lymphocyte%, monocyte%, esinophil% and basophil%) of mice in chloramphenicol and *Spinacia oleracea* extract treated group showed a significant increase (p□0.05) as compared with chloramphenicol treated group and no significant difference (p□0.05) when compared with hematological parameters of mice treated with distilled water (control group) as in table (1). While the hematological parameters in chloramphenicol treated group showed a significant decrease (p□0.05) as compared with distilled water (control group).

*T1= treated with chloramphenicol *T2= treated with chloramphenicol and *Spinacia oleracea* extract* T3= treated with distilled water only.

Histopathological Changes:

The histolopathological section of liver mice treated with chloramphenicol showed the main lesions were characterized by sever Coagulative necrosis , pyknotic or disappear of nuclei of hepatocyte as well as Dilated sinusoid with inflammatory cell infiltration in the lumen (figure 1) and atrophy of hepatic cord, and in the other section Vacular degeneration and congestion of blood vessels (figure 2). While the histopathological section of mice liver treated with chloramphenicol and *Spinagia oleracea*extract showed kupffer cell proliferation, figure (3), in addition to disappearing the sever necrosis with mononuclear cells infiltration particularly Lymphocyte aggregation around blood vessels and central vein (figure 4).

DISCUSSION

The alcoholic extract of leaves of plant was dried and 6.9% of extract eas used, this result agreed with the result reported by(Jai and Loganathan, 2010). But it differ from the percentage obtained by (Erika *et al*.,2012).The results of hematological parameters of in T2 group may be due to the presence of vitamin and mineral contents of the leaves of *Spinaciaoleracea*, these constituents are well known haemopoietic factors that have direct influence on the production of blood in the bone marrow.

Also, may be indicated that the plant extract has the ability to stimulate the erythropoietin release into the kidney which is the humoral regulator of RBC and WBCs production.(Sanchez *etal*., 2004) Erthropoietin increases the number of erythropoietin – sensitive committed stem cells in the bone marrow that are converted to red blood cell and subsequently to mature erythrocytes.(Ganong, 1997), In addition to ability of the plant in enhancing the proper utilization of the iron contained to synthesize heme/haemoglobin for new red blood cells thus leading to an improved Hb, PCV, WBCs and RBC. Interestingly, saponins of *Spinacia oleracea* especially terpene glycosides enhanced the natural resistance and recuperative powers of the body (pathirane *et al*., 1990; Singh *et al*.,1991).

Therefore, the anti- anaemic potential and haemoglobin restoring effect of aqueous extract of *Spinacia oleracea* leaf as suggested by the data in the present study could be attributed in part to its saponins contents.The manganese and copper of *Spinacia oleracea* acted as a co-factor for the antioxidant enzyme, superoxide dismutase. Copper is also required for the production of red blood cells. Zinc of plant also is a co-factor for many enzymes that regulate growth and development, digestion and nucleic acid synthesis(Tang *et al.,*2005).Furthermore, Saponins containing herbs have been successfully had detoxification effect used in the management of liver inflammation, as tonic sedative formulas and to promote and vitalize blood circulation. (Shi *et al*., 2004; Wang *et al*., 2005)

While the hematological parameters results of chloramphenicol treated group can be attributedto produce fatal aplastic anemia which related to reversible bone marrow depression, in addition the chloramphenicol had a haematological adverse effects and caused bone marrow disorders like reticulocytopenia, granulocytopenia andthrombocytopenia(Yuan and Shi, 2008).

Furthermore, Chloramphenicol prohibited apoptosis and in turn caused differentiation of abnormal cells which leads to the development of leukaemia like. It has been suggested that chloramphenicol-induced aplastic anaemia and leukaemia are related to the DNA damage caused by nitroso chloramphenicol, which is a product of the reduction of the para-nitro group of chloramphenicol.(Tripathi, 2003),The histological effect of mice liver in chloramphenicol treated group perhaps regarded to that chloramphenicol had really toxic effect on the liver. Chloramphenicol had earlier been reported as hepatic cytochrome p450 inhibitor.

Moreover, the Chloramphenicol had a degenerative change of the hepatic parenchymel cells, hyperbilirubinaemia was also observed in the animals administered with chloramphenicol. 80% of the total bilirubin was conjugated bilirubin which is a strong indication that the hyper bilirubinaemia was most likely to be of hepatic origin.(Robillart *et al*., 1998)

CONCLUSION

The *Spinacia oleracea* leaves alcoholic extract lead to prevent the adverse effect of chloramphenicol when given together. So in this study, *Spinacia oleracea* leaves alcoholic extract can rightly be mentioned as a plant of considerable importance for improving hematological parameters.

REFERENCES

1. Archer,R.K.(1985).Hematological techniques for use an animals . Oxford ; Blackwell, scientific publication .
2. Asai, A.; Terasaki, M., and Nagao, A. (2004)An epoxide-furanoid rearrangement of spinach neoxanthin occurs in the gastrointestinal tract of mice and in vitro: formation and cytostatic activity of neochrome stereoisomers;134(9):2237-43.
3. Borneo, R. ; LWT, Y. (2008). Food Science and Technology; 41: (10) : 1748–1751.
4. Coles,E.H.(1974).Veterinaryclinicalhistology.2nded.W.B.Sounders company .
5. Douglas, H. (2010). Etymological Dictionary; 2 (3).
6. Dwivedi, G. ;Dwivedi, S. (2007). "History of Medicine: Sushruta – the Clinician – Teacher par Excellence ;Vol.49 pp.243-4.
7. Edenharder, R.; Keller, G.; Platt, K.and Unger K.(2001). Isolation and characterization of structurally novel antimutagenic flavonoids from spinach(Spinaciaoleracea);49(6).
8. Falagas, M. E.; Grammatikos, A. P. and Michalopoulos, A. (2008). "Potential of old-generation antibiotics to address current need for new antibiotics". Expert Review of Anti Infective Therapy; 6 (5).
9. Fullerton, S.J. (2007). The Truth about Food. p. 224.
10. Gaikwad, P.S.; Shete, R.V. and Otari, K.V.(2010). A Pharmacognostic and Pharmacological Overview, International Journal of Research and Ayurveda & pharmacy; 1(1) 78-84.
11. Ganong,W.F. (1997). A review of Medical Physiology Appleton & Lange Pubiisher.; pp. a96.
12. Genannt, B.; Walczyk, T. and Renggli, S.(2008)Oxalic acid does not influence nonhaem iron absorption: a comparison of kale and spinach meals;62(3):336-41.
13. Hanif, R.;Iqbal, Z.; Iqbal, M.; Hanif, S. and Rasheed, M.(2006). Use of vegetables as nutritional food: role in human health , Journal of Agriculture and Biological Science; 1(1).
14. Heaney, R. P. (2006). Calcium in human health. p. 135.
15. Insel, P. M.; Turner, R. E. and Ross, D. (2003). Nutrition. (978); 474.

16. Lucarini, M.; Lanzi, S.; D'Evoli(2006), L. Intake of vitamin A and carotenoids from the Italian population--results of an Italian total diet study;76(3).
17. Luka,C.D. , Abdulkarim, M., Adoga GI, J ijjani, H and Olatund, A (2014). Antianemic potential of aqueous extract of Spinacia oleracea leaf in phenylhydrazine treated rat, Newyour Science Journal ;7(6).
18. Luna,L.G.(1968) . Manual of histologic staining methods of the a rmed forces . Institute of pathology . 3rd Ed . ,McGraw – Hill Book company , N.Y. ,Toronto. London , Sydney ; 12-31 .
19. Makiko, I.; Mutsuko, T.; and Takashi, N. (2005). Influence of the Amount of Boiling Water on the Sensory Evaluation, Oxalic Acid and Potassium Content of Boiled Spinach. Journal of Cookery Science of Japan; 38(4)
20. Manach, C.; Scalbert, A.; Morand, C.; Rémésy, C. and Jiménez, L.(2004)Polyphenols: food sources and bioavailability;79(5):727-47.
21. Maridass M, and A. John D. (2008) Origin of Plant Derived Medicines. Ethnobotanical Leaflets 12, 373.
22. Martini, F. (2007). Anatomy and Physiology; p. 643.
23. Morris, M.C.; Evans, D.A.; Tangney, C.C.; Bienias, J.L. and Wilson, R.S.(2006) Associations of vegetable and fruit consumption with age-related cognitive change. Neurology; 67(8):1370.
24. Mortensen, S.P.; Dawson, E.A. and Yoshiga, C.C.(2005). Limitations to systemic and locomotor limb muscle oxygen delivery and uptake during maximal exercise in humans;566 (pt1): 273-58.
25. Ogbe, R.J.; Adoga, G.I. and Abu, A.H.(2010). Antianemic potentials of some plant extracs on phenyl hydrazine-induced anemia in rabbits. J. Med Plant ; 4,680-684.
26. Okazaki, K.; Oka, N. and Shinano, T. (2008) Differences in the metabolite profiles of spinach (Spinacia oleracea L.) leaf in different concentrations of nitrate in the culture solution. Plant Cell Physio; 49(2).
27. Park, J. Y.; Kim, K. A.; Kim, S. L. (2003). "Chloramphenicol Is a Potent Inhibitor of Cytochrome P450 Isoforms CYP2C19 and CYP3A4 in Human Liver Microsomes". Antimicrobial Agents and Chemotherapy; 47 (11).
28. Pathirana, C.; Gibney,M.; Taylor,T.(1990). Effect of soy protein and saponins on serum and liver cholesterol in rats. Atherosclerosis ;36, 595_599.
29. Pormann, P. E.; Smith, E. S. (2007) Medieval Islamic medicine Georgetown University; p. 48.
30. Robillart, A.; Zeisser, M.; Vailly, B. and Dupeyron, J.P.(1998)Hepatic mono-oxygenases; 7 (2): 149-155.
31. Rolland, A.; Jacques, L.; Sherman, H. and Carol, J. (2006). The Food Encyclopedia. Toronto: Robert Rose. pp. 335–338.
32. Saba A.B; Ola -davies, O; Oyeyemi, M.O and Ajala O. (2000): The toxic effects of prolonged administration of chloramphenicol on the liver and kidney of rats, Afr. J. Biomed: Vol 3; 133 – 137.
33. Sanchez, E.T.; Ramirez, J.R.; Rodriquez, S.F.; Varela, E.K.; Bernabeu, C.Y. and Botelia, L.M. (2004). Acrosstalk between hypoxia and TGF_beta o rchestraies erythropoietin gene reguiation through SPI and Smads ,J.; 336(1).
34. SAS Institute.SAS/STAT,(2012) Guide for personal computers version, 9th Ed. SAS Instutite Inc; Cary NC ,USA. .
35. Sherwood, L. (2011). Human Physiology: From Cells to Systems. pp. 401.
36. Shi, J.;Arunasalam, K.;Yeung, D.; Kakuda, Y.; Mittal, J. and Jiang, Y.(2004). Saponins from edible legumes: chemistry, processing, and health benefits. Journal of Medicine Food.; 7, 67_78.
37. Shoja, M. M.; Tubbs, R. S.; Loukas, M.; Khalili, M.; Alakbarli, F. and Cohen-Gadol, A. A. (2009). "Vasovagal syncope in the Canon of Avicenna: The first mention of carotid artery hypersensitivity". International Journal of Cardiology;134 (3): 297–301.
38. Singh, N.; Verma, P.; Mishara, N.and Nath, R.(1991). A complete, evaluation of some antistress agent of paints origin. Indian J. Pharmacol. ;21:99.
39. Song, W.; Derito, C.M. and Liu, M.K. (2010). Cellular antioxidant activity of common vegetables. ; (11):6621.
40. Sutton, M. (2010). "SPINACH, IRON and POPEYE: Ironic lessons from biochemistry and history on the importance of healthy eating, healthy scepticism and adequate citation; 15(23).
41. Tang, G.; Qin, J. and Dolnikowski,G. (2005).Spinach or carrots can supply significant amounts of vitamin A as assessed by feeding with intrinsically deuterated vegetables;82(4):821-8.
42. Tripathi, K.D.(2003). Essential of Medical pharmacology; p (674_675).
43. Varlay, H. ; Gonlock, A. H. and Bell, M.(1980). Practical clinical biochemistry 5th ed. Williu Heinemann . medical books . Ltd. London

44. Vieria, M.R.; Galzvao, L.C. and Fernandes, M.I.(2000). Relation of the disaccharidases in the small intestine of the rat to the degree of experimentaly induced iron-deficiency anemia;33: 539-544
45. Wang, J.; Xu, J. and Zhong, J.(2005). Effect of Radix notogeineseng saponins on platelet activating molecule expression and aggregation in patient with blood hyperviscosity syndrome. Alternative Medicine Review ;24 , 312_316.
46. Wang, Y.; Chang, C.; Chou, J.; Chen, H.; Deng, X.; Harvey, B. and Cadet, J.(2005) Bickford PC. Dietary supplementation with blueberries, spinach, or spirulina reduces ischemic brain damage;193(1):75-84.
47. Woods, M.; Adrienne, L. (2008). Delmar nurse's drug handbook. Delmar;p. 296.
48. Yang ,Y.; Marczak, E.; Yokoo, M.; Usui, H. and Yoshikawa, M. (2003) Isolation and antihypertensive effect of angiotensin I-converting enzyme (ACE) inhibitory peptides from spinach Rubisco;51(17):4897-902.
49. Yuan, Z. and Shi, Y. (2008). Chloramphenicol induces abnormal differentiation and inhibits apoptosis in activated T cells, cancer Res.;68, 4875_4881.

Table (1):Effect of Alcoholic Extract of *Spinacia oleracea*,on P.C.V., Hb, RBCs and total WBCs Count after 14 days of the Treatment.

Gro-ups	PCV %	Hb g/dl	RBCs x10³/m	WBCs cell/cm³	N %	L %	M %	E %	B%
T1	30.91± 2.66 B	9.06± 0.36 B	4.2 ± 0.46 B	4050 B ± 12.72 B	39.4 ± 1.22 B	40.2 ± 0.9 B	5.1 ± 0.51 B	1.4 ± 0.25 B	1 ± 0.19 A
T2	40.29± 2.07 A	11.4± 0.42 A	5.5 ± 0.42 A	5450± 9.41 A	56.0± 2.61 A	47.0 ± 1.7 A	6.4 ± 0.62 A	3.3 ± 0.30 A	2± 0.21 A
T3	38.3± 2.58 A	12.7± 0.20 A	5.1 ± 0.53 A	5399 ± 9.05 A	58.9 ± 1.80 A	48.2 ± 1.3 A	7.7 ± 0.92 A	3.5 ± 0.21 A	1 ± 0.19 A

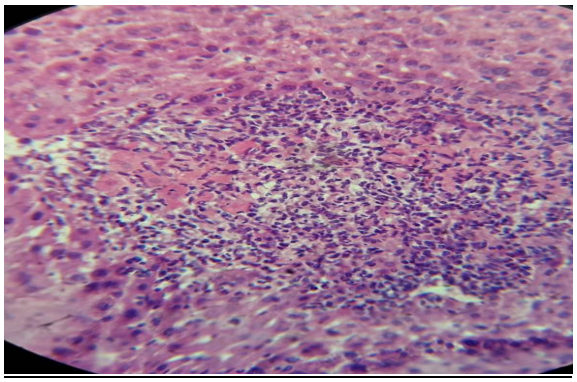

Figure (1): Tissue Section in Liver Mouse Treated with Chloramphenicol Showed the Main Lesions were Characterized by sever Coagulative Necrosis , Pyknotic or Disappear of Nuclei of Hepatocyte. H and E (40X)

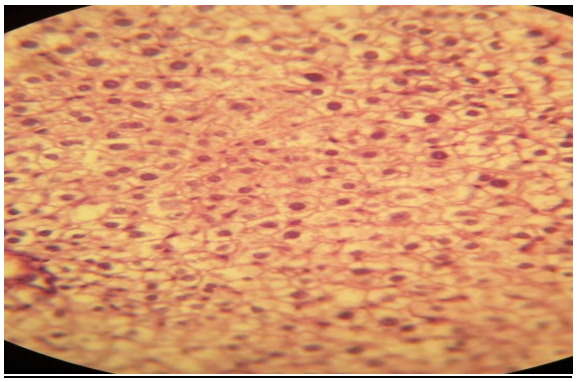

Figure (2):Tissue Section in Liver Mouse Treated with Chloramphenicol Showedatrophy of Hepatic Cord, and in the other Section Vacular Degeneration and Congestion of Blood Vessels.H and E (40X)

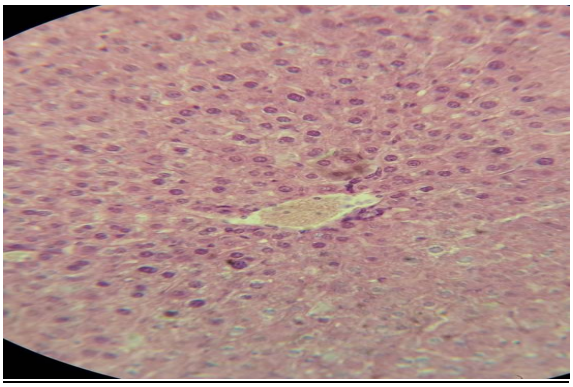

Figure (3): Tissue Section in Liver Mouse Treated with Chloramphenicol and *Spinagia oleracea*extract Showed Kupffer Cell Proliferation.H and E (40X).

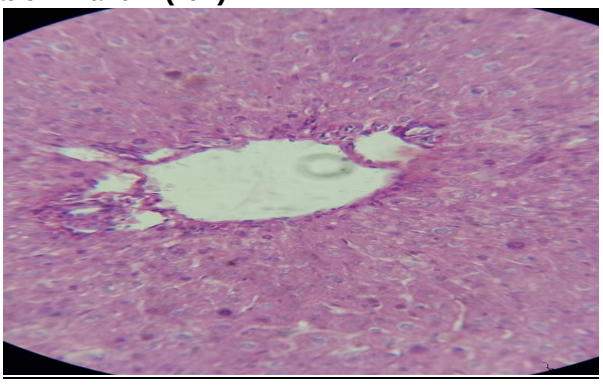

Figure (4): Tissue Section in Liver Mouse Treated with Chloramphenicol and *Spinagia oleracea*extract Showeddisappearing the Sever Necrosis with Mononuclear Cells Infiltration Particularly Lymphocyte Aggregation Around Blood Vessels and Central Vein.H and E (40X).

Indian Journal of Natural Sciences www.tnsroindia.org.in ©IJONS

Vol.8 / Issue 45 / December 2017 *International Bimonthly* *ISSN: 0976 – 0997*

RESEARCH ARTICLE

Prevalence and Molecular Characterization of Methicillin Resistant Staphylococcus aureus in Bovine Raw Milk and Beef Samples from Wayanad District of Kerala

Mahesh S.H[1]*, Prejit[1,3], Vinod V.K[1], B. Sunil[1], Koshy John[2] and Nimisha Soman[1]

[1]Department of Veterinary Public Health, College of Veterinary and Animal Sciences, Pookode, Wayanad, Kerala – 673 576

[2]Department of Veterinary Microbiology, College of Veterinary and Animal Sciences, Pookode, Wayanad, Kerala – 673 576

[3]Centre for One Health, Education, Advocacy, Research and Training,College of Veterinary and Animal Sciences, Pookode, Wayanad, Kerala-6735 76.

Received: 17 Oct 2017 Revised: 22 Oct 2017 Accepted: 25 Nov 2017

*Address for correspondence

Mahesh S.H

M.V.Sc Scholar,Department of Veterinary Public Health,
College of Veterinary and Animal Sciences,
Pookode, Wayanad, Kerala – 673 576
Moblile No: 9483271450
Email: drmaheshshvetvet09@gmail.com

ABSTRACT

Emergence of methicillin resistance in *Staphylococcus aureus* is a major concern of public health. In the present study the meat and milk were analysed for isolation and identification of methicillin resistant *S. aureus*(MRSA) from bovine raw milk and beef samples collected from Wayanad District of Kerala, India. Further, the isolates werecharacterised by *nuc* gene and followed byantibiotic resistant potential targeting *mec*A gene through application of PCR. A total of 120 food samples (60 each of raw milk and meat ;) were collected and analysed for detection of *S.aureus* and MRSA.On biochemical and molecular characterization, 18 *S. aureus* were identified from meat (3.33 %) and milk (15 %) samples.Upon screening of MRSA for *mec*A gene, five milk (8.33 %) samples were found positive. The relevance of contamination of MRSA in food sources poses a potential health hazard, thus it is necessary to monitor the foods of animal origin and hygienic practices in order to reduce the health hazards to consumers.

Key words: *Staphylococcus aureus,*MRSA, Milk, Beef, *mec*A

INTRODUCTION

Staphylococcus aureus has been recognized as one of the major cause of food poisoning. It is a natural inhabitant of skin and nasal cavity of both human and animals. These organisms can multiply, survive and colonise in wide range of changing environmental conditions with ubiquitous adaption capacity, which may enhance the growth and multiplication of the organism and contaminate the meat and milk products (Jakson *et al*., 2013). In addition, Staphylococcal virulence genes producing different toxins and antibiotic resistance pattern leads to healthcare associated infections and hospitalization (Wendlandt *et al*., 2013).

The virulent strains of *S. aureus* are showing resistance pattern to many antimicrobial agents, such as methicillin resistant *S. aureus* (MRSA). Globally, MRSA infections were commonly reported from healthcare settings and emerged as community-associated infections**(**EFSA, E. 2015**).**In recent years, MRSA has been identified as an emerging pathogen from companion animals, livestock and associated with food product of animal origins(Li *et al*., 2014).

Rapid detection of Methicillin resistance together with the identification of *S. aureus* is necessary for diagnostic, therapeutic and epidemiological purposes. Conventional culture methods were time consuming and most have inherent limitations (Maes *et al*., 2002). Polymerase chain reaction (PCR) based detection methods targeting *nuc* and *mec*A gene of MRSA have shown to be sensitive, reliable and rapid approach for identification of MRSA. The presence of *mecA* gene, a mobile genetic element in the staphylococcal cassette chromosome *mec* (SCC*mec*) of methicillin resistance of *S. aureus* is conferred and it codes for penicillin-binding protein (PBP)(Ito *et al*., 2001).

The increased prevalence rate of multidrug resistant and virulent *S. aureus* strains poses a emerging threat to the animal based food industries, which needs a regular monitoring surveillance systems. Hence the study reveals the isolation, identification and molecular characterization of methicillin resistant *S. aureus* isolates from bovine raw milk and beef samples collected from various retail markets of Wayanad District.

MATERIALS AND METHODS

Collection of Food Samples

A total of 120 samples (60 samples each of bovine raw milk and beef samples) were collected during the period august 2016 to March 2017 from different retail outlets of Wayanad District of Kerala. All the samples were collected aseptically and transported to the laboratory in insulated condition. The Samples were processed within 6 hours of collection in the laboratory for further isolation and molecular detection of *S. aureus*.

Isolation and Identification of s*. aureus*

Isolation and identification of different enteric bacterial pathogens was attempted by culture method as described by Agarwal *et al.* (2003). Initially the milk and meat samples were homogenised (BagMixer®CC) and enriched (1:10 dilution) into Braine Heart Infusion (BHI) broth and incubated at 37°C for 24 h. Streaked loopful of enriched culture from BHI broth on to Baird-Parker agar and incubate at 37^0C for 48 h.A shiny, jet black coloured colonieswith opaque zones surrounded by clear halo of *S. aureus* were isolated and further subjected to biochemical confirmation like gram staining, catalase and coagulase production by standard procedure described by Barrow and Feltham, 2003.

Molecular Characterization of MRSA

Molecular detection and characterisation of *S. aureus* isolates from the milk and meat samples were carried out by polymerase chain reaction (PCR) targeting the nuclease gene (*nuc*) and methicillin resistance determinant (*mec*A) gene. Genomic DNA of *S. aureus* isolates were prepared by Phenol: Chloroformmethod as described by Sambrook and Russel, 2001. Genomic DNA of *E. coli* DH5α was considered as negative control DNA template in PCR. The oligonucleotide primers were got synthesized by SciGenom Labs, Kochi, India (Table 1).

The standardized PCR protocol targeting *nuc* and *mec*A genes includes 20 µL reaction having 2.0 µL of 10X PCR buffer, 1.6 µL of 10 mM dNTP mix, 0.4µl of 10 µM primer set containing forward and reverse primers, 0.05 units of Taq DNA polymerase (1U/50µl), 0.5 µL of DNA template and nuclease free water to make up the reaction volume. The cycling conditions of PCR, initial denaturation of DNA template at 94°C for 3 min, followed by 34 cycles each of 40 s denaturation at 94°C, 50s annealing at 58°C and 1 minute extension at 72°C. At the end of all cycles, a final extension at 72°C for 10 min was performed in a T100™Thermal Cycler (Bio-Rad, USA). The amplified PCR products were separated and visualized by gel electrophoresis along with 100bp DNA ladder in 1.2 per cent agarose containing ethidium bromide by electrophoresis using Tris-Acetate- EDTA (TAE) as running buffer and visualised by gel documentation system. Ethidium bromide contaminated materials were disposed as per local guidelines.

RESULTS AND DISCUSSION

In this study, *S. aureus* was detected from both bovine raw milk and meat (beef) samples. The characteristic jet black coloured colonies with opaque zones surrounded by clear halo were presumptively considered as*S. aureus* were isolated from Baird-Parker agar (Fig. 1).Isolating *S. aureus* in food samples depends usually on culturing viable cells on Baird Parker medium (Wehr& Frank, 2004). Out of 120 samples analysed 18 samples were found positive for *S. aureus* upon biochemical characterisation. *S. aureus* were identified from meat (3.33 %) and milk (15 %) samples on PCR targeting *nuc* gene. Kamal *et al*., 2013 reported, out of 35 raw milk samples tested, nearly 94% (33 samples) were contaminated by *S. aureus*. Upon screening of MRSA for *mec*A gene, five milk (8.33 %) samples were found positive in the present study. To support the present study, out of 160 samples analysed for detection of *S. aureus* strains, four isolates were found positive for *mec*A gene from bovine milk samples (Normanno *et al*., 2007).The representation of PCR amplification of *nuc* and *mec*A genes for MRSA were represented in Fig 2.The beef samples analysed in the present study were found negative for MRSA. Similarly, MRSA strains were isolated from animal meat products like beef, veal, mutton, pork and chicken (Boer *et al*., 2009). The study conducted by Weese *et al*., 2010 reported 5.6 per cent occurrence of MRSA from beef samples.

S. aureus strains produce an extracellular thermostable nuclease (thermonuclease) with a frequency similar to coagulase are characterised by PCR targeting amplification of *nuc* gene was found highly sensitive and reliable in nature (Brakstad *et al*. 1992).

The results of the presence study reveals that *S. aureus* is prevalent in raw bovine milk and meat (beef) samples could pose a potential risk factor to consumers at retail milk and meat markets. In addition, detection of *S. aureus* and MRSA by PCR targeting *nuc* and *mec*A genes respectively can be used as a tool for rapid, sensitive and specific identification method.

ACKNOWLEDGEMENTS

The analysis was supported as a part of the State Plan Project, Government of Kerala sanctioned to the Centre for One Health Education, Advocacy, Research and Training (COHEART), KVASU, Kerala.

REFERENCES

1. Agarwal, R. K. (2003). Laboratory manual for the isolation and identification of foodborne pathogens.
2. Brakstad, O. G., Aasbakk, K., &Maeland, J. A. (1992). Detection of Staphylococcus aureus by polymerase chain reaction amplification of the nuc gene. *Journal of clinical microbiology*, *30*(7), 1654-1660.
3. Cowan, S. T., & Steel, K. J. (2003). *Cowan and Steel's manual for the identification of medical bacteria*. Cambridge university press.
4. EFSA, E. (2015). EU Summary Report on antimicrobial resistance in zoonotic and indicator bacteria from humans, animals and food in 2013. *EFSA Journal*, *13*(2), 4036.
5. Frey, Y., Rodriguez, J. P., Thomann, A., Schwendener, S., &Perreten, V. (2013). Genetic characterization of antimicrobial resistance in coagulase-negative staphylococci from bovine mastitis milk. *Journal of dairy science*, *96*(4), 2247-2257.
6. Wendlandt, S., Schwarz, S., &Silley, P. (2013). Methicillin-resistant Staphylococcus aureus: a food-borne pathogen. *Annual review of food science and technology*, *4*, 117-139.
7. Ito, T., Katayama, Y., Asada, K., Mori, N., Tsutsumimoto, K., Tiensasitorn, C., &Hiramatsu, K. (2001). Structural comparison of three types of staphylococcal cassette chromosome mec integrated in the chromosome in methicillin-resistant Staphylococcus aureus. *Antimicrobial agents and chemotherapy*, *45*(5), 1323-1336.
8. Li, G., Wu, C., Wang, X., &Meng, J. (2015). Prevalence and characterization of methicillin susceptible Staphylococcus aureus ST398 isolates from retail foods. *International journal of food microbiology*, *196*, 94-97.
9. De Boer, E., Zwartkruis-Nahuis, J. T. M., Wit, B., Huijsdens, X. W., De Neeling, A. J., Bosch, T,&Heuvelink, A. E. (2009). Prevalence of methicillin-resistant Staphylococcus aureus in meat. *International journal of food microbiology*, *134*(1), 52-56.
10. Normanno, G., Corrente, M., La Salandra, G., Dambrosio, A., Quaglia, N. C., Parisi, A. &Celano, G. V. (2007). Methicillin-resistant Staphylococcus aureus (MRSA) in foods of animal origin product in Italy. *International journal of food microbiology*, *117*(2), 219-222.
11. Kamal, R. M., Bayoumi, M. A., & El Aal, S. F. A. (2013). MRSA detection in raw milk, some dairy products and hands of dairy workers in Egypt, a mini-survey. *Food Control*, *33*(1), 49-53.

Table 1. Details of the Primers used in the Study

Primers	Oligonucleotide sequence (5′-3′)	Amplicon size(bp)	Reference
nuc	F -GCGATTGATGGTGATACGGTT R -AGCCAAGCCTTGACGAACTAAAG	279	(Brakstad *et al*. 1992)
***mec*A**	F -AAA ATC GAT GGT AAA GGT TGG C R -GT TCT GCA GTA CCG GAT TTG C	533	(Frey *et al*. 2013)

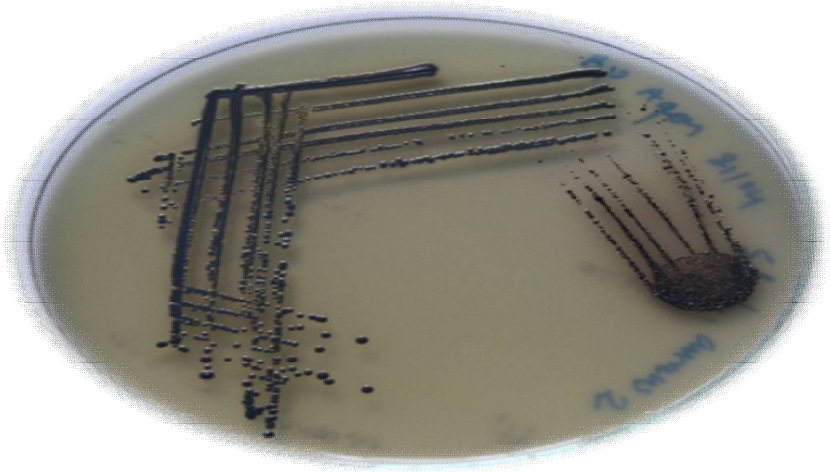

Fig. 1. *S. aureus* on Baird Parker (BP) Agar (Tiny Jet- Black Coloured Colonies)

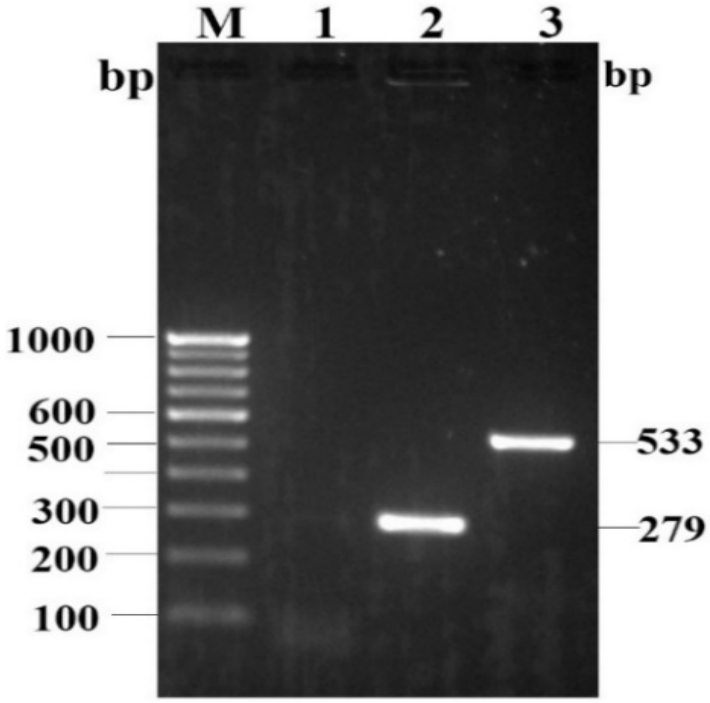

Fig 2. Standardized PCR Protocol for MRSA *nuc*- 279 bp and *mec*A- 533 bp Lane M: 100 ladder; Lane 1. Negative Control Lane 2, 3: PCR Products

Indian Journal of Natural Sciences www.tnsroindia.org.in ©IJONS

Vol.8 / Issue 45 / December 2017 *International Bimonthly* *ISSN: 0976 – 0997*

RESEARCH ARTICLE

Using Geographic Information System to Assess Groundwater Quality in Palani Taluk of Dindigul District, India

G.Noushad[1*] and A.Ilanthirayan2

[1]Research Scholar, Bharathiar University, Department of Geography Coimbatore, Tamilnadu,India
[2]Assistant Professor, Department of Geography, Government Arts College (A), Salem, Tamilnadu, India

Received: 05 Oct 2017 Revised: 23 Oct 2017 Accepted: 25 Nov 2017

[*]**Address for correspondence**
G.Noushad
Assistant Professor,
Department of Civil Engineering,
Ranganathan Engineering College,
Thondamuthur, Tamilnadu, India.
Email: noushadgis@yahoo.com

ABSTRACT

Groundwater plays a vital role in the world. This is the main sources of drinking water in the urban environment, it also used for industrial and domestic purposes. In this study area Groundwater quality assessment has special significance and needs great attention of all concerned since it is the major alternate source of domestic, industrial and drinking water supply. The present study groundwater samples were collected from 77 predetermined open wells and bore wells representing in Palani Taluk. Thematic maps for the study are prepared by visual interpretation of SOI toposheets on 1:50,000 scale using ArcMap version10.3software. The groundwater samples were analyzed for physico-chemical parameters like pH, EC,TDS, TH, Ca, Mg, Cl, SO4, NO3, Na, and K using BIS standard in the laboratory. Also groundwater samples data collected at predetermined locations to generate spatial distribution maps of major water quality parameters are prepared using IDW method in ArcMap software. Final integrated map shows two priority classes such as Suitable and Unsuitable groundwater quality zone of the study area and provides a guideline for the suitability of groundwater for drinking purposes.

Keywords: Groundwater**,** Geographical Information System (GIS), Groundwater quality, Inverse Distance Weighted (IDW).

INTRODUCTION

Groundwater is the only source of drinking water most of the population in India. Pure drinking water is now accepted as an essential right of human beings. The natural impurities in rainwater, which replenishes groundwater systems, get removed while infiltrating through soil strata. Groundwater contaminated by naturally or several types

of human activities, residential, municipal, commercial, industrial, and agricultural activities can all affect groundwater quality. The quality of public health depends on the quality of drinking water, it is result that detailed information about the quality of water systematically collected and monitored. The groundwater is believed to be comparatively much clean and free from pollution than surface water. Assessment of the suitability of groundwater for domestic purpose requires concentrations of physico-chemical parameters. Bureau of Indian Standards (BIS) have specified concentration limits of various constituents for groundwaters for different uses, such as domestic, agriculture and Industrial.

GIS is an effective tool for groundwater quality mapping and essential for monitoring. GIS has been used in the map classification of groundwater quality, based on physico-chemical parameters. In some of the studies, GIS is utilized to find groundwater quality zones suitable for different usages such as domestic, agriculture and Industrial.

Karnath (1987) have evaluated the groundwater quality variation based on physical and chemical parameters. The physical and chemical properties of groundwater are a measure of its suitability for domestic, irrigation, and for industrial and other purposes. Ahmed et al (2002) have evaluate the laboratory results of groundwater in Rajshahi city of Bangladesh they have classified groundwater into various types. Anbazhagan et al (2004) have stated that the use of GIS to present and realize the spatial variation of physicochemical elements in Panvel Basin. Subramani et al (2005) have expressed the variation of groundwater quality of the area is a function of physical and chemical parameters that are greatly determined by geological formations and anthropogenic activities. Sarath Prasanth et al. (2012) have reported that quality of groundwater and its suitability for domestic purpose in the Alappuzha district. Y Srinivas et al (2013) have evaluated the major ion chemistry, the factors controlling water composition, and suitability of water for both drinking and irrigation purposes in and around Nagercoil town. J. Colins Johnny et al. (2014) has reported groundwater quality is a continuously changing phenomenon, variation occurs with time and space, so there is a need to check and revise the water quality parameters and maps, regularly with time and space.

Location and Extent

The Study Area lie between 10°20'2'' North latitudes to 10°38'24'' N as well as longitudes 77°18'6'' E to 77°35'41'' East. The total geographical extent of the study area is 766.83 km^2 shown in Figure 1. Palani Taluk is bounded by Thoppampatti Taluk towards North, Kodaikanal Taluk towards South, Madathukulam Taluk towards west, Oddanchatram Taluk towards East. The review territory comes in Dindigul District of Tamilnadu. The significant source of groundwater is precipitation, south-west season. The normal average rainfall is 690mm. The drainages flowing in the study area are Amravathi, Varthar, Murudanadi and Parappalar.

MATERIALS AND METHODS

Groundwater level determined for the past three years (2014 – 2016), both in Pre & Post monsoon period in 77 existing bore well points shown in Figure 2. Groundwater samples were collected from 77 existing bore well and open well points using field survey for the years 2014 – 2016 in two liters of Polythene containers. The containers were thoroughly washed with tape water the water sample to be collected and then filled up the bottle with the sample leaving only a small air gap at the top, stopper and sealed the bottle. The individual sample locations were plotted in GIS for the study area shown in Figure 2. The groundwater sample locations cover widely includes commercial, industrial, and residential areas. Each of the groundwater samples analysis has been carried out for the parameters such as pH, electrical conductivity (EC), total dissolved solids (TDS), sulphate (SO4), chloride (Cl), sodium (Na), potassium (K), calcium (Ca), magnesium (Mg), Nitrate (NO3), Total alkalinity (CaCO3) and total hardness (TH) using standard protocols recommended by APHA [1] IS: 10500-1994 codes. The spatial variations of individual parameters of water quality spatial distribution maps generated for Palani Taluk.

RESULTS AND DISCUSSION

Groundwater physicochemical values are analysed in the laboratory with reference to BIS drinking water standard protocols and tabulated in Table 1.

- **pH:** pH is one of the essential parameters of water and determines the acidic and alkaline nature of water. The pH of the good quality water ranges from 6.5 to 8. The spatial distribution map for pH was prepared and presented in Figure. 3. The map shows that major parts of study area have the pH value in the desirable range. The villages namely Thalaiyuthu, Pappampatti, Karikkaranpudur, Narikkalpatti, Guranvanvalasu and Marichilambu have the pH value in undesirable range.

- **Electrical Conductivity (EC):** According to the BIS standard, the desirable range of EC 700-3000 00 μmhos/cm. In the study area, EC of the groundwater samples are found to ranges from 167.00 μmhos/cm to 3000 μmhos/cm. The spatial distribution map for EC was prepared and presented in Figure. 4. The map shows that major parts of study area have the EC value in the desirable range. The few villages like Erumanayakkanpatti and Melkaraipatti have the undesirable range (>3000 μmhos/cm) of EC.

- **Total Hardness (TH):** The additional essential parameters of water. The BIS standard value of hardness ranges for a good quality water range is 300-600mg/L. Total hardness was classified to Three ranges (0-300 mg/L, 300-600, >600 mg/L). The spatial distribution map for total hardness was prepared based on these ranges and presented in Figure. 5. From the spatial variation map it was observed that major part of the study area has suitable range (300-600 mg/L). The most of the villages Ayyampalaiyam, Talaiyuthu, Narikkalpatti, and Tumpalapatti have the undesirable range of hardness (> 600 mg/L).

- **Chloride (Cl):** According to the BIS standard, public drinking water standards for chloride is not to exceed 250 mg/L. The normal value of chloride for a good quality water is 250-1000 mg/L. in the stydy area chlorides can be classified into three ranges (0-250 mg/L, 250-1000, >1000 mg/L). The spatial distribution map for chlorides was presented in Figure. 6. This clearly shows that the major parts of tha study area have desirable range of chloride. Ayyampalaiyam, Tatanayakkanpatti, Pushpathur, Talaiyuthu, Narikkalpatti, Tumpalappatti, Toppampatti, Marichchilambu, and Pulampatti villages have the undesirable range of chloride (>1000 mg/L).

- **Total Dissolved Solids (TDS):** It is essential to classify the groundwater depending upon their physico chemical properties based on TDS values for ascertaining the suitability of groundwater for any purpose. In this study area the TDS was classified into three ranges (0-500 mg/L, 500-2000 mg/L, >2000 mg/L). The spatial variation map for TDS was prepared based on these ranges and presented in Figure. 7. From the map it has been observed that major part of the study area has TDS values in the desirable range of 500-2000 mg/L. But the some villages namely Erumanayakkanpatti and Melkaraipatti have a undesirable range of >2000 mg/L.

- **Calcium (Ca):** According to the BIS standard, the desirable range of Ca 75-200 mg/L. The spatial distribution map for calcium has been presented in Figure. 8. From the spatial distribution map, it was observed that northwest part of the study area like Pushpathur, Talaiyuthu, Manoor, Kalayamputhur, Neikarapatti, Keeranur, Kottatturai and Guruvanvalasu have calcium values in the suitable range (0-75mg/L). It was observed that Pulampatti, Amarappundi, Sivagiripatti, Balasamudram and Kanakkanpatti villages, located in the Eastern part of the study area, have the calcium value in the moderate range (75-200 mg/L). But the Erumanayakkanpatti village has the calcium value in beyond the desirable range (<200 mg/L).

- **Magnesium(Mg):** Magnesium is one of the abundant elements in rocks. It causes hardness in water. The high level of magnesium found in hard water, which has some anti-stress actions against heart disease. In the study area the spatial distribution map for magnesium has been obtained and presented in Figure. 9. From the spatial distribution map shows that major part of the study area has magnesium value in the desirable range (30-100 mg/L). Some part of the study area like Erumanayakkanpatti, Sivagiripatti, Kanakkanpatti, Balasamuthiram and Manjanaikenpatti villages have beyond the desirable range (>100 mg/L).

- **Sulphates (SO4):** According to the BIS standard, the desirable range of SO4 200-400 mg/L. In the study area, sulphate content was classified into three ranges (0-200 mg/L, 200-400 mg/L, >400 mg/L) and based on these ranges the spatial distribution map for sulphates has been presented in Figure. 10. The spatial distribution map clearly shows that the study area has the sulphate value below the desirable range.

- **Nitrate (NO3):** The BIS allowable Nitrate concentration in potable waters is 45-100mg/L. Nitrate levels at or above this level the symptoms of blue-baby syndrome can be subtle and often confused with other illnesses. The spatial distribution map for nitrate was prepared based on these ranges and presented in Figure. 11. The study area nitrate was classified to three ranges (0-45mg/L, 45-100 mg/L, >100 mg/L). It shows that major part of the study area has the nitrate value are below the desirable range (0-45mg/L). But the villages namely Kondaimangalam**,** Erumanayakkanpatti and Kanakkanpatti have the desirable range (0-45mg/L) Nitrate concentration.

- **Sodium (Na):** In the study area, sodium content in the groundwater samples was classified into three ranges (0-45 mg/L, 45-100 mg/L, <100 mg/L) and based on these ranges the spatial distribution map for sodium has been presented in Figure. 12. The spatial distribution map clearly shows that the study area has the sodium concentration are found to be very high compared to all other ions. But the some villages namely Talaiyuthu, Pushpathur, Tumbalapatti, Toppampatti, and Narikkalpatti have an desirable range of sodium (45-100 mg/L).

- **Potassium (K)**: In the present study area, potassium content in the groundwater samples was classified into TWO ranges (0-10 mg/l, <10 mg/l) and based on these ranges the spatial distribution map for potassium has been presented in Figure. 13. The spatial distribution map clearly shows that the study area has the potassium concentration are found to be very high (<10 mg/l) major villages. Only few villages have the desirable range of potassium (0-10 mg/l).

Integrated Groundwater Quality Map using GIS

After creating individual spatial distribution maps for drinking water purposes, we integrated the all into a combined map. The integrated Groundwater Quality Map for palani taluk shown in Figure.14. The groundwater quality map indicating the suitability of Groundwater Zones for drinking water. The groundwater quality has been classified quantitatively as suitable, and unsuitable depending on the integration of overall analysis. From the map, it is observed that the most part of the study area is having undesirable groundwater quality, while in the northern part of the study area the groundwater quality is in the good condition. The villages namely thoppampatti, Narikkalpatti, Tumbalapatti and Talaiyuthu have excellent and good groundwater quality zones. The villages namely Vedasandur, Valayapatti, Kalvelipatti and Idayapadi have moderate groundwater quality zones. The villages namely Papampatti, Kondaimangalam, Sandanchettivalasu, Guruvanvalasu, and Kottaturai of Palani taluk have Poor groundwater quality zones.

CONCLUSION

Groundwater quality in Palani Taluk has been analysed in the present work. The groundwater samples conform that overall pH level of groundwater was within limit. The groundwater is acidic in nature and total hardness observed in all samples 13% samples fall very hard category. The total dissolved solids values were more than maximum permissible limit in 4 samples, these sample water are not suitable for drinking purpose. In 2 samples were having Calcium more than maximum permissible limit. The Magnesium values were in 7 samples having the above the permissible limit. The Nitrate concentration in the northern part exceeded the permissible limit. The Chloride values above the permissible limit in 4 samples. Only 1samples were found which are having Sulphates more than 400 not suitable for drinking. In the present study, interpretation of physicochemical analysis displays that the groundwater in area is Medium to hard. Thus groundwater quality map used to demarcate the locational distribution of water quality in a inclusive manner and help in suggesting groundwater suitable for domestic purposes.

REFERENCES

1. S S Ahmed, Q H Mazumder, C S Jahan, M Ahmed, S Islam (2002) "Hydrochemistry and classification of groundwater, Rajshahi City Corporation Area, Bangladesh", Journal of Geological Society of India, Vol.60, pp:411–418.
2. S Anbazhagan, AM Nair (2004) "Geo-graphic information system and groundwater quality mapping in Panvel Basin, Maharashtra, India" ,Journal of Environmental Geology, Vol. 45, pp:753–761.
3. APHA Standard Methods for the Examination of Water and Wastewater, 17th ed. APHA, Washington, DC (1995).
4. Guidelines for Drinking Water Quality, 4th ed., World Health Organization Recommendations, WHO, Geneva,1-4 (2011)
5. Indian Standard Drinking Water Specification, Bureau of Indian Standards, New Delhi, 2-4 (2012)
6. J. Colins Johnny and M. C. Sashikkumar 2014. "Groundwater Quality Assessment in Dindigul District, Tamil Nadu Using GIS". Nature Environment and Pollution Technology, 3(1): 49-56
7. KR Karanth (1987) Ground water assessment, development and management.Tata McGraw Hill, New Delhi, pp 720
8. SV Sarath Prasanth, NS Magesh, KV Jitheshlal, NChandrasekar, K Gangadhar (2012), "Evaluation of groundwater quality and its suitability for drinking and agricultural use in the coastal stretch of Alappuzha District, Kerala, India", Applied Water Sciences, Vol 2, pp:165–175
9. T Subramani., L Elango., S.R Damodarasamy., (2005), "Groundwater quality and its suitability for drinking and agricultural use in Chithar River Basin, Tamil Nadu, India", Environmental Geology , Vol.47, pp: 1099–1110.
10. Y Srinivas., D Hudson Oliver., A.StanleyRaj ,N Chandrasekar.,(2013) "Evaluation of groundwater quality in and around Nagercoil town, Tamilnadu, India: an integrated geochemical and GIS approach", Springer, Application of Water Sciences Vol.3 pp:631–651.

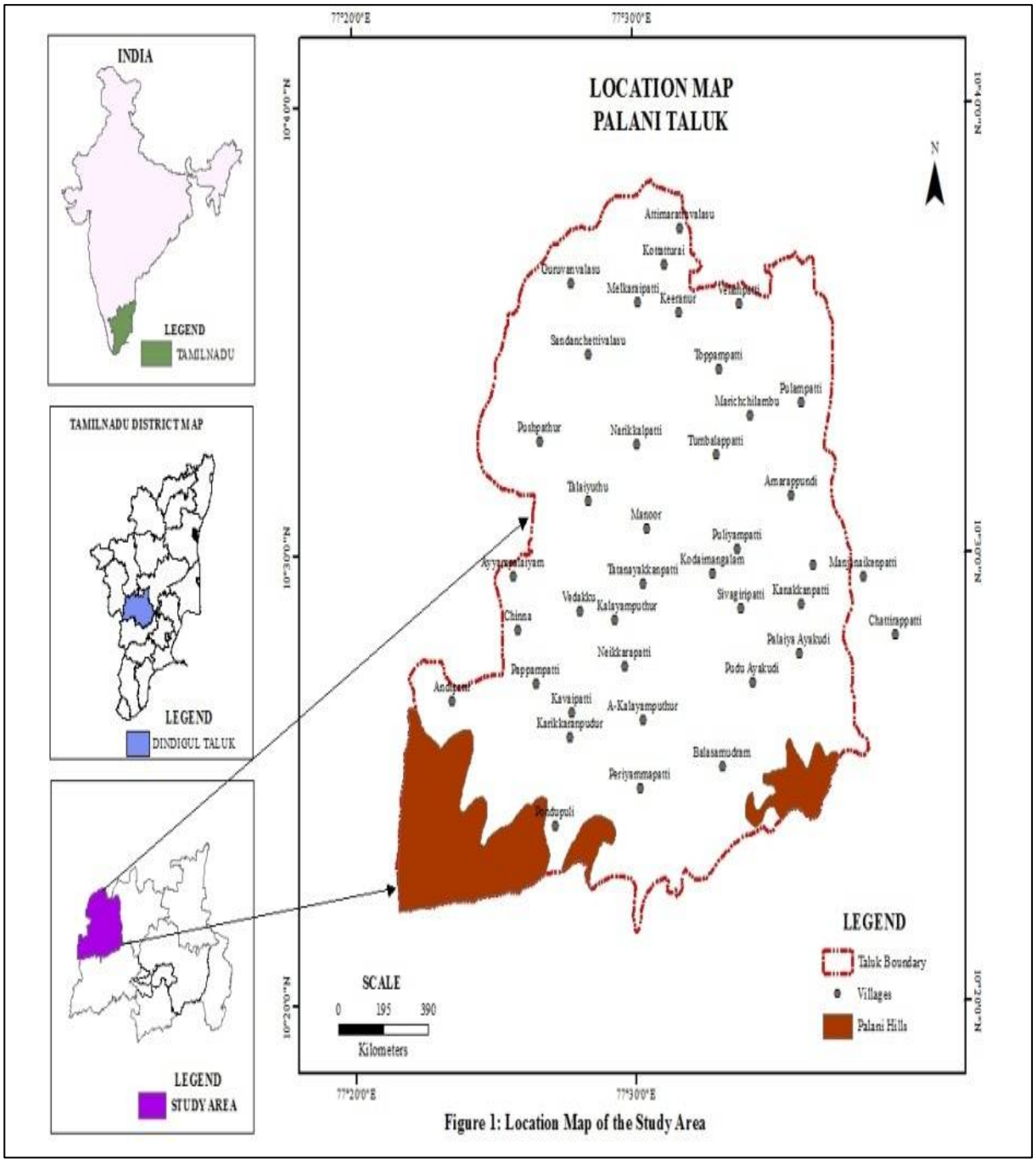

Figure 1: Location Map of the Study Area

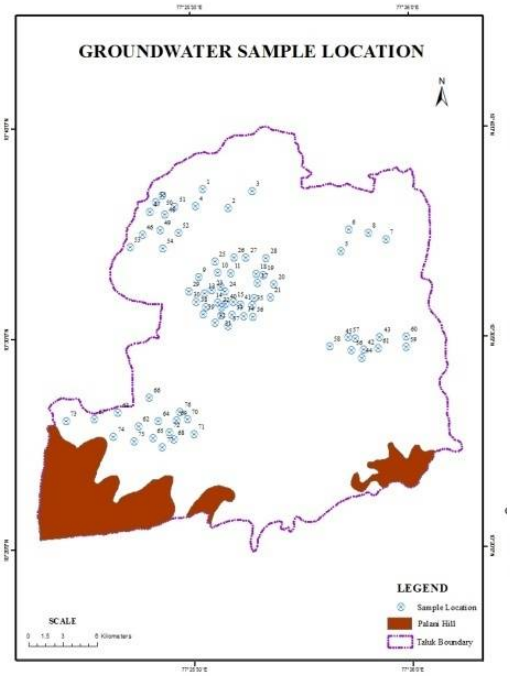

Figure 2: Groundwater Sample Locations

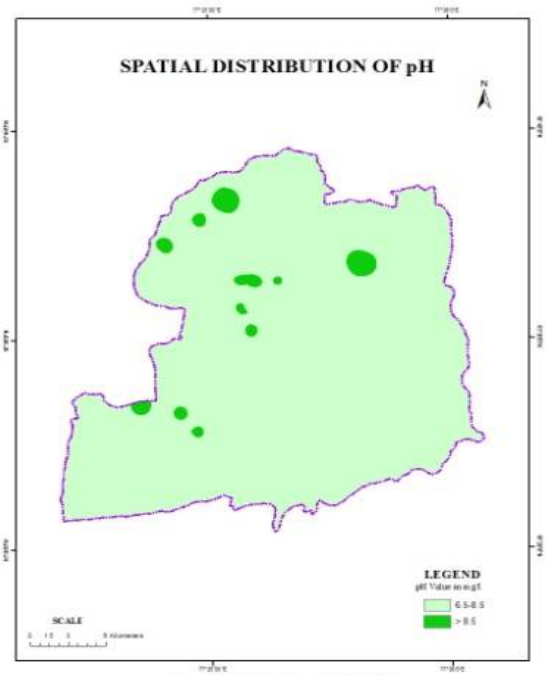

Figure 3:Spatial Distribution of pH in Study Area

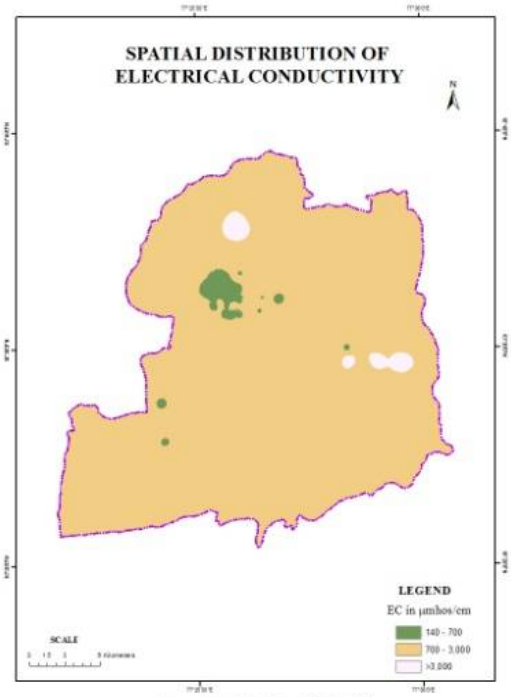

Figure 4:Spatial Distribution of EC in Study Area

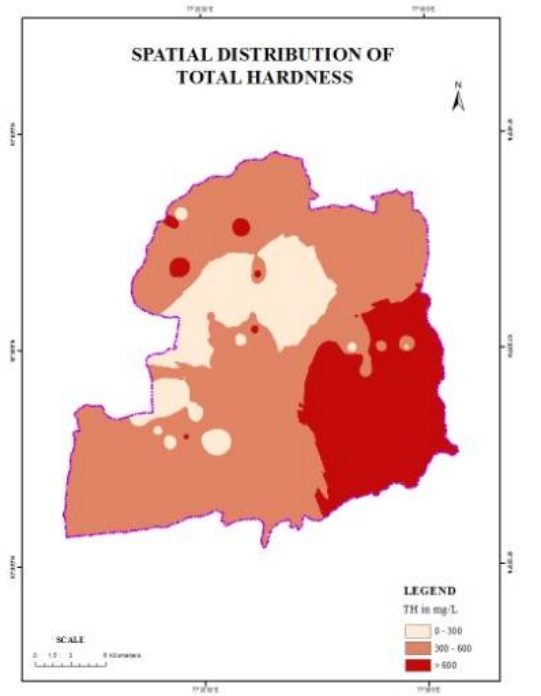

Figure 5:Spatial Distribution of TH in Study Area

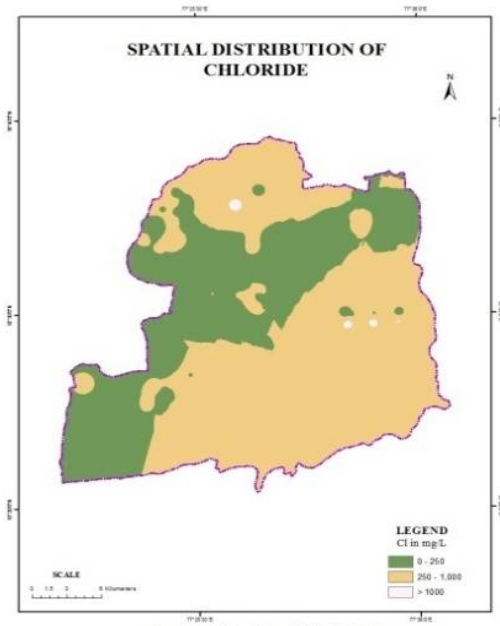

Figure 6:Spatial Distribution of Chloride in Study Area

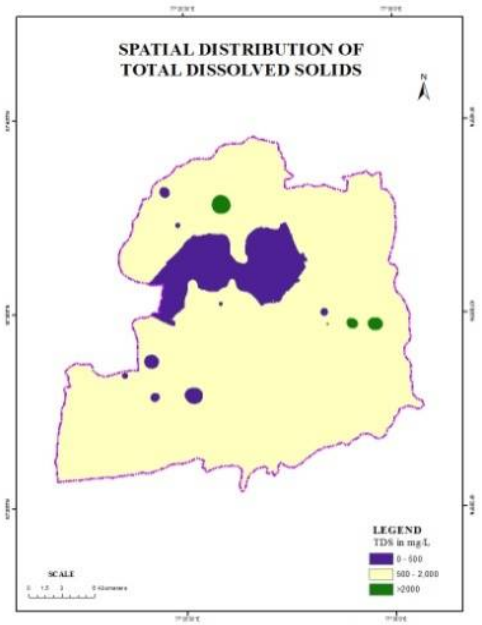

Figure 7:Spatial Distribution of TDS in Study Area

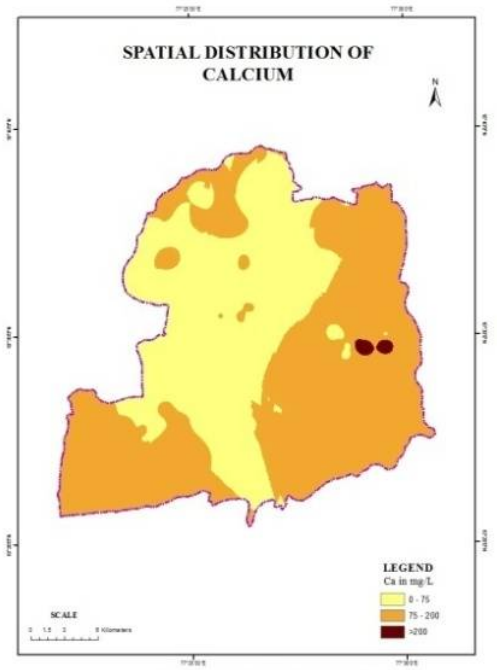

Figure 8:Spatial Distribution of Ca in Study Area

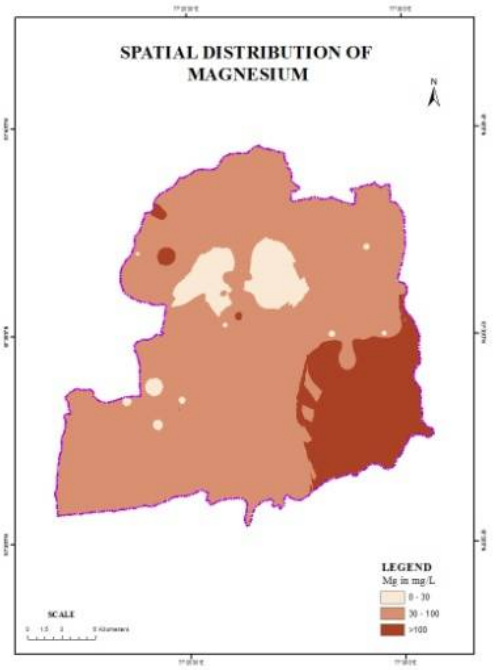

Figure 9:Spatial Distribution of Mg in Study Area

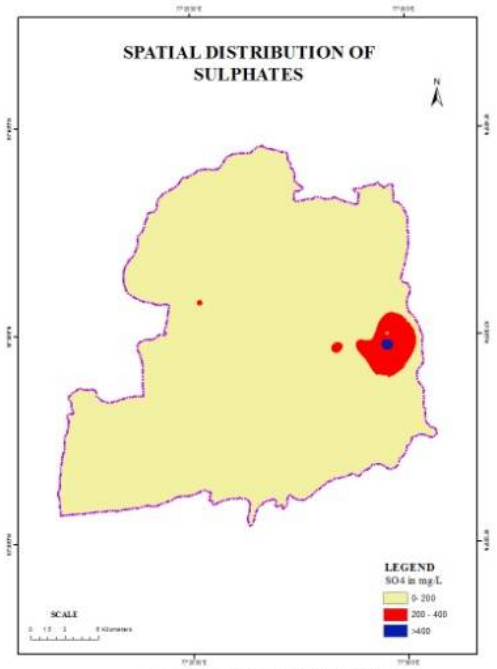

Figure 10:Spatial Distribution of SO4 in Study Area

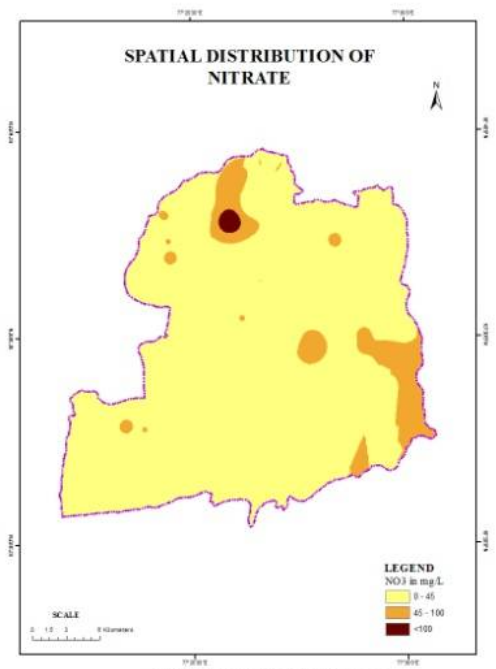

Figure 11:Spatial Distribution of NO3 in Study Area

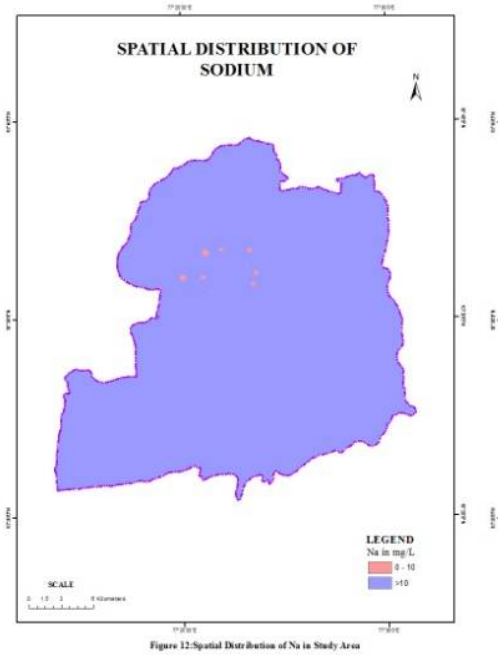

Figure 12:Spatial Distribution of Na in Study Area

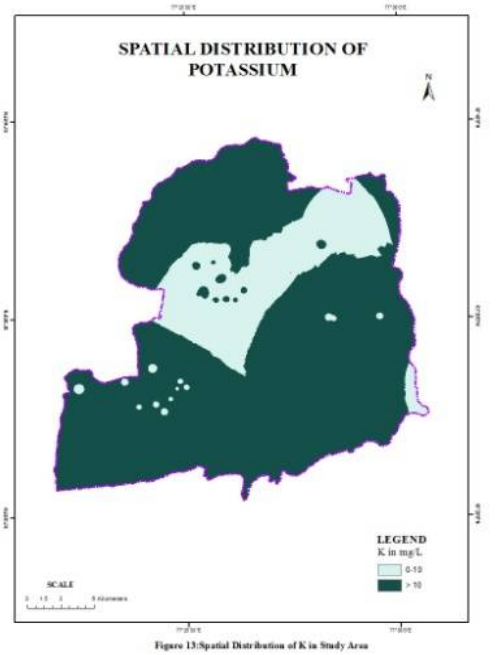

Figure 13:Spatial Distribution of K in Study Area

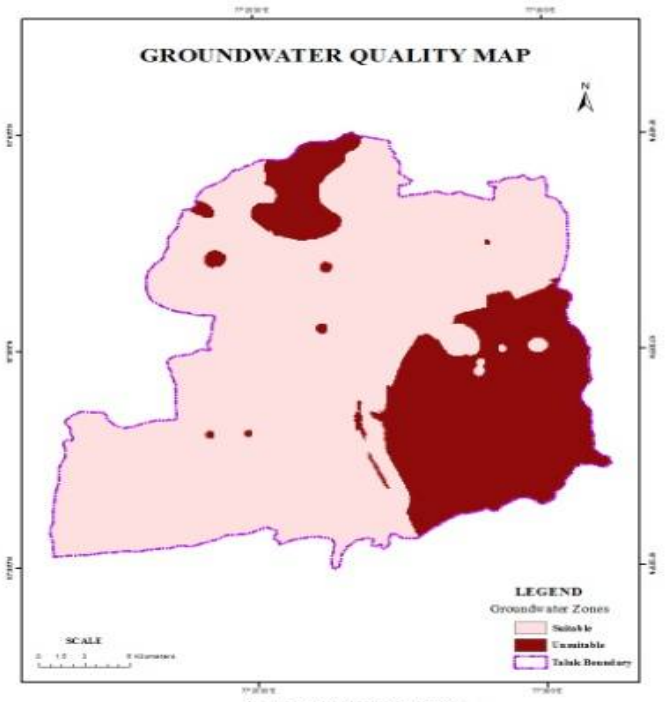

Figure 14: Groundwater Quality Map

Table 1. BIS Drinking Water Standard

S.No.	Name of the Water Quality Parameter	Bureau of Indian Standard (IS-10500:1994)	Parameters Range (mg/L)
1	pH at 25 °C	6.5 - 8.5	7-9
2	Electrical Conductivity (µmhos/cm)	700-3000	140- 5330
3	Total hardness ($CaCO_3$ mg/L)	300-600	45-1660
4	Chloride (as Cl mg/L)	250-1000	14-1425
5	Total Dissolved Solids (mg/L)	500-2000	75-2921
6	Calcium (as Ca mg/L)	75-200	10-400
7	Magnesium (as Mg mg/L)	30-100	2-280
8	Sulphates (as SO_4 mg/L)	200-400	1-514
9	Nitrate (as NO_3 mg/L)	45-100	1-182
10	Sodium (as Na mg/L)	7	11-874
11	Potassium (as K mg/L)	10	1-192

Indian Journal of Natural Sciences www.tnsroindia.org.in ©IJONS

Vol.8 / Issue 45 / December 2017 *International Bimonthly* *ISSN: 0976 – 0997*

RESEARCH ARTICLE

Phytochemical Screening of Ethanol Extract of Aerial Parts of Blumea laevis (EABL)

Yashas R.Kumar*[1], N. Divakaran Nair*[1], Ajith Jacob George*[1], Anoopraj. R*[1], K. S Prasanna*[1], Hamza Palekkodan*[1] and Suja Rani. S*[2]

[1]Department of Veterinary Pathology, College of Veterinary and Animal Sciences,Pookode
Kerala Veterinary and Animal Sciences University, Pookode, Wayanad – 673576,Kerala,India.
[2]Department of Veterinary Pharmacology and Toxicology, College of Veterinary and Animal Sciences,Thrissur & Kerala Veterinary and Animal Sciences University, Pookode, Wayanad – 673576.

Received: 18 Oct 2017 Revised: 28 Oct 2017 Accepted: 25 Nov 2017

***Address for correspondence**
Yashas R Kumar
M.V.Sc. Scholar and Corresponding Author,
Department of Veterinary Pathology,
College of Veterinary and Animal Sciences,
Kerala Veterinary and Animal Sciences University, Pookode,Wayanad – 673576,Kerala,India.
E-mail: dr.yashasrkumar5445@gmail.com

ABSTRACT

Blumea genus belonging to Asteraceae family consists of more than 80 species, among which *Blumea laevis* (Kattappa in Malayalam)is found abundantly sprouting during the post monsoon season and available full-fledged with flowers and fruiting from December to June in different regions of Kerala. The presentstudy was undertaken as several veterinarians reported of high mortality, in goats ascribing of ingesting *Blumea laevis* plant. As initial steps, phytochemical screening had been carried out on ethanol extract of aerial parts of *Blumea laevis* (EABL) to analyze bioactive compounds. The extracts were prepared using ethanol in soxhlet apparatus at40-50ºC which showed the presence of several bioactive compounds such as carbohydrates, flavonoids, saponins,phytosterols, and terpenoids

Keywords: EABL, *Blumea laevis*(Kaattappa), carbohydrates, phytosterols, saponins, terpenoids, flavanoids.

INTRODUCTION

Plants and animals are related to each other and evolved together. Some animals consume entire plants destroying them completely, whereas others only eat a portion of the plant allowing the plant to recover. The relationship is always asymmetric with animals benefited and plants harmed. This made the plants to evolve with multiple defense mechanism to combat both biotic and abiotic factors (Mazid *et al*., 2011) with high range of secondary metabolites

that account for the major contribution for specific taste, odour and colour which attract the herbivores. A large number of toxic plants may be ingested accidentally or willful consumption during grazingwhich leads to extreme toxicity. Poisonous properties correlated with toxicity or aversive conditioning with evolution (Laycock, 1978).

Animals are more likely to eat toxic plants which possess high nutrient value or when deficit of certain nutrients. Most toxins at higher concentrations make plant unpalatable, which makes the animals tough to browse. With coexistence, the animals also have adapted to the wide range of evolutionary changes to detoxify plant poisons but fail at times leading to illness and death.

Prolonged usage of herbs to a large extent has received strong attention from the public and rural populace because of their indiscriminate use for treating diseases. Lack of awareness on toxic metabolites of medicinal herbs and their haphazard use can result in toxicity associated health problems. Plants with secondary metabolites such as cyanide, alkaloids, tannins, saponins, phenolic compounds and terpenoids, when ingested can cause acute or chronic illness affecting the normal physiology and productivity leading to severe livestock loss (Pavarini *et al.,* 2012).Recently, many veterinarians working in Malappuram district of Kerala have reported heavy mortality in goats, ascribing the cause as ingestion of *Blumea laevis* locally called "Kaattappa". Consequently, repeated requests are mounting up from different parts of Kerala to explore and validate the toxic effects of *Blumea laevis*.*Blumea laevis,* belonging to family Asteraceae (Compositae), are herbs growing about 10-180cm in height with rhizomes deeply spread and fibrous, stem are simple or branched, glabarous or sparingly pilose. Leaves are sessile with the apical lobe and terminal lobes obovate to oblanceolate and lateral lobes broadly triangular, florets and fruiting stage usually from December to June which are tubular and marginal with yellow to creamy white in color, widely distributed in the moist decidious and semi-evergreen forests of India including parts of Andaman and Nicobar islands, Bhutan, Cambodia, Malaysia, Laos, Pakistan, Myanmar, Srilanka, Thailand, Phillipines and Vietnam(Randeria, 1960; Anderberg, 1994; Anderberg and Eldena, 2007; Pompongrungueng *et al.,*2016).

MATERIALS AND METHODS

Plant Material

Aerial parts of *Blumea laevis* plant (Figure. 1) in its flowering stage was collected, identified and authenticated by botanist, Dr. A. K. Pradeep and was assigned with the accession No.88480 herbarium and passport data sheets of plant was prepared accordingly and voucher specimen was deposited in Department of Botany, University of Calicut.

METHODS

Preperation of Ethanol extract of *Blumea laevis*

Aerial parts of *Blumea laevis* was cleaned and shade dried at room temperature. After shade drying, the aerial parts of *Blumea laevis* was grinded through blender and converted into course powder. The powder was extracted by continuous hot extraction using the Soxhlet apparatus with 95% ethanol. The extract was then concentrated and reduced under pressure through Rotary vacuum evaporator (M/S Buchi, Switzerland) at temperature ranging from 40-50ºC. The concentrated extract was air dried at room temperature for about 24hrs and placed in suitable containers and preserved in refrigerator for further studies. The percentage extract yield was calculated separately using the formula below:

$$\text{Extractive yield (\%)} = \frac{\text{Weight of the extract}}{\text{Weight of the sample taken}} \times 100$$

Phytochemical screening of aerial parts of *Blumea laevis*

Ethanol extract of aerial parts of *Blumea laevis* was subjected to phytochemical screening by various qualitative tests for detection of bioactive molecules which includes alkaloids, carbohydrates, cardiac glycosides, fat tests, flavonoids, proteins and amino acids, phenolic compounds, tannin, steroids as per Harborne (1991) and Raaman (2006).

Results and discussion

The percentage extractive yield of aerial parts of *Blumea laevis* was found to be 8.051 % in ethanol**.**The preliminary phytochemical analysis from aerial parts of *Blumea laevis* was first of its kind and showed the presence of secondary phytochemical constituents such as saponins (Foam test) (Fig.2), terpenoids (Salkowskis test) (Fig.3), flavonoids (Alkaline reagent test) (Fig. 4), Phytosterols (Leibermann Burchards test)(Fig.5) and carbohydrates (Molish test) (Fig.6)as shown in theTable1.Phytochemical analysis has aided in the rapid and accurate methods of screening plants for determining particular bioactive compounds (Harborne, 1993). The phytochemicals are grouped into two main categories namely primary constituents which includes amino acids, common sugars, proteins and chlorophyll etc., and secondary constituents consisting of alkaloids, essential oils, flavonoids, phenolic compounds, saponins, tannins, terpenoids and others (Edeoga *et al*., 2005;Krishnaiah *et al*., 2007).Phytochemical analysis is a method that helps in elucidating the phytochemical constituents of the plant. The knowledge of the bioactive molecules of a plant helps to apprehend the medicinal/toxic effects. In the recent studies *Blumea* genus enumerates its presence of various bioactive compounds such as alkaloids, flavonoids, saponins, tannins, terpenoids, and reducing sugars on phytochemical analysis (Das *et al*., 2015; Kumari *et al*., 2016).

In the present study the qualitative phytochemical screening of ethanol extract of *Blumea laevis* showed the presence of carbohydrates, saponins, flavonoids, phytosterols and terpenoids. Although no such previous reports are available on phytochemical screening of *Blumea laevis,* Kumari *et al.,* 2016 reported a similar findings on phytochemical analysis of *Blumea balsamifera*.

Saponins are class of glycosides known for its foaming nature. Substantial quantities of harmful saponins possess life threatening toxic substance for certain species of animals, which include hemolytic action on the membranes and bloat production (Palo and Robbins, 1991) Flavanoids are ubiquitously present throughout plant kingdom. Over 4000 flavonoids have been identified and purified, which are known for their antioxidant and antiradical properties (Das *et al.,* 2015; Kumari *et al*., 2016). The detection of flavonoids from *Blumea laevis* wasfound similar to repeated occurrence of flavonoids in *Blumea balsamifera* (Huang *et al*., 2006; Chen *et al*., 2010; Sati and Joshi, 2011; Kumari *et al*., 2016) and *Blumea lacera* (Das *et al*., 2015; Mishra *et al*., 2015; Zahan *et al*., 2015). Phytosterols are compounds present in plants with similar structure and functions to cholesterol (Ogbe *et al*., 2015).

In the present study the ethanol extract of *Blumea laevis* was found to be a rich source of terpenoids. This findings is in corroboration with the observation on studies of phytochemical analysis of *Blumea balsamifera* by Kumari *et al*., 2016 and *Blumea lacera* Agarwal *et al.,* 1995. Terpenoids are volatile substances mainly present in leaves, flowers and fruits. Terpenoids are further classified based on the number of carbon atoms present in the configuration such as monoterpenoids, sesquiterpenoids, diterpenoids, sesterpenoids, troterpenoids, tetraterpenoids and polyterpenoids (Yadav *et al*., 2014). Of the different forms, sesquiterpenes and sesquiterpene lactones are responsible for severe livestock poisoning (Palo and Robbins 1991; Rodriguez *et al.,* 1976). Hence, it can be assumed that the terpenoids present in *Blumea laevis* would have caused the deaths in goats when they ingested large quantities of this plant.

CONCLUSION

Though, the phytochemical analysis revealed the presence of secondary metabolites such as saponins, flavonoids, terpenoids, phytosterolsand carbohydrates, it is the terpenoids present in the *Blumea laevis*that would have caused the reported mortality in goats. The present study was a preliminary study. There is a huge scope for further studies so as to figure out the class of terpenoids present in this plantthat helps in finding suitable treatment measures in livestock after ingestion of *Blumea laevis*plant.

ACKNOWLEDGMENTS

I would like to thank Kerala Veterinary and Animal Sciences University for providing research grants and rendering facilities to carry out this work. A special note of thanks to my teachers Drs. N. Divakaran Nair, Ajith Jacob george, Anoopraj. R, K. S Prasanna, Hamza palekkodanand Suja rani. S for their constant support and expert guidance.

REFRENCES

1. Mazid, M., Khan, T.A. and Mohammad, F. Role of secondary metabolites in defense mechanisms of plants. *Biol. Med.* 2011. 3: 232-249.
2. Laycock, W.A. Coevolution of poisonous plants and large herbivores on rangelands. *J. Range Mgmt*. 1978. 335-342.
3. Pavarini, D.P., Pavarini, S.P., Niehues, M. and Lopes, N.P., Exogenous influences on plant secondary metabolite levels. *Animal Feed Sci. and tech*. 2012. *176*: 5-16.
4. Randeria, A.J. The composite genus *Blumea,* a taxonomic revision. *Blumea-Biodivers. Evol. Biogeograph. Pl.* 1960. 10: 176-317.
5. Pornpongrungrueng, P., Gustafsson, M.H., Borchsenius, F., Koyama, H. and Chantaranothai, P. Blumea (Compositae: Inuleae) in continental Southeast Asia. *Kew Bull.* 2016. 71: 1.
6. Agarwal, R., Singh, R., Siddiqui, I.R. and Singh, J. Triterpenoid and prenylated Phenol Glycosides from *Blumea lacera*. *Phytochem*. 1995. 38: 935-938.
7. Anderberg A.A. Tribe Inuleae. In: Bremer, K. (ed.), *Asteracea: Cladistics* and *classification.* Timber Press, Portland,1994. 273 – 291.
8. Anderberg, A. A. and Eldena's, P. XVII. Tribe Inuleae Cass. In: Kadereit, J.W., Jeffrey, C. (eds.), *Thefamilies and genera of vascular plants. Flowering plants-eudicot,Asterales. Springer, Berlin.* 2007. 374 – 390.
9. Harborne, J.B., Mabry, T.J. and Mabry, H. *The Flavonoids,* Chapman and Hall Publishers, London, 1978. 45- 77.
10. Harborne, J.B. *Phytochemical Methods- A guide to modern techniques of plant analysis.* Chapman and Hall Publishers, London, 1998. 1-32.
11. Raaman, N. 2006. *Phytochemical techniques.* New India publishing Agency, New Delhi. 40p
12. Das, K. D., Prakash, S. and Yadav, K.The effect of varying concentrations of sambong leaves (*Blumea balsamifera*) decoction on wound healing.*Wld. J. Pharm. Pharm. Sci.*2015. 5: 1099-1116
13. Chen, M., Qin, J.J., Fu, J.J., Hu, X.J., Liu, X.H., Zhang, W.D. and Jin, H.Z.,. Blumeaenes A–J, sesquiterpenoid esters from *Blumea balsamifera* with NO inhibitory activity. *Planta medica*. 2010. *76*(9): 897-902.
14. Sati, S.C. and Joshi, S., Aspects of antifungal potential of ethnobotanically known medicinal plants. *Res. J. of Med. Plants*,2011. *5*: 377-391.
15. Chen, M., Qin, J.J., Fu, J.J., Hu, X.J., Liu, X.H., Zhang, W.D. and Jin, H.Z.,. Blumeaenes A–J, sesquiterpenoid esters from *Blumea balsamifera* with NO inhibitory activity. *Planta medica*. 2010. *76*(9): 897-902.
16. Krishnaiah, D., Devi, T., Bono, A. and Sarbatly, R. Studies on phytochemical constituents of six Malaysian medicinal plants. *J. Med. Pl. Res.* 2009.3: 67-72.
17. Krishnaiah, D., Sarbatly R., Bono, A. Phytochemical antioxidants for health and medicine – A move towards nature. *Biotech. Mol. Bio. Rev*. 2007.1: 97-104.

18. Kumari, N., Shukla, K. and Sharma, H.P. Phytochemical screening and biopesticidal efficacy of some plants of East singhbhum, Jharkhand. *Indo Am. J. Pharm. Res.*2016.6: 6716-6724.
19. Palo, R.T. and Robbins, C.T. *Plant defenses against mammalian herbivory*. CRC Press. 1991. 83-103.
20. Mishra, P., Raguverrichhiaya and Mishra, S.M. Phytochemical investigation and spectral studies of isolated flavinoid from ethanolic extract of whole plant *Blumea LaceraD.C*. *J. Pharmacogn.* and *Phytochem.* 2015. 4: 01-04.
21. Edeoga, H.O., Okwu, D.E. and Mbaebie, B.O. Phytochemical constituents of some Nigerian medicinal plants. *Afr. J. Biotech.* 2005. 4: 685-688.
22. Huang, Y.L., Zhao, Z.G. and Wen, Y.X., Determination of total flavonoid in different sections of Blumea balsanifera [J]. *Guihaia*, 2006. 26:453-5.
23. Ogbe, R.J., Ochalefu, D.O., Mafulul, G. and Olaniru, O.B., A review on dietary phytosterols: Their occurrence, metabolism and health benefits. *Asian J. Plant Sci. Res*,2015. *5*:10-21.
24. Pornpongrungrueng, P., Borchsenius, F., Englund, M., Anderberg, A.A. and Gustafsson, M. H. Phylogenetic relationships in Blumea (Asteraceae: Inuleae) as evidenced by molecular and morphological data. *Pl. Syst. Evol.*2007.269: 223-243.
25. Yadav, N., yadav, R. and Goyal, A.Chemistry of terpenoids. *Int. J. Pharm. Sci. Rev. Res.*201427: 272-278.
26. Zahan, M.N., Reza, M.A., Talukder, M.S., Ali, M.S., Paul, T.K. and Parvej, M. S. *Blumea lacera* plant poisoning in cattle; epidemiology and management. *Turk. J. Agric-Food Sci.Tech.* 2015. 3: 635-638.
27. Rodriguez, E., Towers, G.H.N. and Mitchell, J.C. Biological activities of sesquiterpene lactones. *Phytochem.*, 1976. *15*: 1573-1580.

Table 1. Phytochemical Screening of Secondary Metabolites of Plant Extracts.

Sl. No	Phytochemical constituents	Reagents	Observation	Results
1	Saponins	Foam test	Presence Honeycomb froth appears	**+++**
2	Flavonoids	Alkaline reagent test	Presence of Increase intensity of yellow color	**+++**
3	Terpenoids	Salkowskis test	Presence of Reddish brown ring at the junction	**+++**
4	Phytosterols	Liebermann-Burchard's test	Presence of Brown ring at the junction	**+++**
5	Carbohydrates	Molish's test	Presence reddish violet ring at the junction	**++**
6	Alkaloids	Dragendroff's test	Absence of orange red precipitate	**-**

7	Fat test	Spot test	Absence of oil stain on the filter paper	**-**
8	Proteins and amino acids	Biuret test	Absence of pink color	**-**
9	Cardiac glycosides	Keller-kiltani test	Absence of violet ring formation	**-**
10	Reducing sugars	Benedict's test	Absence of orange red precipitate	**-**
11	Tannins	Ferric chloride test	Blue black discoloration was not observed	**-**
12	Phenolic compounds	Ferric chloride and lead acetate test	Absence of blue black color/ white precipitation	**-**

Table 1: **+++**: important Presence, ++: average Presence and +: weak presence

Fig. 1. *Blumea Laevis*: The Experimental Herb

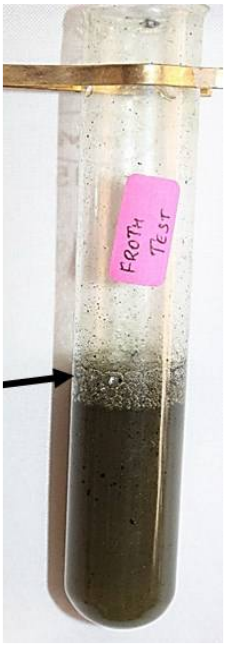

Fig. 2. Foam Test: Appearance of Honey Comb Froth (Arrow)- Positive for Saponins

Fig. 3. Salkowoski's Test: Appearance of Reddish Brown Ring at the Junction (Arrow) -Positive for Terpenoids

Fig. 4. Alkaline Reagent Test: Increased Intensity of Yellow Colour (Arrow) - Positive for flavanoids

Fig. 5. LB Test: Brown Ring Formation at the Junction (Arrow)-Positive for Phytosterols

Fig. 6. Molisch's Test: Reddish Violet Ring at the Junction (Arrow)-Positive for Carbohydrates

Indian Journal of Natural Sciences www.tnsroindia.org.in ©IJONS

Vol.8 / Issue 45 / December 2017 *International Bimonthly* *ISSN: 0976 – 0997*

RESEARCH ARTICLE

Comparison of Different Methods of AgNOR Staining for Indexing Fibroblast Proliferation

K.V.Sabeer Hussain[1*], N. Divakaran Nair[2], Ajith Jacob George[3], K.S Prasanna[4], V. N Vasudevan[5], R Anoopraj[4], B Dhanush Krishna[6] and Hamza Palekkodan[4]

[1]Post graduate Scholar, Department of Veterinary Pathology, College of Veterinary and Animal Sciences, Pookode, Wayanad, Kerala- 673576.
[2]Professor and Head, Department of Veterinary Pathology, College of Veterinary and Animal Sciences, Mannuthy, Thrissur, Kerala- 680 651.
[3]Associate Professor and Head, Department of Veterinary Pathology, College of Veterinary and Animal Sciences, Pookode, Wayanad, Kerala- 673576.
[4]Assistant Professor, Department of Veterinary Pathology, College of Veterinary and Animal Sciences, Pookode, Wayanad, Kerala- 673576.
[5]Assistant professor, Department of Livestock Product Technology and Meat Technology Unit, College of Veterinary and Animal Sciences, Mannuthy, Thrissur-680651.
[6]Assistant Professor, Department of Veterinary Pathology, College of Veterinary and Animal Sciences, Mannuthy, Thrissur, Kerala- 680 651.

Received: 24 Oct 2017 Revised: 20 Nov 2017 Accepted: 25 Nov 2017

[*]**Address for correspondence**
Sabeer Hussain K.V
Post graduate Scholar,
Department of Veterinary Pathology,
College of Veterinary and Animal Sciences,
Kerala Veterinary and Animal Sciences University,
Pookode, Wayanad, Kerala-673576,India.
Email – sabeerhussainkv@gmail.com

ABSTRACT

The study was conducted in the Department of Veterinary Pathology, College of Veterinary and Animal Sciences, Pookode. Three different method of silver nitrate staining were compared for indexing fibroblast proliferation using a novel biomaterial. The first method was described by Ploton and coworkers, which used incubation in acid alcohol and toning in 10% sodium thiosulphate. The second method was described by Bancroft and the third method was a modification of Bancroft'smethod with addition of neutral red as counter stain. The major parameters of comparison were contrast of Argyrophilic Nucleolar Organizer Region (AgNOR) dots and cellular out line and retention potential of

stain after exposure to light. From this study, the method described by Ploton and coworkers was found better over others in the compared parameters.

Keywords – AgNOR stain, Acid alcohol, 10% Sodium thiosulphate, Neutral red counter stain, Retention potential.

INTRODUCTION

Nucleolar organizer regions (NORs) have attracted much attention because it claims that their frequency within nuclei is significantly higher in malignant cells than in normal, reactive or benign neoplastic cells. These are chromosomal loops of DNA, involved in ribosomal synthesis (Gall and Pardue, 1967). NORs can be located by staining, since the nucleolar proteins associated with NORs have special affinity towards silver nitrate. Thus, the silver nitrate staining is one of the methods used commonly in neoplastic conditions to assess its prognosis. The potential of silver nitrate staining technique for demonstrating fibroblast proliferation index was demonstrated by Umashankar*etal*(2001) and it was found beneficial especially in the case of biomaterial research works. But the staining procedure adopted for demonstrating NORs is crucial, since the size and distribution of NORs within the fibroblast nuclei may not evident enough as in the case of neoplastic condition. The reliability of different silver nitrate staining procedure should be evaluated in order to find out best among them for indexing fibroblast proliferation.

MATERIALS AND METHODS

A novel biomaterial studied using rat subcutaneous model was used for demonstrating fibroblast proliferation index with different staining procedure. Total nine samples (explanted biomaterial with host tissue) were taken and slides were prepared after standard histopathological processing. Slides were stained for NOR using three different staining protocols which included, a) method described by Ploton*etal*(1986), b) method described by Bancroft(2002) and, c) counter stain with neutral red.

Preparation of staining solution

Solution A: The solution was prepared by dissolving 500 mg gelatin powder in 25 ml distilled water at 37^{o}C and then 250μl formic acid was added. Continuous shaking for about 10 min at 37^{o}C was sufficient to dissolve the gelatin and the solution was filtered using Whatman no 4 filter paper and clear solution was obtained.

Solution B: It comprised of silver nitrate and distilled water. 8g of silver nitrate was weighed and kept in a small capped bottle and as much as 50 w/v concentrated solution of silver nitrate in distilled water was prepared just before staining.

Working solution

This was prepared just before use (since it degrades quickly) by mixing one part by volume of solution A with two parts by volume of solution B.

The AgNOR staining

For the comparison of three staining protocols, three sets of tissue sections of four micrometer thickness were obtained from formalin fixed paraffin embedded tissues (explanted biomaterial with host tissue). First set of sections were stained according to the protocol described by Ploton *et al* (1986). Briefly, tissue sections were deparaffinized in

two changes of xylene and descending alcohol concentration. The hydration was then performed in two changes of distilled water. The tissue was then incubated at 37°C in acid alcohol (three parts ethanol: two parts acetic acid) for five minutes and then rinsed in two changes of distilled water. The sections were then serially placed on a slide stand which is kept in a humidified tray. Sufficient amount of freshly prepared silver nitrate working solution (silver nitrate staining solution consisted of two parts of a 50% solution of silver nitrate and one part 2% gelatin in 1% formic acid solution) was poured over each slidewhich were kept in a dark humidified chamber and incubated for 45 min at 37°C and then washed with distilled water. Ploton *etal* (1986) introduced 10% sodium thiosulphate in distilled water as toning agent to improve the staining. As per this method the sections were incubated in 10% sodium thiosulphate at 37°C for 5 minutes. The sections were then washed in distilled water, dehydrated in graded alcohol and then xylene and mounted with coverslip. The tissue was then ready for counts.Distilled water was used for preparation of all solutions.

Second set of sections were stained following the protocol designed by Bancroft (2002).After deparaffinizing and rehydration, tissue sections were directly incubated with freshly prepared working solution without using incubation in acid alcohol. The third set was also stained in the same way as described above and additionally, counter stained with freshly prepared neutral red for 30 seconds. None of these two methods used 10% sodium thiosulphate as toning agent.

Parameters of comparison

Normally AgNOR stained areas appear as variable number of black dots in nucleus with yellowish background. The cellular outline and contrast of dark dots will vary in different methods of staining procedure. Most challenging part is to retain the stain even after the light exposure. Gradual fading of the stain after staining, even if we keep the slides in dark chamber, makes it difficult for slide evaluation and interpretation. At times, the stain may fade even before DPX mounting. Therefore, contrast of AgNOR dots and cellular outline and the retention potential of stain even after light exposure were the major parameters of comparison.

RESULTS

Only the first set of sections was fully satisfied with the observed parameters. The cellular outline and AgNOR dots in first set of sections were well differentiated (Fig. 1). The retention ability was also found superior by retaining the silver nitrate stain for more than three months. Even after three months the cellular outline and AgNOR dots were clearly visible.

Cellular outline in the second set of stained tissue was good. But the AgNOR dots were poorly visible in majority of the cells, except few cells. The retaining ability of the stain was also poor. The tissue sections were found visible maximum for 24 hours(Fig. 2).

In the third set of tissue with neutral red counter stain, both the cellular outline and AgNOR dots were poorly visible. In some cells the AgNOR dots were not at all visible. None of the sections retained the stain after 12 hours and showed only counter stain and the sections became reddish(Fig. 3).

DISCUSSION

Silver nitrate staining is an unavoidable task especially in case of tumour diagnosis and biomaterial induced fibroblast proliferation indexing. The credulity of this method totally depends on staining procedure because in poorly stained sections only larger AgNOR dots will be visible and other small dots will be unclear even though they are present. It gives false result since the proliferation index and mean AgNOR count totally depend on size and

distribution of AgNOR dots which are unclear in some staining procedure(Derenzini and Ploton, 1991). The major parameters we compared here were contrast of AgNOR dots and cellular outline and retention potential of stain. Compared to first and second set of procedure, an addition of neutral red counter staining was there in the third set. But the counter staining didn't give an added benefit over other for both the compared parameters (Bukhari *et al*, 2007)

An addition of incubation with acid alcohol and toning with sodium thiosulphate in the first method made the AgNORs more clear and the retention potential of the stain was also found superior. This method can be used for preserving slides for future reference and is also economically more feasible.

CONCLUSION

In this study, we compared three methods of silver nitrate staining procedure using fibroblast proliferation indexing. The method described by Ploton *etal* (1986)wasundoubtedly found superior over others in both the compared parameters and can be used as the protocol of choice for demonstrating AgNORs in tumour studies and biomaterial research.

REFERENCES

1. Bancroft J.D. 2002. Cytoplasmic granules, organelles and neuroendocrine. In: Theory and Practice of Histological Techniques, 5th edn, p. 350 (eds J. D. Bancroft, M. Gamble) New York: Churchill Livingston.
2. Bukhari, M.H., Niazi, S., Khan, S.A., Hashimi, I., Perveen, S., Qureshi, S.S., Chaudhry, N.A., Qureshi, G.R. and Hasan, M. 2007. Modified method of AgNOR staining for tissue and interpretation in histopathology. *Int. J. Exp. Path.***88**: 47-53.
3. Derenzini M. & Ploton D. 1991. Interphase nucleolar organizer regions in cancer cells. *Int*. *Rev*. *Exp*. *Pathol*. **32**: 150–192.
4. Gall J.G. & Pardue M.L. 1969. Formation and detection of RNA-DNA hybrid molecules in cytological preparations.*Proc*. *NatlAcad*. *Sci*. U.S.A. **63**: 378–383.
5. Ploton, D., Menager, M., Jeannesson, P., Himber, G., Pigeon, F. and Adnett J.J. 1986. Improvement in the staining and the visualization of the argyrophilic proteins of the nucleolar organizer region at the optical level. *Hitched J.* **18**: 5–14.
6. Umashankar, P. R. 2001. Efficacy of Argyrophilic Nucleolar Organizer Region Count Test for *in vivo* Biomaterial Evaluation. *M.V.Sc thesis*, Kerala Agricultural University, Thrissur, 68p.

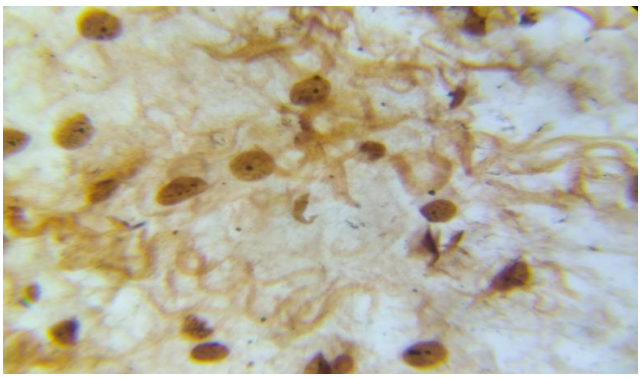

Fig. 1 – Ploton Method- Cellular Outline and AgNOR Dot Size and Dispersion are Clearly Visible (1000X)

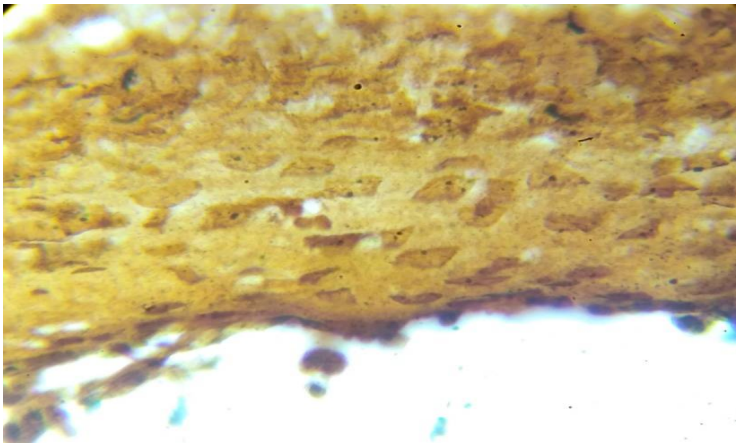

Fig. 2–Bancroft Method -The AgNOR Dots have become Blurred due to dim background and less Clearly Visible (1000X)

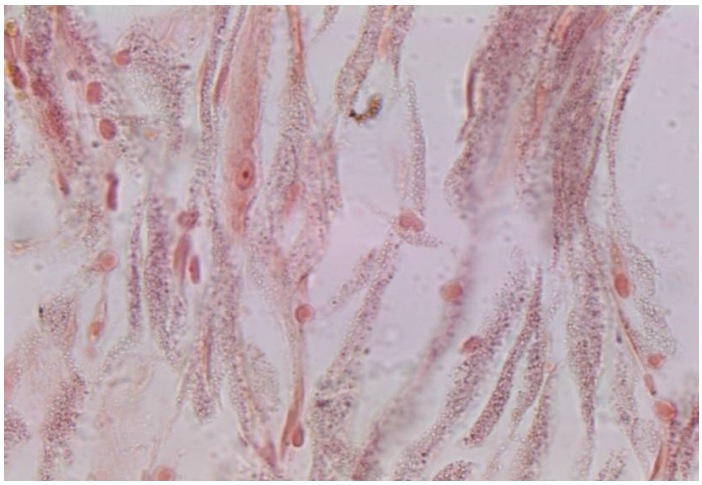

Fig. 3 – Counter Stain Method - Cellular Outline and AgNOR Dot Dispersion were less Clearly Visible in Counter Stained Sections (1000X)

Indian Journal of Natural Sciences www.tnsroindia.org.in ©IJONS

Vol.8 / Issue 45 / December 2017 *International Bimonthly* *ISSN: 0976 – 0997*

RESEARCH ARTICLE

Neuromuscular Stimulation Studies to Evaluate Neuromuscular Blockade Produced by Atracurium in Dogs

Binu S. Joselin*, Sooryadas S., John Martin K. D., Dinesh P.T., and Reji Varghese

Department of Veterinary Surgery and Radiology, College of Veterinary and Animal Sciences, Kerala Veterinary and Animal Sciences University, Pookode, Wayanad, Kerala – 673576.

Received: 10 Oct 2017 Revised: 15 Nov 2017 Accepted: 25 Nov 2017

*Address for correspondence
Dr Binu S Joselin
M.V.Sc Student, Department of Veterinary Surgery and Radiology,
College of Veterinary and Animals Sciences,
Kerala Veterinary and Animal Sciences University, Pookode, Wayanad – 673576,Kerala,India.
E-mail : binu6989@gmail.com

ABSTRACT

Six dogs of various breeds presented at the Teaching Veterinary Clinical Complex, College of Veterinary and Animal Sciences, for various elective surgeries like orthopaedic surgeries of the limbs and laparotomy surgeries, were taken for the study. The animals were fasted 12 hours prior to the procedure. On the day the procedure, supra-maximal current (minimal current required to produce the slightest of twitch by a muscle bundle) was estimated for neuromuscular stimulation study. The animals were pre-medicated with dexmedetomidine, midazolam and ketamine to induce anaesthesia, which was then maintained with inhalant anaesthesia using isoflurane. Animals were then administered atracurium @ 0.1mg/kg body weight, immediately followed by continuous rate infusion @ 0.1mg/kg/hour. The train-of-four was then monitored every 5 minutes till the end of procedure. Reduced respiratory rates with no changes in the haemodynamic parameters as a result of atracurium administration could be recorded. The train-of-four was reduced initially following administration of atracurium bolus, which recovered shortly, even though under continuous rate infusion of atracurium. Hence the particular dose of atracurium in continuous rate infusion was insufficient in producing muscle relaxation as inferred from the neuromuscular stimulation studies. But the bolus injection of atracurium at the rate of 0.1 mg/kg bodyweight produced sufficient muscle relaxation, without any haemodynamic variations and minimal disturbances in the respiratory system.

Key-words: Neuromuscular blocker, Atracurium, Neuromuscular stimulation, Muscle relaxation, Train-of-four.

INTRODUCTION

Neuromuscular blocking drugs produce profound muscle relaxation when compared with the conventional benzodiazepines. The degree of muscle relaxation can be evaluated using parameter like train-of-four (TOF). The skeletal muscle relaxant atracurium used in this study is a non-depolarising muscle relaxant. The particular study emphasizes on the evaluation of muscle relaxation produced by atracurium using a Neuromuscular stimulator-mapper-locator (NSML) unit by visually assessing the TOF elicited.

MATERIALS AND METHODS

Six dogs of various breeds presented for various elective surgeries like orthopaedic surgeries of the limbs and laparotomy surgeries, which required substantial muscle relaxation was taken for this study. The animals were fasted 12 hours prior to the procedure.

On the day of surgery, Supramaximal current - the minimum current required to elicit the slightest twitch of a muscle bundle supplied by a nerve trunk, was estimated before the start of anaesthesia by placing the leads of the neuromuscular monitor on the lateral aspect at the hock joint and over the course of the peroneal nerve and TOF was noted as pre-induction TOF. The animal was then premedicated using dexmedetomidine, midazolam, ketamine and anaesthesia maintained under isoflurane. TOF was then noted as post-induction TOF.

Animals were then administered atracurium at the dose rate of 0.1 mg/kg bodyweight as a bolus injection and immediately followed by continuous rate infusion of the drug at the rate of 0.1 mg/kg/hour. The TOF was then recorded every 5 minutes till the end of procedure.

RESULTS AND DISCUSSION

In the present study, all animals were induced with the same anaesthetic protocol involving dexmedetomidine, midazolam and ketamine and then anaesthesia maintained using isoflurane under 100% oxygen through a rebreathing ventilatory circuit. Animals were evaluated for physiological and haemodynamic changes. Animals did not show any significant changes in either and all the parameters were in their respective normal ranges (Hackett *et al.,* 1989).

Respiration rates were reduced to significantly lower levels and thus manual assisted ventilation were administered by bagging (Meyer *et al*., 1986).

The supramaximal current recorded for each animal was different, which would have been due to the difference in threshold of the muscle bundle in each animal (Flores *et al.,* 2011). The TOF recorded was 4 with an equal strength of all four twitches.

The TOF recorded after induction of anaesthesia using dexmedetomidine, midazolam and ketamine, showed similar results of TOF, as obtained before induction of anaesthesia, but was reduced in intensity, which might have been due to the insufficient muscle relaxation obtained without the neuromuscular blocking drug.

Following administration of atracurium at the rate of 0.1 mg/kg body weight and initiation of continuous rate infusion of atracurium at the rate of 0.1 mg/kg/hour, the character of muscle twitches changed into a step-down fashion, in which each of the twitch of TOF reduced in intensity with respect to the preceding twitch, characteristic of the non-depolarizing skeletal muscle relaxant (Adams *et al.,* 2001). This observation was made 4-5 minutes after

administration of bolus injection of atracurium. The peak muscle relaxation according to TOF was obtained between 12-14 minutes after administration of atracurium, and was recorded as 2.

18-20 minutes after the bolus injection of atracurium, the TOF started to return to 3 and finally to 4, but still retaining the step-down fashion of the twitches. This continued till the end of atracurium administration and 5 minutes after termination of continuous rate infusion of atracurium. This might have been due to the insufficient dose of continuous rate infusion. But the step-down fashion of twitches which was retained might have been due to the additive effect of the isoflurane by which the anaesthesia was maintained in the dogs. This could have also been due to the hypothermia produced in the animals both due to the reduced muscular activity resulting from the anaesthetic plane maintained using isoflurane and the skeletal muscle relaxation produced by atracurium (Meyer *et al.,* 1986).

SUMMARY

The present study on the assessment of muscle relaxation produced by a skeletal muscle relaxant like atracurium, using neuromuscular stimulation studies revealed that, atracurium can be successfully used as a drug to induce profound muscle relaxation by intermittent bolus injection. It is evident from the study that a continuous rate infusion of the drug immediately following the bolus injection was insufficient to produce a substantial muscle relaxation. But the lower dose of atracurium at the rate of 0.1 mg/kg body weight, proved to be safe for administration without resulting in any untoward complication associated with the drug like, causing respiratory paralysis.

REFERENCES

1. Adams, W. A., Robinson, K. J., Mark Senior, J. and Jones, R. S. 2001. The use of non-depolarising neuromuscular blocking drug cis-atracurium in dogs. *Vet. Anaesth. Analg*. 28: 156-160.
2. Clutton, R. E., Boyd, C., Flora, R., Payne, J. and McGrath, C. J. 1992. Autonomic and cardiovascular effects of neuromuscular blockade antagonism in the dog. *Vet. Surg.* 21(1): 68-75.
3. Flores, M. M., Lau, E. J., Campoy, L., Erb, H. N. and Gleed, R. D. 2011. Twitch potentiation: a potential source of error during neuromuscular monitoring with acceleromyography in anaesthetized dogs. *Vet. Anaesth. and Analg.* 38. 328-335.
4. Knuttgen, K., Jahn, M., Ziedler, D. and Doehn, M. 1999. Atracurium during thoracic surgery: Impaired efficiency in septic processes. *JCVA*. 13(1): 26-29.
5. Meyer, R. E., Page, R. L., Thrall, D. E., Dewhirst, M. W. and Vose, D. L. 1986. Determination of continuous atracurium infusion rate in dogs undergoing whole body hyperthermia. *Cancer Research*. 46: 5599-5601.

Indian Journal of Natural Sciences www.tnsroindia.org.in ©IJONS

Vol.8 / Issue 45 / December 2017 *International Bimonthly* *ISSN: 0976 – 0997*

RESEARCH ARTICLE

Isolation and Passaging for Rapid Culture and Expansion of Multipotent Mesenchymal Cells from Amniotic Membrane: a High Throughput Source in Cell Therapy

Elavarasi, S.*, Nancy Mary, A and Horne Iona Averal

Research Department of Zoology, Holy Cross College (Autonomous), Tiruchirappalli -2, Tamil Nadu, India.

Received: 21 July 2017 Revised: 21 Oct 2017 Accepted: 17 Nov 2017

***Address for correspondence**
Elavarasi, S.,
PG and Research Department of Zoology,
Holy Cross College (Autonomous),
Tiruchirappalli -2, Tamil Nadu, India.
E.mail: elavarasi888@gmail.com

ABSTRACT

Vertebrates in general have extra embryonic tissues known as placental membranes. In humans they are composed of the so-called reflected membranes. Their origin along with their structural and functional complexity has recently been receiving attention due to its composition of the various extracellular connective tissue components and stem cell properties of their epithelial stromal cells. Inner cell mass differentiation are beginning to be known, however understanding of cell fate decisions during human embryonic development still remains limited. Hoping to use these cells for clinical applications, promising results have been achieved, in particular using fibroblast like cells isolated from the amnion and chorion. Indeed, these foetal membranes are no longer seen as waste tissues but as a source of cells and bioactive molecules for therapeutic applications.

Key words: Multipotent mesenchymal cells, amniotic membrane, cell therapy.

INTRODUCTION

Stem cell therapy has breathed a new hope to repair tissue damage caused by diseases, degenerative processes or injury and holds promise in a clinical setting by the ability of stem cells to integrate and reconstitute the desired tissue type. The perinatal tissue obtained post-delivery offers many advantages as a source of stem cells such as unlimited supply, easy access and has no ethical issue associated with their use (Warrier, 2012). Mesenchymal stem cells are cells with high *in vitro* expansion potential and self-renewal capacity which were first isolated from bone marrow (Prockop, 1997; Pittenger *et al*., 1999; Baksh *et al.,* 2004). Beside their ability to differentiate into multiple mesoderm-type lineages, e.g. osteoblasts, chondrocytes and adipocytes, bone marrow derived- MSCs are also able to differentiate into endothelial cells *in vitro* (Oswald *et al*, 2004); this opens new possibilities for promoting angiogenesis through cell-based therapeutic strategies (Alviano, 2007). Human amniotic membrane and amniotic

fluid have attracted increasing attention in recent years as a storehouse of stem cells that maybe useful for clinical application in regenerative medicine. Many studies have been conducted to date in terms of the differentiation potential of these cells, demonstrating that mesenchymal stem cells (MSCs) from both the amniotic fluid and membrane display high differentiation potential (Kadam *et al*., 2010). In addition, cells from the amniotic membrane have also shown to display immunomodulatory properties both *in vivo* and *in vitro*, which could make them useful under an allotransplantation setting (Wolbank *et al.,* 2007).

Mesenchymal cells derived from amniotic membrane have been referred to in various ways by different research groups, including human amnion/amniotic mesenchymal stromal cells (hAMSC[s]), amniotic membrane mesenchymal stem cells (AM-MSC), amniotic membrane-human mesenchymal stromal cells (AM-hMSC), amnion-derived MSC, amniotic mesenchymal fibroblasts, human amnion stromal cells (hASC), human amniotic mesenchymal tissue cells (AMTC), human amniotic mesenchymal cells (HAMc), mesenchymal cells derived from human amniotic membrane (MC-HAM), human amniotic mesenchymal stem cells (hAMs), human amniotic membrane-derived mesenchymal cells (hAMCs or hAM-MSC) and human amnion-derived fibroblast-like cells (HADFIL) (Insausti *et al.,* 2010). During the first meeting of "International Placenta Stem Cell Society" (IPLASS) in 2007, it was agreed that the nomenclature of these cells should be unified as "human amniotic mesenchymal stromal cells" (hAMSC) (Parolini *et al.,* 2008). hAMSC are derived from the extraembryonic mesoderm (Parolini *et al.,* 2008) and are found dispersed in the collagenous stroma underlying the epithelial monolayer of the amniotic membrane (Bilic *et al*., 2008; Manuelpillai *et al.,* 2011; Lindenmair *et al*., 2012). Experimental and clinical studies have demonstrated that amniotic membrane transplantation promotes re-epithelialisation, decreases inflammation and fibrosis (Solomon *et al*., 2005) and modulates angiogenesis (Dua *et al.,* 2004). Several growth factors produced from amniotic membrane are involved in these processes, such as Transforming Growth Factor-β (TGF-β), basic Fibroblast Growth Factor (bFGF) (Shimazaki *et al.,* 1997), Epidermal Growth Factor (EGF), Transforming Growth Factor-α (TGFα), Keratinocyte Growth Factor, and Hepatocyte Growth Factor (Koizumi *et al.,* 2000). Thus, the present study aims to isolate the mesenchymal stem cells from the amniotic membrane and passaging for rapid culture and expansion of the multipotent cells.

MATERIALS AND METHODS

Isolation and expansion of hAMSC (Lindenmair *et al.,* 2012):

Amniotic membrane is mechanically peeled off the chorionic membrane by blunt dissection, washed several times in a buffered solution and cut into small pieces. In most cases, hAMSC are obtained in subsequent enzymatic digestions. After complete removal of human amniotic epithelial cells (hAEC) by trypsin digestion, hAMSC are digested with various types and concentrations of collagenase (0.75-2 mg/mL) with or without adding DNase (20-75 µg/mL) (In 't Anker *et al.,* 2004; Kim *et al.,* 2012). According to Parolini *et al*., (2008) one single amnion should theoretically contain 5 × 108 hAMSC. Typically, one gram tissue yields in about 1-2 × 106 hAMSC (Bilic *et al*., 2008).

Media used for expansion are usually composed of a basal medium, supplemented with fetal calf serum, antibiotics and antimycotics. One characteristic property of mesenchymal stem cells such as hAMSC is their plastic adherence. To remove non-adherent cells, medium is removed after a time of two h (Paracchini *et al.,* 2012) up to seven days (Lisi *et al.,* 2012) after cell seeding. After reaching confluence of 70%-100%, cells are usually detached with trypsin (0.05% or 0.25%) with or without EDTA (0.02%) (Diaz-Prado *et al.,* 2010). Expansion of hAMSC is possible for at least five passages without any morphological alterations (Lisi *et al*., 2012).

RESULTS AND DISCUSSION

In the present study, we directed our attention towards an alternative source that is easily accessible, high in yield and ethically acceptable. In particular we succeeded in isolating a multipotent stem cell population that is still of fetal origin and may be superior in proliferation and differentiation potential to cells deriving from adult tissues. AM-hMSCs were isolated through both mechanical and enzymatic digestion. The yield of MSCs from the enzyme treated amnion was higher. After two weeks of culture a homogeneous population of mesenchymal cells was isolated by collagenase treatment from human amniotic membrane and reached confluence (Plate-1). This population could be successfully passaged. Subsequent isolations were performed by trypsin/collagenase and were passaged up to passage 3 to remove any contaminating epithelial population. Culture of umbilical cord tissue pieces yielded an adherent growing cell population with a diverse morphology of small and large cells (Majore *et al.,* 2009). Thus amniotic membranes may represent a reservoir of multipotent mesenchymal stem cells every bit as good as bone marrow. In this context, the development of a regenerative medicine based on stem cell therapy may hold unprecedented prospects (Deans and Moseley, 2000). Therefore it is evident that alternative cell sources for attempting therapeutic neo-vascularization in adults are available but it should be emphasized that the efficacy of such options remains to be determined in humans.

CONCLUSION

The present observations focusing on the expansion and differentiation potential of AM-hMSCs suggest that this population may be a remarkable source of pluripotent cells available for future efforts in cell therapy. Further studies are required to fully understand the potential of AM-hMSCs as a candidate in cell therapy strategies.

ACKNOWLEDGMENTS

The authors thank The Management and The Principal, Holy Cross College (Autonomous), Trichy for providing the necessary facilities.

REFERENCES

1. Alviano, F., Fossati, V., Marchionni, C., Arpinati, M., Bonsi, L., Franchina, M., Lanzoni, G., Cantoni, S., Cavallini, C., Bianchi, F., Tazzari, P.L., Pasquinelli, G., Foroni, L., Ventura, C., Grossi1, A and Bagnara, G.P. 2007. Term amniotic membrane is a high throughput source for multipotent mesenchymal stem cells with the ability to differentiate into endothelial cells *in vitro. BMC Developmental Biology*, 7:11.
2. Baksh, D., Song, L and Tuan, R.S. 2004. Adult mesenchymal stem cells: characterization, differentiation, and application in cell and gene therapy. *J Cell Mol Med*, 8(3):301-316.
3. Bilic, G., Zeisberger, S. M., Mallik, A. S., Zimmermann, R and Zisch, A. H. 2008. Comparative characterization of cultured human term amnion epithelial and mesenchymal stromal cells for application in cell therapy. *Cell Transplant.* 17, 955-968.
4. Deans, R. J and Moseley, A. B. 2000. Mesenchymal stem cells: Biology and Potential clinical uses. *Exp. Hematol.,* 28: 875-884.
5. Diaz-Prado, S., Muinos-Lopez, E., Hermida-Gomez, T., Rendal-Vazquez, M.E., Fuentes-Boquete, I., de Toro, F.J and Blanco, F.J. 2010. Multilineage differentiation potential of cells isolated from the human amniotic membrane. *J. Cell Biochem. 111*, 846-857.
6. Dominici, M., Le Blanc, K., Mueller, I., Slaper-Cortenbach, I., Marini, F., Krause, D., Deans, R., Keating, A., Prockop, DJ and Horwitz, E. 2006. Minimal criteria for defining multipotent mesenchymal stromal cells. The International Society for Cellular Therapy position statement. *Cytotherapy.,* 8:315-7.

7. Dua, H. S., Gomes, J. A., King, A. J and Maharajan, V.S. 2004. The amniotic membrane in ophthalmology. *Surv Ophthalmol.,* 49:51-77.
8. In 't Anker, P. S., Scherjon, S. A., Kleijburg-van der Keur, C., de Groot-Swings, G. M., Claas, F. H., Fibbe, W. E and Kanhai, H. H. 2004. Isolation of mesenchymal stem cells of fetal or maternal origin from human placenta. *Stem Cells.* 22, 1338-1345.
9. Ingrida Majore., Pierre Moretti., Ralf Hass and Cornelia Kasper. 2009. Identification of subpopulations in mesenchymal stem cell-like cultures from human umbilical cord. *Cell Communication and Signaling*., 7:6 doi:10.1186/1478-811X-7-6.
10. Insausti, C. L., Blanquer, M., Bleda, P., Iniesta, P., Majado, M. J., Castellanos, G and Moraleda, J. M. 2010. The amniotic membrane as a source of stem cells. *Histol. Histopathol.,* 25, 91-98.
11. Kadam, S. S., Sudhakar, M., Nair, P.D and Bhonde, R.R. 2010. Reversal of experimental diabetes in mice by transplantation of neo-islets generated from human amnion derived mesenchymal stromal cells using immuno-isolatory macrocapsules. *Cytotherapy* 12(8): 982-91.
12. Kim, J., Park, S., Kang, H. M., Ahn, C. W., Kwon, H. C., Song, J. H., Lee, Y. J., Lee, K. H., Yang, H., Baek, S.Y., *et al.* 2012. Human insulin secreted from insulinogenic xenograft restores normoglycemia in type i diabetic mice without immunosuppression. *Cell Transplant.* doi: 10.3727/096368912X636803.
13. Koizumi, N. J., Inatomi, T.J., Sotozono, C. J., Fullwood, N. J., Quantock, A. J and Kinoshita, S. 2000. Growth factor mRNA and protein in preserved human amniotic membrane. *Curr Eye Res.,* 20:173-177.
14. Lindenmair, A., Hatlapatka, T., Kollwig, G., Hennerbichler, S., Gabriel, C., Wolbank, S., Redl, H and Kasper, C. 2012. Mesenchymal Stem or Stromal Cells from Amnion and Umbilical Cord Tissue and Their Potential for Clinical Applications. *Cells,* 1, 1061-1088; doi:10.3390/cells1041061
15. Lisi, A., Briganti, E., Ledda, M., Losi, P., Grimaldi, S., Marchese, R and Soldani, G. 2012. A combined synthetic-fibrin scaffold supports growth and cardiomyogenic commitment of human placental derived stem cells. *PLoS One,7*, e34284.
16. Manuelpillai, U., Moodley, Y., Borlongan, C. V and Parolini, O. 2011. Amniotic membrane and amniotic cells: Potential therapeutic tools to combat tissue inflammation and fibrosis? *Placenta.* 32 (Suppl. 4), S320-S325.
17. Oswald, J., Boxberger, S., Jorgensen, B., Feldmann, S., Ehninger, G., Bornhauser, M and Werner, C. 2004. Mesenchymal stem cells can be differentiated into endothelial cells in vitro. *Stem Cells,* 22(3):377-384.
18. Paracchini, V., Carbone, A., Colombo, F., Castellani, S., Mazzucchelli, S., Gioia, S.D., Degiorgio, D., Seia, M., Porretti, L., Colombo, C., *et al.* 2012. Amniotic mesenchymal stem cells: A new source for hepatocyte-like cells and induction of cftr expression by coculture with cystic fibrosis airway epithelial cells. *J. Biomed. Biotechnol.* 575471.
19. Parolini, O., Alviano, F., Bagnara, G. P., Bilic, G., Buhring, H. J., Evangelista, M., Hennerbichler, S., Liu, B., Magatti, M., Mao, N., *et al.* 2008. Concise review: Isolation and characterization of cells from human term placenta: Outcome of the first international workshop on placenta derived stem cells. *Stem Cells,* 26, 300-311.
20. Pittenger, M.F., Mackay, A.M., Beck, S.C., Jaiswal, R.K., Douglas, R., Mosca, J.D., Moorman, M.A., Simonetti, D.W., Craig, S and Marshak, D.R. 1999. Multilineage potential of adult human mesenchymal stem cells. *Science,* 284:143-147.
21. Prockop, D.J. 1997. Marrow Stromal cells as stem cells for non-hematopoietic tissues. *Science.,* 276: 71-74.
22. Shimazaki, J., Yang, H. Y and Tsubota, K. 1997. Amniotic membrane transplantation for ocular surface reconstruction in patients with chemical and thermal burns. *Ophthalmology.* 104:2068-2076.
23. Solomon, A., Wajngarten, M., Alviano, F., Anteby, I., Elchalal U, Pe'er J and Levi-Schaffer F. 2005. Suppression of inflammatory and fibrotic responses in an in-vitro model of allergic inflammation by the amniotic membrane stromal matrix. *Clin Exp Allergy.* 35(7):941-948.
24. Warrier, S., Haridas, N and Bhonde, R. 2012. Inherent propensity of amnion-derived mesenchymal stem cells towards endothelial lineage: Vascularization from an avascular tissue. *Placenta,* 33: 850-858.
25. Wolbank, S., Peterbauer, A., Fahrner, M., Hennerbichler, S., Van Griensven, M., Stadler, G., et al. 2007. Dose-dependent immunomodulatory effect of human stem cells from amniotic membrane: a comparison with human mesenchymal stem cells from adipose tissue. *Tissue Eng*., 13:1173-83.

Plate 1: Isolation of hMSCs from Amniotic Membrane

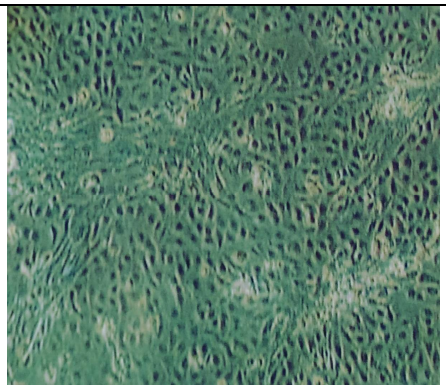

Fig. 1: Morphology at Passage 0 with 60% Confluency (Mag. 40X)

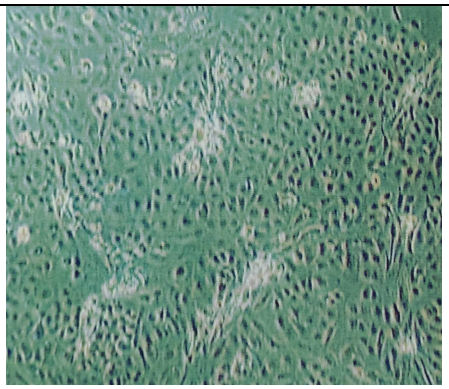

Fig. 2: Morphology at Passage 0 with 70% Confluency (Mag. 40X)

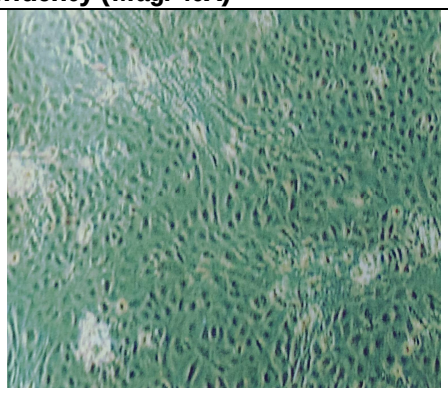

Fig. 3: Morphology at Passage 0 with 80% Confluency (Mag. 40X)

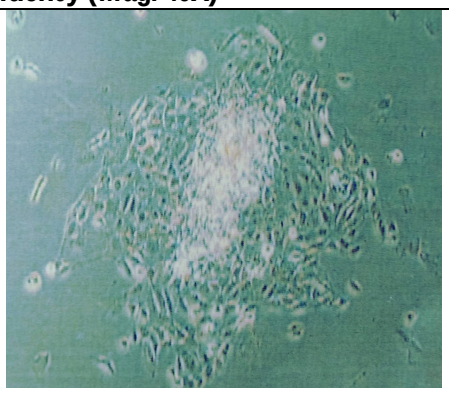

Fig. 4: Morphology at Passage 1 day 9 with small population of MSCs (Mag. 40X)

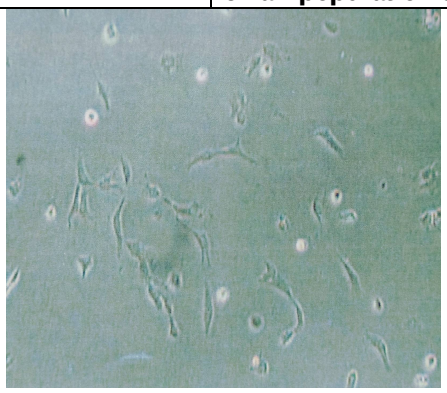

Fig. 5: Morphology at Passage 1 day 9 with 20% Confluency (Mag. 40X)

Indian Journal of Natural Sciences www.tnsroindia.org.in ©IJONS

Vol.8 / Issue 45 / December 2017 *International Bimonthly* *ISSN: 0976 – 0997*

RESEARCH ARTICLE

Investigation of Nucleon Momentum Distributions and Elastic Form Factors for Some FP-Shell Nuclei

Ahmed N. Abdullah*

Department of Physics, College of Science, University of Baghdad, Baghdad, Iraq.

Received: 17 Oct 2017 Revised: 24 Oct 2017 Accepted: 26 Nov 2017

***Address for correspondence**
Ahmed N. Abdullah
Department of Physics,
College of Science, University of Baghdad,
Baghdad, Iraq.
E.mail: Ahmednajim@scbaghdad.edu.iq

ABSTRACT

The nucleon momentum distributions (NMD)for some odd-A fp-shell nuclei, such as ^{51}V,^{53}Cr, ^{55}Mn and ^{57}Fe nuclei are calculated within the coherent density fluctuation model (CDFM) using the theoretical and experimental nucleon density distributions (NDD).The NMD evaluated by the CDFM exhibit high- momentum components (at $k \geq 2$ fm^{-1}) and this feature agrees with the experimental data. For completeness, also elastic electron scattering form factors, F(q) are evaluated within the same framework.The calculated elastic charge form factors for considered nuclei are in a good agreement with the experimental data.

PACS Nos.: 21.10.Ft, 25.30.Bf.

Keywords: Elastic electron scattering,Nucleon density distributions, Nucleon momentum distributions.

INTRODUCTION

The systematic investigations of the nucleon momentum distributions in nuclei extend the scope of the nuclear ground-state theory. Until the mid-seventies more attention in the theory had been paid to the study of quantities such as the binding energy and the nuclear density distribution $\rho(r)$. This is related to the ability of the widely used Hartree-Fock theory to describe successfully these quantities, which, however, are not very sensitive to the dynamical short-range correlations. The experimental situation in recent years concerning the interaction of particles with nuclei at high energies, in particular the nuclear photo effect, meson absorption by nuclei, inclusive proton production in proton-nucleus collisions, and even some phenomena at low energies such as giant multipole resonances, makes it possible to study additional quantities. One of them is the nucleon momentum distribution $n(k)$ [1,2] which is specifically related to the processes mentioned above. However, it has been shown [3] that, in

principle, it is impossible to describe correctly both momentum and density distributions simultaneously in the Hartree-Fock theory. The reason is that the nucleon momentum distribution is sensitive to short-range and tensor nucleon-nucleon correlations. It reflects the peculiarities of the nucleon-nucleon forces at short distances which are not included in the Hartree-Fock theory. This requires a correct simultaneous description of both related distributions $\rho(r)$ and $n(k)$ in the framework of nuclear correlationmethods.

The main characteristic feature of the nucleon momentum distribution obtained by various correlation methods [1,2,4-6] is the existence of high-momentum components, for momenta k > 2 fm^{-1}, due to the presence of short-range and tensor nucleon correlations. This feature of $n(k)$ has been confirmed by the experimental data on inclusive and exclusive electron scattering on nuclei. In general, the knowledge of the momentum distribution for any nucleus is important for calculations of cross-sections of various kinds of nuclear reactions. The coherent density fluctuation model (CDFM) has been suggested in [1,2] as a model for studying characteristics of nuclear structure and nuclear reactions based on the local density distribution as a variable of the theory and using the essential results of the infinite nuclear matter theory.

Abdullah [7] have been study the NMD and elastic electron scattering form factors for some even mass nuclei of *fp*-shell nuclei like ^{50}Cr, ^{52}Cr and ^{54}Cr isotopes using the framework of CDFM. The calculated NMD and elastic form factors of all considered nuclei have been in very good agreement with experimental data.

Hamoudi*et al*. [8, 9,10] have studied the nucleon momentum distributions (NMD) and elastic electron scattering form factors for *p*-shell [8], *sd*-shell [9] and *fp*- shell [10] nuclei using the framework of coherent density fluctuation model (CDFM). They [8, 9,10] derived an analytical form for the NDD based on the use of the single particle harmonic oscillator wave functions and the occupation number of the states. The derived NDD's, which are applicable throughout the whole *p*-shell [8], *sd*-shell [9] and *fp*- shell [10] nuclei, have been used in the CDFM. The calculated NMD and elastic form factors of all considered nucleihave been in very good agreement with experimental data.

In the present study, we follow the work ofHamoudi*et al*. [8, 9,10] and utilize the CDFM with weight functions originated in terms of theoretical NDD of some *fp*-shell nuclei such as ^{51}V, ^{53}Cr, ^{55}Mn and ^{57}Fe nuclei. It is found that the theoretical weight function $|f(x)|^2$ based on the derived NDD is capable to give information about the NMD and elastic charge form factors as do those of the experimental data.

THEORY

The nucleon density distribution (NDD)of one body operator can be written as [8]:

$$\rho(r) = \frac{1}{4\pi} \sum_{n\ell} \xi_{n\ell}\, 4(2\ell+1) \left|R_{n\ell}\right|^2 \qquad (1)$$

Where $\xi_{n\ell}$ is the nucleon occupation probability of the state $n\ell$ ($\xi_{n\ell}$= 0 or 1 for closed shell nuclei and 0 < $\xi_{n\ell}$<1 foropen shell nuclei) and $R_{n\ell}$ is the radial part of the single particle harmonic oscillator wave function.

To derived an explicit form for the NDD of *fp*-shellnuclei, we follow the method of [10] and assume that there are filled 1*s*, 1*p* and 1*d* orbitals and the nucleon occupation numbers in 2*s*, 1*f* and 2*p* orbitals are equal to, respectively, (4-α), (*A*-40-β) and (α+β) not to 4, (*A*-40) and 0 as in the simple shell model. Using this assumption in Eq. (1), an analytical form for the ground state NDD is obtained as:

$$\rho(r)=\frac{e^{-r^2/b^2}}{\pi^{3/2}b^3}\left\{10-\frac{3}{2}\alpha+\left(\frac{11}{3}\alpha+\frac{5}{3}\beta\right)\left(\frac{r}{b}\right)^2+\left(8-2\alpha-\frac{4}{3}\beta\right)\left(\frac{r}{b}\right)^4+\left[\frac{20}{105}\beta+\frac{8}{105}(A-40)+\frac{4}{15}\alpha\right]\left(\frac{r}{b}\right)^6\right\} \quad (2)$$

where A is the nuclear mass number, b is the harmonic oscillator size parameter, the parameters α and β are the deviation of the nucleon occupation numbers from the prediction of the simple shell model ($\alpha=\beta=0$).

From Eq. (2) the central NDD, $\rho(r=0)$, is given by:

$$\rho(0)=\frac{1}{\pi^{3/2}b^3}\left(10-\frac{3}{2}\alpha\right) \quad (3)$$

From Eq. (3) the parameter α can be calculated as:

$$\alpha=\frac{2}{3}\left(10-\rho(0)\pi^{3/2}b^3\right) \quad (4)$$

In the CDFM the NMD, $n(k)$, is given by [11]:

$$n(k)=\int_0^\infty |f(x)|^2 n_x(k)dx, \quad (5)$$

where

$$n_x(k)=\frac{4}{3}\pi x^3\theta(k_F(x)-|\vec{k}|), \quad (6)$$

with θ being a step function, is the Fermi-momentum distribution of a system with A nucleons uniformly distributed in a sphere with radius x and a density $\rho_0(x)=3A/4\pi x^3$ and

$$k_F(x)=\left(\frac{3\pi^2}{2}\rho_0(x)\right)^{1/3}\equiv\frac{V}{x} \quad (7)$$

is the Fermi momentum.

The weight function $|f(x)|^2$ can be determined by the local density ρ [11]:

$$|f(x)|^2=\frac{-1}{\rho_0(x)}\frac{d\rho(r)}{dr}\bigg|_{r=x} \quad (8)$$

This relation holds for monotonically decreasing density distributions ($d\rho(r)/dr\leq 0$).

From Eqs. (5)-(8) the NMD can be obtained as a functional of the density ρ[11]:

$$n_{CDFM}(k)=\left(\frac{4\pi}{3}\right)^2\frac{4}{A}\int_0^{V/k}\left[6\rho(x)x^5dx-\left(\frac{V}{k}\right)^6\rho\left(\frac{V}{k}\right)\right], \quad (9)$$

where $V=(9\pi A/8)^{1/3}$ with a normalization condition:

$$\int n(k)\frac{dk}{(2\pi)^3}=A \quad (10)$$

The NMD of *fp*-shell nuclei is also determined by the shell model using the single particle harmonic oscillator wave functions in momentum representation and is given by [10]:

$$n(k)=\frac{b^3}{\pi^{3/2}}e^{-b^2k^2}\left[10+8(bk)^4+\frac{8(A-40)}{105}(bk)^6\right] \quad (11)$$

The elastic form factor, $F(q)$,of the nucleus in the CDFM can be writtenas [5]:

$$F(q)=\frac{1}{A}\int_0^{\infty}|f(x)|^2\,F(q,x)\,dx \quad (12)$$

where $F(q,x)$ is the form factor of uniform charge density distribution given by:

$$F(q,x)=\frac{3A}{(qx)^2}\left[\frac{\sin(qx)}{qx}-\cos(qx)\right] \quad (13)$$

Inclusion the corrections of the finite nucleon size $F_{fs}=exp\ (-0.43q^2/4)$ and the center of mass $F_{cm}(q)=exp\ (b^2q^2/4A)$ in the calculations needs multiplying the form factor of Eq. (12) by these corrections.

The NDD of two- parameter Fermi (2PF) model is given by [12]:

$$\rho(r)=\frac{\rho_0}{1+e^{(r-c)/z}} \quad (14)$$

The experimental weight function is obtained by substituting Eq. (14) into Eq. (8):

$$|f(x)|^2_{2PF}=\frac{4\pi x^3\rho_0}{3Az}\left(1+e^{\frac{x-c}{z}}\right)^{-2}e^{\frac{x-c}{z}} \quad (15)$$

Moreover, the theoretical weight function is obtained by substituting Eq. (2) into Eq. (8):

$$|f(x)|^2_{th} = \frac{8\pi x^2}{3Ab^2}\rho(x) - \frac{16x^4}{3A\pi^{1/2}b^5}\left\{\frac{11}{6}\alpha + \frac{5}{6}\beta + \left(8 - 2\alpha - \frac{4}{3}\beta\right)\frac{x^2}{b^2} + \left(\frac{4}{35}(A-40) + \frac{2}{5}\alpha + \frac{2}{7}\beta\right)\frac{x^4}{b^4}\right\} e^{-\frac{x^2}{b^2}} \quad (16)$$

RESULTS AND DISCUSSION

The nucleon momentum distributions (NMD)for some odd-A *fp*-shell nuclei, such as ^{51}V, ^{53}Cr, ^{55}Mn and ^{57}Fe nuclei are calculated within the coherent density fluctuation model (CDFM) using the theoretical and experimental nucleon density distributions (NDD). For completeness, also electron scattering form factors, F(q) are evaluated within the same framework. In the present work, the NDD for *fp*-shell nuclei are formulated by means of the wave functions of a harmonic oscillator potential with the assumption that the occupation numbers of the states in real nuclei differ from the predictions of the simple shell model.

Table-1 displays the values of the parameters b,α andβ together with the other parameters employed in the present calculations for selected nuclei. The parameterα is determined by Eq. (4), while the parameterβ is assumed as a free parameter to be adjusted to obtain agreement with the experimental NDD. In Table-2, we present the calculated occupation numbers of nucleons in the orbitals 2*s*, 1*f* and 2*p* orbitals which are equal to (4-α), (*A*-40-β) and (α+β), respectively, together with the calculated rms$\langle r^2\rangle^{1/2}_{cal}$ and those of experimental data $\langle r^2\rangle^{1/2}_{\exp}$ [13].Itis clear from Table-2 that the calculated results of rms radii showed excellent agreement with experimental data.

Figs. 1(a)-1(d) demonstrate the calculatedNDD for ^{51}V,^{53}Cr, ^{55}Mn and ^{57}Fe nuclei, respectively. The dotted symbols are the experimental results [14,15] whereas the blue and red curves are the calculated NDD, using Eq. (2), with(α = β=0) and($\alpha \neq \beta \neq 0$), respectively. It is evident from this figure that the blue curves deviate slightly from the dotted symbols especially at small *r*. Taking the effect of the higher orbitalsby introducing the parameters α andβ in the calculations tends to remove these deviations from the region of small *r* as seen in the red curves. It is obvious from thesefigures that the calculated NDD represented by the red curves are in excellent accordance with those of experimental data hence they coincide with each other throughout the whole range of *r*.

The results of the NMD for ^{51}V, ^{53}Cr, ^{55}Mn and ^{57}Fe nuclei obtained by CDFM using the theoretical (the red curves) and experimental (the dotted symbols) NDD are presented in Figs. 2(a)-2(d), respectively, compared with those calculated by the harmonic oscillator shell model (the blue curves). It can be noted that the blue curves show a steep decrease up to k <2 fm^{-1}, which are in inconsistent with the studies [1, 2]. This is due to that the short-range correlation (SRC) does not included in to the ground state wave function of the shell model calculations which is responsible for the behavior of NMDin the high momentum [16, 17]. Besides, it can be noted that the CDFM results describe satisfactorily the experimental data throughout all values of *k*. The most important feature of NMDobtained within the CDFM is the presence of high-momentum components (at k≥ 2 fm^{-1}). This is in agreement with the available experimental information. The latter can be considered as an evidence for an effective account of the SRC in the model.

Figs. 3(a) -3(d) explore the elastic form factors of ^{51}V, ^{53}Cr, ^{55}Mn and ^{57}Fe nuclei, respectively. The solid curves are the calculated results whereas the dotted symbols are the experimental data [14,15]. It shows that the experimental data of these nuclei are very well explained by the calculated curves up to the momentum transfer (q ≈ 1.9 *fm*$^{-1}$) whereas for higher momentum transfer the calculated form factors do not give a satisfactory results with the experiment data.Moreover, the locations of the first and second diffractions minimum, for the experimental and calculated results, are coincide with each other.

CONCLUSIONS

The nucleon momentum distributions (NMD)for some odd-A fp shell nuclei, such as ^{51}V,^{53}Cr, ^{55}Mn and ^{57}Fe nuclei are calculated within the coherent density fluctuation model (CDFM) using the theoretical and experimental nucleon density distributions(NDD). For completeness, also elastic form factors, F(q) are evaluated within the same framework.From the present work, it is possible to draw the following conclusions:

- Including the effect of α and β (i.e. considering higher orbits) improves the calculated nucleon density distributions (NDD) and makes them in agreement with the experimental data.
- The calculated nucleon momentum distributions in the coherent density fluctuation model are mainly characterized by the long-tail behavior at high momentum *k* and this feature agrees with the experimental data.
- The calculated nucleon momentum distributions in the shell model (using the single particle harmonic-oscillator wave functions in the momentum space) are mainly characterized by the steep-slope behavior at high momentum *k*, i.e., the nucleon momentum distributions decrease rapidly with increasing *k*.
- The calculated elastic form factors in the coherent density fluctuation model are (in general) in a good agreement with the experimental data and this agreement proves the reality of this model in calculating the nucleon momentum distributions and form factors of the nuclei under study.

REFERENCES

1. A. N. Antonov, P. E. Hodgson and I. Z. Petkov, *Nucleon momentum and density distribution in nuclei* (Clarendon, Oxford 1988).
2. A. N.Antonov, P. E. Hodgson and I. Z.Petkov, *Nucleon correlation in nuclei* (Springer-Verlag, Berlin–Heidelberg–New York **,**1993).
3. M. Jaminon, C. Mahaux, H. Ngo, *Phys. Lett.* **158** B (1985) 103.
4. J.G. Zabolitzky and W. Ey, *Phys. Lett.* **76** B (1978) 527.
5. A. N. Antonov, P. E. Hodgson and I. Z. Petkov, *Z. Physik A***297** (1980) 257.
6. A.N. Antonov, I.S. Bonev, C.V. Christov and I. Z. Petkov.*NuovoCimento* A **100** (1988)779.
7. A. N. Abdullah, *Iraqi Journal of Science,* **57** (3A) (2016)1723.
8. A. K. Hamoudi, M. A. Hasan and A. R. Ridha, *Pramana Journal of Physics* (Indian Academy of Sciences) **78** (5) (2012) 737.
9. A. K. Hamoudi, G. N. Flaiyh and S. H. Mohsin, *Iraqi Journal of Science***53** (4), (2012) 819.
10. A. K Hamoudi and H. F. Ojaimi, *Iraqi Journal of Physics***12** (24) (2014) 33.
11. A. N. Antonov, C. V. Christov, I. Z. Petkovand I. S. Bonev, *NuovoCim A***101** (1989) 639.
12. H. D. Vries, C. W. Jager, and C. Vries,*Atom. Data and Nucl. Data Tables***36** (1987) 495.
13. I. Angeli and K. P. Marinova, *Atom. Data and Nucl. Data Tables***99** (2013) 69.
14. H. D. Wohlfahrt, E. B. Shera and M. V. Hoehn,*Phys. Rev. C***23**(1981) 533.
15. E. B. Shera*et al.Phys. Rev. C***14** (1981) 731.
16. M. Traini and G. Orlandini, *Z. Physik A***321** (1985) 479.
17. M. D.Ri, S. Stringari and O. Bohigas, *Nucl. Phys. A***376** (1982) 81.

Table-1: Parameters used in the Present Calculations for Selected Nuclei.

Nuclei	Z	Model	c	z	ρ_{exp} (0) (fm^{-3})	*b* (fm)	α	β
^{51}V	23	2PF	3.830	0.55	0.1798	1.966	1.5901	1.0214
^{53}Cr	24	2PF	3.922	0.55	0.1754	1.981	1.5998	1.0195
^{55}Mn	25	2PF	3.996	0.55	0.1732	2.0	1.5196	1.3280
^{57}Fe	26	2PF	4.073	0.55	0.1705	2.014	1.4916	1.4562

Table-2: Calculated Occupation Numbers of 2*s*, 1*f* and 2*p*Orbitals of the Considered Nuclei together with $\langle r^2 \rangle_{cal}^{1/2}$ and $\langle r^2 \rangle_{\exp}^{1/2}$

Nuclei	Occupation No. of 2*s*(4-α)	Occupation No. of 1*f*(*A*-40-β)	Occupation No. of 2*p*(α+β)	$\langle r^2 \rangle_{cal}^{1/2}$ (fm)	$\langle r^2 \rangle_{\exp}^{1/2}$ (fm) [13]
^{51}V	2.4098	9.9786	2.6115	3.6	3.60±0.002
^{53}Cr	2.4001	11.9805	2.6193	3.651	3.651±0.007
^{55}Mn	2.4803	13.6720	2.8476	3.707	3.705±0.002
^{57}Fe	2.5083	15.5438	2.9478	3.753	3.753±0.002

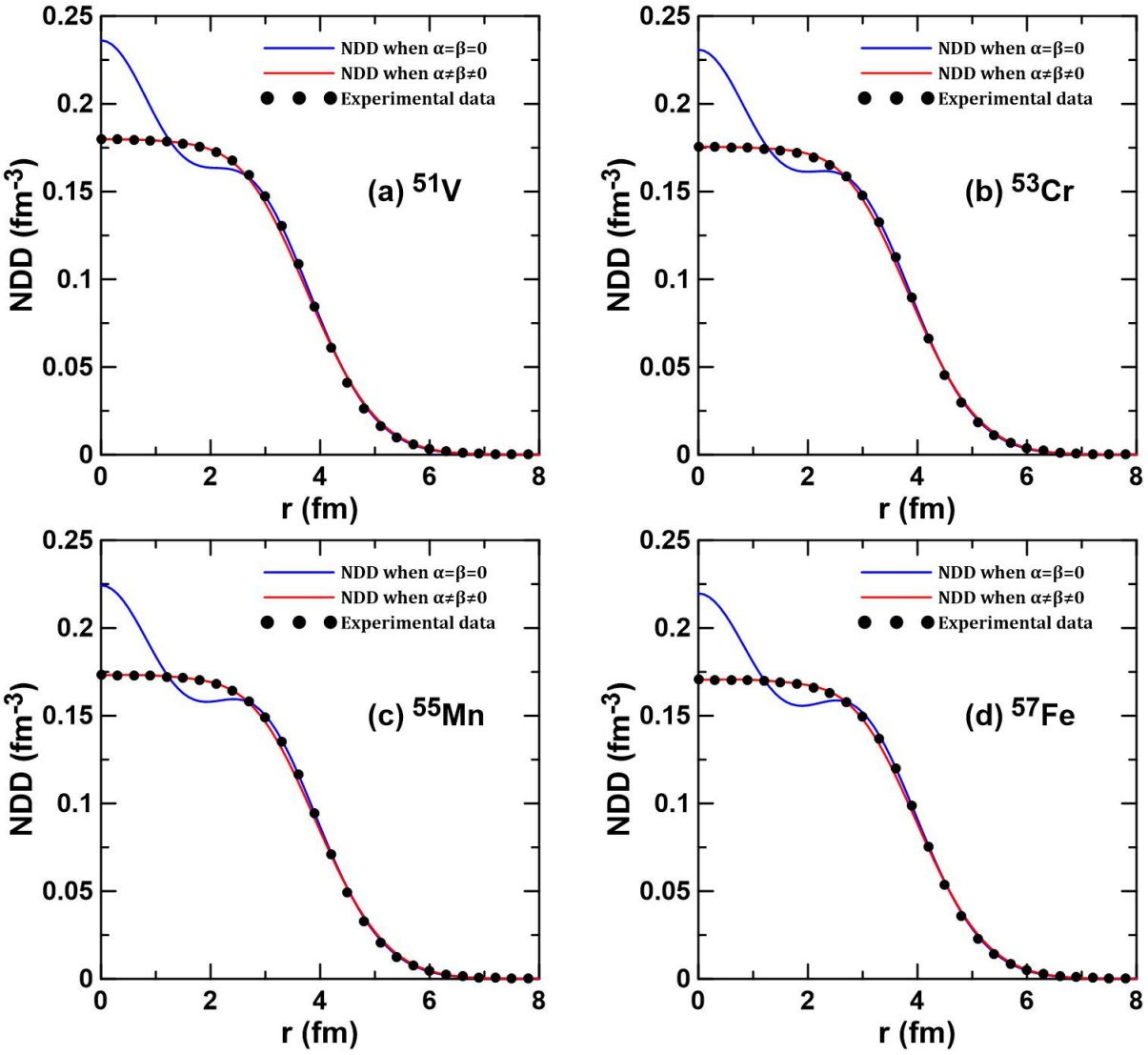

Fig. 1: The Nucleon Density Distributions (NDD) for (a) ^{51}V, (b) ^{53}Cr, (c) ^{55}Mn and (d) ^{57}Fe nuclei.

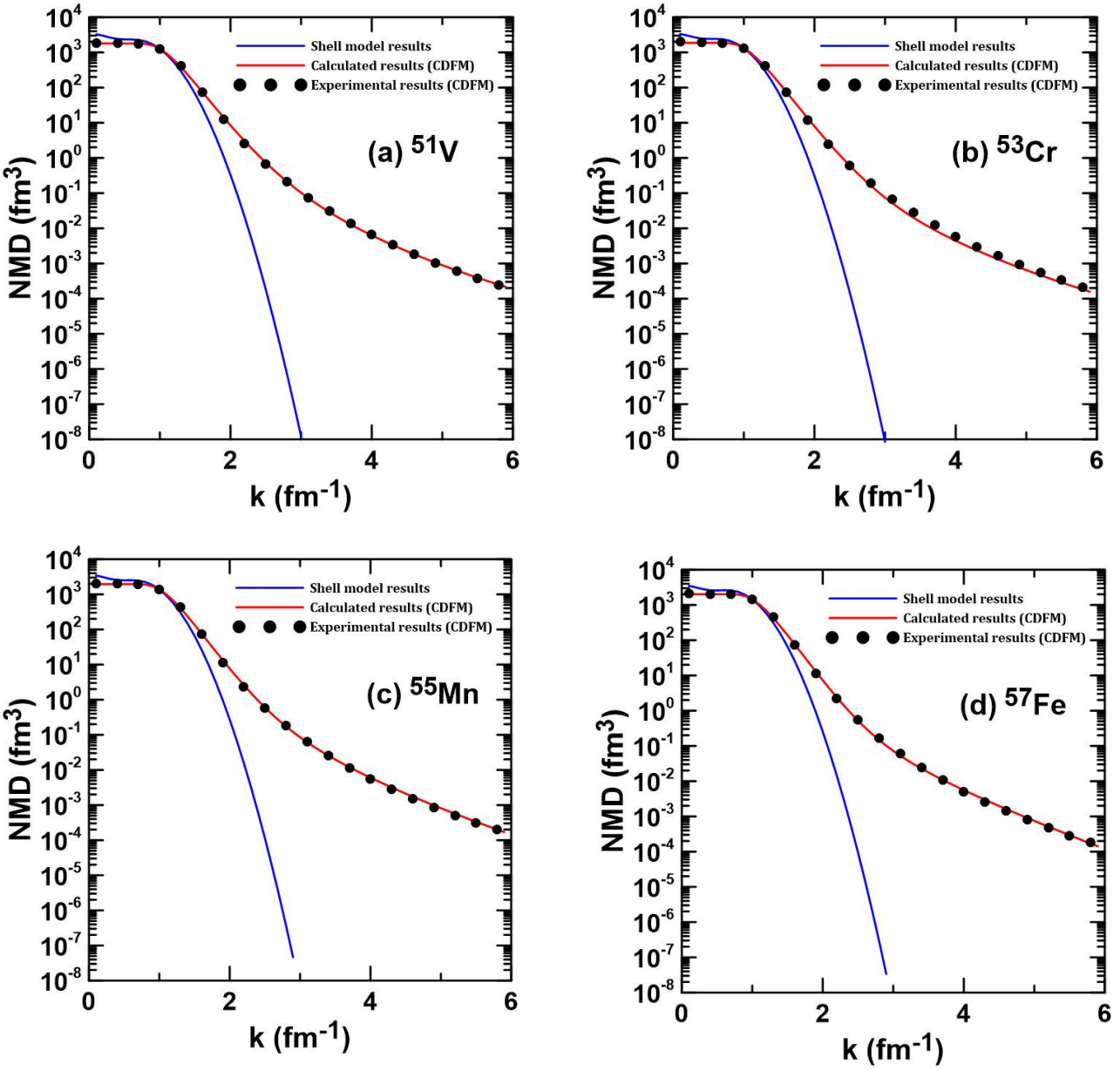

Fig. 2: Calculated Nucleon Momentum Distributions (NMD) for (a) ^{51}V, (b) ^{53}Cr, (c) ^{55}Mn and (d) ^{57}Fe nuclei.

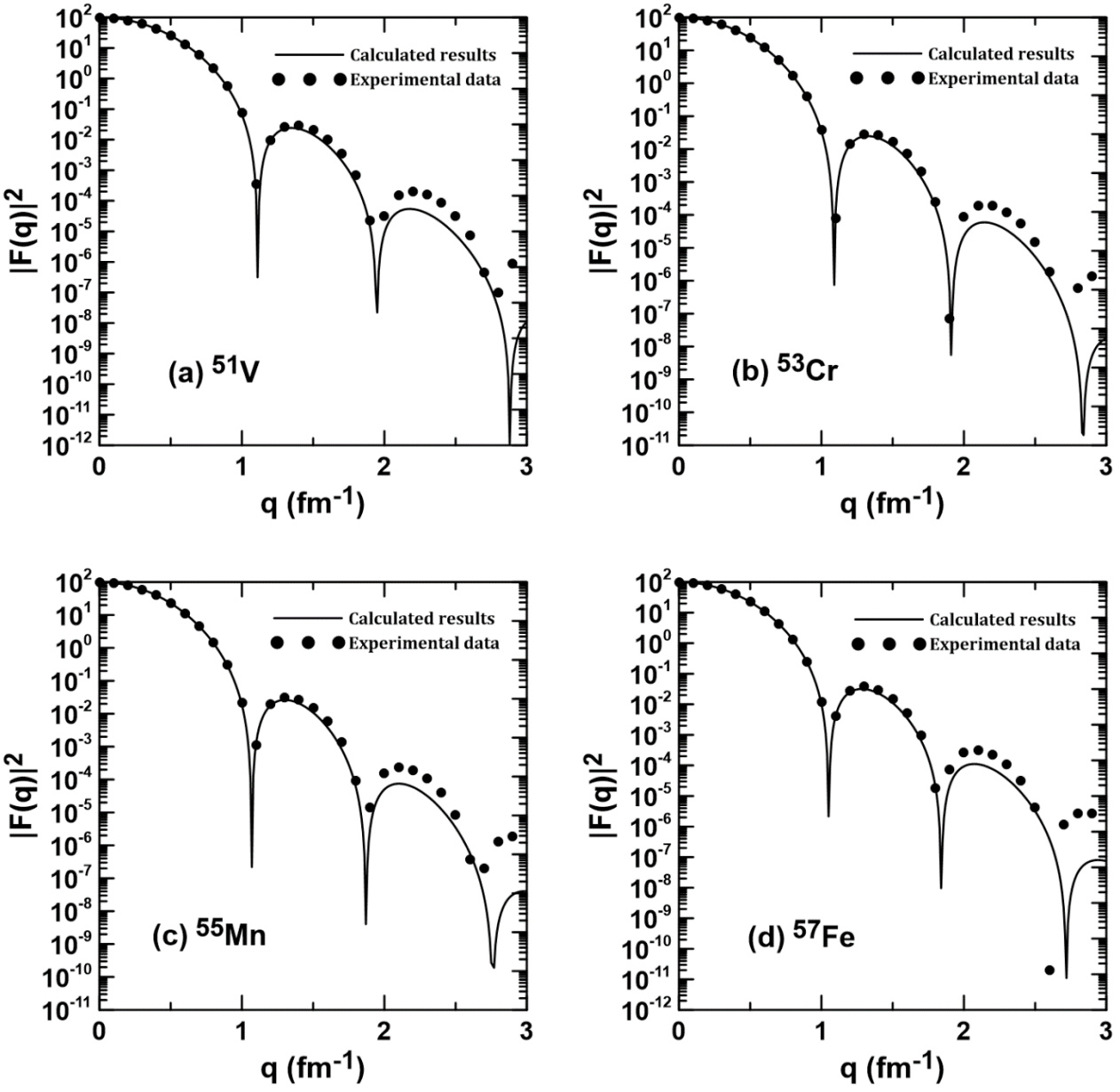

Fig. 3: The elastic form factors for (a) ^{51}V, (b) ^{53}Cr, (c) ^{55}Mn and (d) ^{57}Fe nuclei.

Connecting People with Nature

INDIAN JOURNAL OF NATURAL SCIENCES

ISSN: 0976-0997

MJL& Cited by Thomson Reuters for Zoological survey in 2012

ISI Impact Factor :1.233 , NAAS Rating :3.56,IC Value: 47.65

Tamil Nadu Scientific Research Organization is working for the promotion of society by transferring science & technology since 1997. We are very keen in appreciating and recognizing the contribution of every one of you. We are publishing **Indian Journal of Natural Sciences** - **IJONS** from **August 2010**. The Journal is peer reviewed International Journal for publication of Original Research papers /Reviews/ Short communications/Book reviews/Reports on conferences/Seminar, Important events, News of interest, Special articles, General Articles etc.

Call for Papers: Investigations related to science in all branches

Highlights

- International Quality
- Published Bi-Monthly
- Fast acceptance and Quick Publication
- Low price
- High Rank Editorial Board
- Online manuscript submission
- Publish original Research Works and Reviews

Subscription Fee (Annual 6 Issues)

- For Individuals Rs.1000/-
- For students Rs.750/-
- For Institutions Rs.1200/-

Publication fee for Authors

- **Rs.3000/- (**Processing fee)
- **USD 90/-** for Foreign author

Send all correspondence to

----------Chief Editor ----------

Indian Journal of Natural Sciences (IJONS)

C/o TNSRO, 39 Mura Bhavan,Koodal Nagar,Rajagopalapuram Post

Pudukkottai-622003,TamilNadu,India.

Phone:04322-261088 Mobile: 99528 86637

E-mail: ijonstnsro@gmail.com.,**www.tnsroindia.org.in**

Plant More Trees ***Love Animals*** ***Conserve our Nature***

Indian Journal of Natural Sciences www.tnsroindia.org.in ©IJONS

Vol.8 / Issue 45 / December 2017 *International Bimonthly* *ISSN: 0976 – 0997*

RESEARCH ARTICLE

Study the Electronic and Spectroscopic Properties of Bare and H Passivatedwurtzoid AlN Nanotubes

Mohammed T. Hassein[1]*, Mudar Ahmed.Abdulsattar[2] and Tasneem H. Mahmood[3]

[1]University of Baghdad ,College of Science, Physics Department.
[2]Ministry of Science and Technology, Baghdad, Iraq.
[3]University of Baghdad, College of Science for Women, Physics Department.

Received: 03 Oct 2017 Revised: 17 Oct 2017 Accepted: 01 Nov 2017

***Address for correspondence**
Mohammed T. Hassein
Department of Physics,
College of Science, University of Baghdad,
Baghdad, Iraq.
E.mail: mohammedtake@gmail.com

ABSTRACT

AlNwurtzoid nanostructures properties are investigatedusing wurtzoid molecules. The investigated properties include energy gap, Highest occupied molecular orbital (HOMO),Lowest unoccupied molecular orbital (LUMO), infrared and Raman spectra. Wurtzoid molecules are a collection of molecules that simulated the wurtzite structure of hexagonal lattice. These molecules are described as a capped bundle of (3,0) nanotubes that have dimension that can related to **a** and **c** lattice parameters of hexagonal wurtzite structure. Results show that experimental bulk gap is generally confined between bare and H passivated wurtzoids. Structural parameters such as bond lengths and bond angle are in agreement with experimental bulk values. Results of vibrational frequencies are red shifted with respect to experimental bulk.

Key words :AlNwurtzoid molecules, Nanotubs, DFT.

INTRODUCTION

AlN is termed group III-V semiconductors with a wide band gap that many be used in optoelectronics, solar cell, LED and a greatly promising candidatefor developing efficient laser devices [1]. AlNnanocrystals is interest because of the great potential applications in micro-and nano optoelectronics. In the present work we shall investigate the electronic and spectroscopic properties of AlNwurtzitenanocrystals approached for bare and H passivated wurtzoids structure using density function theory methods.

THEORY

Gaussian 09 computational chemistry package is used to perform the AlN molecular geometrical optimization and molecular vibrational frequency calculations with all-electron density functional theory (DFT) at the level of B3LYP with valence triplet-zetabasis 6-311G** [2]

In the present work bare and H passivated molecular nanotube wurtzoid of AlN will be investigated. The smallest AlN molecule is Aluminum mononitrideafter complete H passivation. It is assigned the formula $AlNH_6$. While the mostinteresting molecule is called cyclohexane $Al_3N_3H_{12}$. This hexagonal ring shaped molecule is building block of both wurtzoids and diamondoids.

The wurtzoids molecules need to specify two indices (a and c) as in the ordinary wurtzite (hexagonal) structure [3]. These molecules are a bundle of AlN (3,0) nanotube. The symmetry of their structure enables them to form bare and H passivated structures without facing appreciable structure reconstruction. Investigated bare and H passivated cluster AlNwurtzoid nanotube are shown in fig.(1)

RESULTS AND DISCUSSION

Fig.(2) shows gap of bare and hydrogen passivatedwurtzoid of AlN as a function of total of Al and N atoms. It is found that hydrogen passivated wurtzoids follow quantum confinement effect of decreasing energy gap as a function of increasing of total number of atoms. Experimental bulk AlNwurtzite hexagonal structure energy gap is close to 6 eV.

Fig.(3) shows cohesive energy of AlN bare and hydrogen passivated wurtzoids as a function of total number of Al and N atoms. It shows that H passivated wurtzoid have higher cohesive energies than bare wurtzoids. While the experimental cohesive energy is higher than the both of bare and passivated wurtzoids except at H passivatedtriwurtzoids.

Fig.(4) shows the distribution of bond length of bare and H passivatedAlNwurtzoid. There are three type of bonds exist i.e. N-H, Al-H and AlN [4,5]. The strong bond length are N-H bonds followed by Al-H bonds. These bonds are in agreement with experimental values. While AlN is the widest distribution because the calculations are like surface calculation in which reconstruction deviates many bond from their ideal length.

Fig.(5) shows the distribution of bond angles (angles between two bonds) in H passivated wurtzoid compare with bulk wurtzite has bond angle 120^o as shows by an arrow with highest peak of the molecule.

Fig.(6) shows the highest reduced mass mode used for molecules and manocrystal to determine the longitudinal optical mode at bulk structure. This figure shows two distinguished region for the bare structure and three for H passivated structure. These region are vibrations of Al approximately (170-500) cm^{-1}, N approximately (500-800) cm^{-1}. The highest reduced masses are for Al atoms follow by N and H passivated molecules have reduced mass nearly equal to 1 atomic mass unit. The highest reduced mass mode vibrations are shifted with respect to bulk experiment LO mode HRMM for bare and H passivatedAlNwurtzoid are 550 and 750 cm^{-1} respectively compared with LO experiment bulk wurtzite of (893) cm^{-1}.

Fig.(7) shows IR and Raman spectra for AlN bare and H passivated wurtzoid structure. It is observed two regions for H passivated the first (500-1000) cm^{-1} where the center peak at 744 cm^{-1} and the second region center at 1888 cm^{-1} and Raman spectra are very low intensity in these two bonds. While bare wurtzoid have two different bands one at 722 cm-1 are the second at 893 cm^{-1}.

CONCLUSION

Electronic and spectroscopic properties of AlNwurtzoids approach to nanocrystal and bulk limits. The geometrical structural properties such as bond lengths and bond angles have distribution in which the highest peaks are very close to ideal bulk values. Results of vibrational frequencies are red shifted with respect to experimental bulk. Results show that experimental bulk gap is genrally confined between bare and H passivated wurtzoids.

REFERENCES

1. Yen Chih Chiang, Chung Lin, Hao Chung Kuo, "Novel thin GaN LED structure adoped micro abraded surface to compare with conventional vertical LEDs in ultraviolet light ", Nanoscal Res. Lett. 10,182, (2015).
2. Omkar K. Jani, "Development of wide-band gap InGaN solar cells for high efficiency photovoltaics", PHD thesis, Georgia insttute of technology, (2008).
3. Mudar Ahmed Abdulsattar," Molecular approach to hexagonal and cubic diamond nanocrystals", carbon let., 16, 192, (2015).
4. K. Balasubramanian, "Geometric and bond energies of GaHn, AND GaHn+(n=1-3)", chem.phys.lett., 164, 231,(1989).
5. C. Stampfl, C.G.VandeWalle, "Density functional calculations for III-V nitrides using the local-density approximation and the generalized gradient approximation", phys. Rev 1359, 5521, (1999).

(a) AlN bare

AlN

Al_3N_3 Cyclohexane

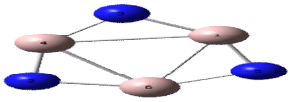

Al_7N_7 wurtzoid

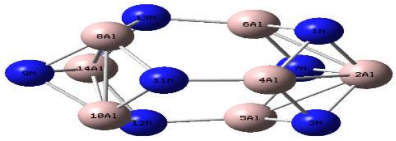

$Al_{13}N_{13}$ wurtzoid2c

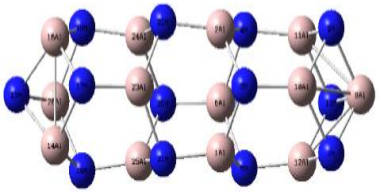

(b) AlNpassivated H

AlNH

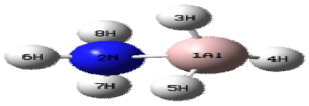

$Al_3N_3H_{12}$ Cyclohexane

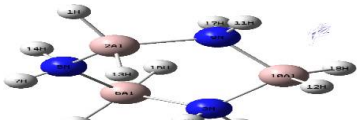

Al_7N_7 H_{14} wurtzoid

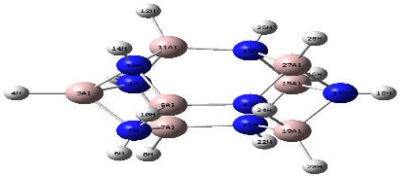

$Al_{13}N_{13}H_{26}$ wurtzoid2c

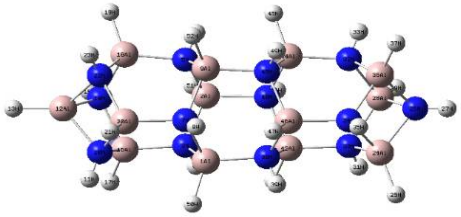

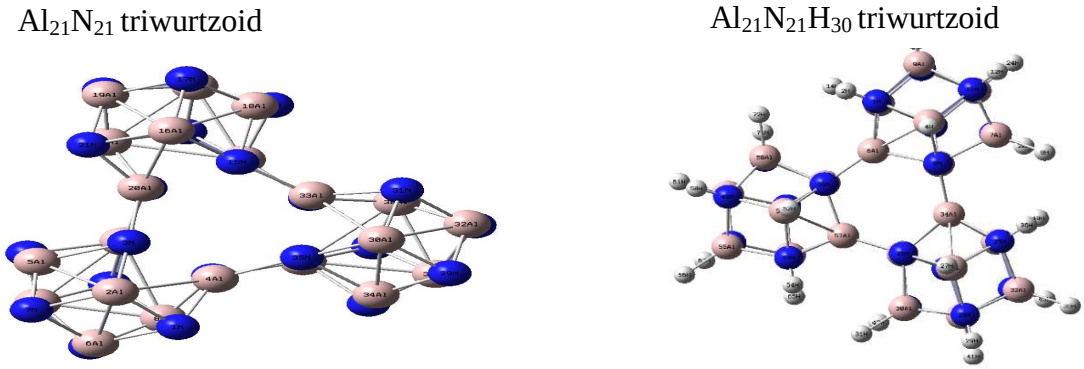

Fig.(1) AlN (a) Bare and (b) H Passivated Wurtzoids Nanotube Geometrical Optimization Structure.

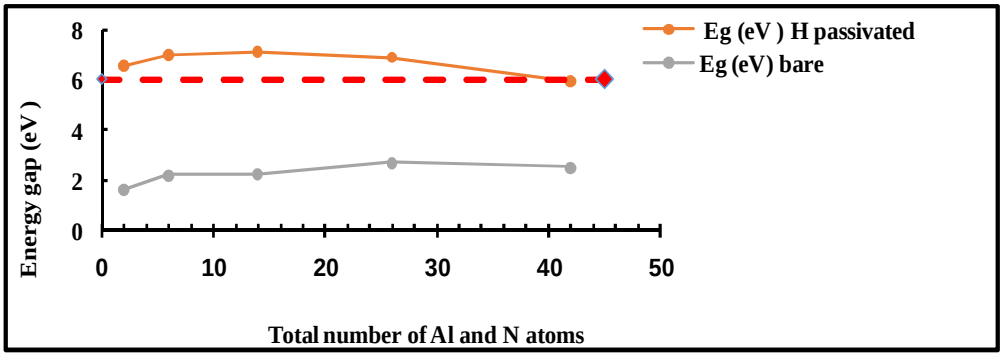

Fig.(2) Energy Gap of Bar and Passivated Wurtzoids as a Function of total number of Al and N Compare with Bulk Experimental Wurtzite Energy Gap[3,4].

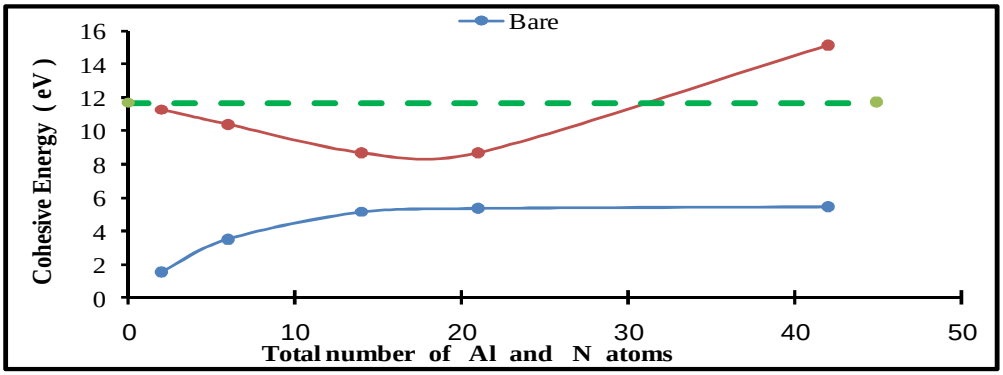

Fig.(3) Cohesive Energy per atom for Bare and H PassivatedaInwurtzoids. Experimental Bulk Wurtzite Value is (11.669 eV).

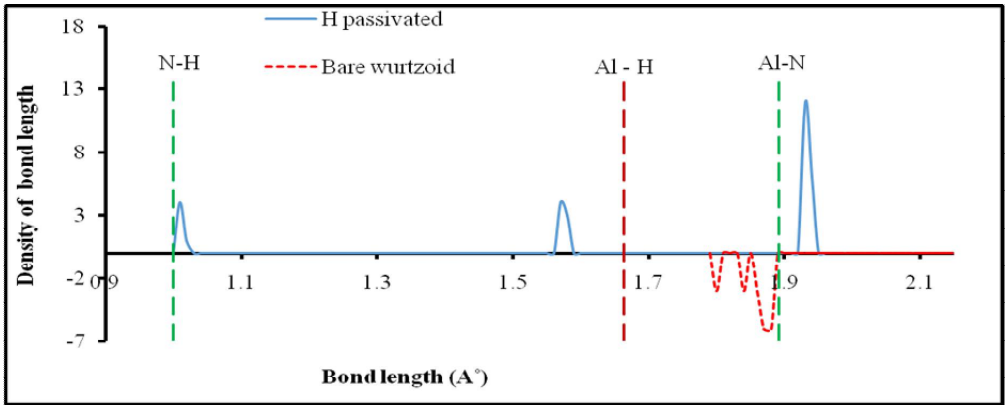

Fig.(4) Bond Lengths of the bare and H PassivatedaInwurtzoid Compare with Experimental Values N-H, Al-H, and Al-N .

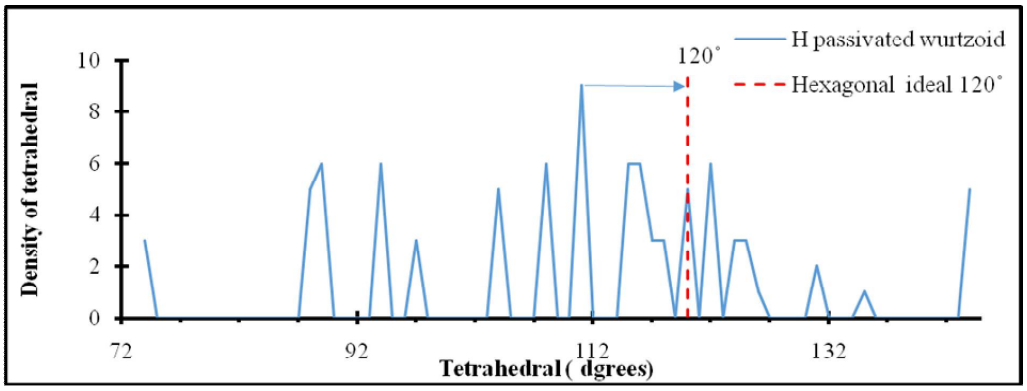

Fig.(5) Tetrahedral (Bond Angles) of Hydrogen Passivated Wurtzoid Compare with Bulk Wurtzite.

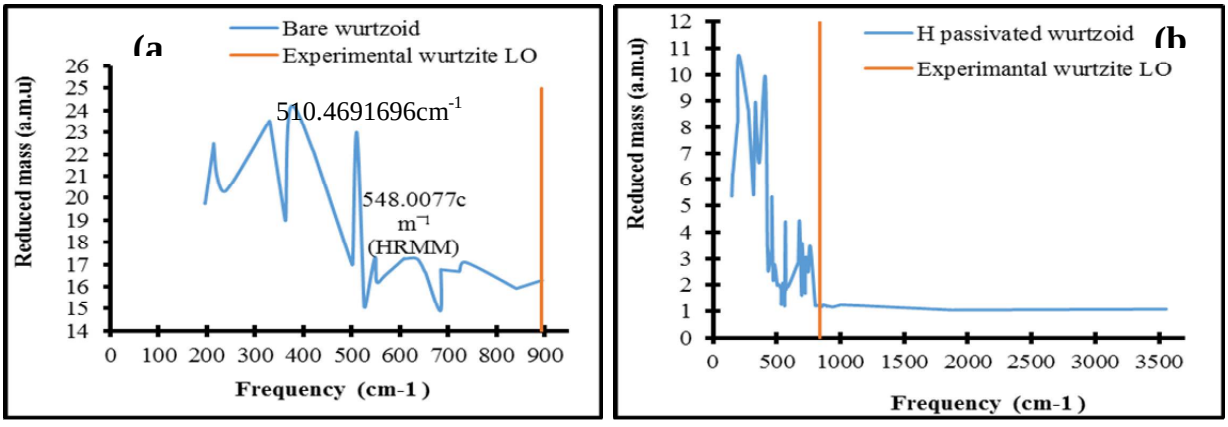

Fig.(6) Reduced Masses of AlN (a) Bare Wurtzoid (b) H Passivated Wurtzoid.

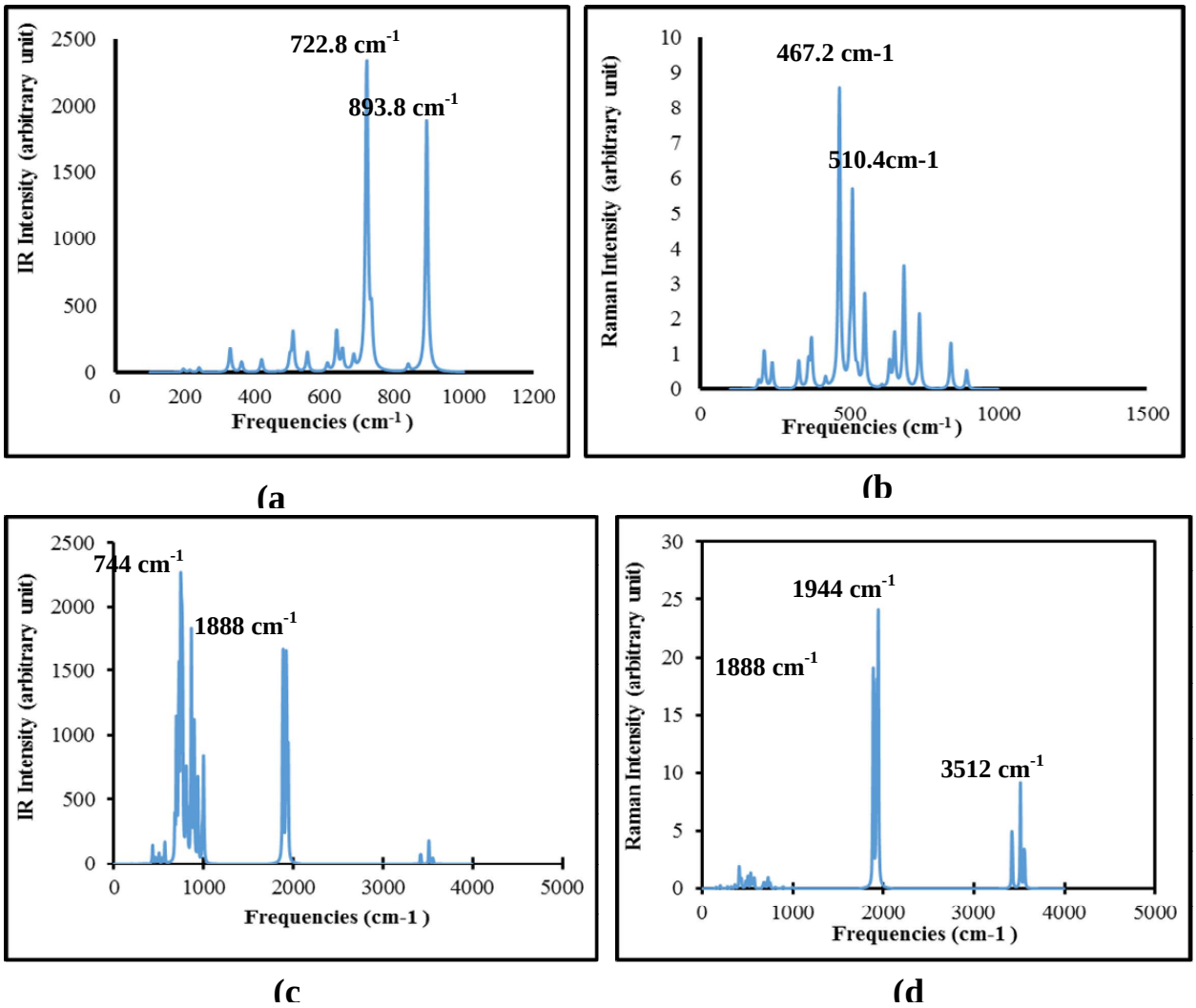

Fig.(7) IR and Raman Spectrum for Bare and H Passivated Wurtzoid.(a) IR of Al_7N_7 Bare Wurtzoid, (b)Raman of Al7N7 Bare Wurtzoid (c)IR of Al7N7H14 wurtzoid (d)Raman of Al7N7H 14 Passivated Wurtzoid.

Indian Journal of Natural Sciences www.tnsroindia.org.in ©IJONS

Vol.8 / Issue 45 / December 2017 *International Bimonthly* *ISSN: 0976 – 0997*

RESEARCH ARTICLE

Investigation of Agro-Industrial Waste under the Working Parameters on Fluidized Gasification System

M.Mathanmohan[1]* and S.Vivekanandan[2]

[1]Research Scholar Department of Mechanical Engineering, Annamalai University, Chidambaram–608 002., Tamilnadu, India

[2]Associate Professor Department of Mechanical Engineering, Annamalai University, Chidambaram–608 002.. Tamilnadu, India

Received: 17 Oct 2017 Revised: 24 Oct 2017 Accepted: 26 Nov 2017

***Address for correspondence**

M.Mathanmohan

Research scholar Department of Mechanical Engineering,

Annamalai University,

Chidambaram – 608 002, Tamilnadu, India.

E.mail: mathanmohanenergy1984@gmail.com

ABSTRACT

The objective of the present work was to assess the agro-industrial residuals in a fluidized bed gasification process. The experiments were performed in a pilot scale auto-thermal fluidized bed gasifier (FBR) were wheat husk, rice husk and saw dust was used as the feed stock after analyzing phsio-chemical analysis with physical pre-treatment by using air as gasifying agent. The working parametric such as bed temperature (t), equivalence ratio (e), pressure (p), feed size (f_s) and fuel consumption rate (f_c) with optimum condition considered to improve producer gas efficiency, tar yield efficiency and ash content efficiency. Experiments were conducted between the 't' range of 650-900°C, using 'e' ranges 0.2 to 0.35, 'f_s' between of 75 to 300 μm and 'f_c' range of 5 to 20 kg/hr. In the present investigation, an empirical relationship was developed to predict the process of generating producer gas with better quality through gasification of biomass in a FBR using response surface methodology (RSM). The full potentiality of wheat husk, rice husk and saw dust for gasification was investigated via RSM. Higher f_s and e resulted in more gas yield due to increases in the exothermic reactions. The developed model was made a good prediction for the experimental data as well as predicated data.

INTRODUCTION

An agro-industrial waste could be utilized for the recovery of energy. Biomass such as wheat husk, rice husk and saw dust. Used as reasonably due to high energy content 10<18 MJ/kg [1-4]. In many countries, moist of surplus, agro wastes are disposed by direct burning in open heaps, which result in energy loss and units emission of various pollutants to the environment. The process of converting carbonaceous substance into gaseous products using a

gasifying agent such as air, O_2 and steam has been considered as one of the visible alternative to combustion of low density [5]. Agro-industrial residue further the gasification process is 80% thermodynamically efficient in converting the organic substance of the feed into a product gas with the mixture containing Co_2, Co, H_2, CH_4, N_2 and other minor organic compounds such as tars, ammonia, sulfur formed in case of air is used as gasifying agent beside the gasification system products a clean fuel gas can be used in a combined cycle for generation power may achieve 40% efficiency. An integrated combined cycle of gasification system offer higher efficiency than that of a convention direct combustion pulverized coal fixed process [6].

Nowadays, gasification technology that coverts solid biomass into syngas for combined integrated cycle, coal covert liquid products and chemical products [7-9]. The gasification technology has been developed for woody agriculture biomass is carbon-neutral as eco- friendly CO_2 emission when solid biomass used. However, biomass has a low heating value transportation, storage cost and density and also the problem of shortages of this fuel due to seasonally and the potentially necessity to have large size gasifier [10].

Gasification system are of two types, they are fixed bed and fluidized bed gasifier, according to many reports the fluidized gasifying system offer more advantages than the conventional draft type gasifying system, for converting low density. Agro – biomass such as wheat husk, rice husk and saw dust into energy in gasifying process may generate low calorific value fuel gas. The fluidized bed gasifier seems to the suitable option for such biomass with better conditions of gasifier temperature in isothermal conditions. Conversion of wheat husk, rice husk and saw dust into heat, steam and gases or liquid fuels could bring benefits and to minimum conventional energy resources [11-15]. Besides wheat husk, rice husk has low contents of sulfur and of heavy metals and is relatively low pollutions. It can serve as eco- friendly fuel than fossil fuels because, even it is burned emitter carbon accumulated in the plant body by photosynthesis [16].

The generation of energy from rice husk and wheat husk, could also generate income as a co-generation of power to the national grid system could save the fuel cast and cost of treatment however, many technologies have been developed for utilizing biomass as gasification to generate power by using Agro- biomass to drive generator to producer energy [17-20]. very few investigation have been done related to different working parameter in a fluidized bed gasifier using woody biomass, hence the present work was aimed to develop fluidized bed gasifier using air of gasifying agent by incorporating the process parameter like bed temperature, equivalent ratio, pressure, feed rate, particle size and to investigate the effect of producer gas, tar, ash efficiency [21].

EXPERIMENTAL INVESTIGATION

Agro biomass

The feed material such as wheat husk, rice husk and saw dust was selected to study the fluidized bed gasification process. These biomass were collected from rural area from Chidambaram, Cuddalore district, India. The phsio-chemical properties of biomass as feed material are presented in Table 1. The test materials were dried and then sieved in a standard sieves, as particle size was distributed as 196 μm, 298 μm and 285 μm as followed by wheat husk, rice husk and saw dust [22]. The specific gravity of the selected materials was measured using bottle method; the moisture content, volatile matter, fixed carbon and ash content was determined by ASTM procedures (ASTM, E - 871, 872 and 830) respectively [23]. The feed elemental composition was analyzed by PERKIN ELMAR 2400 Series II. The bed material was used as lime stone and may used particle size as selected as 0.4 mm. The fluidization velocity was determined by using U-tube manometers are used to measure the pressure drop above and below the distributor plate and at different heights of fluidized bed gasifier. The air velocity determined to the peak pressure drop gives the experimental value of minimum fluidization velocity.

Experimental setup

A 20 kg/hr fluidized bed gasifier has been developed and the experimental investigation was carried out on agro-industrial biomass such as wheat husk, rice husk and saw dust. The schematic line diagram of experimental setup is shown in figure 1 and table 2 shows the experimental design specification and operating parameters. The gasifier is made up of carbon steel material with the inside diameter of 108 mm and height of 1400 mm having inside refractory lining of thickness 0.1 m and multiple hole distributor plate of 105 mm diameter was used for air distribution. Lime stone was used as bed material fitted with gasifier, arrangement is made to discharge the ash periodical disposal system. The screw feeder used to feed the feed material and to maintain the bed in a fluidized stage air was introduced at the bottom of gasification system using blowers. The air flow was estimated by orifice meter placed in a feed pipe to measure the pressure drop with proper controlling and regulating valves. The calibration of orifice prior to the experiment with two instruments; namely a anemometer (make: Dantec, Denmark) and micro-manometer (make: Furnace Control, England). The pressure drop between the orifice were measured in the manometer with respect to flow rates by the anemometer. At different equivalent ratio pressure drop were noted to measure the air flow rate.

Pre-heating the bed material with help of electrical heaters during startup to achieve the bed temperature, feed was controlled in a screw feeder using speed drive properly into the gasifier to prevent the combustion outside the chamber. The deserved equivalent ratio was achieved by controlling the air supply to the gasification system. The cyclone separator used to separate the solid particles from the producer gas. The bag filter used to clean up the gas by removing dust and other Corse particles. The water cooling systems were used to cool the producer gas and remove the tar by condensation.

EXPERIMENTAL TESTING AND OPERATING CONDITIONS

Temperature (t)

Investigation carried out by maintain the desired bed temperatures as the selected feed material such as wheat husk, rice husk and saw dust. One of the important features of biomass gasification is that the bed temperature can be kept as low as 650–950°C, thereby preventing sintering and agglomeration of carbon ash during the conversion process. Low temperature requires catalyst for producing hydrogen and nitrogen. The bottom part of the gasifier, temperature is stable for all the fuel around 650 °C. High temperature above 950 °C will change the gas composition.

Equivalent ratio (e)

Quantity of air required to burn a portion of the fuel to release heat by supporting the endothermic reactions, to prevent the heat losses in Solid, liquid and gaseous product by maintaining the required temperature termed as equivalence ratio as an important factor in a gasification process. Experiment were carried out with a equivalence ratio 0.2 - 0.5 with wheat husk, rice husk and saw dust by varying equivalence ratio at 0.25, 0.30 and 0.35.

Pressure (p)

The chemical cycle when the production of hydrogen may affects, if the pressure rises above 5 bar and if the pressure less than 1 bar producer gas generates with low purity.

Feed size (f_s)

The biomass less than 75 μm implied more conversions leads to lower solid temperatures in the system may affect the concentration of producer gas. Feed size above 500 μm leads to devolatilization period and may reduce the pre-treatment cost.

Fuel consumption rate (f_c)

Biomass gathers on the bottom forming a solid bed with a feed rate was less than 5 kg/hr, If the fuel consumption rate was less than 20 kg/hr, may decrease the residence time of the feed inside the gasifier and thus decrease its exposure to melting inside. Hence, the gasifier used for the present work designed with the maximum feed rate of 20 kg/hr.

DESIGN MATRIX ON EXPERIMENTATION

From the investigation the agro-industrial biomass as a predominant factor may have the greater influence on the quality of the solid (ash), liquid (tar) and gaseous (producer gas) have been identified [24-29]. The biomasses such as wheat husk, rice husk and saw dust are used in the present investigation. Owing to a wide range of factors such as temperature, pressure, equivalence ratio, feed size and fuel consumption rate. The use of five factors and central composite rotatable design matrix was chosen to minimize number of experiments. The number of tests required for the CCRD includes the standard 2k factorial with its origin at the center, 2k points fixed axially at a distance, say α, from the center to generate the quadratic terms, and replicate the experiment tests at the center point; where number of variables represent by k. The axial points are chosen such that they allow rotatability, which ensures that the variance of the model prediction is constant at all points equidistant from the design center. By adding axial points which extend, the design will provide protection against the curvature from twisting. Hence, the design was extended up to $\pm \alpha$. The value of α is chosen to maintain rotatability and depend upon the number of experimental runs in the factorial portion of the CCD, as shown in Equation (3.1)

$$\alpha = [\text{number of factorial points}]1/4 \quad (3.1)$$

If full factorial for α is evaluated using

$$\alpha = [23]1/4 = \pm 1.682 \quad (3.2)$$

When ◎ > 1, each factor is run at five levels (–◎, –1, 0, +1, + ◎) instead of the three levels of –1, 0, and +1. The reason for running the CCD with ◎ > 1 is to have a rotatable design. However, the factorial portion can also be a fractional factorial design of resolution. The center values for the variables were carried out at least six times for the estimation of error, and single runs for each of the other combinations. For full replication of the test at the center an independent and more uniform estimate of the prediction variance over the entire design as shown in Table 3 the ranges of factors are considered. For the convenience of recording and processing the experimental data, the upper and lower levels of the factors are coded as +1.682 and -1.682 respectively. The coded values of any intermediate value can be calculated by using the Equation (3.3).

$$Xi = 1.682\,[2X - (Xmax - Xmin)] / (Xmax - Xmin) \quad (3.3)$$

Where, Xi is the required coded value of a variable X, and X is any value of the variable from Xmin to Xmax
Xmin is the lower level of the variable.
Xmax is the upper level of the variable.
Xmax is the upper level of the variable.

Design matrix consisting of 20 sets of coded conditions 8 factorial points, 6 corner points and six center points was chosen in this study [30-34]. Table 4 shows the experimental results and actual results for 20 sets of coded and actual values.

The experimental data and those were compared with the predicted values of the developed model. The producer gas energy is assessed with the variable ACE (Ash conversion efficiency). This variable represents the ratio between the energy content of the producer gas (HHVgas) and the energy content of the initial agro-biomass. (HHVbiomass) without taking into account the heat input in the reactor:

$$\text{ACE} = 100\ (\text{Carbon content in the gas} \times \text{Gas yield}) / (\text{Ash content in biomass material} \times \text{Total feed}) \quad (1)$$

At the end of the experiment the tar were weighed and stored in a sealed recipient for further characterization. The tar yield is expressed as the ratio of the residual tar to the initial mass of biomass

$$\text{YTar\%} = [(\text{MTar}) / (\text{Mbiomass})] \times 100 \quad (2)$$

APPLYING DESIGN MATRIX ON EXPERIMENTATION

In the present work, to correlate the working parameters and the quality of the producer gas, a second order quadratic model was developed. In this study, the Response Surface Methodology provides a quantitative form of relationship between the desired response (Quality of the Producer gas) and the independent input variables (Biomass ratio), Wheat husk (W), Rice husk (R), and Saw dust (S), and can be expressed as a function, as in Equation (3)

$$\text{Quality of the Producer gas (Q)} = f(\text{W, R, S}).....\quad (3)$$

The mathematical relationship must include the main and interaction effects of all factors by selecting polynomial expressed as follows:

$$Y = bo + \circledcirc bi\ xi + \circledcirc bii\ xi^2 + \circledcirc bij\ xi\ xj \quad (4)$$

For three factors, the selected polynomial could be expressed as

$$\text{Quality of the Producer gas (Q)} = \{b0 + b1\ (\text{W}) + b2\ (\text{R}) + b3\ (\text{S}) + b11\ (\text{W}) + b22\ (\text{R}) + b33\ (\text{S}) + b12\ (\text{WR}) + b13(\text{WS}) + b23\ (\text{RS})\} \quad (5)$$

where $b0$ is the average of responses () and $b1$, $b2$, $b3$… $b11$, $b12$, $b13$… $b22$, $b23$, $b33$, are the coefficients that depend on their respective main and interaction factors, which can calculated using the expression given below,

$$Bi = (\circledcirc (Xi, Yi)\ )/n \quad (6)$$

Where 'i' varies from 1 to n, in which Xi the corresponding coded value of a factor and Yi is is the corresponding response output value obtained from the experiment and 'n' is the total number of biomass feed considered. All the coefficients were obtained applying CCRD matrix including the Design Expert statistical software package. By determining the significant coefficients (at higher confidence level), the final relationship was developed including only these coefficients. The final empirical relationship obtained by the above procedure to

estimate producer gas generation, tar yield and ash content of various biomass feed under fluidized bed gasification is given below;

Producer Gas Efficiency

Producer Gas = + 72.555 – 2.546*(W) –0.528 *(R) –0.397 (S) –4.305 x 10-3 *(WR)
+ 9.277x 10–3* (WS) + 9.446x 10–3* (RS)
+ 0.072* (W^2) + 3.208x 10–3 (R^2) + 0.053*(S^2)

Tar yield efficiency

Producer Gas = + 14.537 –0.499 *(W) –0.138 *(R) –0.163 (S)
–5.342 x 10-4 *(WR) –1.236x10-3 (WS) + 8.975x 10–4 * (RS)
+ 0.014* (W^2) + 1.384x 10–3 (R^2) + 0.015* (S^2)

Ash Content Efficiency

Producer Gas = + 90.192 –2.759*(W) –0.557*(R) –0.539(S) –5.185x 10-3 *(WR)
+ 0.0126*(WS) + 0.013*(RS) + 0.078*(W^2)
+ 2.882x 103 (R^2) + 0.052*(S^2)

To find the main significant and interaction factors by using Analysis of Variance technique. The results of second order response surface model fitting as Analysis of Variance (ANOVA) are given in the Table 4. The determination coefficient (*r*2) indicated the goodness of fit for the model. The Model F-value of (ACE = 5.76, PGE = 5.88, TYE = 4.66) implies the model is significant. There is only a 0.01% chance that a "Model F-Value" this large could occur due to noise.

Producer Gas Efficiency

Values of "Prob > F" less than 0.0500 indicate model terms are significant. In this case R, S, W are significant model terms. Values greater than 0.1000 indicate the model terms are not significant. If there are many insignificant model terms (not counting those required to support hierarchy), model reduction may improve your model. The "Lack of Fit F-value" of 4.22 implies there is a 7.00% chance that a "Lack of Fit F- value" this large could occur due to noise. Lack of fi t is bad -- we want the model to fit. This relatively low probability (<10%) is troubling. The "Pred R-Squared" of 0.0275 is not as close to the "Adj R-Squared" of 0.7128 as one might normally expect; *i.e*. the difference is more than 0.2 [37]. This may indicate a large block effect or a possible problem with your model and/or data. Things to consider are model reduction, response transformation, outliers, etc. All empirical models should be tested by doing confirmation runs."Adeq Precision" measures the signal to noise ratio. A ratio greater than 4 is desirable. The present ratio of 7.858 indicates an adequate signal.

Tar yield

Values of "Prob > F" less than 0.0500 indicate model terms are significant. In this case W, R, S are significant model terms. Values greater than 0.1000 indicate the model terms are not significant. If there are many in significant model terms (not counting those required to support hierarchy), model reduction may improve your model. The "Lack of Fit F-value" of 2.62 implies the Lack of Fit is not significant relative to the pure error. There is a 15.66% chance that a "Lack of Fit F-value" this large could occur due to noise. Non-significant lack of fit is good -- we want the model to fit. A negative "Pred R-Squared" implies that the overall mean may be a better predictor of you response than the current model "Adeq Precision" measures the signal to noise ratio [35]. A ratio greater than 4 is desirable. The present ratio of 6.072 indicates an adequate signal.

Ash Content Efficiency

Values of "Prob > F" less than 0.0500 indicate model terms are significant. In this case R, S, W are significant model terms. Values greater than 0.1000 indicate the model terms are not significant. If there are many insignificant model terms (not counting those required to support hierarchy), model reduction may improve your model. The "Lack of Fit F-value" of 3.12 implies the Lack of Fit is not significant relative to the pure error. There is 11.89% chance that a "Lack of Fit F-value" this large could occur due to noise. Non-significant lack of fit is good -- we want the model to fit. The "Pred R-Squared" of 0.0121 is not as close to the "Adj R-Squared" of 0.6926 as one might normally expect; *i.e.* the difference is more than 0.2. This may indicate a large block effect or a possible problem with your model and/or data. Things to consider are model reduction, response transformation, outliers, etc. All empirical models should be tested by doing confirmation runs. "Adeq Precision" measures the signal to noise ratio. A ratio greater than 4 is desirable [36]. The present ratio of 7.484 indicates an adequate signal.

RESULT AND DISCUSSIONS

Agro industrial waste is a predominant biomass used for the gasification. The influences of addition of rice husk clearly demonstrated that, because of the thermal instability of carbon, a higher percentage heating value in a lesser degree of carbon conversion. Generally, increasing the gas efficiency since the heating value of the produced gas will increase with pressure and temperature [38-42]. It is reported that higher conversion of fuel during gasification of wheat husk causes an increases in tar yield. However, higher gas yield is reported with an increase in feed rate in the fuel as a consequence of higher concentration of hydrocarbons. The wheat husk as a biomass plays a key role in the production of more tar during gasification in comparison with other feedstock components. In the case of saw dust due to the low heating value ash carbon conversion efficiency reported more.

All of this, result indicates a perfect suitability of the regression model. Each of the predicated values compared with the experimental values shown in the Fig.2. A scatter points of the two variables indicates a straight line provides a suitable fit to the experimental data. The differences between two responses are termed as residuals, this shows the measure of the closeness of agreement of the experimental value and the predicted responses; hence, they provide a measure of the adequacy of the fitted model [43, 44]. The difference in the experimental and the predicted responses, with dark points, is the residuals. The linear fit approximates the experimental data points very well; the sum of squares of residual is all very close as shown in the Table 5. Some residuals are one important indicator of the adequacy of a regression fit.

CONCLUSIONS

- The present investigation was focused on the agro industrial biomass such as Wheat husk, Rice husk and Saw dust in a pilot scale fluidized bed reactor. To examine the producer gas efficiency, tar yield efficiency and ash content efficiency.
- The gasifier was operated at bed temperatures ranging from 650 °C to 950 °C with varying equivalence ratios of 0.2 – 0.5 , pressure 1 to 5 bar, feed rate 5 -20 kg/hr and particle size 70 -500 μm to investigate the efficiencies.
- The empirical relation was developed in order to quantify the gas efficiency of producer gas. This model gave results with high accuracy showing similar trends in predicting the variation of gas species concentrations in line with experimental data.
- It was noticed that the producer gas efficiency more in rice husk. However, ash content efficiency more in the case of saw dust and tar yield reported high in wheat husk.
- On comparing the efficiency of the producer gas shows better performance in the rice husk when comparing the other feed.

REFERENCES

1. Bridgwater, A.V.: The technical and economic feasibility of biomass gasification for power generation. Fuel. 74(3), 631–53 (1995).
2. Boateng, A.A., W.P. Walawender, L.T Fan and C.S.Chee : Fluidized bed steam gasification of rice hull. Bio resource Technology. 40(2), 235–9 (1992).
3. E.C. Beagle, "Rice-husk conversion to energy", 1978.
4. T.C. Luan and T.C. Chou, "Recovery of silica from the gasification of rice husks/coal in the presence of a pilot flame in a modified fluidized bed", Industrial & engineering chemistry research, Vol. 29, No. 9, Pp. 1922-1927, 1990.
5. Ghaly, A.E., A.M. Al-Taweel and Mackay: GDM project report renewable energy division. Canada, Ottawa, Ontario: Energy Mines and Resources; 1986.
6. Natarajan, A. Nordin and A.N. Rao, "Overview of combustion and gasification of rice husk in fluidized bed reactors", Biomass and Bioenergy, Vol. 14, No. 5, Pp. 533-546, 1998.
7. Xu, S., Y. Ren, B.Wang, Y. Xu, L. Chen and Wang and X. Xiao: Development of a novel 2-stage entrained flow coal dry powder gasifier. Appl. Energy, 113, 318–322 (2014).
8. Corella, J., J. M. Toledo and G.Molina: A. Review on dual fluidized bed biomass gasifier. Ind. Eng. Chem. Res., 46, 6831–6839 (2007).
9. Seo, M.W., J.H. Goo, S.D.Kim, S.H. Lee and Y.C. Choi: Gasification characteristics of coal/biomass blend in a dual circulating fluidized bed react. Energy Fuels, 24, 3108–3118 (2010).
10. Ahmed, I.I. and A.K. Gupta Kinetics of woodchips char gasification with steam and carbon dioxide. Appl. Energy, 88, 1613–1619 (2011).
11. Prabowo, B., K.Umeki, M. Yan, M.R.Nakamura, M.J. Castaldi and K.Yoshikawa : CO2–steam mixture for direct and indirect gasification of rice straw in a downdraft gasifier: Laboratory-scale experiments and performance prediction. Appl. Energy, 113, 670–679 (2014).
12. Prega national technical experts. [internet] demonstration of rice rusks fired power plant in an giang province: a prefeasibility study report. Hanoi, vietnam: vietnam institute of energy. Available at: http://www.adb.org/clean-energy/documents/vie-pfs-rice-power-plant.pdf; 2004
13. Sarkar, M., A. Kumar, J.S. Tumuluru, K.N. Patil and D.D. Bellmer: Gasification performance of switch grass pretreated with torrefaction and densification. Appl. Energy, 127, 194–201 (2014).
14. Pinto F., C. Franco, A.R. Neto, C.Tavares, M. Dias, I. Gulyurtlu and I. Cabrita: Effect of experimental conditions on cogasification of coal, biomass and plastics wastes with air/steam mixtures in a fluidized bed system. Fuel, 82, 1967–1976 (2003).
15. Jones J. M., M.Kubaki, K.Kubica K., A.B. Ross and A.Williams: Devolatilization characteristics of coal and biomass blends. J. Anal. Appl. Pyrolysis, 74, 502–511 (2005).
16. Rizkiana, J., G. Guan, W.B.Widayatno, X. Hao X. Li, W. Huang and A. Abudula: Promoting effect of various biomass ashes on the steam gasification of low-rank coal. Appl. Energy, 133, 282–288 (2014).
17. Hernandez, J.J., G. Aranda-Almansa and C.Serrano: Co-gasification of biomass wastes and coal–coke blends in an entrained flow gasifier: An experimental study. Energy Fuels, 24, 2479–2488 (2010).
18. Peter, M.K.: Energy production from biomass (part 2): Conversion Technologies. Bioresource Technology, 83 (1) 47–54 (2002).
19. Sims, REH: Bioenergy to mitigate for climate change and meet the needs of society, the economy and the environment. Mitigation and Adoption Strategies for Global Change, 8: 349–370 (2003.).
20. Lin, C.L., M.L. Wey and S.D. You: The effect of particle size distribution on minimum fluidization velocity at high temperature. Powder Technol.126, 297–301(2002).
21. Natarajan, E., A. Nordin and A.N.Rao: Overview of combustion and gasification of rice husk in fluidized bed reactors. Biomass Bioenergy. 14(5/6), 533–46 (1998).

22. S.A. Hartiniati and M. Youvial, "Performance of a pilot scale fluidized bed gasifier fueled by rice husks, pyrolysis and gasification", Proceedings of the international conference in Luxembourg, Pp. 23-25, 1989.
23. Bin ZainalAlauddin, Z.A., L. Pooya, M. Mohammadi and A.R. Mohamed: Gasification of lignocellulosic biomass in fluidized beds for renewable energy development. A review. Renewable and Sustainable Energy Reviews 14, 2852– 2862 (2010).
24. Natarajan, A. Nordin and A.N. Rao, "Overview of combustion and gasification of rice husk in fluidized bed reactors", Biomass and Bioenergy, Vol. 14, No. 5, Pp. 533-546, 1998.
25. Simin Shabani, MojtabaAghajani Delavar and Mohammadreza Azmi : Investigation of biomass gasification hydrogen and electricity co-production with carbon dioxide capture and storage, international jornal of hydrogen energy 38, 3630-3639 (2013),
26. Koc, R., N.K. Kazantzis and Y. Hua Ma: A process dynamic modeling and control framework for performance assessment of Pd/ alloy-based membrane reactors used in hydrogen production. Int J Hydrogen Energy 36, 4934-51. (2011)
27. Mathieu, P. and R. Dubuisson: Performance analysis of a biomass gasifier. Energy Convers. Manage. 43, 1291–1299 (2002).
28. Lin, C.L., M.L. Wey and S.D. You: The effect of particle size distribution on minimum fluidization velocity at high temperature. Powder Technol. 126 (2002), 297–301.
29. Drift, A.V., J. Doorn and J.W. Vermeulen: Ten residual biomass fuels for circulating fluidized-bed gasification. Biomass Bioenergy 20, 45–56 (2009).
30. Luoa, S., B. Xiao, Z. Hua, S. Liua, Y. Guana and L. Caia : Influence of particle size on pyrolysis and gasification performance of municipal solid waste in a fixed bed reactor. Bioresource Technology.101(16), 6517–6520 (2010).
31. Susana Martı´nez-Lera and Jose´ TorricoJavier Pallare´s Antonia Gil: Design and fi rst experimental results of a bubbling fluidized bed for air gasification of plastic waste, J Mater Cycles Waste Manag. 15, 370–380(2013)
32. Risberg M., Ohrman O.G.W., Gebart B.R., Nilsson P.T., Gudmundsson A. and Sanati M. Influence from fuel type on the performance of an air-blown cyclone gasifier, Fuel 116, 751–759 (2014).
33. Mansaray, K.G., A.E. Ghaly, A.M Al-Taweel, F. Hamdullahpur and V. Ugursal: Air gasification of Corn Stalk in a dual distributor type fluidized bed gasifier. Biomass Bioenergy.17, 315–32 (1999).
34. Kaupp Albrecht : Gasification of rice hulls. Theory and practices. Deutsches Zentrum Fuer Entwicklungs Technologien (GATE): Eschborn; (1984).
35. Schiefelbein, G.F.: Biomass thermal gasification research, recent results – UnitedStates DOE's research program. Biomass 19, 145–59 (1989).
36. Bin Zainal Alauddin Z.A., L. Pooya, M. Mohammadi and A.R. Mohamed: Gasification of lignocellulosic biomass in fluidized beds for renewable energy development, Renewable and Sustainable Energy Reviews 14, 2852–2862 (2010).
37. Kurkela, E.; P. Stahlberg: Air Gasification of Peat, Wood and Brown Coal in Pressurised Fluidized Bed Reactor. I. Carbon Conversion, Gas Yield, and Tar Formation. Fuel Process. Technol. 31, 1-21 (1992)
38. Corella, J., M. P Aznar, J. Delgado, E. Aldea and P. Martı´nez, : Fuel and Useful Gas by Steam Gasification of Biomass in Fluidized Bed Followed by Tar Cracking Fluidized Bed of Dolomite/ Limestone/ Magnesite. In Biomass for Energy Industry and Environment (6th EC Conference); Grassi, G., et al., Eds.; Elsevier Applied Science: London, pp 714-721 (1992).
39. Walawender, W. P., D. Hoveland and L. T. Fan : Steam Gasification of Alpha Cellulose in a Fluid Bed Reactor. In Fundamentals of Thermochemical Biomass Conversion; Overend, R. P., et al., Eds.; Elsevier Applied Science: London; pp 897-910 (1985).
40. Illerup, J. B., K.Dam-Johansen and Lunden, K; High-Temperature Reaction between Sulfur Dioxide and Limestone- VI. The Infl uence of High Pressure. Chem. Eng. Sci., 48, 2151-2157 (1993).
41. Mathieu, P. and R.Dubuisson : Performance analysis of a biomass gasifier. Energy Convers. Manage..Eqivalent ratio & Feed rate. 43, 1291–1299 (2002).

42. Fermoso, J, B. Arias, M.V. Gil, M.G. Plaza, C. Pevida and JJ Pis :. Cogasification of different rank coals with biomass and petroleum coke in a high-pressure reactor for H2-rich gas production. Bioresource Technol 101(9):3230-5 (2010).
43. Seo, M.W., J.H. Goo, S.D. Kim, S.H. Lee and Y.C. Choi:. Gasifi cation characteristics of coal/biomass blend in a dual circulating fl uidized bed reactor. Energy Fuel;24:108-18 (2010).
44. Collot, A.G, Y. Zhuo, D.R. Dugwell and R. Kandiyoti Co-pyrolysis and co-gasification of coal and biomass in bench scale fixed-bed and fluidised bed reactors. Fuel; 78(6):667-79 (1999).

Table 1: Ultimate and proximate analysis of biomass

Ultimate analysis				Proximate analysis			
Components	**Percent**			**Components**	**Percent**		
	Wheat husk	**Rice husk**	**Saw dust**		**Wheat husk**	**Rice husk**	**Saw dust**
Carbon	40.10	50.48	31.54	Volatile matter	84.10	70.60	54.91
Hydrogen	6.40	6.51	4.07	Fixed carbon	5.68	2.97	11.51
Nitrogen	1.35	1.49	3.99	Moisture	9.92	9.45	11.43
Oxygen	51.79	41.40	25.87	Ash	1.63	17.09	22.14
Sulphur	0.36	0.20	0.96	Heating value (MJ/kg)	17.94	19.81	15.52

Table 2: Design and operating features of Fluidized Bed Gasifier

Parameters	**Range**
Gasifier	Fluidized Bed Gasifier
Gasifier specifications	Diameter (Inner) : 108 mm Total height : 1400 mm
Heating	Electric heating
Coolant	Water
Biomass capacity	20 kg / hr
Feeding method	Screw feeder
Gasifying agents	Air
Temperature	650-950 ºC
Operating parameters	Bed Temperature, Pressure, Feed rate, Equivalence ratio and Particle size.
Purification	Cyclone, Water scrubber, Dry filter

Table 3: Important factors and their levels

Factors	Units	Notation	Factors levels				
	%		–1.682	–1	0	+1	+1.682
Wheat husk		W	0	6	15	24	30
Rice husk		R	0	12	30	48	60
Saw dust		S	0	5	12.5	20	25

Table 4 : ANOVA Test results

Source	Ash Content Efficiency		Producer Gas Efficiency		Tar Yield	
	F value	p-value Prob>F	F value	p-value Prob>F	F value	p-value Prob>F
Model	5.76	0.0057	6.24	0.0042	4.27	0.0101
A-Wheat husk	3.23	0.1025	3.39	0.0952	2.11	0.1587
B-Rice husk	7.05	0.0241	7.77	0.0192	3.00	0.1008
C-Saw dust	28.25	0.0003	31.79	0.0002	19.24	0.0009
AB	0.11	0.7515	0.084	0.7775	0.030	0.8601
AC	0.11	0.7471	0.068	0.7997	0.024	0.7844
BC	0.53	0.4833	0.28	0.6071	0.060	0.8044
A2	11.04	0.0077	10.87	0.0080	10.01	0.0077
B^2	0.24	0.6376	0.34	0.5743	1.32	0.2358
C^2	2.38	0.1537	2.86	0.1218	4.98	0.0228

Table 5: Experimental Results

S. NO	Wheat Husk			Rice Husk			Saw dust		
	Ash content efficiency (%)	Producer gas efficiency (%)	Tar Yield (%)	Ash content efficiency (%)	Producer gas efficiency (%)	Tar Yield (%)	Ash content efficiency (%)	Producer gas efficiency (%)	Tar Yield (%)
1.	35.89	60.61	3.50	31.29	64.11	4.60	38.99	55.77	5.24
2.	35.60	61.00	3.40	31.00	64.50	4.50	38.76	56.11	5.13
3.	35.30	61.15	3.55	30.70	64.65	4.65	38.46	56.24	5.30

4.	35.46	61.62	2.92	30.86	65.12	4.02	38.77	56.65	4.58
5.	36.62	60.49	2.89	32.02	63.99	3.99	39.79	55.67	4.54
6.	34.78	61.41	3.81	30.18	64.91	4.91	37.94	56.47	5.59
7.	34.88	61.36	3.76	30.28	64.86	4.86	38.04	56.42	5.54
8.	34.70	62.45	2.85	30.10	65.95	3.95	38.13	57.37	4.50
9.	35.72	60.94	3.34	31.12	64.44	4.44	38.88	56.06	5.06
10.	36.98	60.31	2.71	32.38	63.81	3.81	40.15	55.51	4.34
11.	36.30	60.65	3.05	31.70	64.15	4.15	39.46	55.81	4.73
12.	36.38	60.61	3.01	31.78	64.11	4.11	39.55	55.77	4.68
13.	35.54	61.03	3.43	30.94	64.53	4.53	38.70	56.14	5.16
14.	36.10	60.75	3.15	31.50	64.25	4.25	39.27	55.89	4.84
15.	35.70	60.95	3.35	31.10	64.45	4.45	38.86	56.07	5.07
16.	35.04	61.28	3.68	30.44	64.78	4.78	38.21	56.35	5.44
17.	37.58	59.01	3.41	32.98	62.51	4.51	40.48	54.38	5.14
18.	36.24	61.63	2.13	31.64	65.13	3.23	39.66	56.66	3.68
19.	36.22	60.69	3.09	31.62	64.19	4.19	39.39	55.84	4.77
20.	37.28	60.76	1.96	32.68	64.26	3.06	40.62	55.90	3.48

Wheat husk

Rice husk

Saw dust

Figure 1. Photographic view of different biomass

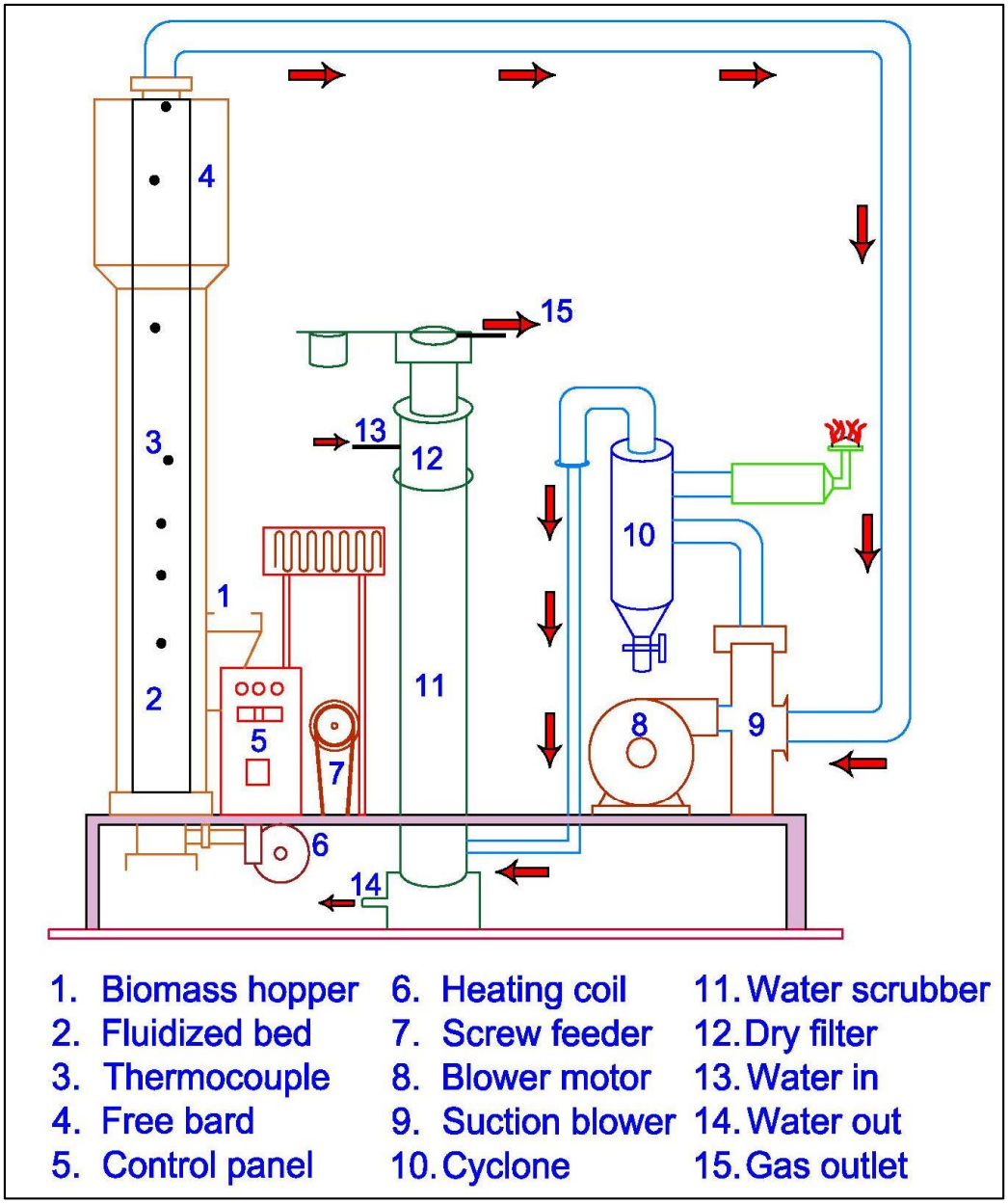

Figure 2. Layout of experimental setup

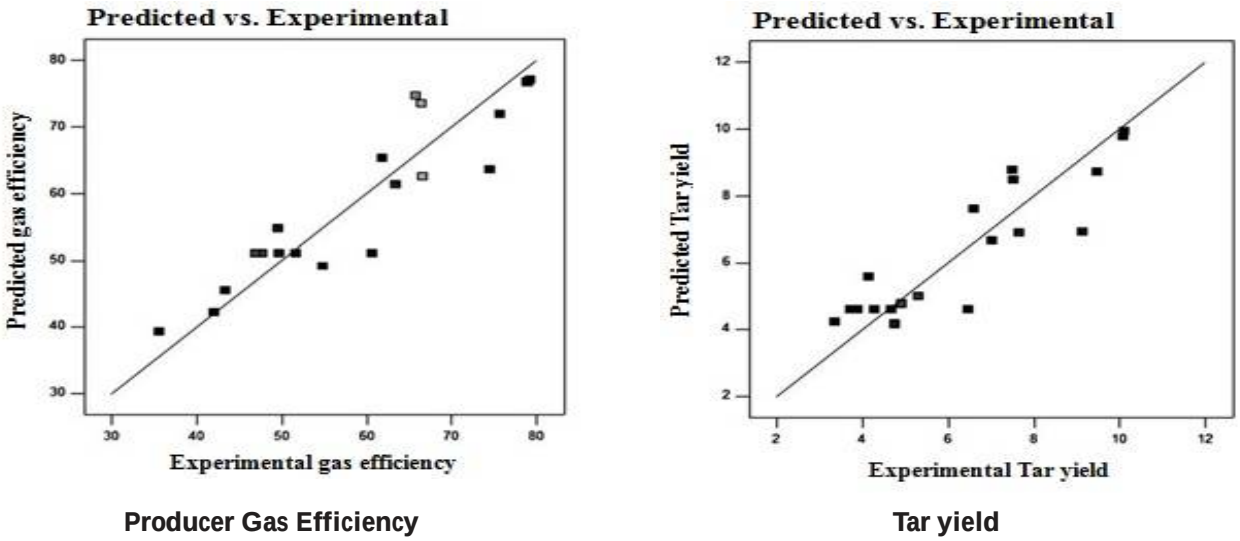

Producer Gas Efficiency **Tar yield**

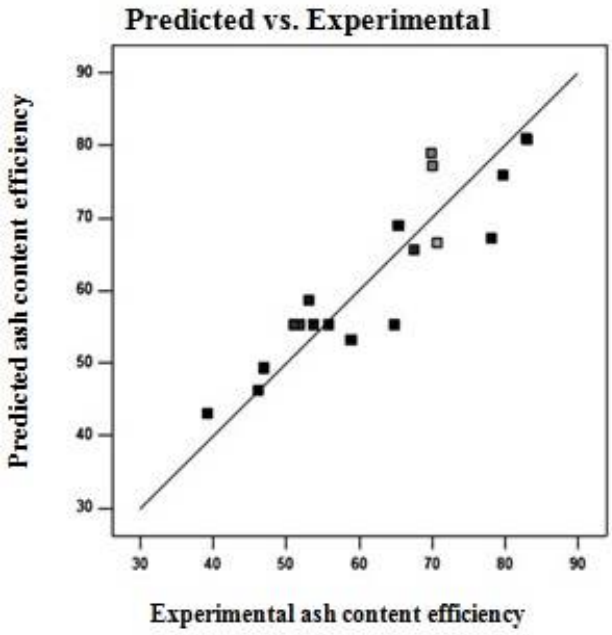

Ash content efficiency

Figure 3. Predicted vs Experimental